Geological setting, mineralogy, alteration, and nature of ore fluid of the H zone, the Chatree deposit, Thailand

By

Kamonporn Kromkhun

BSc. (Khon Kaen University, Thailand)

A thesis submitted in partial fulfilment for the degree of Master of Exploration Science

Centre for Ore Deposit Research (CODES SRC)
University of Tasmania, Australia

March, 2005

เดินทางบ่สุดเส้น

อย่าถอยหลังให้เขาเหยียบ

ตายขอให้ตายหน้าพุ้น

เขาสิเอิ้นว่าหาญ

Iddhipada: The Four paths of accomplishment

1. Chanda: will ; aspiration; intention,
2. Wiriya: energy; effort; exertion,
3. Citta: thoughtfulness; active thought,
4. Vimamsa: investigation; examination.

DISCLAIMER

This thesis contains results of research undertaken at University of Tasmania from March 2003 to March 2005. It contains no material that has been accepted for the award of higher degree or graduate diploma in any tertiary institution and contains no material previously published or written by another person, except when due acknowledgment is made in the text of this thesis.

i) I agree/do not agree that the thesis may be available for loan.

ii) I agree/do not agree that the thesis may be available for photocopying

Kamonporn Kromkhun

Kamonporn Kromkhun
University of Tasmania
March 2005

CONFIDENTIAL THESIS

Restricted access only. Embargo applies till June 2006

This thesis shall be made available by the University for consultation but, for a period of 1.5 years after the thesis is lodged, it **shall not be made available for loan or photocopying** without written consent of the author and in accordance with the laws of copyright Act 1968.

Kamonporn Kromkhun

Kamonporn Kromkhun

ABSTRACT

The Chatree gold deposit occurs within the Permo-Triassic volcanic rocks of the Loei-Phetchabun Volcanic Belt and is located at the boundary of Phetchabun and Phichit Provinces, central Thailand. The Chatree deposit (geological resource of 33 Mt @ 1.7 g/t Au and 11 g/t Ag) is classified as a low-sulphidation epithermal deposit and has been subdivided into several distinct zones. This study concentrates on the H zone. The stratigraphy of the H zone consists of plagioclase pyroxene phyric andesite, andesitic lithic breccias, crystal-rich andesitic pumice breccias, crystal-rich quartz feldspar lithic breccia, quartz-rich volcanic sandstone/mudstone and limestone. Andesitic-dacitic and basaltic dykes have intruded the host rocks and mineralised veins. Whole rock geochemistry indicates that the host rock composition ranges from sub-alkaline and calc-alkaline basalt to andesite. These volcanic rocks formed in a volcanic arc, with most rocks of continental volcanic arc affinity. The environments of host rock deposition are mainly subaerial to shallow submarine.

Five stages of vein mineralisation have been identified by petrography, PIMA and electron microprobe. These include Stage 1: hydrothermal breccia; Stage 2: gold - bearing quartz - calcite vein including quartz - calcite - chlorite - illite - illite/smectite - sericite - ankerite - dolomite - epidote - adularia - pyrite - hematite - rhodochrosite - chalcedony - sphalerite - galena - chalcopyrite - electrum; Stage 3: quartz - K-feldspar - carbonate - epidote - pyrite vein; Stage 4: calcite veinlet; and Stage 5: laumontite coating. Stage 2 mineralised veins occur in a NE trending dilational jog, dipping 45°NW in the southern part of the H zone and slightly flatter (to 20°NW) at the northern end of the H zone.

Mineralised vein textures include colloform-crustiform bands, comb, breccia and vuggy textures. Gold occurs as electrum in the forms of (1) inclusions within pyrite, (2) disseminated and (3) in contact with pyrite, chalcopyrite, galena and sphalerite within fine-grained quartz and calcite gangue. The deposit has a gold/silver ratio of approximately 1:4 and gold fineness ranging from 544 to 690 with an average of 609.

Gold-bearing veins are associated with four separate hydrothermal alteration zones. The mineralogy of these zones has been identified by PIMA, electron microprobe and

petrography. The zones include: Zone I (Kaolinite - montmorillonite - illite - pyrite); Zone II (Quartz - carbonates - illite - chlorite - pyrite - sericite - adularia); Zone III (Illite - chlorite - adularia - quartz - carbonate - epidote - sericite - albite); Zone IV (Epidote - chlorite - illite) and supergene enrichment. The alteration assemblages suggest that ore fluids were neutral to alkaline, reduced chloride waters with high concentrations of dissolved CO_2 and temperatures ranging from 100 to 300°C.

$\delta^{34}S$ values from pyrite grains within the mineralised veins range from –1.7 to +5.2‰, suggesting that the sulphur has been derived from a predominantly magmatic source. $\delta^{18}C$ values from calcite in various paragenetic stages and altered limestone range from –0.8 to –7.3‰. Corresponding $\delta^{18}O$ values range from +7.5 to +14.9‰. The initial composition of fluids has $\delta^{13}C$ and $\delta^{18}O$ values of -3‰ and +2‰, respectively. The carbon and oxygen isotope data suggests that carbonate minerals precipitated from the mixture of two fluids (magmatic and meteoric waters), accompanied by cooling and fluid-wallrock interaction.

ACKNOWLEDGMENTS

Throughout the duration of this study, the author has greatly benefited from the knowledge, advice, encouragement, and friendship of many people.

First, I would like to express gratitude to Royal Thai Government for the financial support. My dream would not have been possible without the special chance from the Thai government.

I would like to thank my supervisors Dr. Khin Zaw, Dr. David Cooke and Dr. Anthony Harris. Thanks Khin Zaw for offering an opportunity to do research at CODES, financial support for the project, advice and patience. Anthony has always encouraged and pushed me until the final stage.

Discussions with staff at CODES were very helpful; Thanks to Wally Herrmann, his advice is very valuable and kept me going; Dr. Garry Davidson guided me in dealing with stable isotope; Dr. Tony Crawford helped revising chapters and cheered me up. Many other staff at University of Tasmania have helped my work run smoothly; Mrs. Nilar Hlaing, Mrs. Katie McGoldrick, Mr. Simom Stephen, Mr. Phil Robinson, Dr. David Steel, Mr. Keith Harris and Mrs. Christine Cooke.

This project was supported by Kingsgate Consolidated NL. and Akara Mining. Many staff from the companies provided very helpful data and suggestions. Thanks to Dr. Marcus Tomkinson, Mr. Ron James and Mr. Mike Garman. Thanks also to Thai Akara staffers P' Tor and P' Kai, P' Maso, P' Maung, P' Kae, P' Toa, P' Ae, Nong Ae, Nong Phu, Nong Jeab and Nong Nui.

I have also received much support from many DMR staff and my Thai friends. Thanks guys for making me smile and always listening to me.

My work could not have been done without the encouragement, generosity, sense of humour and advice from friends at CODES; Bryan Bowden, Mawson Croaker, Wallace Mackay and Steve Lewis. I would especially like to thank my best friend, Rodney Maier, who was extremely helpful in various ways, his warm friendship, moral support, encouragement with my English and always being there whenever I need help.

Finally, I would like to thank my family; my father, Mr. Petch Kromkhun who is my role model and teaches me how to be optimistic; my mother, Mrs Pawinee Kromkhun who always encourages and pacifies me; my sister 'Ked' who posted many Thai entertainments to me; and to my other relations in Thailand. All of their encouragement helped me walk through the problems.

TABLE OF CONTENTS

ABSTRACT I

ACKNOWLEDGMENTS III

TABLE OF CONTENTS V

LIST OF FIGURES XII

LIST OF TABLES XVIII

CHAPTER 1 INTRODUCTION 1-1

1.1. Introduction 1-1

1.2. Location 1-1

1.3. Exploration history 1-6

1.4. Previous work 1-8

1.5. Mineralisation along the Loei Volcanic Belt 1-9

1.6. Aims of the study 1-10

1.7. Research designs and methods 1-11

CHAPTER 2 REGIONAL GEOLOGY 2-1

2.1. Introduction 2-1

2.2. Tectonic Evolution of Thailand 2-1

2.3. Tectonic Evolution of the Loei Volcanic-Plutonic Belt 2-4

2.3.1. Late Devonian-Early Carboniferous rocks 2-4

2.3.2. Permo-Triassic rocks 2-6

2.3.3. Tertiary rocks 2-7

2.4. Geochronology of the Loei-Phetchabun Volcaic Belt 2-7

CHAPTER 3 LOCAL GEOLOGY 3-1

3.1. Introduction 3-1

3.2. General Geology of the Chon Daen-Thap Klo Area 3-1

3.2.1. Stratigraphy of the Chon Daen-Thap Klo Area 3-1

3.3. Age of host rock 3-3

3.4. Geology of H Zone 3-4

3.4.1 Host Rocks 3-10

3.4.1.1. Plagioclase-pyroxene-phyric andesite 3-10

3.4.1.2. Andesitic lithic breccias 3-12

3.4.1.3. Crystal-rich andesitic pumice breccias 3-12

3.4.1.4. Crystal rich quartz-feldspar lithic breccia 3-14

3.4.1.5. Quartz-rich volcanic sandstone/mudstone 3-15

3.4.1.6. Limestone 3-16

3.4.2. Intrusive rocks 3-18

3.4.2.1. Andesite-dacite dyke 3-19

3.4.2.2. Basalt dyke 3-20

3.5. Whole rock geochemistry 3-21

3.5.1. Sampling and analytical techniques 3-22

3.5.2. Whole rock grouping 3-22

3.5.3. Major and trace elements 3-22

3.6. Depositional setting and environment 3-30

3.7. Summary 3-32

CHAPTER 4 VEIN MINERALOGY AND PARAGENESIS **4-1**

4.1. Introduction 4-1

4.2. Methodology 4-1

4.3. Vein morphology, texture, mineralogy and paragenesis 4-1

4.3.1. Stage 1 4-1

4.3.2. Stage 2 4-2

4.3.2.1. Vein texture 4-3

4.3.2.2. Vein mineralogy 4-6

4.3.3. Stage 3 4-8

4.3.4. Stage 4 4-9

4.3.5. Stage 5 4-9

4.4. Ore mineralogy 4-11

4.4.1. Electrum and sulphide mineral paragenesis 4-13

4.4.2. Ag:Au Ratios 4-15

4.5. Discussion 4-19

4.5.1. Vein mineralogy 4-19

4.5.2. Ore mineralogy 4-20

4.5.2.1. Ag:Au ratio 4-20

4.5.2.2. Chalcopyrite disease 4-21

4.5.2.3. Sphalerite content 4-21

4.5.3. Comparison vein study of the H zone with the A, D and C zones 4-22

4.6. Summary 4-24

CHAPTER 5 HYDROTHERMAL ALTERATION **5-1**

5.1. Introduction 5-1

5.2. Methodology 5-1

5.3. Alteration and mineralogy 5-2

5.3.1. Silicic alteration assemblages 5-2

5.3.2. Albitic alteration assemblages 5-3

5.3.3. Argillic alteration assemblages 5-4

5.3.4. Carbonate alteration assemblages 5-5

5.3.5. Chloritic alteration assemblages 5-6

5.3.6. Potassic alteration assemblages 5-7

5.3.7. Phyllic alteration assemblages 5-8

5.3.8. Propylitic alteration assemblages 5-10

5.3.9. Sulphide minerals 5-12

5.3.10. Zeolitic alteration assemblages 5-14

5.4. Discussion 5-15

5.4.1. Alteration zone and equilibrium alteration assemblages 5-15

5.4.1.1. Zone I (Kaolinite-illite-montmorillonite-pyrite) 5-15

5.4.1.2. Zone II (Quartz-carbonate-illite-chlorite-pyrite-sericite–adularia) 5-17

5.4.1.3. Zone III (Illite-chlorite-adularia-quartz-carbonate-epidote–sericite-albite) 5-18

5.4.1.4. Zone IV (Epidote–chlorite-illite) 5-18

5.4.1.5. Supergene enrichment 5-18

5.4.2. The Fe/(Fe/Mg) of chlorite and Au grade 5-19

5.4.3. Chlorite geothermometry 5-19

5.4.4. Comparison between the H zone and low-sulphidation epithermal deposits 5-21

5.5. Summary 5-23

CHAPTER 6 SULPHUR, CARBON AND OXYGEN ISOTOPES 6-1

6.1. Introduction 6-1

6.2. Sulphur Isotopes 6-1

6.2.1. Methodology 6-1

6.2.2. Results 6-2

6.2.2.1. $\delta^{34}S$ values of the H zone 6-2

6.2.2.2. Comparison of $\delta^{34}S$ values from the H zone with the A, C and D zones 6-4

6.2.3. Discussion 6-6

6.1.3.1. Source of sulphur 6-6

6.1.3.2. Sulphur isotope composition 6-7

6.1.3.3. Sulphur isotope and boiling 6-7

6.3. Carbon and Oxygen Isotopes 6-8

6.3.1. Methodology 6-8

6.3.2. Results 6-9

6.3.2.1. $\delta^{13}C$ and $\delta^{18}O$ values of the H zone 6-9

6.3.2.2. The $\delta^{13}C$ and $\delta^{18}O$ values of the A, C, D and H zones 6-11

6.3.3. Discussion 6-14

6.3.3.1. Data interpretation and. source of fluid 6-14

6.3.3.2. Carbon and oxygen plot 6-18

6.3.3.3. Initial composition of fluid 6-18

6.3.3.4. Carbon species 6-20
6.3.3.5. Fluid-rock interaction 6-22
6.3.3.6. The carbon-oxygen isotope temperature relationships 6-23
Fluid mixing 6-24
6.4. Summary 6-26

CHAPTER 7 CONCLUSIONS, DISCUSSION AND GENETIC MODEL 7-1
7.1. Introduction 7-1
7.2. Geological setting 7-1
7.3. Vein mineralogy and paragenesis 7-2
7.4. Hydrothermal alteration 7-3
7.5. Sulphur, carbon and oxygen isotopes 7-4
7.6. Geochemistry of the ore fluid 7-5
7.6.1. Temperature 7-5
7.6.2. pH and salinity 7-5
7.7. Depositional process 7-6
7.7.1. Conductive cooling 7-6
7.7.2. Boiling 7-7
7.7.3. Fluid mixing 7-8
7.7.4. Water-rock interaction 7-8
7.8. H zone compared to other low-sulphidation epithermal deposits 7-8
7.9. Genetic model 7-12

REFERENCE 8-1

APPENDICES

Appendix A: XRF analysis

Appendix B: PIMA

Appendix C: Electron Microprobe analysis

Appendix D: Carbon, oxygen and sulphur isotopes

Appendix E: List of samples

Appendix F: Gold and silver assay

Appendix G: Sample and drill hole location

LIST OF FIGURES

CHAPTER 1 INTRODUCTION

Figure 1.1. Map of the location of the Chatree and Phu Thap Fha deposit 1-2

Figure 1.2. Map of the location of the Chatree deposit 1-3

Figure 1.3. Photograph showing the Chatree deposit (Khao Mo and Khao Pong) 1-4

Figure 1.4. Photograph showing the Chatree deposit (Khao Mo) 1-4

Figure 1.5. Locations of the A, D, C and H Zones 1-5

Figure 1.6. Map of eight prospects at the initial exploration stage 1-7

Figure 1.7. Map of mineral deposits along Loei Volcanic Belt 1-10

CHAPTER 2 REGIONAL GEOLOGY

Figure 2.1. Map of Thailand showing Shan-Thai and Indochina terranes 2-2

Figure 2.2. Paleo-geographical distribution of Southeast Asian terranes and Gondwanaland 2-3

Figure 2.3. Distribution of volcanic rocks along the Loei Volcanic Belt 2-5

Figure 2.4. Tectonic model for the evolution of the Loei Volcanic Belt in Late Devonian 2-6

Figure 2.5. Tectonic models for the evolution the Loei Volcanic Belt in Permo-Triassic 2-6

Figure 2.6. Tectonic models for the evolution the Loei Volcanic Belt in Tertiary 2-7

Figure 2.7. Map of Ar-Ar data a long the Loei Volcanic Belt 2-8

Figure 2.8. Ages of volcanic rock along the Loei Volcanic Belt 2-9

CHAPTER 3 LOCAL GEOLOGY

Figure 3.1. Geology of the Chon Daen-Thap Klo area 3-2

Figure 3.2. Location of the A, C, D and H zones and major structures 3-5

Figure 3.3. Geologic map of H zone with location of drill cores 3-6

Figure 3.4. Cross-section of H zone, section 6100 3-7

Figure 3.5. Cross-section of H zone, section 6200 3-8

Figure 3.6. Cross-section of H zone, section 3500 3-9

Figure 3.7. Photograph of andesitic lithic breccia and plagioclase-pyroxene-phyric andesite 3-10

Figure 3.8. Photograph of plagioclase-pyroxene-phyric andesite 3-11

Figure 3.9. Photomicrograph of clinopyroxene phenocryst 3-11

Figure 3.10. Photograph of andesitic lithic breccia 3-12

Figure 3.11. Outcrop of footwall showing contacts between two units 3-13

Figure 3.12. Outcrop of crystal-rich pumice lithic breccia 3-13

Figure 3.13. Photograph of crystal-rich quartz-feldspar lithic breccia 3-14

Figure 3.14. Photomicrograph of crystal-rich quartz-feldspar lithic breccia 3-15

Figure 3.15. Outcrop of bedded quartz-rich volcanic sandstone/mudstone 3-16

Figure 3.16. Photograph of limestone 3-17

Figure 3.17. Photomicrograph showing fossils in limestone 3-17

Figure 3.18. Outcrop at H pit showing late dyke crosscutting hanging wall 3-18

Figure 3.19. Outcrop of contact between late dyke and sheared hanging wall 3-18

Figure 3.20. Petrography and texture of late andesitic dyke 3-19

Figure 3.21. Characteristic and texture of andesitic to dacitic late dyke 3-19

Figure 3.22. Characteristic and texture of basaltic late dyke 3-20

Figure 3.23. Igneous classification from TAS diagram 3-24

Figure 3.24. Igneous rock classification diagram by Nb/Y and Zr/TiO_2 3-25

Figure 3.25. Igneous rock classification diagram by Nb/Y and Zr/TiO_2 3-26

Figure 3.26. Plot of SiO_2 and FeO showing a trend of calc-alkali basalt 3-27

Figure 3.27. Plots of Zr/P_2O_5*10000 with TiO_2 (A) and Nb/Y (B) 3-27

Figure 3.28. Plot of Zr and Zr/Y showing continental and oceanic arc setting 3-28

Figure 3.29. Plot of Zr and Ti for tectonic setting 3-28

Figure 3.30. Plot of 2Nb-Zr/4-Y for tectonic setting 3-29

Figure 3.31. Ti-Zr-Y discrimination diagram for basalt 3-29

CHAPTER 4 VEIN MINERALOGY AND PARAGENESIS

Figure 4.1. Photograph of vein Stage 1 grey quartz (hydrothermal breccia) 4-2

Figure 4.2. Photograph of vein Stage 2 at the H pit 4-3

Figure 4.3. Photograph showing crustiform - colloform band 4-3

Figure 4.4. Photograph showing crustiform - colloform texture of Stage 2 vein 4-4

Figure 4.5. Photograph showing comb texture 4-4

Figure 4.6. Photograph showing breccia texture 4-5

Figure 4.7. Photograph showing carbonate-leached vuggy quartz vein 4-5

Figure 4.8. Photograph of quartz-carbonate-chlorite-hematite-pyrite-sericite vein 4-7

Figure 4.9. Photograph of vein Stage 2 quartz-calcite-chlorite bands 4-7

Figure 4.10. Photograph showing vein Stage 3 crosscutting vein Stage 2 4-8

Figure 4.11. Photograph showing quartz-pyrite vein of Stage 3 4-8

Figure 4.12. Photograph of calcite veinlet crosscutting andesitic dyke 4-9

Figure 4.13. Photograph of laumontite coating calcite veinlet 4-9

Figure 4.14. Mineral paragenesis of vein stages 4-10

Figure 4.15. Photomicrograph of electrum 4-11

Figure 4.16. Photomicrograph of electrum 4-11

Figure 4.17. Photomicrograph of electrum 4-12

Figure 4.18. Photomicrograph of electrum 4-12

Figure 4.19. Photomicrograph of electrum 4-12

Figure 4.20. Photomicrograph of opaque minerals and calcite and quartz gangue 4-12

Figure 4.21. Photomicrograph of electrum and sulphide minerals within gangue 4-12

Figure 4.22. Chalcopyrite disease in sphalerite grain 4-14

Figure 4.23. Paragenetic relationship between sulphide minerals and electrum 4-15

Figure 4.24. Map of gold grade contour of Section 6200N 4-16

Figure 4.25. Map of silver and gold contour of Section 6200N 4-17

Figure 4.26. Distribution of gold fineness 4-19

CHAPTER 5 HYDROTHERMAL ALTERATION

Figure 5.1. Photograph of silica alteration in andesitic lithic breccia 5-2

Figure 5.2. Photomicrograph of fine-grained quartz alteration 5-3

Figure 5.3. Photograph of argillic alteration 5-4

Figure 5.4. Photograph of calcite infilling open-spaces 5-5

Figure 5.5. Photograph of rhodochrosite in quartz-carbonate vein 5-6

Figure 5.6. Photograph of chlorite replacement in quartz-carbonate vein 5-6

Figure 5.7. Photograph of K-feldspar and chlorite alteration 5-7

Figure 5.8. Photograph of K-feldspar halo around quartz vein 5-7

Figure 5.9. Photograph of K-feldspar alteration observed by staining 5-7

Figure 5.10. Photomicrograph of adularia alteration 5-8

Figure 5.11. Photomicrograph of adularia in quartz-carbonate mineralised vein 5-8

Figure 5.12. Photograph of sericite alteration halo 5-9

Figure 5.13. Photomicrograph of sericite alteration 5-9

Figure 5.14. Photograph of epidote alteration in carbonate-quartz vein 5-10

Figure 5.15. Photomicrograph of epidote and prehnite alteration 5-11

Figure 5.16. Photograph of hematite alteration 5-11

Figure 5.17. Photomicrograph of hematite and chlorite alteration 5-12

Figure 5.18. Photograph of cubic pyrite in hanging wall of the H pit 5-13

Figure 5.19. Photograph of pyrite alteration in quartz -chlorite vein 5-13

Figure 5.20. Photograph of laumontite coating in fractures 5-14

Figure 5.21. Cross-section showing alteration zones 5-16

Figure 5.22. Relationship between Au grade and Fe/(Fe+Mg) ratio of chlorite 5-21

Figure 5.23. Comparison of low-sulphidation alteration pattern 5-22

CHAPTER 6 SULPHUR, CARBON AND OXYGEN ISOTOPES

Figure 6.1. Distribution of $\delta^{34}S$ at Section 6200N 6-3

Figure 6.2. Frequency distribution histogram of $\delta^{34}S$ values 6-4

Figure 6.3. Comparison of the $\delta^{34}S$ values at the Chatree 6-5

Figure 6.4. The $\delta^{34}S$ values with different sources of sulphide minerals 6-6

Figure 6.5. Plot of $\delta^{34}S$ with Au grade 6-8

Figure 6.6. Histogram of the $\delta^{13}C$ values 6-10

Figure 6.7. Histogram of the $\delta^{18}O$ values 6-11

Figure 6.8. Comparison of the $\delta^{13}C$ values between the A, C, D and H zones 6-12

Figure 6.9. Comparison of the $\delta^{18}O$ values between the A, C, D and H zones 6-13

Figure 6.10. The $\delta^{13}C$ values comparing with source of carbon and the other epithermal deposits 6-15

Figure 6.11. The $\delta^{18}O$ values of the H zone and the A, C and D zones compare with source of oxygen 6-17

Figure 6.12. Plot of $\delta^{13}C$ and $\delta^{18}O$ values for an initial composition of fluid and initial position of fluid model 6-19

Figure 6.13. Plot of $\delta^{13}C$ and $\delta^{18}O$ values of carbonates from the H zone with the H_2CO_3 and HCO_3^- curves 6-21

Figure 6.14. Plot of $\delta^{13}C$ and $\delta^{18}O$ values of altered limestone showing fluid-wall rock interaction 6-22

Figure 6.15. Plot of the $\delta^{13}C$ and $\delta^{18}O$ values and cooling trend 6-24

Figure 6.16. Plot of the $\delta^{13}C$ and $\delta^{18}O$ values and mixing trend 6-25

CHAPTER 7 CONCLUSIONS, DISCUSSION AND GENETIC MODEL

Figure 7.1. Major NW fault movement and dilation jogs 7-12

Figure 7.2. Schematic diagram showing mixing of the meteoric water with magmatic volatile fluids 7-13

Figure 7.3. Cartoon to illustrate schematically the hydrothermal breccia 7-14

Figure 7.4. Cartoon to illustrate schematically the deposition of silica gangue minerals 7-15

Figure 7.5. Cartoon to illustrate schematically the blanket of kaolinite, montmorillonite, illite-smectite and pyrite by steam heated water 7-16

Figure 7.6. Cartoon to illustrate schematically the sheared hanging wall and late dyke crosscutting ore vein 7-17

LIST OF TABLE

CHAPTER 3 LOCAL GEOLOGY

Table 3.1. Geochemical data of major and trace elements of samples 3-22

CHAPTER 4 VEIN MINERALOGY AND PARAGENESIS

Table 4.1. Sphalerite composition and FeS content 4-14

Table 4.2. Compositional variation and relation of electrum 4-18

Table 4.3. Comparison of vein mineralogy and characteristics 4-23

Table 4.4. Summary of vein studies 4-24

CHAPTER 5 HYDROTHERMAL ALTERATION

Table 5.1. Characteristic of the alteration zones 5-20

Table 5.2. Mineral alteration assemblage of the H zone, the Chatree deposit 5-23

Table 5.3. Characteristics of the alteration zones at the H zone 5-24

CHAPTER 6 SULPHUR, CARBON AND OXYGEN ISOTOPES

Table 6.1. The sulphur isotope values of the H zone and gold grades 6-2

Table 6.2. $\delta^{13}C$ and $\delta^{18}O$ analysis from carbonate minerals of the H zone 6-10

Table 6.3. Summary of sulphur, carbon and oxygen isotope studies 6-26

CHAPTER 7 CONCLUSION, DISCUSSION AND GENETIC MODEL

Table 7.1 Comparison of characteristics of the H zone and
other low-sulphidation epithermal deposits 7-11

Chapter 1
Introduction

1.1. Introduction

Thailand has a long history of gold mining and exploration. The first recorded placer gold mining occurred in 1750 from the Ban Pa Ron, Bang Saphan, Prachuap Khiri Khan areas (DMR, 2002). Other gold occurrences have been found throughout Thailand, and these are typically found in volcanic-plutonic belts. In recent years, there are two areas that have been recognised as hosting significant gold resources (Figure 1.1). These are the Chatree gold deposit, which has been in production since 2001, and the Phu Thap Fha deposit, which is under development. The Chatree Gold Mine ranks as one of the lowest cost gold producers in the world. Total production at Chatree for the year ended 30 June 2004 was 149,979 ounces of gold and 395,346 ounces of silver from a total resource of 33 million tonnes at 1.7 g/t Au and 11 g/t Ag (http:// www.kingsgate.com. au).

1.2. Location

The Chatree deposit is located on the boundary between Thap Klo District, Phetchabun Province and Wang Pong District, Phichit Province, central Thailand (Figure 1.2). It is approximately 280 kilometres north of Bangkok and about 35 kilometres southeast of Phichit. Coordinates of the mine are approximately 100° 36′ E and 16° 19′ N. The climate of the area is tropical monsoon and is characterised by a long dry season and a wet season from June to October. There are two main landforms in the area, including lower lying country predominantly used for agriculture and isolated hills (Khao Mo and Khao Pong; Figures 1.3 and 1.4). Khao Mo rises steeply 100 metres above the level of the plain, whereas Khao Pong rises gently for 30 metres above the lower land.

The Chatree gold mine covers an area of 7.5 km by 2.5 km and consists of at least 5 gold-rich vein systems (A, C, D, H and Mar). H zone is located in Tawan pit (C-H), in the western part of the deposit (Figure 1.5). The ore reserves and resources of C-H zone at 30 June 2004 were 8,197 tonnes with grade of 2.3 g/t of Au and 10 g/t of Ag (http://www. kingsgate.com.au).

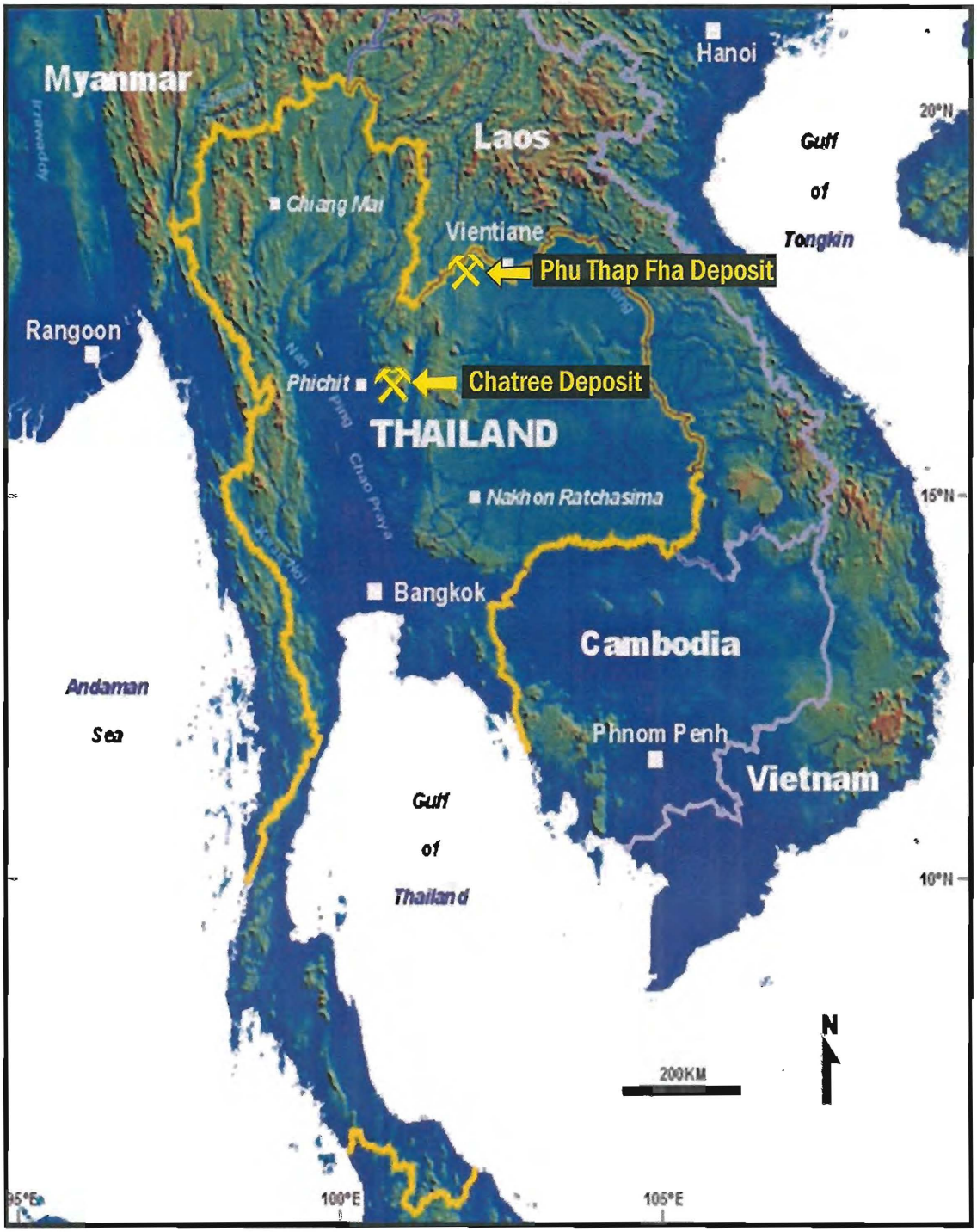

Figure 1.1. Map showing the location of the Chatree and Phu Thap Fha deposits in Thailand (http://www.kingsgate.com.au).

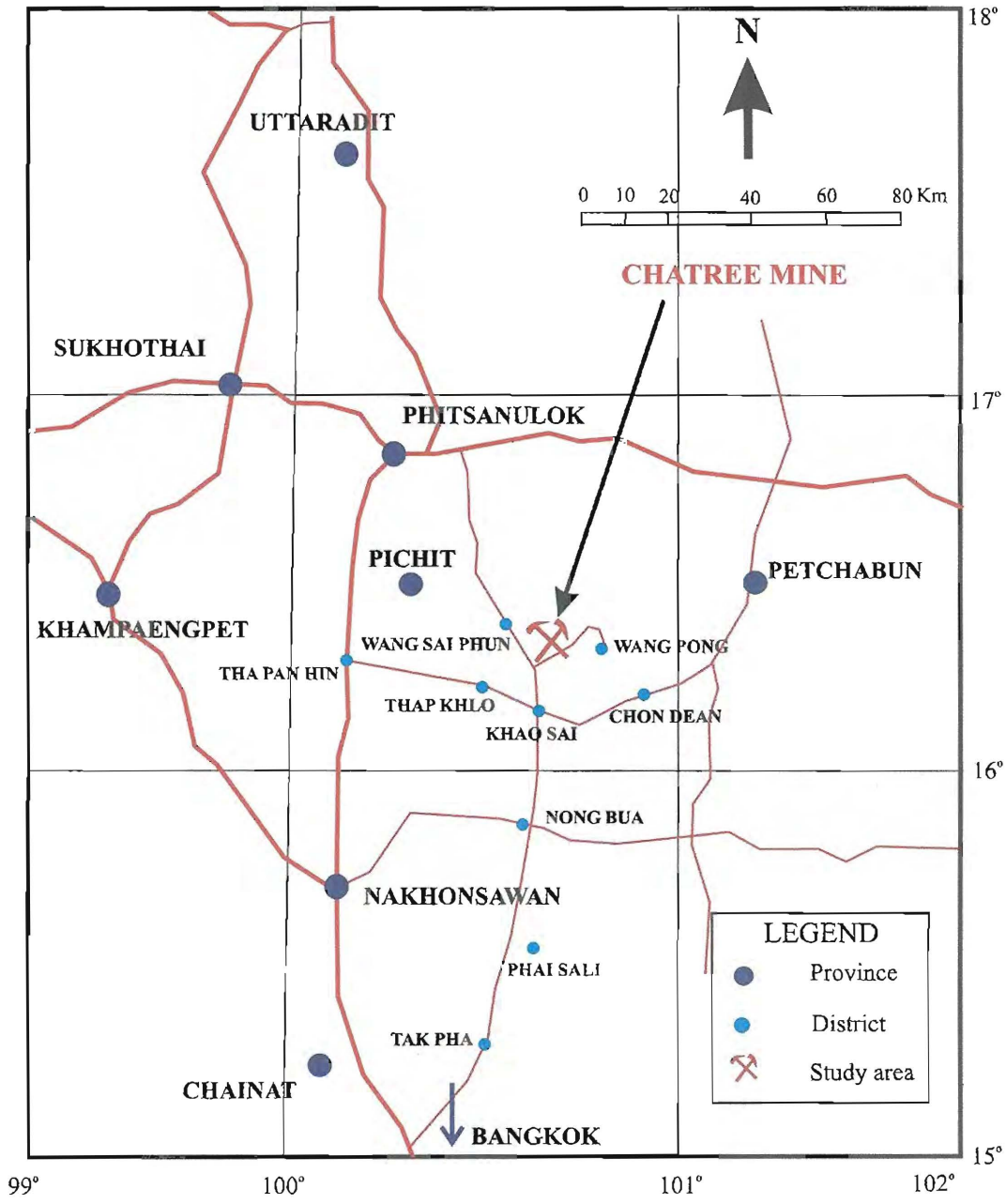

Figure 1.2. Map showing the location of the Chatree deposit, central Thailand.

Figure 1.3. Photograph showing the Chatree prospect; Khao Mo is in the left of the frame and Khao Pong is in the right (Greener, 1999).

Figure 1.4. Photograph showing the Chatree deposit, Khao Mo is in the right of the frame, February, 2004.

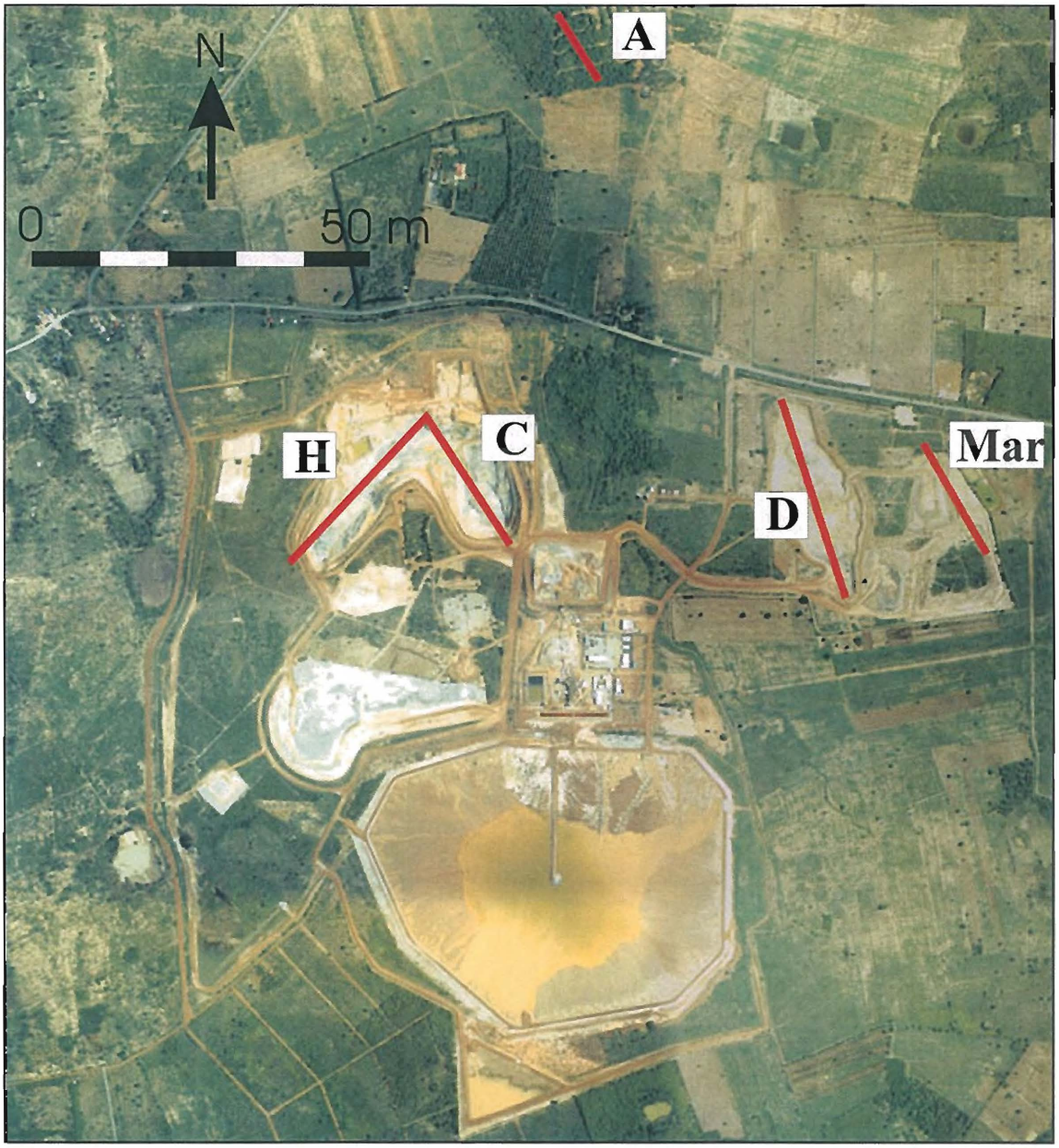

Figure 1.5. Locations of A, C, D, H and Mar Zones of Chatree Mine (Photo from Akara Mining).

1.3. Exploration history

In 1987, Thai Goldfields Limited explored along the Loei–Phetchabun Volcanic Belt (Deimar, 1990). Initial exploration targets were based on a porphyry copper and related epithermal gold system model and included griding, mapping, soil sampling, trenching, auger drilling, rotary air blast drilling and diamond core drilling. Epoch Mining NL in a joint venture with Kulim Limited and a private Australian partner also undertook exploration at Chatree.

In 1991 - 1992, the Department of Mineral Resources (DMR) conducted gold prospecting in Thap Klo District, Phichit Province, and Chon Daen and Wang Pong Districts, Phetchabun Province. The DMR conducted follow-up soil geochemical exploration at B Prospect, trenching at A and B Prospects and carried out a ground electromagnetic conductivity survey in the vicinity (DMR, 1994).

In 1993, several major Australian, Canadian, French and Dutch groups entered into discussion regarding a joint venture at Chatree but failed to commit. Epoch Mining NL from Australia pulled out the exploration management. In mid 1993, the Thai interests were sold to Kingsgate Consolidated NL. In late 1993, Kingsgate Consolidated NL signed a contract with Ban Pu Co., Ltd giving them a 51% participating interest, and a joint venture company Akara Mining Limited was formed.

In 1995, Akara Mining Limited was granted a license to explore the Chatree area. In 1996, the company carried out grid-based auger laterite geochemical exploration in the area between A and B Prospects, which led to the discovery of C, D, E, F, H and J Prospects (Figure 1.6).

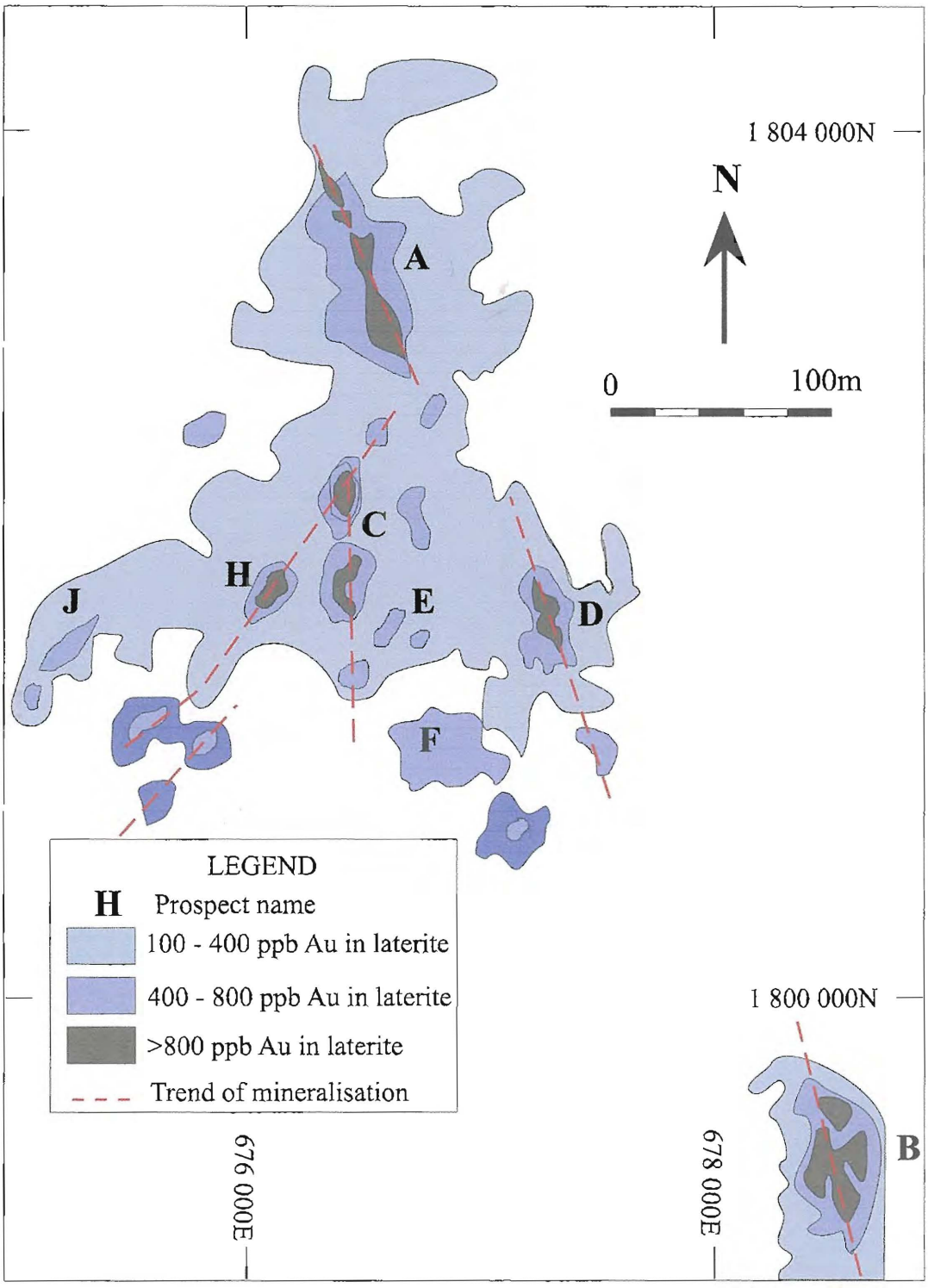

Figure 1.6. The eight prospects of the Chatree deposit after the initial stage of exploration and development (modified after Diemar, http://www.smedg.org.au/chatree2.html).

1.4. Previous work

The Loei – Phetchabun Volcanic Belt, which hosts the Chatree deposit has been documented in published research papers by Bunopas and Vella (1983), Hutchinson (1989), Barr and McDonald (1991) and Jungyasuk and Khositanont (1992).

Bunopas and Vella (1983), Hutchinson (1989) and Bunopas (1991) interpreted the geological history of Thailand using plate tectonic models and suggested that Thailand consists of the Shan-Thai and Indochina Terranes, which are cratonic fragments of Gondwanaland. Barr and McDonald (1991) used the tectonostratigraphic terrane models to determine an early Mesozoic tectonic model of Thailand and proposed the existence of Sukhothai Fold Belt separating the Shan-Thai and Indochina Terranes. Jungyasuk and Khositanont (1992) described the distribution of volcanic rocks in Thailand and suggested that they were of Permo-Triassic to Jurassic ages. The study also indicated that associated economic mineral deposits with volcanic rocks of Thailand include gold, silver, base metals, iron, manganese and antimony. Intasopa (1992) reported on characteristics of volcanic rocks in the Central Thailand Volcanic Belt and indicated that the rock types include Devonian rhyolite, Middle Devonian-Lower Carboniferous basalt and Permo-Triasic andesite. Intasopa (1992) suggested that partial melting of continental crust had generated these volcanic rocks.

Unpublished university BSc (Honour) research at the Chatree deposit includes:

1) Dedenczuk (1998) who studied the geology, mineralogy, geochemistry, and geothermometry at Prospects A and D. The study indicates that gold mineralisation occurs within quartz-carbonate veins at the A and D zones. Dedenczuk (1998) indicates that mineralisation is hosted by altered andesite, suggesting it has formed in a volcanic arc setting. This study documents the alteration minerals at the A and D zones, including quartz, adularia, chlorite, illite and pyrite. Temperatures for fluid inclusions in quartz from the mineralised veins in A and D zones of between 130°C to 240°C with low salinities (< 2.5 wt%) are reported. Dedenczuk (1998) proposed that the style of mineralisation at the Chatree deposit was consistent with a low-sulphidation epithermal gold deposit.

2) Greener (1999) who documented wall rock alteration and vein mineralogy at Prospect C. Greener (1999) indicates that gold mineralisation at the C zone occurs in quartz-calcite veins, hosted by andesitic rocks, and is associated with adularia, quartz, chlorite, pyrite, illite, epidote and calcite alterations. Temperatures of

fluid inclusions in quartz from the mineralised veins in the C zone of ~97°C to 150°C and 250°C to 296°C with low salinities (< 3 wt%) are reported. Greener (1999) proposed that the style of mineralisation at the Chatree deposit was consistent with a low-sulphidation epithermal gold deposit.

3) Cumming (2004) who documented volcanic facies architecture of the Chatree deposit. Cumming (2004) indicates that the Chatree deposit host rocks include andesitic lithic breccia, feldspar-phyric pumice breccia, andesite sills and late andesitic to basaltic dykes. Cumming (2004) proposed that they have formed in a submarine environment.

An unpublished report by Barron (1998) involved petrological and mineragraphic examination of 20 rock samples from Chatree and classified the host rocks as volcanic and volcaniclastic rocks.

Deimar (1999) presented an overview of the Chatree deposit with data and observations drawn from the previous investigations.

1.5. Mineralisation along the Loei Volcanic Belt

Porphyry, skarn type Cu-Au, and epithermal Au deposits occur in the Loei Volcanic Belt (Khin Zaw et al, 1999; Figure 1.7).

The Erawan prospect is a low-sulphidation epithermal vein-breccia Au deposit. Mineralisation is associated with dyke-like diorite intrusions and fine-grained porphyritic andesite (Khin Zaw et al., 1999).

The Ban Bothong deposit is a Cu±Au skarn deposit, which formed due to the intrusion of hornblende-diorite porphyry into metasedimantary rocks including limestones (Pisutha-Arnond et al., 1984). Mineralisation occurs as thin elongate bands where limestone has been replaced by garnet, wollastonite, epidote, hedenbergite and diopside.

The Phu Thap Fha deposit is a Au±Cu skarn deposit. Mineralisation occurs as a pyrrhotite-rich garnet-epidote-pyrite skarn with abundant late carbonate veins. The host rocks are andesitic rocks intercalated with limestone. Skarn alteration is developed around dioritic intrusions. Gold occurs in early garnet and late retrograde epidote-carbonate assemblages (Rodmanee, 2000).

The Phu Lon deposit is a Cu±Au skarn deposit. Mineralisation occurs in irregular replacement bodies at the contact between a granodiorite intrusion and

andesitic volcanic rock and calcareous sedimentary rock. Skarn minerals are garnet and epidote formed in carbonate wall rock (Kamvong, 2004).

The Chatree deposit at Khao Mo and Khao Pong is a low-sulfidation epithermal Au deposit (Dedenczuk, 1998; Greener, 1999; Diemar, 1999). Gold mineralisation occurs in adularia – sericite epithermal system within quartz-calcite veins and is hosted by andesitic rocks.

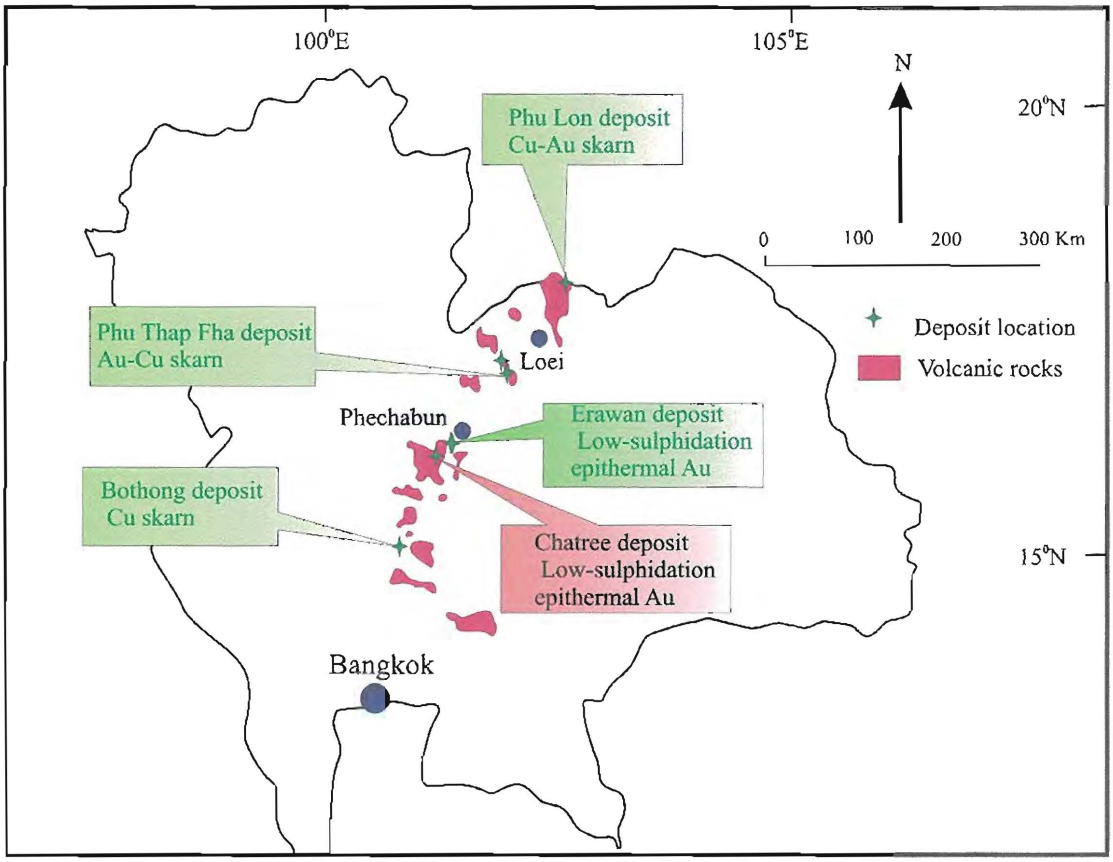

Figure 1.7. Map showing mineral deposits at the Loei Volcanic Belt (modified after Khin Zaw et al., 1999).

1.6. Aims of the study

Previous studies at the Chatree deposit have been undertaken in the A, C and D zones by Dedenczuk (1998) and Greener (1999) respectively. These studies suggest that the A, C and D zones represent a low-sulphidation epithermal system. This interpretation is based on the characteristics of ore veins and alteration mineral assemblages. The H zone, which occupies the western part of the Chatree deposit, is the subject of this study. There are a number of important differences between the H zone and the other zones of the Chatree deposit. Mineralised veins in the H zone have a

significantly different orientation to the other zones. In addition, these veins occur within a well defined shear zone. This leaves open the possibility that mineralisation in the H zone has resulted from different processes.

The main aims of this study are:

1) to describe and interpret the geological characteristics of the H zone at the Chatree deposit, including the alteration and vein mineralogy, mineral zonation and overprinting relationships;

2) to trace the chemistry of the mineralising fluids based on the observed alteration assemblages and stable isotope analysis;

3) to interpret the Chatree deposit within the context of its regional and district scale geological settings, and

4) to provide a model for ore genesis.

1.7. Research design and methods

Prior to the commencement of the field sampling program, a literature review was conducted in order to collate all previous information pertinent to the Chatree deposit.

Field investigations were undertaken during two visits to the Chatree mine between the 1st and 21st of September, 2003 and between 16th and 28th February 2004. This work involved sampling of key alteration assemblages from the H pit, utilising the existing geological map provided by Akara Mining company. Drill core logging was conducted along three selected sections (6100N, 6200N and 6350N) in the H zone. A total of nineteen holes were logged for a combined distance of 1,317 m. A total of 175 samples were collected for petrography and geochemical analysis from the open pit (n= 48), drill cores (n=121) and surrounding district (n=6).

Laboratory work conducted at the University of Tasmania included;

1) Petrography and electron microprobe analysis; Standard petrographic studies were undertaken using thin sections (n=34) and polished thin sections (n=30) to observe the nature and characteristics of the host rocks and alteration products. Ore minerals were observed using polished thin sections and standard reflected light microscopy. Petrographic studies aimed to identify ore and alteration mineralogy, textural relationships and mineral associations for the veins and altered rocks. Electron microprobe analysis was undertaken to determine chemical compositions of the

electrum (n=20), sphalerite (n=11) and chlorite (n=37). Electron microprobe analyses were performed at the Central Science Laboratory (CSL), University of Tasmania.

2) Hydrous mineral identification (e.g. kaolinite, montmorillonite, illite etc.) and alteration mineral mapping in the study area was undertaken using a Portable Infrared Multispectral Analyser (PIMA). This instrument is capable of measuring the spectral reflectance of rocks and minerals in the short-wavelength infrared (SWIR) portion of the electromagnetic spectrum. A total of 97 host rock and vein samples from the H zone were analysed with PIMA.

3) Whole rock and trace element analysis; major and trace-elements composition were analysed for 14 rock samples by X-ray fluorescence (XRF) spectrometry at School of Earth Sciences, University of Tasmania.

4) Isotope geochemistry; stable isotope analyse of sulphur, oxygen and carbon isotopes of ore and alteration minerals were conducted at the Central Science Laboratory, University of Tasmania. A total of 12 sulphide minerals and 17 carbonates were analysed for their stable isotope composition.

Chapter 2
Regional Geology

2.1. Introduction

Thailand is one of the largest countries of mainland of Southeast Asia, lying between latitudes 5° 37′ N, 20° 27′N and 97° 22′ E, 105° 37′ E covers an area of 518,000 km^2. It shares borders with Myanmar to the west and north, Laos to the north and northeast, Cambodia to the east and Malaysia to the south. The country is divided into four major physiographical regions (Mantajit, 1997); i.e., the mountainous highlands in the north and northwest; the central plain; the Khorat Plateau in the northeast, and the southern peninsula lying between the Andaman Sea and the Gulf of Thailand. Rocks of Thailand range in age from Precambrian to Quaternary.

2.2. Tectonic Evolution of Thailand

The Shan-Thai Terrane occurs in the west of Thailand with the Indochina Terrane in the east (Figure 2.1). These terranes are joined along the Nan Suture (Bunopas, 1981). Both terranes had their origins on the northern margin of Gondwanaland during the Late Palaeozoic (Figure 2.2; Sengor, 1984; Metcalfe, 1986; Burett and Stait, 1987; Burett et al., 1990).

The Shan-Thai Terrane underlies eastern Myanmar, western Thailand, western peninsular Malaysia, and northern Sumatra and comprises a basement of Precambrian granitoids and high-grade metamorphic rocks, overlain by sedimentary and metamorphic sequences of Palaeozoic, Mesozoic, and Cenozoic ages. The Shan-Thai Terrane has been derived from northwest Australian Gondwanaland (Metcalfe, 1984, 1986, 1988, 1990; Gatinsky et al., 1984). It separated from Gondwanaland causing formation of the Palaeo-Tethys (Bunopas, 1981, 1992). Burrett et al. (1990) suggested that the Shan-Thai Terrane must have remained attached to or close to Australia until the Carboniferous to Early Permian, based on Palaeontology data.

The Indochina Terrane comprises eastern Thailand, Laos, Cambodia and parts of Vietnam. This terrane comprises mainly Middle Palaeozoic rocks and Permian platform carbonates and deep-water clastic rocks (Wielchowsky and Young, 1985). These rocks were intruded by Carboniferous to Cretaceous granites of the Loei Fold Belt and covered by gently folded Mesozoic continental sedimentary sequences of the Khorat

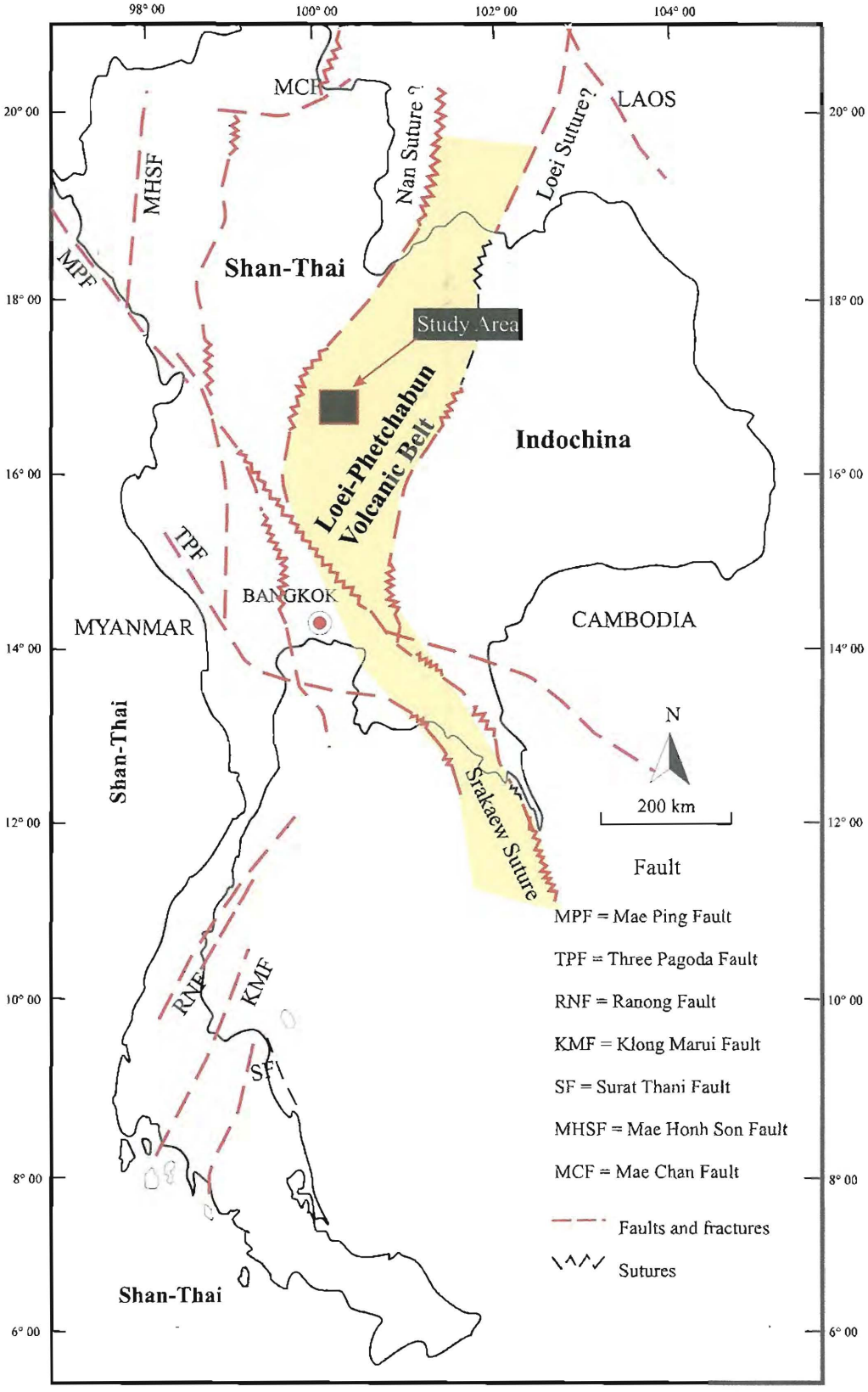

Figure 2.1 Map of Thailand showing two terranes (Shan-Thai and Indochina Terranes), major sutures and fault systems (modified after Charusiri et al., 2002).

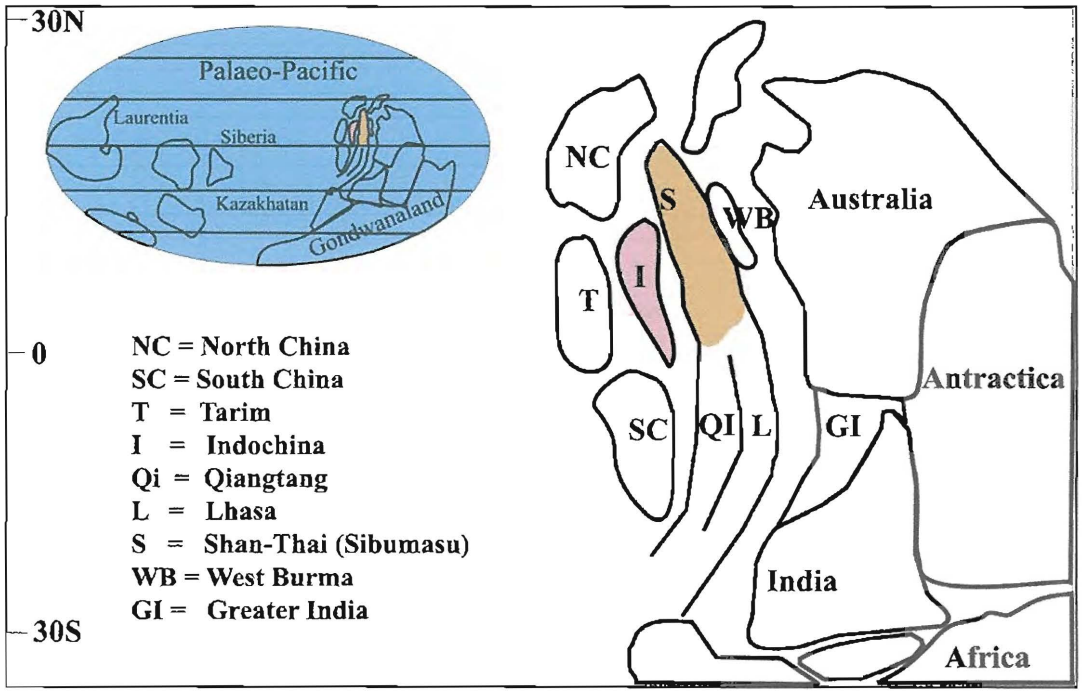

Figure 2.2 Palalaeoeo-geographical distribution of eastern Gondwanaland for the Cambro-Ordovician showing the postulated positions of the East and Southeast Asian Terranes (modified after Metcalfe, 1996).

Group. Based on an unconformity of Late Devonian-Early Carboniferous age, the Indochina Terrane rifted away from Gondwanaland in the middle to late Palaeozoic (Bunopas, 1981, 2002; Metcalfe, 1990).

The boundary of the Shan-Thai and Indochina Terranes is represented by the Nan Suture (Figure 2.1; Barr and McDonald, 1987; Barr and James, 1990). It has been an area of repeated orogenic movement since the Palaeozoic and most workers consider it to be the product of a Late Triassic continental collision (e.g. Chaodumrong, 1992).

The Shan-Thai Terrane began to collide with the Indochina Terrane during the Late Permian and was largely completed by the Late Triassic (Bunopas, 1981; Chaodumrong, 1992). After the collision, the Shan-Thai Terrane was a relatively stable landmass with only mild orogenic movement during the Middle Jurassic (Meesook et al., 1994).

During the Cenozoic, most of the tectonic features in Thailand formed in association with the India-Eurasia collision (Molnar and Tapponier, 1975; Tapponier et al., 1986). Several strike-slip faults were activated as the Indian Plate moved northward against the Eurasian Plate (Intasopa, 1993). The Southeast Asian crustal block was rotated clockwise and then underwent several hundreds kilometres of southeast-

northwest directed extension (Achache et al., 1983; Lin and Watts, 1988). During extension, a series of basins extending from the Gulf of Thailand to the South China Sea formed with normal block faulting beginning in the Early Oligocene, based on stratigraphic records (Harder, 1991).

2.3. Tectonic Evolution of the Loei-Phetchabun Volcanic Belt

The Chatree deposit lies within the Loei-Phetchabun Volcanic Belt in which volcanic rocks extend from northern Laos through central Thailand to Ko Chang Island (Figure 2.3). Quaternary alluvium occurs on the Loei-Phetchabun Volcanic Belt, making it difficult to establish stratigraphic and intrusive relationships. Volcanic rocks along the Loei-Phetchabun Volcanic Belt formed in several stages from Late Devonian and extending to the late Tertiary, with features indicating a diverse range of tectonic settings (Intasopa, 1993).

2.3.1. Late Devonian-Early Carboniferous rocks

Rhyolitic and basaltic rocks formed during the older magmatic episode, at a spreading centre in the ocean basin between the Shan-Thai and Indochina cratonic blocks (Figure 2.4; Intasopa, 1993). Ocean-floor spreading resulted in westward subduction beneath the eastern margin of Shan-Thai. During the Late Devonian to Early Carboniferous, ocean floor volcanism and subduction were related to the evolution of the Late Carboniferous Chiang Rai belt and Chiang Mai back arc basin rift on the western margin of Shan-Thai (Barr et al., 1990).

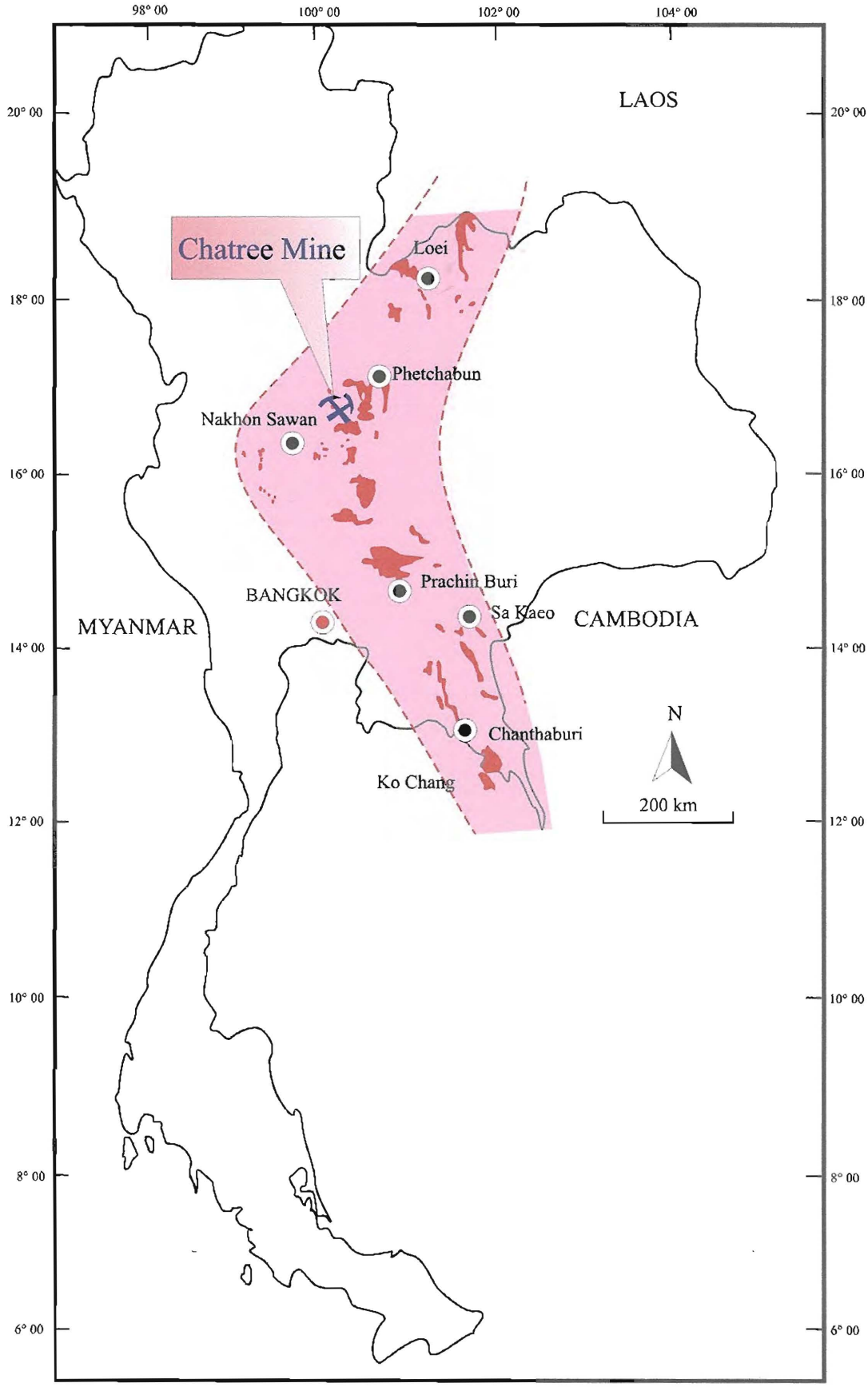

Figure 2.3 Map of Thailand showing distribution of volcanic rocks along Loei-Phetchabun Volcanic belt (modified after Jungyusuk and Khosotanont, 1992).

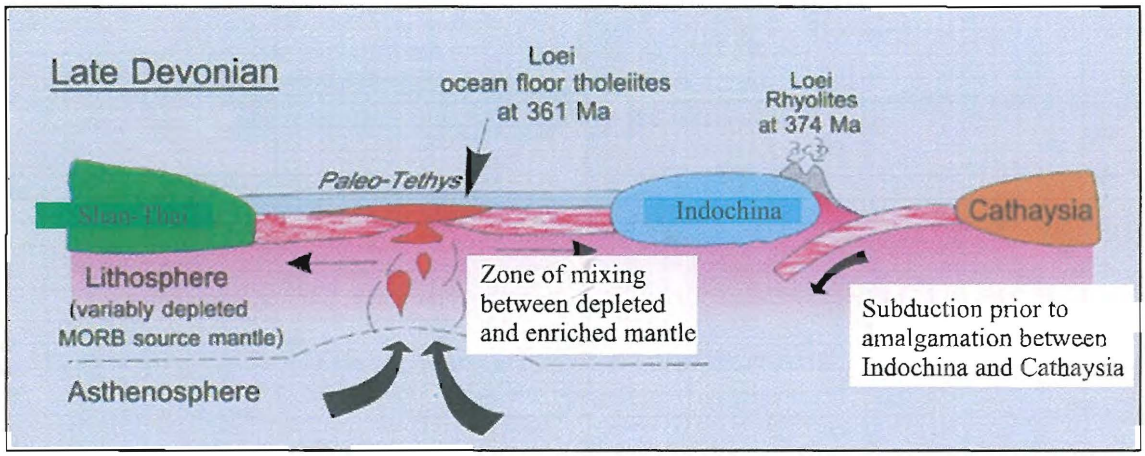

Figure 2.4. Speculative tectonic models for the evolution of the volcanic-plutonic rocks along the Loei Volcanic Belt in Late Devonian (modified after DMR, 1999 this figure was originally presented in Intasopa's unpublished thesis, 1993).

2.3.2. Permo-Triassic rocks

Permo-Triassic volcanic-plutonic rocks consist of andesite, basaltic andesite and basalt with associated diorite and granite. The association of diorite and granite led Bunopas (1981) to suggest that the Permo-Triassic rocks along the Loei volcanic-plutonic belt are related to subduction (Figure 2.5).

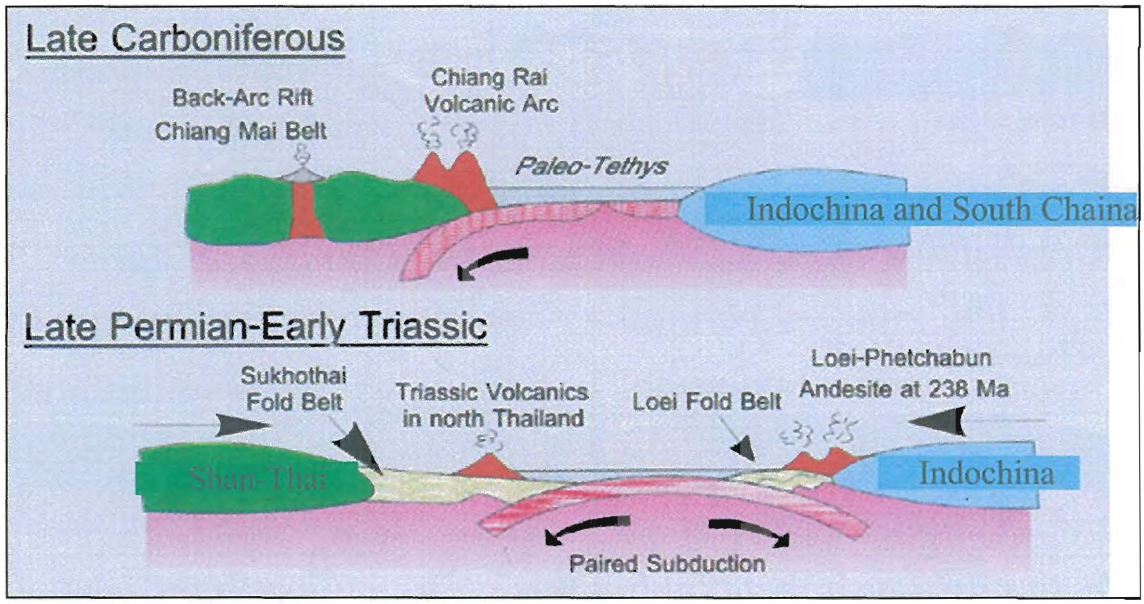

Figure 2.5. Speculative tectonic models for the evolution of the volcanic-plutonic rocks along the Loei Volcanic Belt during the Permo-Triassic (modified after DMR, 1999 this figure was originally presented in Intasopa's unpublished thesis, 1993).

2.3.3. Tertiary rocks

Tertiary volcanism produced mildly alkaline olivine tholeiitic basalt, trachyandesite, dacite and rhyolite (Intasopa, 1993). Basaltic and silicic volcanic rocks have close spatial and temporal associations.

Cenozoic tectonic activity in Southeast Asia is generally regarded as the consequence of the collision between the Indian and Eurasia plates (e.g., Molnar and Tapponnier, 1975; Tapponnier et al., 1986; Dewey et al., 1988, 1989; Hutchison, 1989). The north of the Indian continent collided with Southeast Asia at approximately 65 Ma (Songpope et al., 1991).

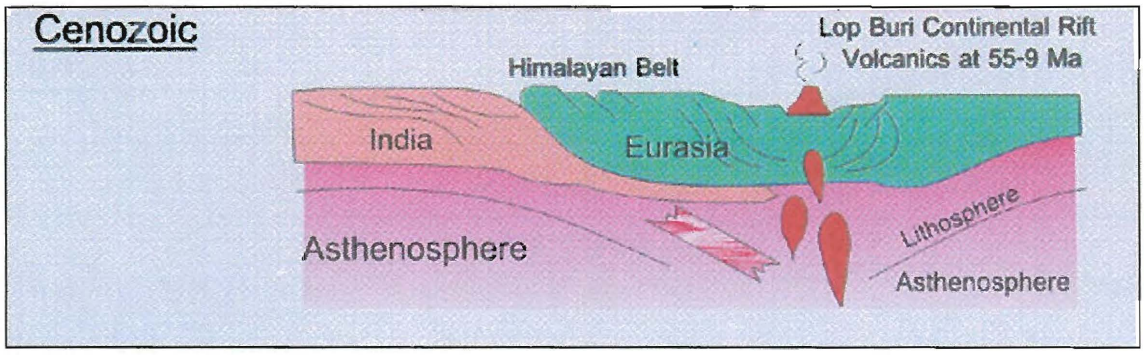

Figure 2.6. Speculative tectonic models for the evolution of the volcanic-plutonic rocks along the Loei Volcanic Belt during the Tertiary (DMR, 1999 this figure was originally presented in Intasopa's unpublished thesis, 1993).

2.4. Geochronology of the Loei-Phetchabun Volcanic Belt

The geochronological data of Charusiri (1989), Intasopa (1993) and Khin Zaw et al. (1999) show that the rocks of the Loei-Phetchabun Volcanic Belt are Triassic to Miocene in age (Figures 2.7 and 2.8). By using $^{40}Ar/^{39}Ar$ and Rb/Sr geochronological data, Intasopa (1993) suggested that there are three magmatic episodes along the belt (Figure 2.8), including;

- 373-361 Ma,
- 225-275 Ma,
- 9-57 Ma.

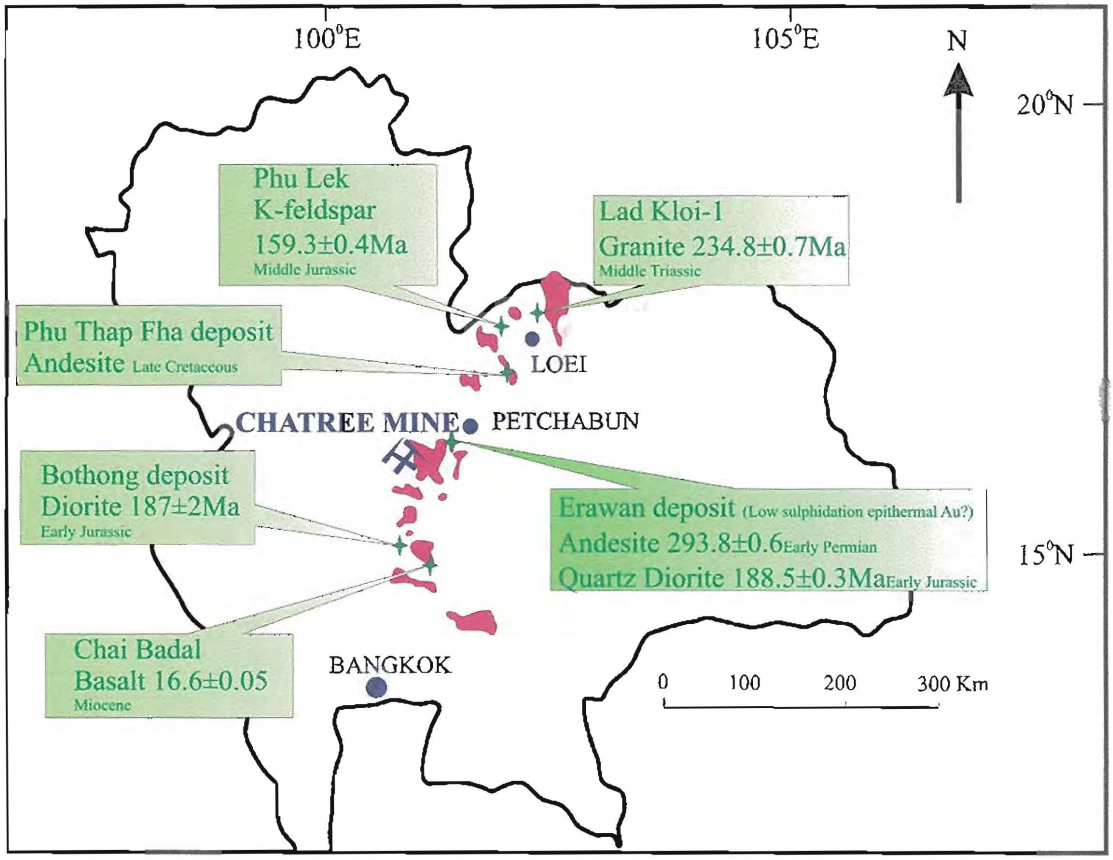

Figure 2.7. Map showing laser ablation Ar-Ar geochronological data along the Loei-Phetchabun Volcanic Belt (Modified after Khin Zaw et al., 1999).

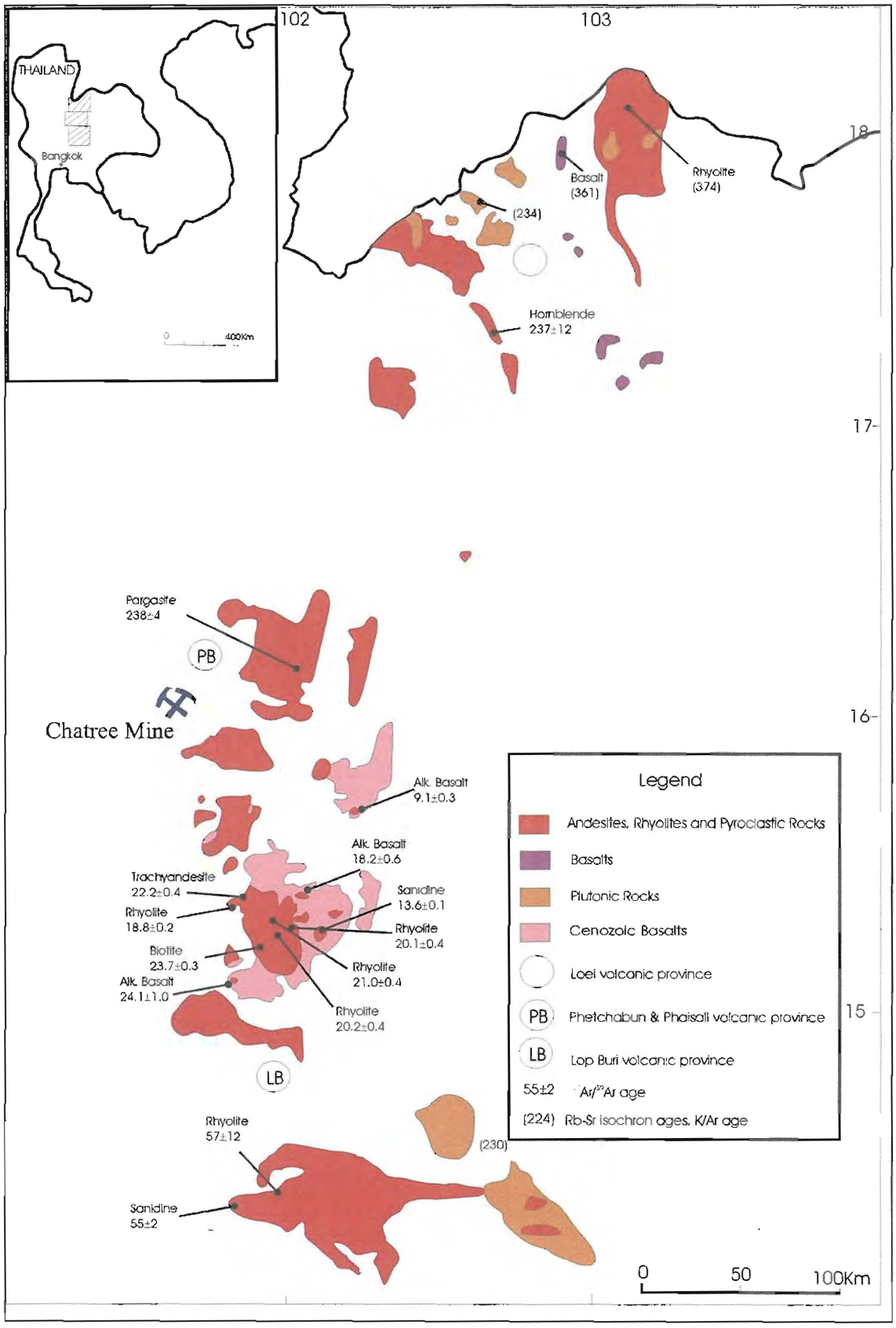

Figure 2.8. Ages of volcanic rock along the Loei-Phetchabun Volcanic Belt (after Intasopa, 1993).

Chapter 3
Local Geology

3.1. Introduction

This chapter documents the district scale geology of Chon Daen-Thap Klo area, the geology of H zone, and the other Chatree ore zones (A, D and C zones). It contains petrographic descriptions of rocks in the area, which consist of an andesitic volcaniclastic succession and related intrusive rocks. Late dykes crosscut the volcanic stratigraphy and sub-volcanic intrusions. Whole rock geochemistry is used to classify the rock types and interpret the tectonic setting. The geology of the H zone is based on observations made during pit mapping and drill core logging in selected cross-sections (section 6100N, 6200N and 6350N). It integrates data from Akara Mining Company.

3.2. General Geology of the Chon Daen-Thap Klo Area

The following description of the geology of the Chon Daen-Thap Klo District, which encompasses the Chatree deposit, is largely based on a mineral exploration report of the Chon Daen-Thap Klo area, Phetchabun, Phichit and Phitsanulok Provinces by the Department of Mineral Resources of Thailand (DMR, 1994) and the author's own field investigation.

3.2.1. Stratigraphy of the Chon Daen-Thap Klo Area

The Chon Daen-Thap Klo area within the Loei-Petchabun Volcanic Belt is underlain by both sedimentary and igneous rocks ranging in age from Carboniferous to Quaternary. The stratigraphy can be divided into three main groups: sedimentary rocks, igneous rocks and unconsolidated sediments (Figure 3.1).

A. Sedimentary rocks

a) Carboniferous Unit (C): The Carboniferous package consists mainly of limestone containing crinoid and coral fossils that are Lower to Mid-Carboniferous in age (DMR, 1994). Adjacent to dykes, the limestone has undergone contact metamorphism forming marbles.

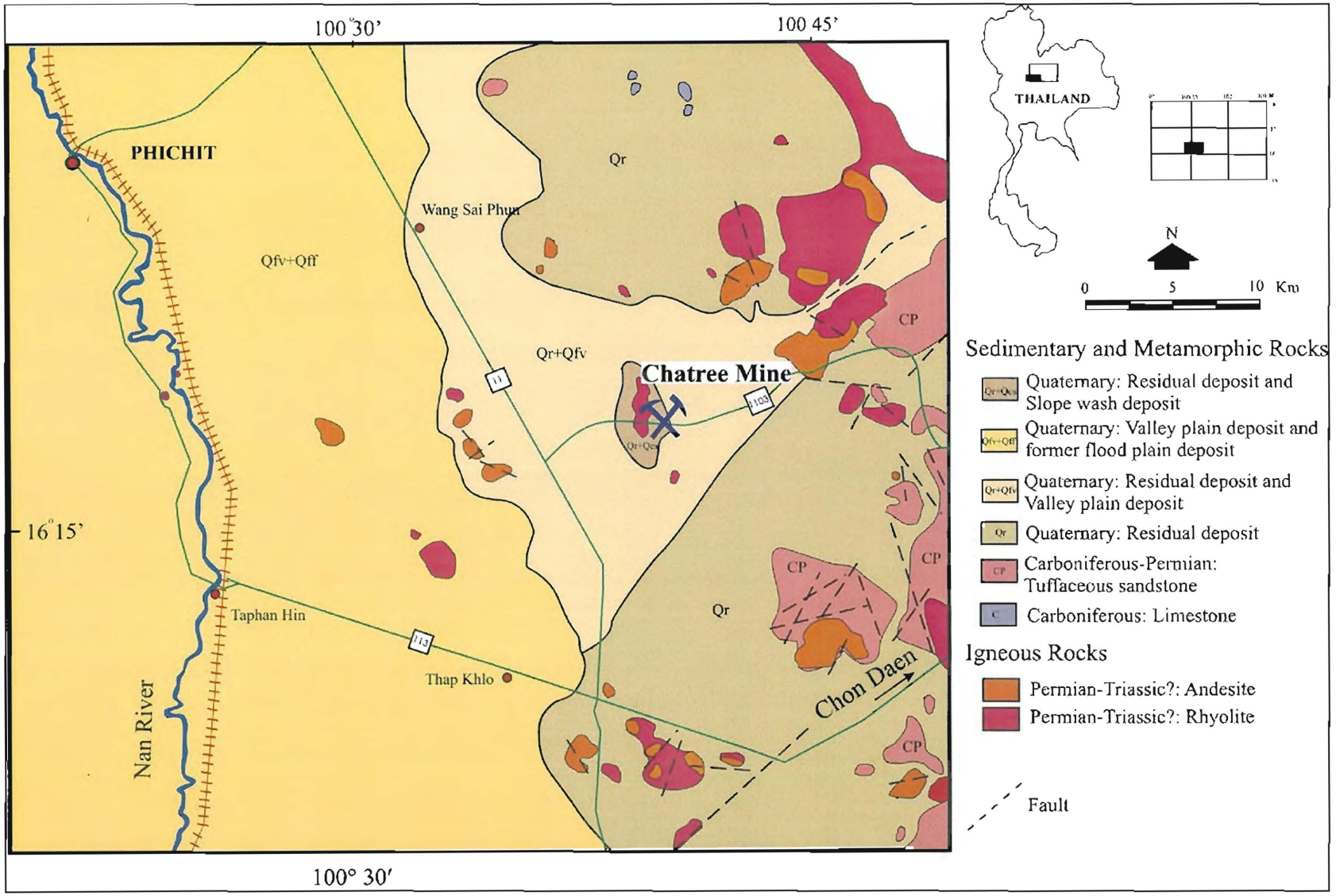

Figure 3.1. Geology of the Chon Daen-Tap Klo area (modified after DMR, 1994).

b) Upper Carboniferous-Permian Unit (CP): This formation conformably overlies the Carboniferous unit. It consists of sandstone (in part volcanic derived), shale, conglomerate and chert. Generally, this formation strikes NE-SW and dips SE. The rocks are locally metamorphosed along the contact with granodiorite.

B. Igneous rocks

Volcanic to sub-volcanic and deeper level plutonic igneous rocks occur in the area.

1) Volcanic rocks: Volcanic rocks with mafic to felsic compositions occur as lava flows, pyroclastic deposits, and dykes and sills. The volcanic rocks are predominantly andesite, andesitic tuff, basaltic andesite, andesitic breccia, rhyolite and rhyolitic tuffaceous rocks. Their ages range from Middle-Upper Permian to Lower Jurassic (Jungyusuk and Khosithanont, 1992).

2) Plutonic rocks: Plutonic rocks are covered by unconsolidated sediment, however, airborne magnetics indicate that dykes and stocks of granite and granodiorite intrude in the area such as in the southern part of the Chatree deposit. Stratigraphic relations constrain the age of these plutonic rocks to a minimum Triassic age (DMR, 1994).

C. Unconsolidated sediments

These cover approximately 80% of the Chon Daen-Thap Klo area, and are divided into five Groups (Figure 3.1; Wongsomsuk, 1989). These are: slope wash deposits (Qcs), valley plain deposits (Qfv), braided plain deposits (Qfr), former flood plain deposits (Qff) and residual deposits (Qr).

3.3. Age of Host Rocks

No geochronological work has been undertaken on the host rocks at the Chatree deposit, but quartz diorite, andesitic volcaniclastics and breccia veins of the same units at the Erawan prospect northeast of the Chatree deposit (see Figure 1.7 in Chapter 1) were dated using laser $^{40}Ar/^{39}Ar$ method (Khin Zaw et al., 1999). The Erawan prospect is a gold-rich vein system similar to that found at Chatree (Khin Zaw et al., 1999). K-feldspar from the quartz diorite gives an age of 188.5 ± 0.3 (Early Jurassic). The age of andesitic volcaniclastic groundmass is 293.8 ± 0.6 Ma (Early Permian). A breccia vein yielded an age of 206.1 ± 0.3 Ma (Late Triassic – Early Jurassic).

3.4. Geology of H Zone

The H zone occupies the western side of the Chatree deposit and covers an area of 7.5 km by 2.5 km. It merges with the C zone in the northern part of the deposit (Figures 3.2). As of February, 2004, mining of the H zone has extended to bench 59, which is approximately 59 m below the surface. The sub-surface geological map of the H zone is based on pit mapping (Akara Mining Company mapping and author's field observation) of 59 m level and drill core logging. Three cross-sections of H zone, the northern (6350N), middle (6200N) and southern (6100N) of the area (Figures 3.3 to 3.6) were selected for detailed study.

Rock types at the H zone are dominantly andesitic lithic breccia, plagioclase-pyroxene-phyric andesite and crystal-lithic breccia units. Minor host rocks include limestone and quartz-rich volcanic sandstone. All units have been hydrothermally altered and cut by mineralised veins. Basaltic and andesitic-dacitic dykes cut all earlier units and veins. All rock units are overlain by laterite and alluvium.

Major NNW, NW and NE structures in the Chatree deposit are evident on air photos, landsat imagery and widely spaced regional aeromagnetic data (Figure 3.2). Major structures of most zones (the A, C and D zones) are NNW and NW but the trend of the H zone is NE (Figure 3.2). The central structure (possibly a fault zone) at the H zone strikes at 040 and dips 20° to 45° to the NE. The fault has been inferred to have normal movement in an extensional structure setting. The H zone shows a major hanging wall shear and subordinate footwall shear (Figure 3.3). The shearing has possibly originated as thrusts during compression. Diemar (1999) suggested that the major structures of the H zone show strong evidence of pre, syn and post mineralisation movement. The post mineralisation movements are interpreted to be Tertiary (Diemar, 1999) and are represented by uncemented breccias. Diemar (1999) suggested that the age of mineralisation of the Chatree is Triassic, thereby the structural movements have been active between the Upper Permian and Tertiary. The quartz veins adjacent to the footwall shear of the H zone show chlorite slickensides that suggest continual syn- and post-mineralisation fault movements. The mineralised veins of the H zone immediately below the hanging wall shear suggest that the mineralised veins do not penetrate the shear zone. Minor faults, late dykes and sills crosscut the host rock and ore veins (Figtures 3.3 to 3.6). Brecciation is widespread, with quartz-cemented breccias containing fragments of earlier formed vein quartz. The breccias vary from clast- to

matrix-supported, and clasts are generally angular to sub-rounded and comprise altered host rock and earlier brecciated vein material. Stockwork veins are also common in the wall rock.

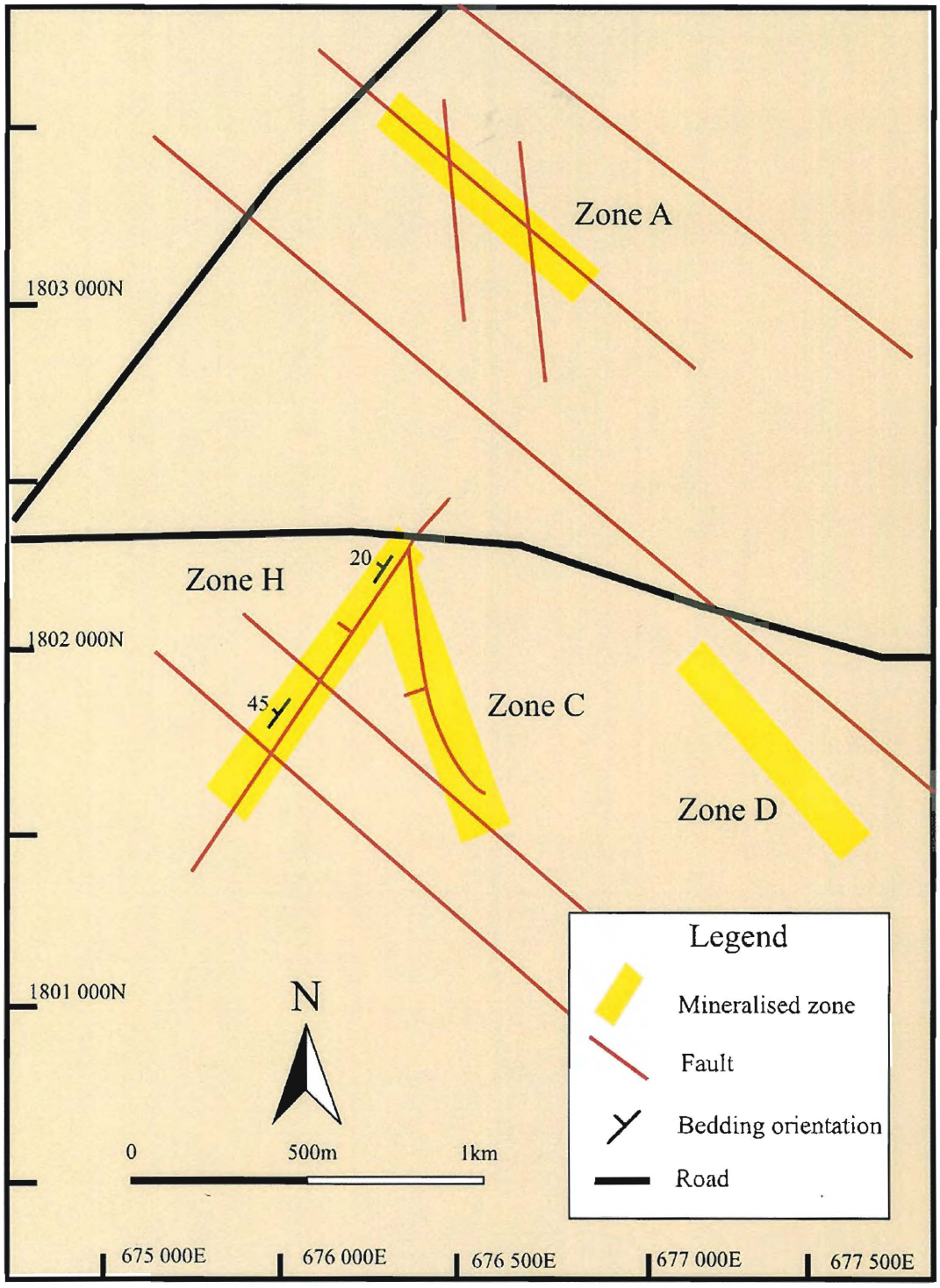

Figure 3.2. Map of the Chatree deposit showing locations of the A, C, D and H zones and major structures including, NNW, NW and NE (modified after Diemar, 1999).

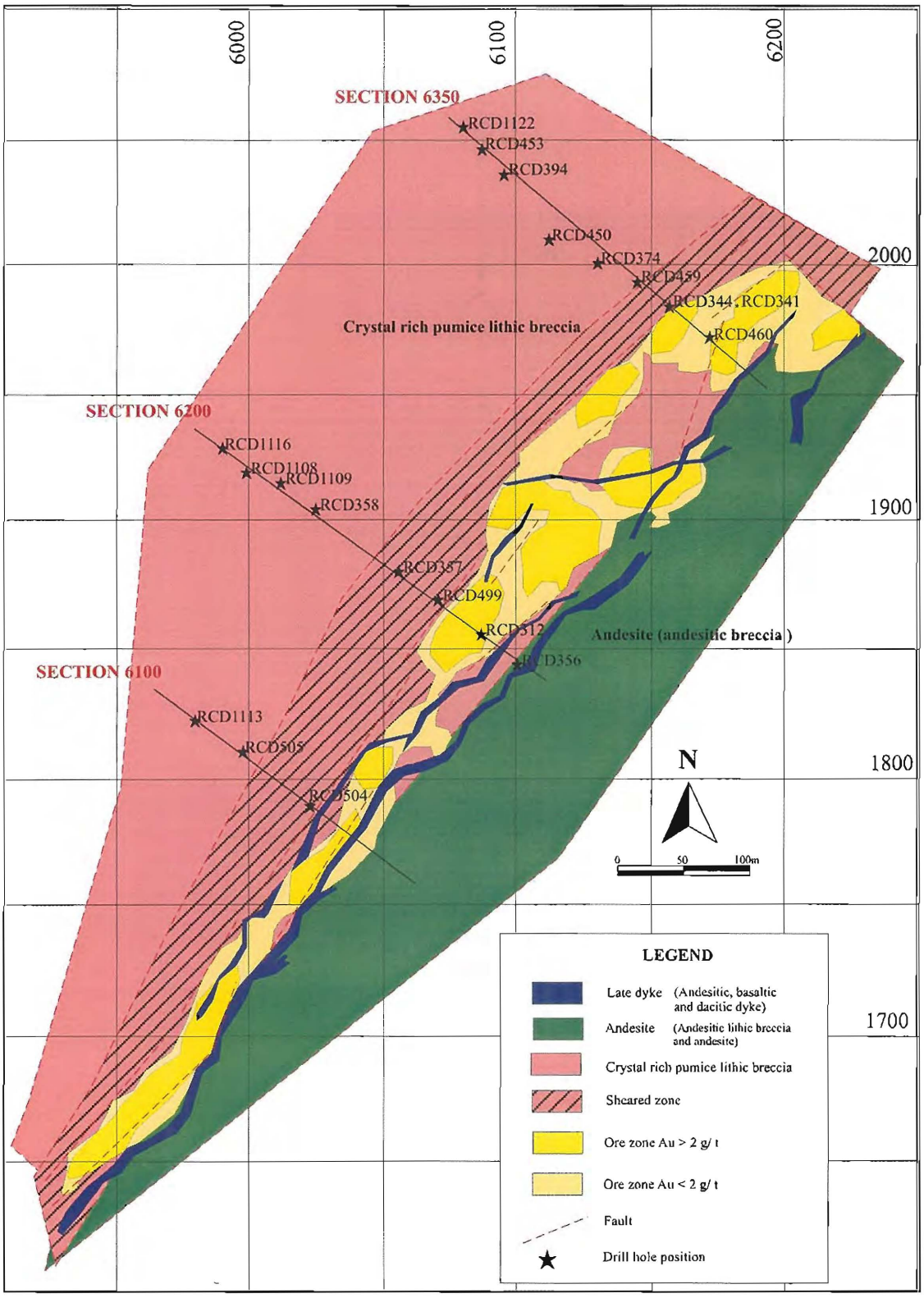

Figure 3.3. Geologic map of the H zone at the Chatree deposit with location of drill holes sampled in this study, note that the footwall shear clearly delineates the base of mineralisation.

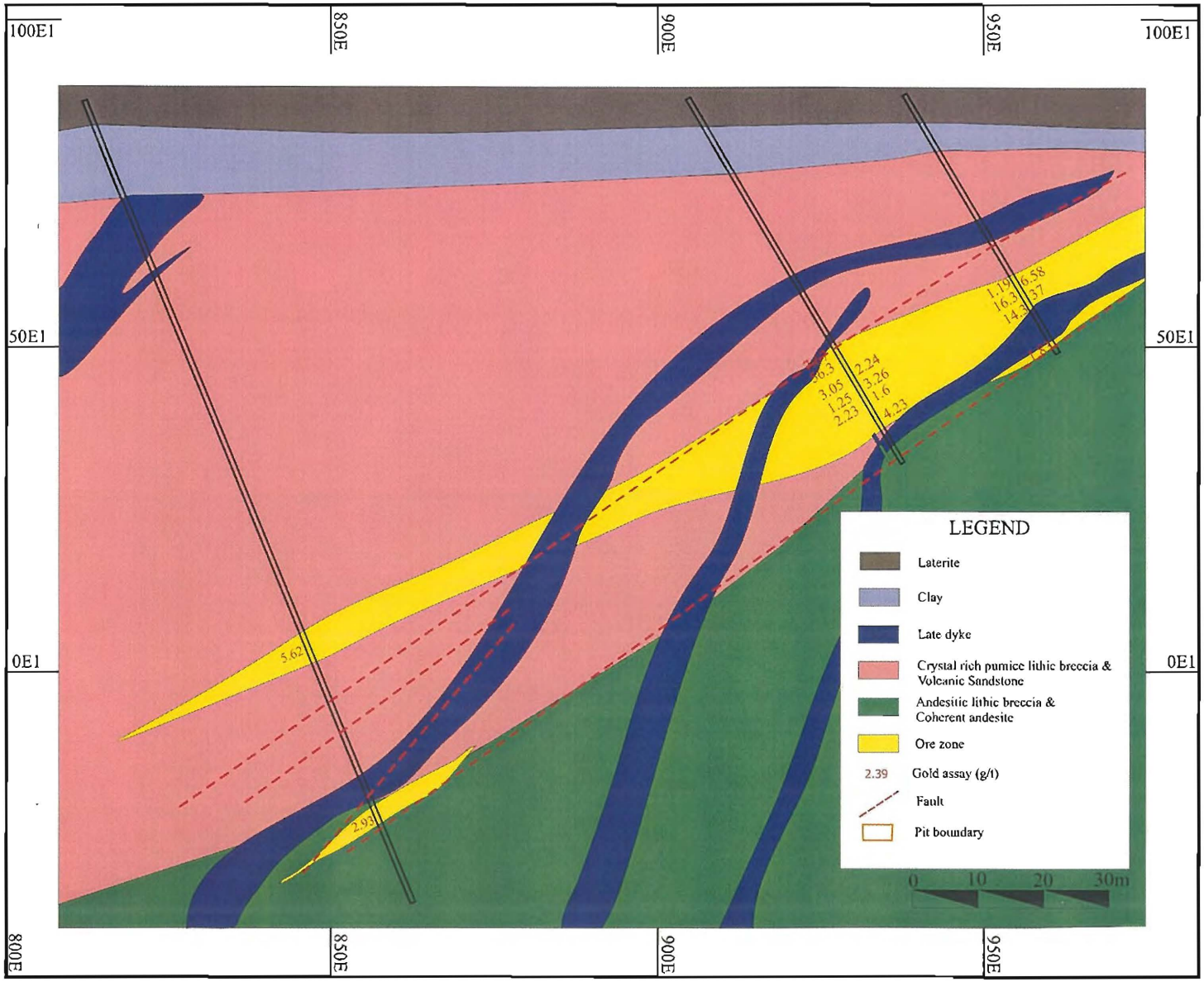

Figure 3.4. Geological cross-section of the H zone, section 6100N showing rock units and high gold grades.

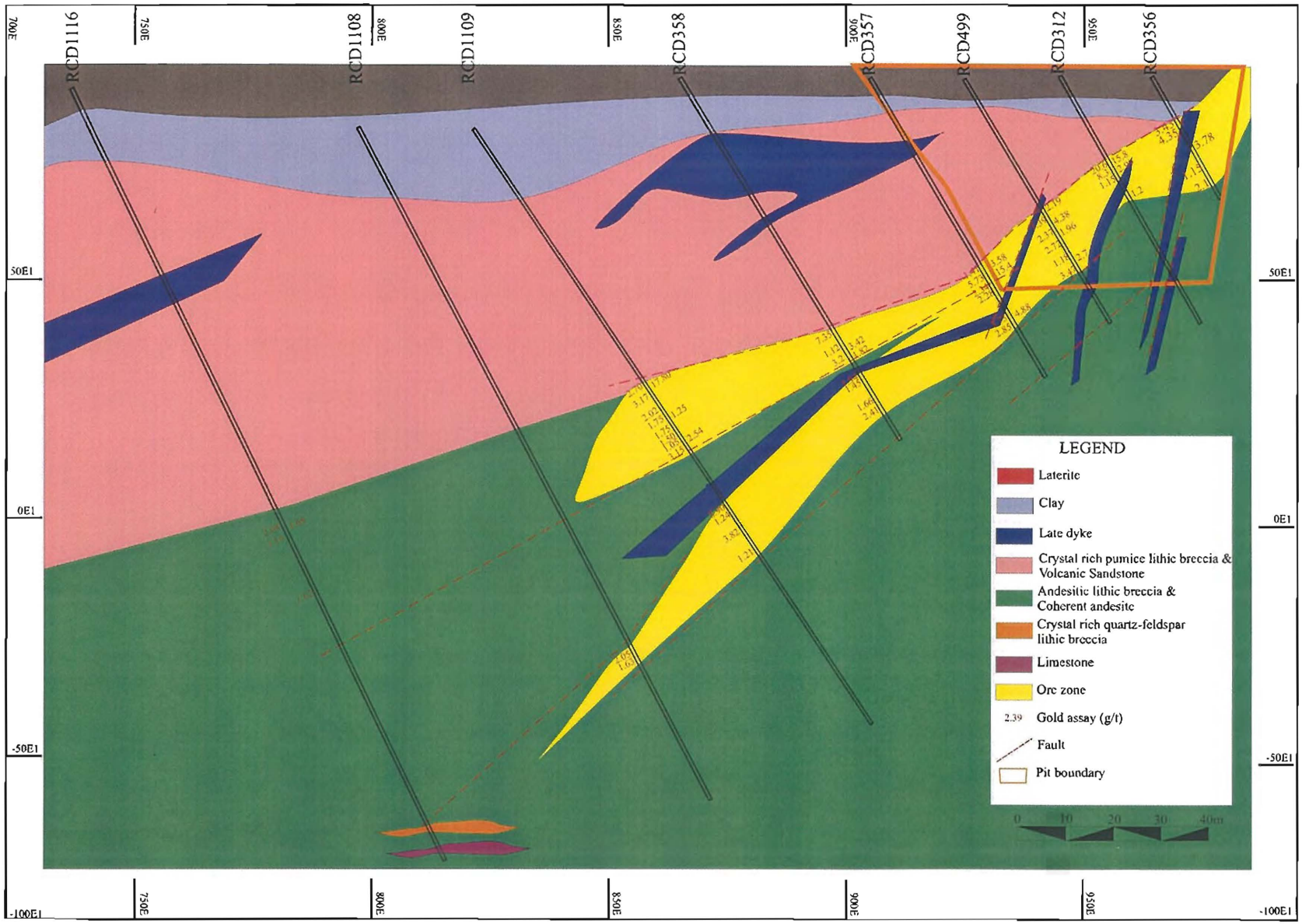

Figure 3.5. Geologic cross-section of the H zone, section 6200N showing rock units and high gold grades.

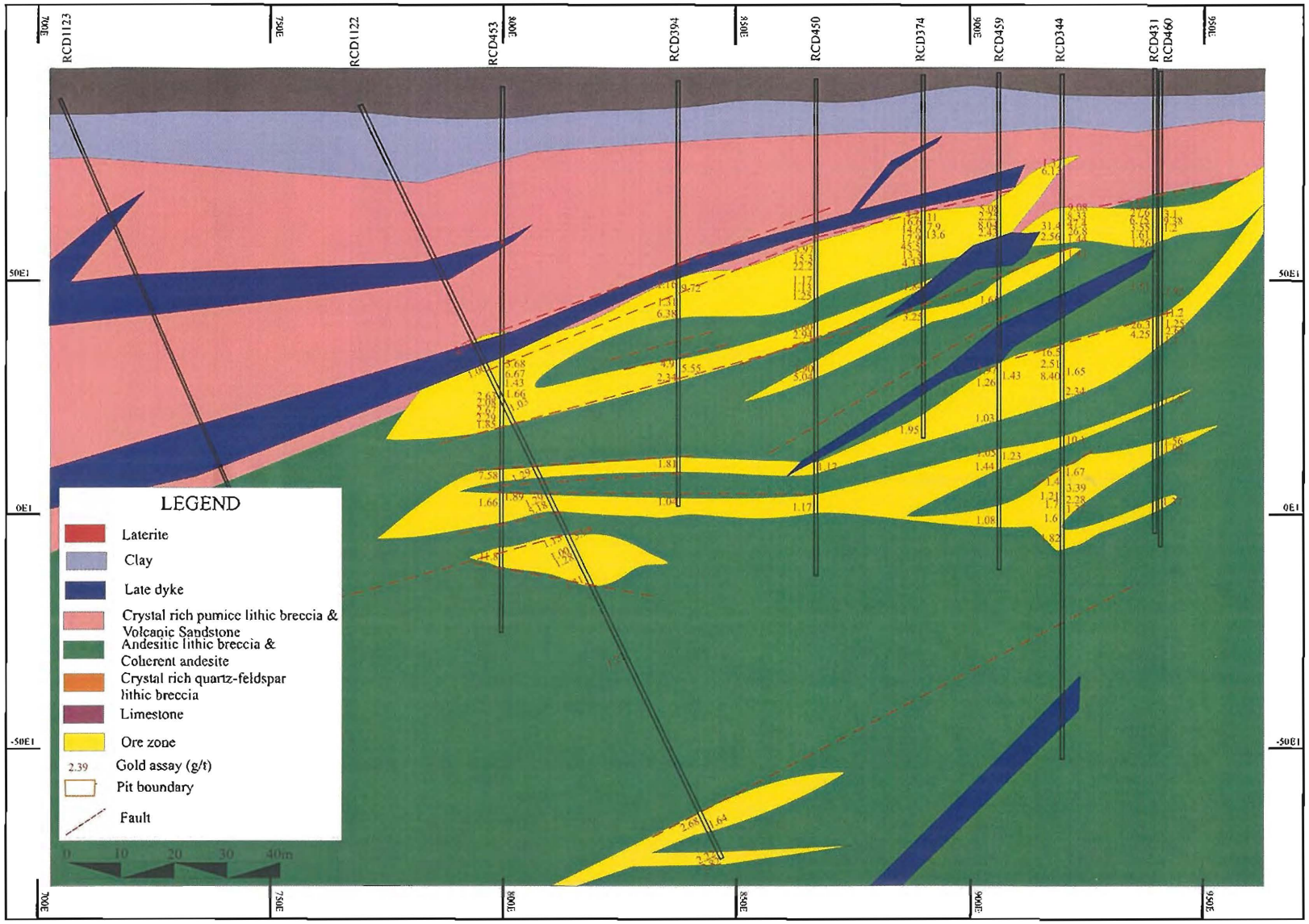

Figure 3.6. Geologic cross-section of the H zone, section 6350N showing rock units and high gold grades.

3.4.1. Host Rocks

3.4.1.1. Plagioclase-pyroxene-phyric andesite

Plagioclase-pyroxene-phyric andesite units occur as sills or dykes cutting andesitic lithic breccia and crystal-rich lithic breccia. Figure 3.7 shows the contact relationships between the two rock types. It forms most of the footwall sequence with thickness up to 20 m. The unit is medium-grey (Figure 3.8) and massive in form. Euhedral to subhedral phenocrysts of plagioclase (30-45 vol%), clinopyroxene (10 vol%) and amphibole (1-3 vol%) occur within groundmass. The plagioclase phenocrysts are tabular to blocky shapes and are partially to completely replaced by albite and/or sericite and preserved as single crystals or in clusters. Clinopyroxene has been strongly altered to chlorite (Figure 3.9). The groundmass consists of plagioclase microlite, clinopyroxene and cryptocrystalline material. The rock contains 2-3% primary magnetite, as both phenocrysts and groundmass phases.

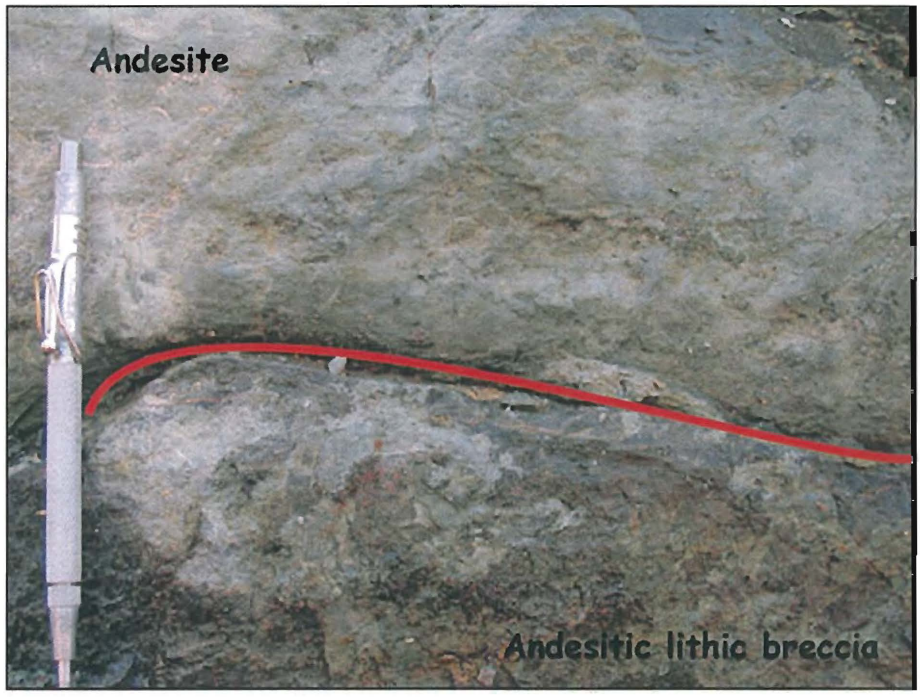

Figure 3.7. Outcrop showing contacts between andesitic lithic breccia and plagioclase-pyroxene-phyric andesite.

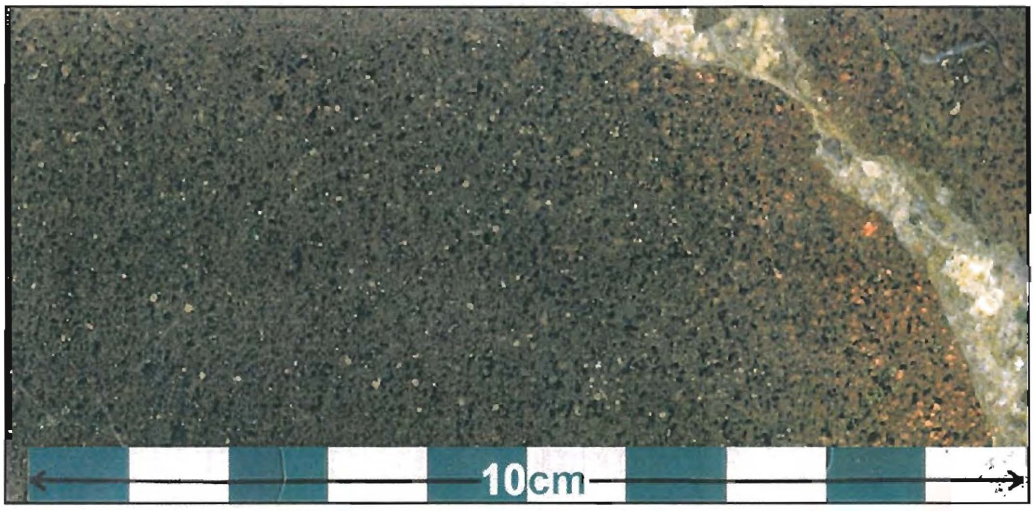

Figure 3.8. Photograph showing typical petrography of plagioclase-pyroxene-phyric andesite, Sample No. RCD 357.93, note calcite vein.

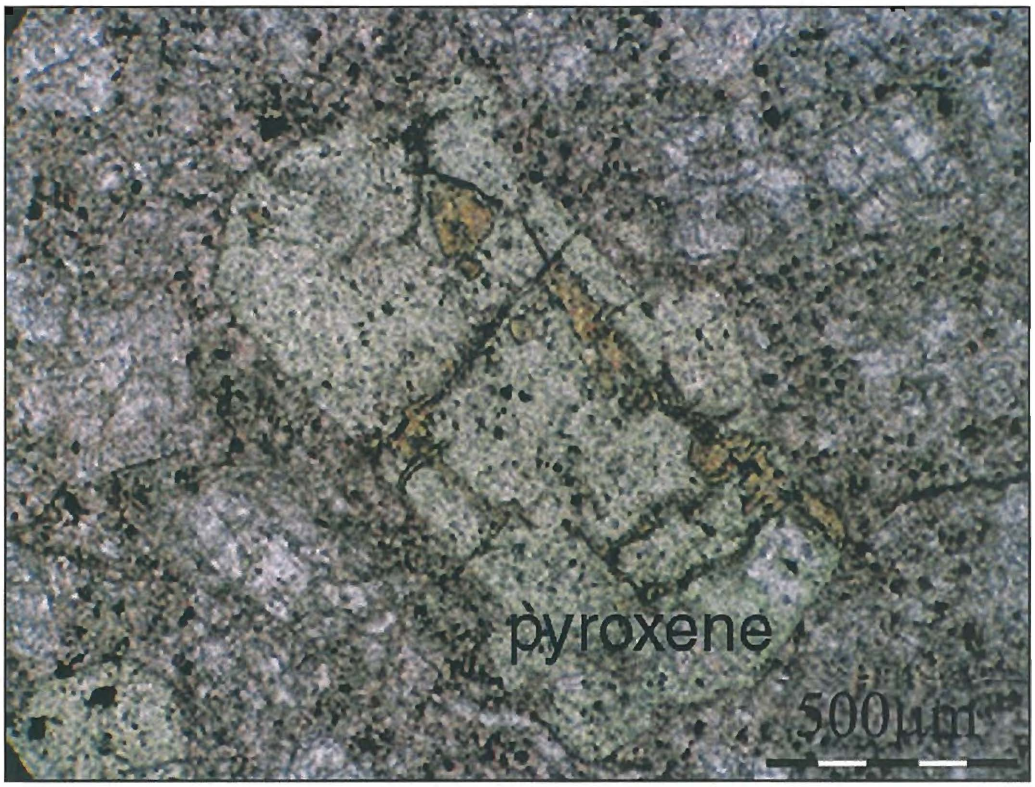

Figure 3.9. Photomicrograph showing clinopyroxene phenocryst replaced by chlorite, Sample No. RCD 341.02.

3.4.1.2. Andesitic lithic breccias

The andesitic lithic breccias occur in the footwall of the H zone, overlain by the plagioclase-phyric andesite units (Figure 3.7). This unit forms dense and resistant outcrops. The andesitic lithic breccias are typically lithic-rich, poorly sorted and clasts have a jigsaw-fit texture (Figure 3.10). The lower part of the unit typically consists of coarse clast-supported breccias with angular clasts. The middle part of the unit typically consists of matrix-supported breccia with coarse clasts. Pebble size clasts dominant, but range up to 1 m in diameter. Breccia clasts are mainly greyish green to medium-grey and composed of porphyritic, and feldspar-pyroxene-phyric andesite. The clast population is clearly polymictic despite the effects of clast-selective alteration including K-feldspar and chlorite alteration. The breccia matrix consists of plagioclase-phyric andesite.

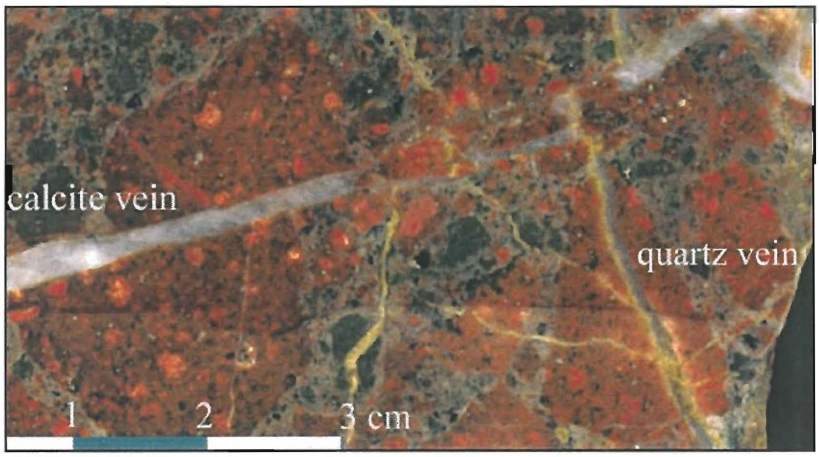

Figure 3.10. Photograph showing general character of andesitic lithic breccia, Sample No. RCD 1116.149, note poorly sorted, rounded lithic fragment; calcite and quartz veins.

3.4.1.3. Crystal-rich andesitic pumice breccia

Strongly altered and sheared crystal-rich andesitic pumice breccias mostly occur in the hanging wall of the H zone. The thickness of this sequence exceeds 30 m (from drill core logging). The contact with the underlying andesite unit and polymictic andesitic lithic breccias is not seen in the H zone, however the contact between units can be seen in the hanging wall out crop of the C zone (Figure 3.11). This unit is creamy pink to greenish grey, massive and poorly sorted, and mostly characterised by volcanic lithic breccia (Figure 3.12). The breccias consist of quartz, plagioclase, pumice clasts, pyroxene crystals and monomicitic to polymictic, andesitic volcanic lithic clasts in a plagioclase crystal-rich, very fine grained to mud matrix. The breccias are mainly

matrix-supported although locally they maybe clast-supported. The size of the clasts in the breccia sequence varies throughout the area, with a mean diameter of 0.5 cm across. Clast shape varies from angular to subrounded. The common clast types, in order of decreasing abundance, consist of: 1) quartz crystals, 2) plagioclase crystals, 3) plagioclase-phyric andesite, and 4) pumice clasts. The quartz and plagioclase crystals are euhedral to subhedral, and are commonly broken, displaying subround and subangular shapes. Most other minerals are altered, with illite, chlorite, sericite and pyrite replacing the original minerals.

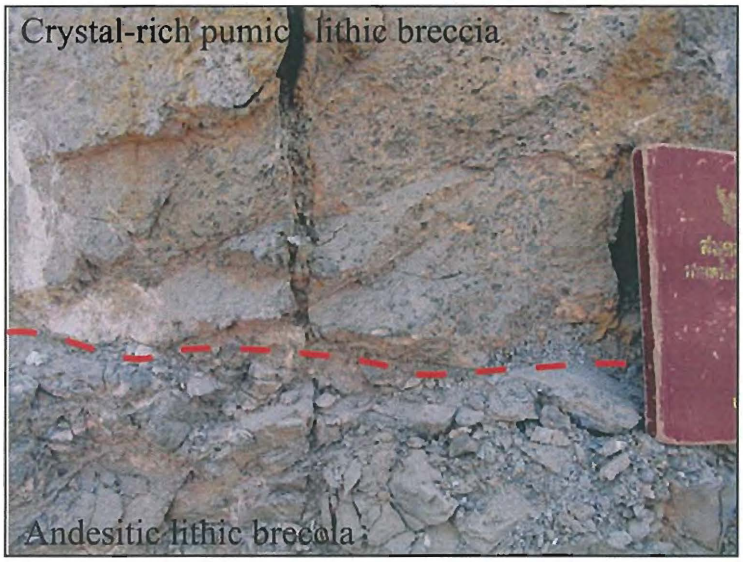

Figure 3.11. Outcrop at the C pit (footwall of the H zone) showing contacts between crystal-rich pumice lithic breccia and andesitic lithic breccia.

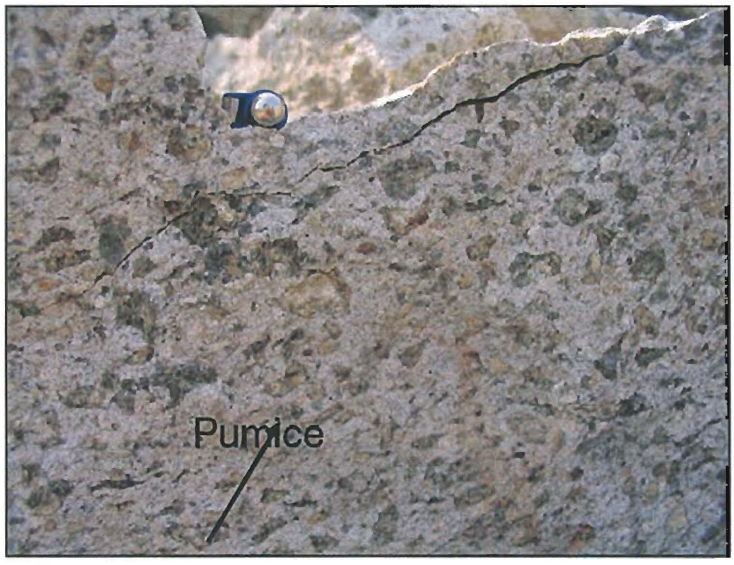

Figure 3.12. Outcrop at H pit showing texture of crystal-rich pumice lithic breccia.

3.4.1.4. Crystal rich quartz- feldspar lithic breccia

Crystal-rich quartz-feldspar lithic breccia occurs as thin lenses 30-50 cm thick. The unit is orange-grey, moderately sorted, and characterised by angular fragments (Figure 3.13). The breccia consists of felspar and quartz as major constituents with lithic clasts and mudstone fragments in a polymictic, fine sand to mud matrix. The abundance of clasts within the breccia sequence is variable, but commonly ranges up to 30 vol%. Clast shapes vary from subrounded to angular, but are typically subangular. Clast diameters are mostly 2mm across. The common clast types, in order of decreasing abundance are: 1) subangular granular polycrystalline quartz and quartz crystals, 2) tabular feldspar, 3) andesitic to basaltic clasts and 4) mudstone. Clasts of this unit are subrounded or subangular (Figure 3.14). Feldspar and lithic clasts are intensely replaced by adularia, clay minerals, hematite, chlorite and quartz. Quartz clasts have undergone less altered than feldspar and lithic clasts.

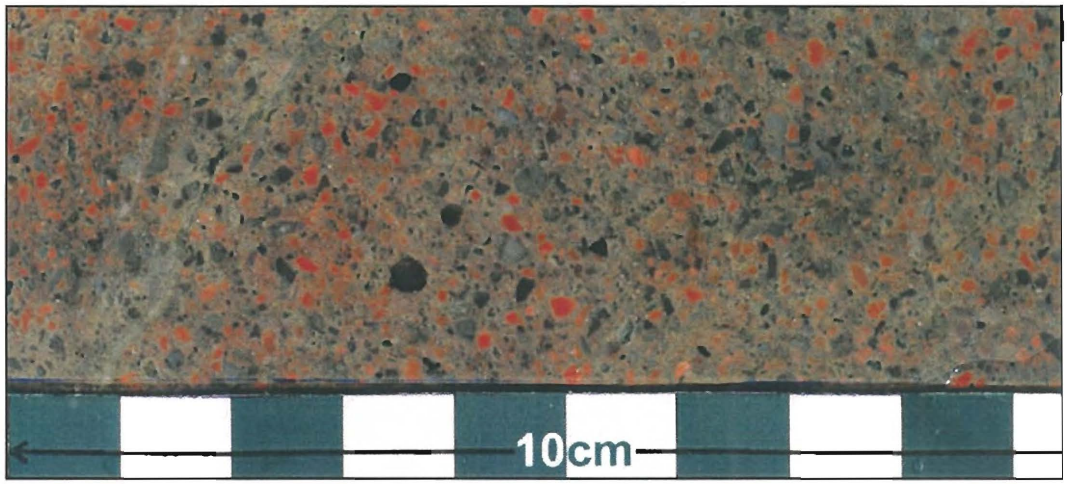

Figure 3.13. Photograph showing typical petrography of crystal-rich quartz-feldspar lithic breccia, Sample No. RCD 344.07.

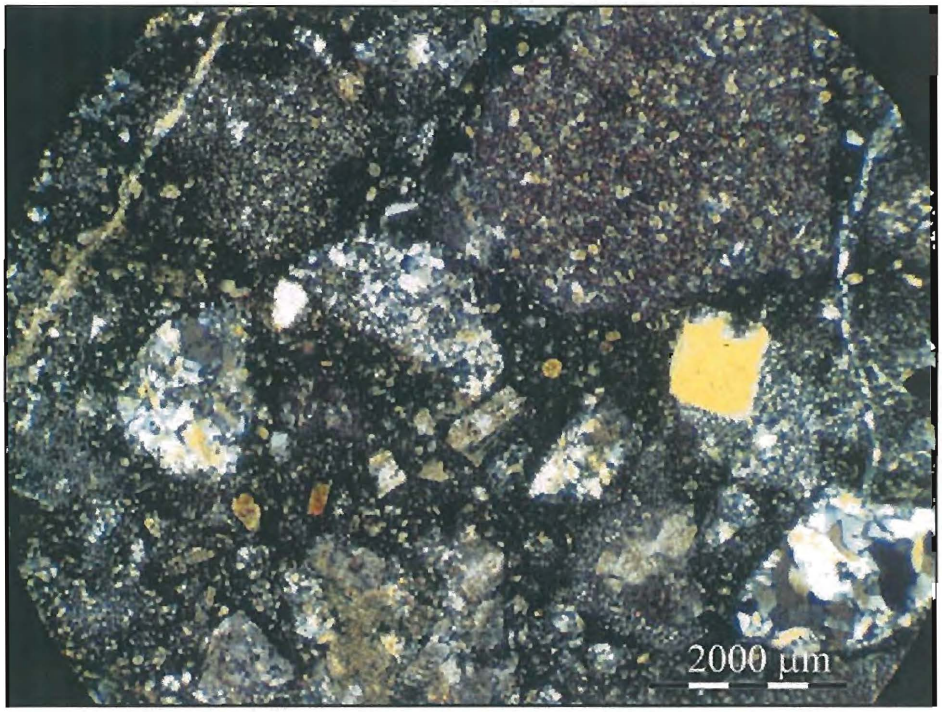

Figure 3.14. Photomicrograph showing petrography of crystal-rich quartz-feldspar lithic breccia in cross-polarised light, Sample No. RCD 344.15.

3.4.1.5. Quartz-rich volcanic sandstone/mudstone

Quartz-rich volcanic sandstone and mudstone are exposed in the upper part of the hanging wall, along with the strongly altered and sheared crystal-rich andesitic pumice breccias. The unit consists predominantly of mudstone and thin-bedded sandstone (Figure 3.15).

Typically, the grey fine-bedded sandstone shows normal grading from silt-sized particles to very coarse-grained, subrounded, 1-2 mm across grains of recrystallised quartz and minor plagioclase. Quartz and mudstone form angular to rounded fragments less than 2 mm in diameter. This unit is crystal/clast-supported with matrix of silt to clay size. Quartz crystal shapes show recrystallisation textures. Most other grains are completely replaced by chlorite, sericite and clay.

Figure 3.15. Outcrop showing bedded quartz-rich volcanic sandstone/mudstone in hanging wall at the H pit.

3.4.1.6. Limestone

Limestone is found in RCD 1116 at the depth 176.30 to 177.20 m. The limestone is dark-grey and very fine-grained and occurs as a thin lens within quartz-rich volcanic sandstone and andesitic lithic breccia. It consists of skeletal fragments such as bryozoa, mollusc and crinoid stems and minor lithic clasts and crystals (Figures 3.16 and 3.17) and is classified as wackestone. Original skeletal fragments are replaced by carbonate and the lithic clasts are replaced by K-feldspar, sericite and chlorite.

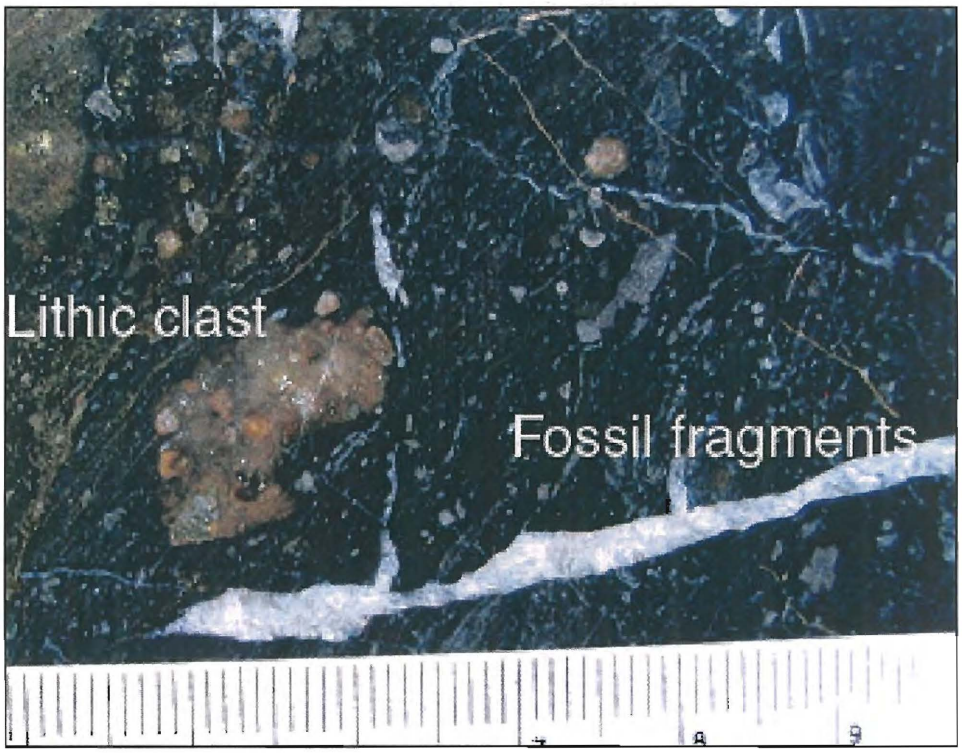

Figure 3.16. Photograph showing the limestone with lithic clasts and fossil fragments, Sample No. RCD 1116 .50, note calcite veinlets.

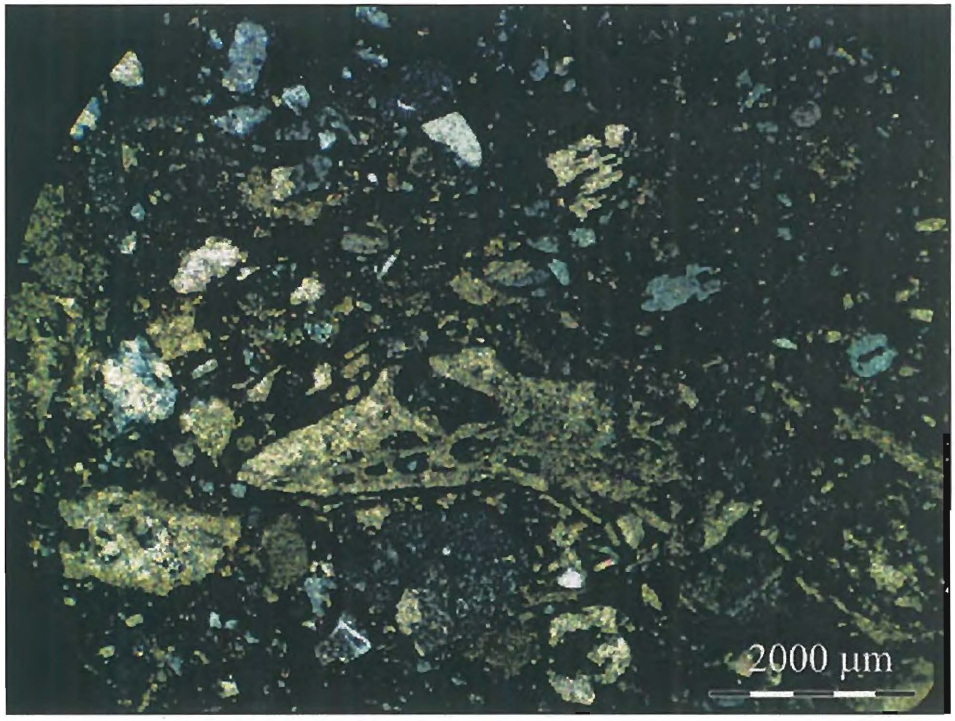

Figure 3.17. Photomicrograph showing fossils such as gastropod, crinoid and bivalve that were replaced by calcite in cross polarised light, Sample No. RCD 1116.64.

3.4.2. Intrusive rocks

Intrusive rocks mainly dykes, in the H zone cross cut the early units and most of the veins. Most are 15 cm to 3 m wide with an average of 50 cm (Figures 3.18 and 3.19). They are commonly of basaltic, andesitic and dacitic compositions and moderately magnetic.

Figure 3.18. Outcrop at H pit showing late dyke crosscutting into hanging wall.

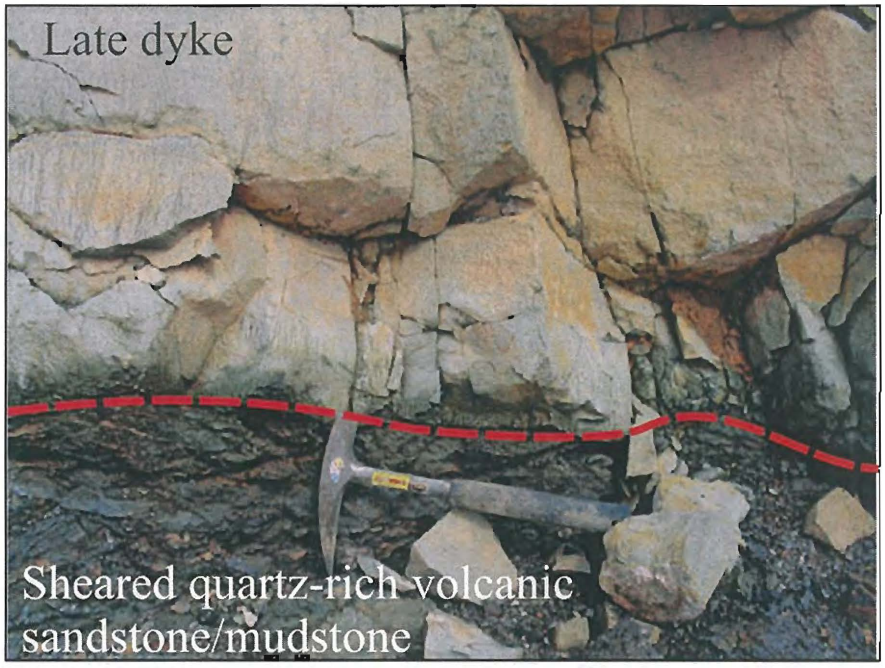

Figure 3.19. Outcrop at H pit showing contact between late dyke and sheared quartz-rich volcanic sandstone/mudstone on hanging wall.

3.4.2.1. Andesite-dacite dyke

Andesitic to dacitic sills or dykes are greenish grey and porphyritic with coarser phenocrysts and finer groundmass than the earlier units. This unit commonly consists of plagioclase phenocrysts with tabular or blocky shapes ranging from 1 to 4 mm (Figure 3.20). Some dykes or sills show andesite-dacite composition reflected in a higher modal abundance of quartz (Figure 3.21). Their groundmass is composed of plagioclase microlaths, clinopyroxene and cryptocrystalline material. Andesite-dacite dykes and sills also show amygdale textures with carbonate infill and K-felspar rims.

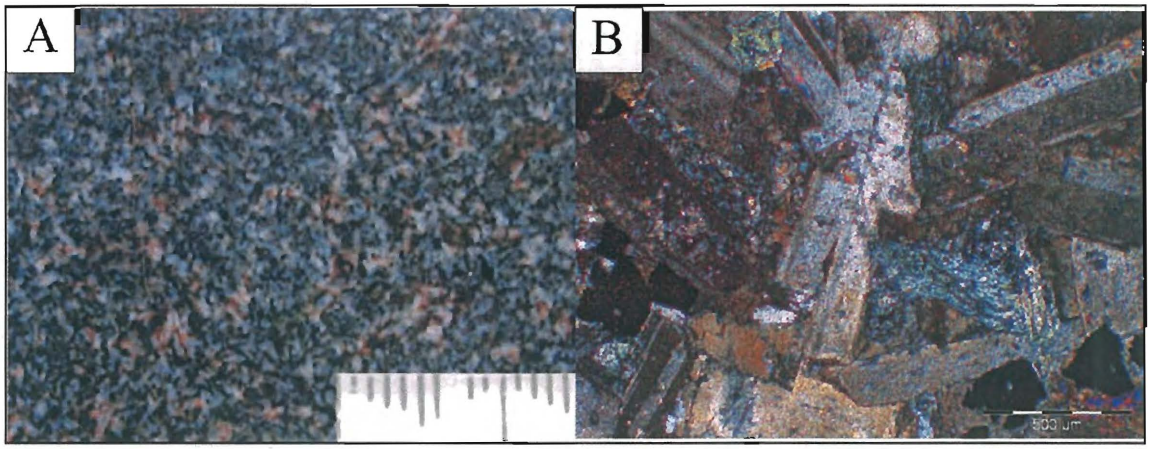

Figure 3.20. Photograph (A) and photomicrograph (B) showing characteristic petrography and texture of late andesitic dyke, Sample No. HP04. Note cross polarised light in B.

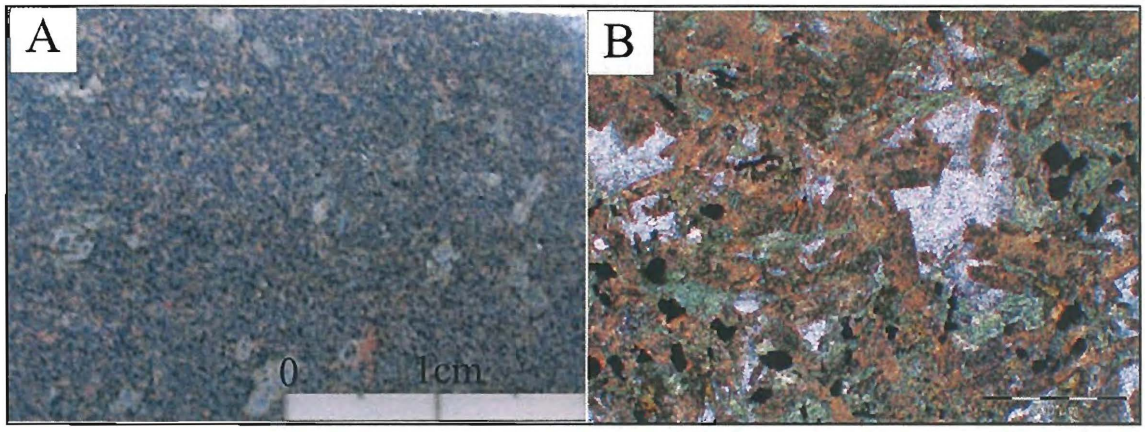

Figure 3.21. Photograph (A) and photomicrograph (B) showing characteristic petrography and texture of andesitic to dacitic late dyke, Sample No. HP08. Note cross polarised light in B.

3.4.2.2. Basalt dyke

Basalt is typically greenish grey and consists of subhedral grains of olivine with elongate plagioclase prisms and pyroxene. Plagioclase also appears to cement aggregate of olivine and pyroxene (Figure 3.22). Chlorite and other clay minerals replace olivine, plagioclase and pyroxene.

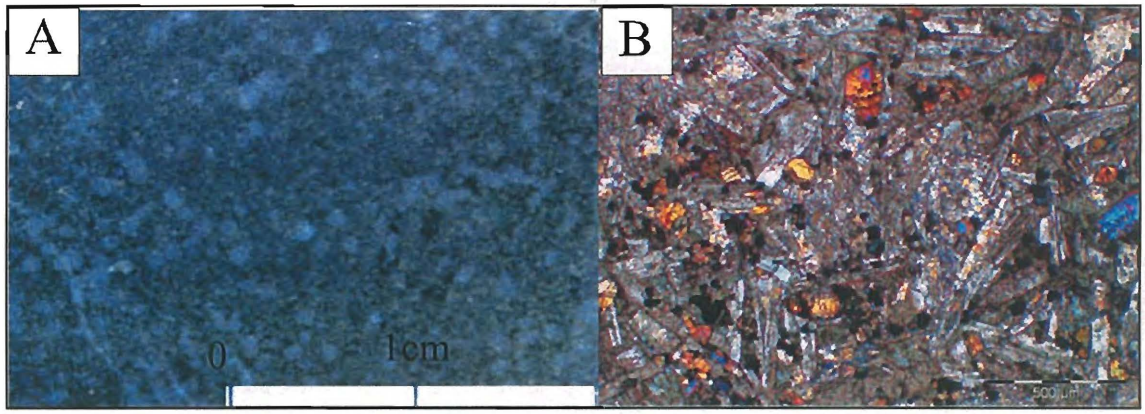

Figure 3.22. Photograph (A) and photomicrograph (B) showing characteristic petrography and texture of late basaltic dyke, Sample No. RCD 505.109. Note cross polarised light in B.

3.5. Whole rock geochemistry

Whole rock geochemistry can be used for the classification of rock types and to interpret tectonic settings (Rollinson, 1993).

3.5.1. Sampling and analytical techniques

Quantitative analyses for major and trace elements have been determined to define and distinguish different rock types. Most drill hole and outcrop samples for this study collected from the H zone have undergone significant hydrothermal alteration and most samples show significant losses on ignition (LOI).

A total of fourteen samples were crushed using a tungsten carbide ring mill and analysed for SiO_2 ,TiO_2, Al_2O_3, total Fe as FeO, MnO, MgO, CaO, Na_2O, K_2O, P_2O_5, BaO and loss in ignition (LOI) and a range of trace elements (S, Y, U, Rb, Th, Pb, As, Bi, Zn, Cu, Ni, Nb, Zr, Sr, Cr, Ba, Sc, V, La, Ce and Nd). Major and trace element compositions were determined by X-Ray Fluorescence (XRF). The chemical compositions are presented in Table 3.1.

3.5.2. Whole rock grouping

Petrographic observations suggest that rocks in the H zone can be classified into three groups. These are; 1) plagioclase-pyroxene-phyric andesite, 2) andesitic lithic breccias and crystal-rich andesitic pumice breccias, and 3) late dykes. Whole rock chemical compositions for each group are consistent with petrographic classification.

Although samples are altered, least altered samples can be used to identify the primary chemical affinities by using selected elements and element ratios.

3.5.3. Major and trace elements

The geochemical data shows LOI for all samples. Therefore re-calculation of all analyses to 100 % volatile (LOI)-free is used in this study (Table 3.1).

The classification schemes of Peccerillo and Taylor (1976) and Ewart (1982) assign rock names based on silica content (basalt <52 wt%, andesite 52-60 wt%, dacite 61-69 wt% and rhyolite >69 wt% SiO_2). Using this scheme, plagioclase-pyroxene-phyric andesite from the H zone is classified as andesite and basalt. In the second group, the breccia was also classified as andesite and dacite. The late dyke samples were classified as having andesitic compositions.

Table 3.1. Geochemical data of major and trace elements of sample, H zone, Chatree deposit, Thailand.

Sample No.	SiO_2	TiO_2	Al_2O_3	Fe_2O_3	MnO	MgO	CaO	Na_2O	K_2O	P_2O_5	BaO	Total	Loss inc S-
Plagioclase-pyroxene-phyric andesite													
RCD 341.02	53.93	0.58	18.76	10.51	0.46	5.35	4.91	1.71	3.48	0.13	0.19	100	4.39
RCD 499.10	54.17	0.73	16.86	8.82	0.29	3.46	4.79	0.10	10.33	0.29	0.17	100	6.29
RCD 394.39	53.03	0.49	18.88	8.17	0.71	5.07	4.25	1.24	7.73	0.11	0.31	100	3.87
HP 07	44.42	1.95	18.44	11.80	0.29	5.57	13.77	0.27	3.21	0.27	0.01	100	13.94
HP 09	51.54	1.06	18.59	9.52	0.21	5.44	8.22	4.19	0.92	0.25	0.06	100	5.27
Andesitic lithic breccia and crystal-rich andesitic lithic breccia													
RCD1108.70	59.22	0.61	15.72	7.24	0.35	4.27	3.38	0.45	8.39	0.23	0.14	100	4.43
F 03	72.56	0.37	9.77	4.87	0.29	1.96	4.26	0.71	4.93	0.14	0.15	100	4.3
HP 02	69.34	0.35	15.05	4.07	0.11	1.36	5.13	3.11	1.36	0.08	0.05	100	6.64
HP 06	66.51	0.50	12.00	10.10	0.46	4.16	3.28	0.03	2.75	0.17	0.05	100	6.65
HP 10	58.94	0.69	16.48	8.54	0.40	3.11	2.52	1.45	7.32	0.26	0.29	100	3.64
Late dyke													
RCD 312.102	56.78	1.54	15.70	10.14	0.18	4.41	4.88	4.37	1.55	0.42	0.03	100	6.06
RCD 505.109	51.97	1.12	18.98	9.76	0.19	5.47	8.03	3.51	0.68	0.25	0.03	100	3.76
HP 05	54.95	0.81	18.90	7.58	0.19	4.69	7.50	4.31	0.88	0.17	0.02	100	4.66
HP 11	54.97	1.55	16.46	9.77	0.19	4.26	6.99	4.02	1.35	0.42	0.02	100	3.66

Table 3.1. Geochemical data of major and trace elements of sample, H zone, Chatree deposit, Thailand (continued).

Sample No.	Y	U	Rb	Th	Pb	As	Bi	Zn	Cu	Ni	Nb	Zr	Sr	Cr	Ba	Sc	V	La	Ce	Nd
detection limit (ppm)	1	1.5	1	1.5	1.5	3	2	1	1	1	1	1	1	1	4	2	1.5	2	4	2
Plagioclase-pyroxene-phyric andesite																				
RCD 341.02	11	<1.5	68	<1.5	<1.5	<3	<2	85	216	14	1	25	247	19	1671	37	324	<2	6	3
RCD 499.10	14	<1.5	145	<1.5	3	17	<2	101	58	17	3	70	127	7	1325	28	247	7	18	7
RCD 394.39	8	<1.5	92	<1.5	2	14	<2	74	124	9	2	17	357	22	2574	30	270	<2	4	<2
HP 07	29	<1.5	56	<1.5	10	13	<2	101	62	80	5	129	71	146	110	38	267	5	11	12
HP 09	16	<1.5	12	<1.5	3	12	<2	78	34	25	3	76	535	52	482	23	233	5	17	12
Andesitic lithic breccia and crystal-rich andesitic lithic breccia																				
RCD1108.70	14	<1.5	134	<1.5	2	12	<2	75	91	12	3	63	103	10	1137	24	291	6	12	8
F 03	9	<1.5	66	<1.5	18	21	<2	86	154	8	2	36	98	14	1282	14	128	3	7	3
HP 02	18	<1.5	14	<1.5	0	<3	<2	48	15	2	3	69	105	6	380	18	63	4	11	8
HP 06	13	<1.5	56	<1.5	373	102	<2	1056	69	11	3	50	41	9	448	20	202	4	16	6
HP 10	16	<1.5	112	<1.5	2	9	<2	90	118	14	3	68	136	8	2274	24	233	7	14	4
Late dyke																				
RCD 312.102	27	<1.5	23	2	6	6	<2	99	122	22	6	196	121	34	275	28	292	13	32	21
RCD 505.109	18	<1.5	10	<1.5	4	4	<2	91	65	26	3	78	631	54	246	26	247	6	18	12
HP 05	11	<1.5	9	<1.5	2	5	<2	103	37	47	2	59	223	136	138	23	191	5	15	10
HP 11	33	<1.5	17	2	6	8	<2	116	126	29	7	213	403	40	199	25	290	19	40	25

Classification by using the total alkalis-silica diagram (TAS; Le Maitre et al., 1989) is normally intended for fresh volcanic rocks but samples from the H zone are clearly altered. Petrological study suggests that most host rocks of the H zone consist of andesitic composition with andesitic, basaltic and dacitic dykes. The TAS of host rocks that is shown in Figure 3.23 shows unusual contents of some major elements (e.g. K_2O and SiO_2). The chemical composition of the altered rocks reflects the compositional changes due to alteration. For example, enrichment of K_2O (e.g. RCD 499.10, RCD 1108.70 and RCD 394.39) is resulted from the rocks have been potassically altered; samples F 03, HP 02 and HP 06 have high SiO_2 contents that maybe resulted from silicic alteration. Despite the effects of alteration, classification using the TAS diagram shows that most samples have basaltic-andesitic composition.

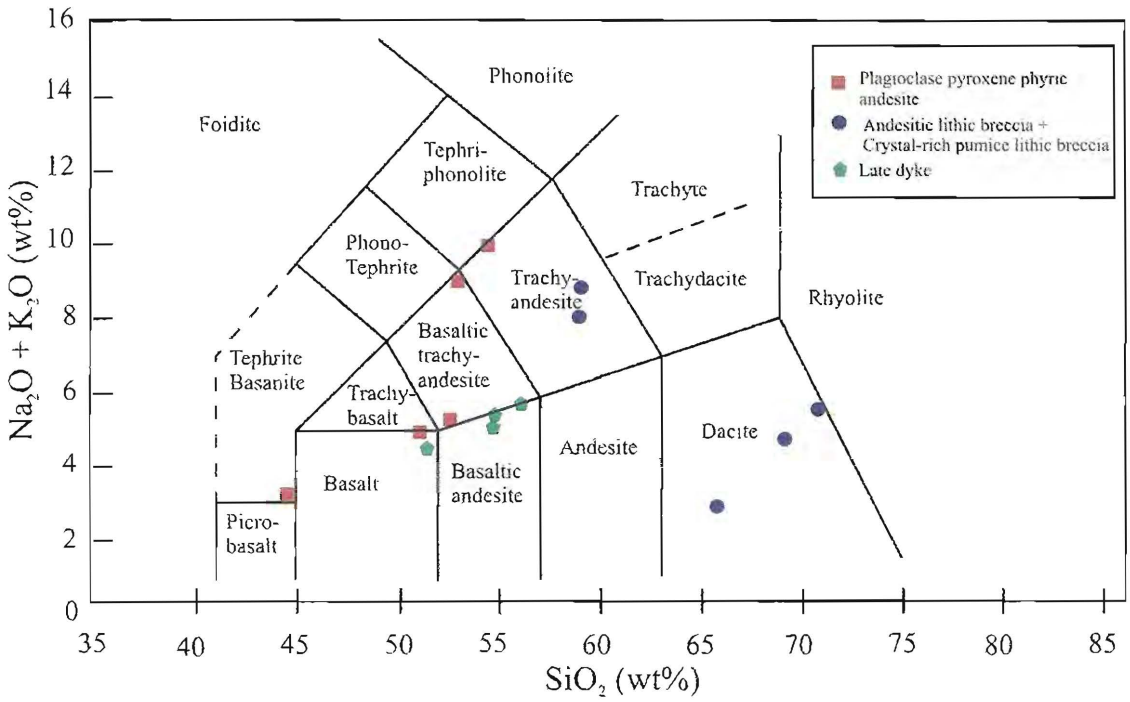

Figure 3.23. Igneous rock classification of samples from the H zone by TAS diagram of Le Maitre et al. (1989).

Geochemically altered rock can be studied by using trace element data. Trace elements are those which occur in a rock in concentrations of less than 0.1 wt% (Rollinson, 1993). Trace element studies are more capable of discriminating between petrological processes than major elements. There are mathematical models to describe trace element distributions. Therefore, studying trace elements are most applicable to processes controlled by crystal-melt or crystal-fluid equilibria.

The data are also plotted on a Zr/TiO_2 – Nb/Y diagram (Figure 3.24; Winchester and Floyd, 1977). This method is more reliable than the total alkali elements versus silica plot because each component of the plot used has been shown to be relatively immobile and therefore insensitive to modification by hydrothermal processes. Classification of the rocks using the Winchester and Floyd diagram indicated that samples from the H zone have a range of composition from andesite, andesite-basalt to subalkaline basalt. Figure 3.25 shows a revised diagram of the Zr/TiO_2 – Nb/Y classification system by Pearce (1996), using a high-quality database of modern volcanics. When plotted using the Pearce (1996) revised diagram, rocks for the H zone have a basaltic composition and only one sample has basaltic-andesitic to andesitic composition.

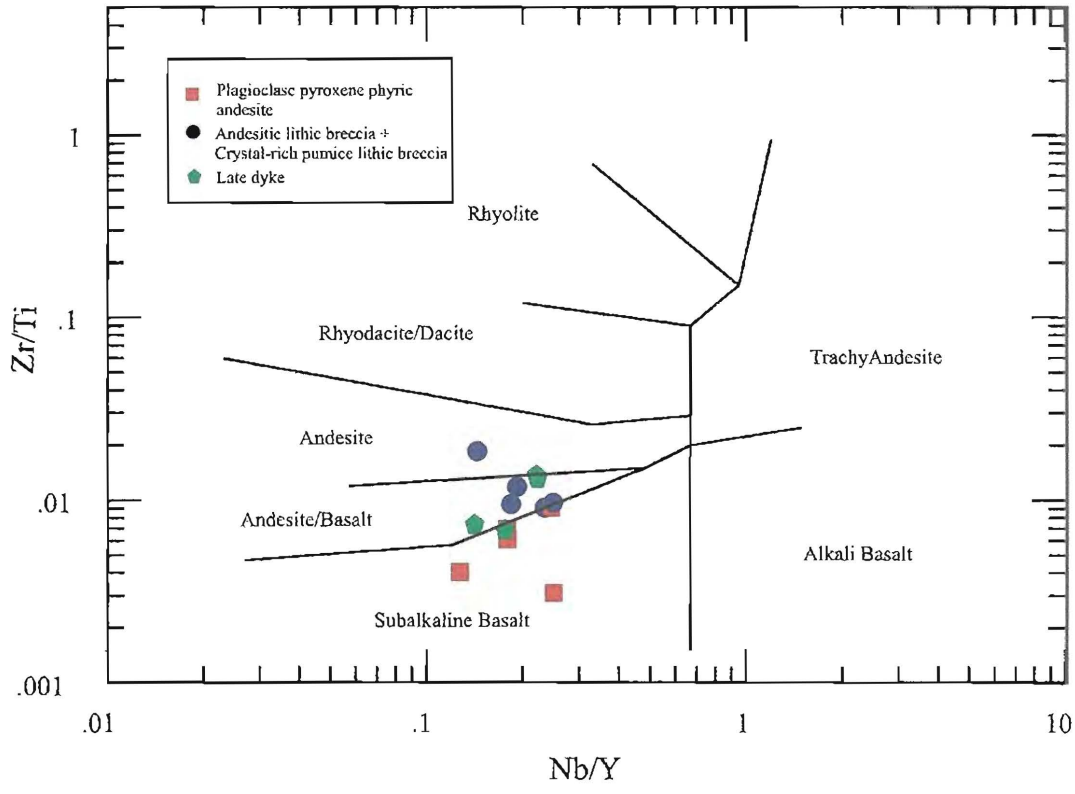

Figure 3.24. Igneous rock classification diagram by Nb/Y and Zr/TiO_2 ratios (Winchester and Floyd, 1977).

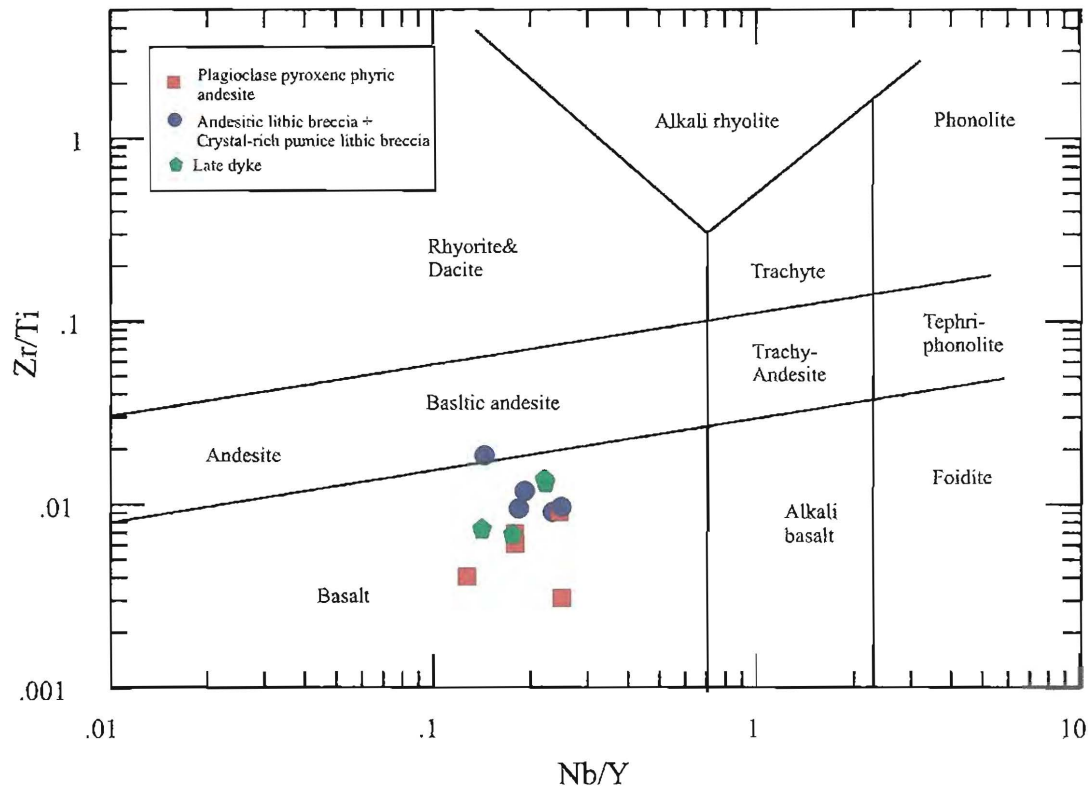

Figure 3.25. Igneous rock classification diagram by Nb/Y and Zr/Ti ratios (Pearce, 1996).

Geochemical data of the rock samples are plotted using different discrimination diagrams to determine the tectonic setting. Generally using several different diagrams is required to discriminate effectively. Ideally, most diagrams are designed for unaltered rocks to reflect melt compositions, especially basaltic rocks.

From the plot of SiO_2 against FeO (total iron as FeO), the trend indicates calc-alkaline affinity (Figure 3.26). The samples of the H zone are plotted in the sub-alkali basalt field by using relationships between $Zr/P_2O_5*10^4$ - TiO_2 and $Zr/P_2O_5*10^4$ - Nb/Y (Figure 3.27; Winchester and Floyd, 1976). The Zr and Zr/Y plot (Figure 3.28) shows that the host rocks of the H zone were erupted in both continental and oceanic arc setting with most rocks falling within the field of continental arc setting (Pearce et al., 1983). The Zr/Ti ratio (Pearce, 1982) indicates that most samples plot in the volcanic arc field with a few in MORB (mid-ocean ridge basalt: Figure 3.29). The 2Nb - Zr/4 - Y plot (Meschede, 1986) indicates that the volcanic rocks from the Chatree deposit have a volcanic-arc affinities (Figure 3.30). In a Zr - Ti, Zr - Ti/100 - Y*3 plot (Pearce and Cann 1973), the data plots in all fields with one cluster in the calc-alkali basalts (Figure 3.31) suggesting several sources for the volcanic rocks.

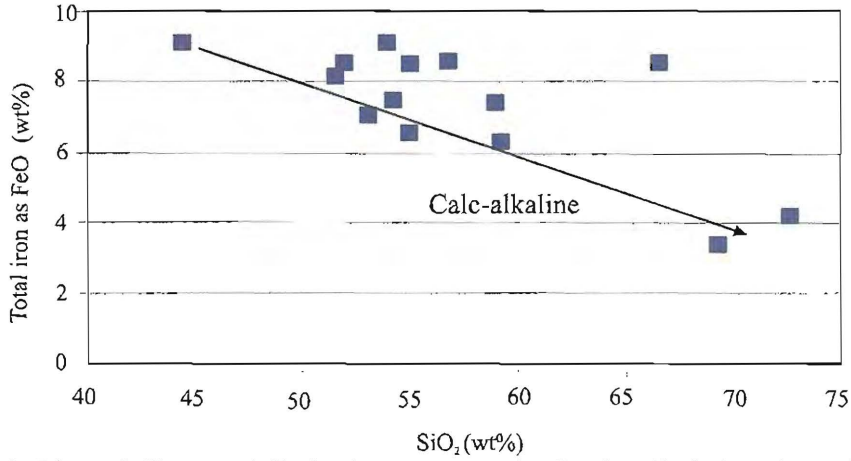

Figure 3.26. Plot of SiO_2 and FeO shows a trend of calc-alkali basalt (After Harker, 1909).

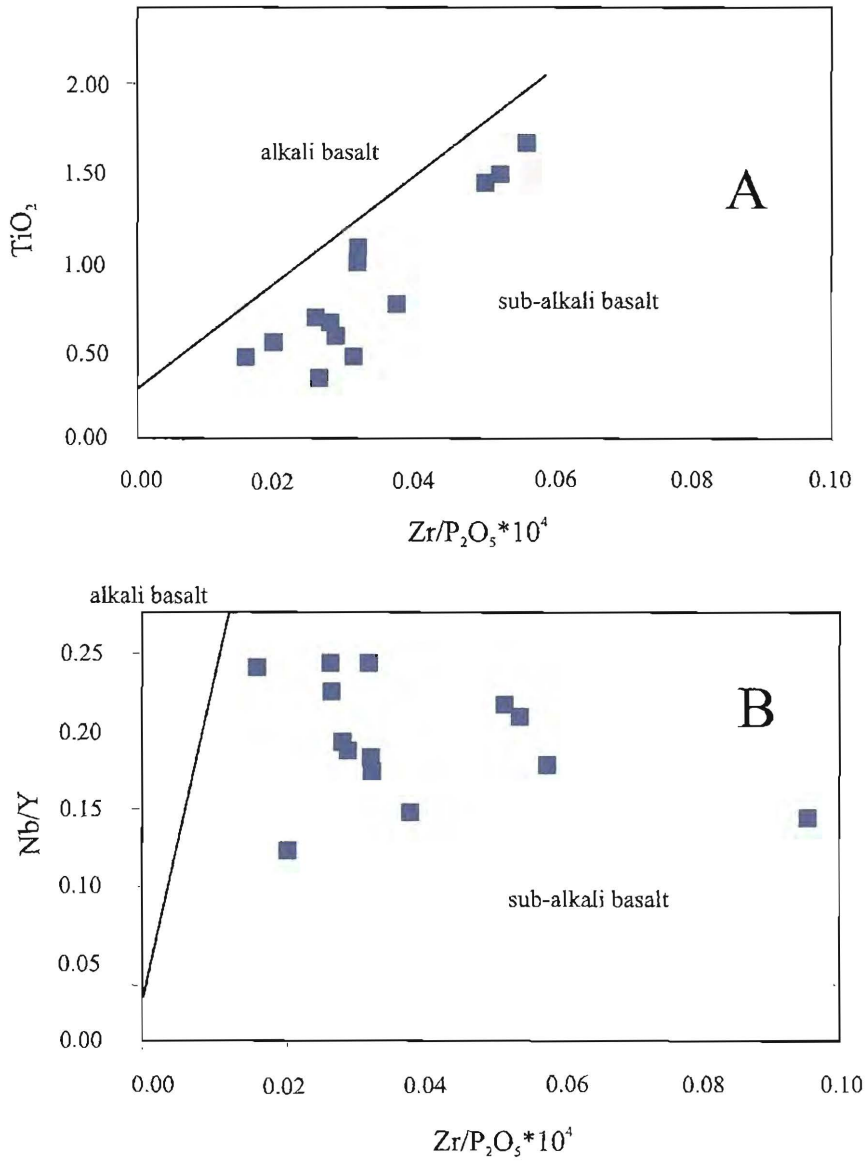

Figure 3.27. Plots of $Zr/P_2O_5*10^4$ with TiO_2 (A) and Nb/Y (B) by Winchester and Floyd (1976); using all samples.

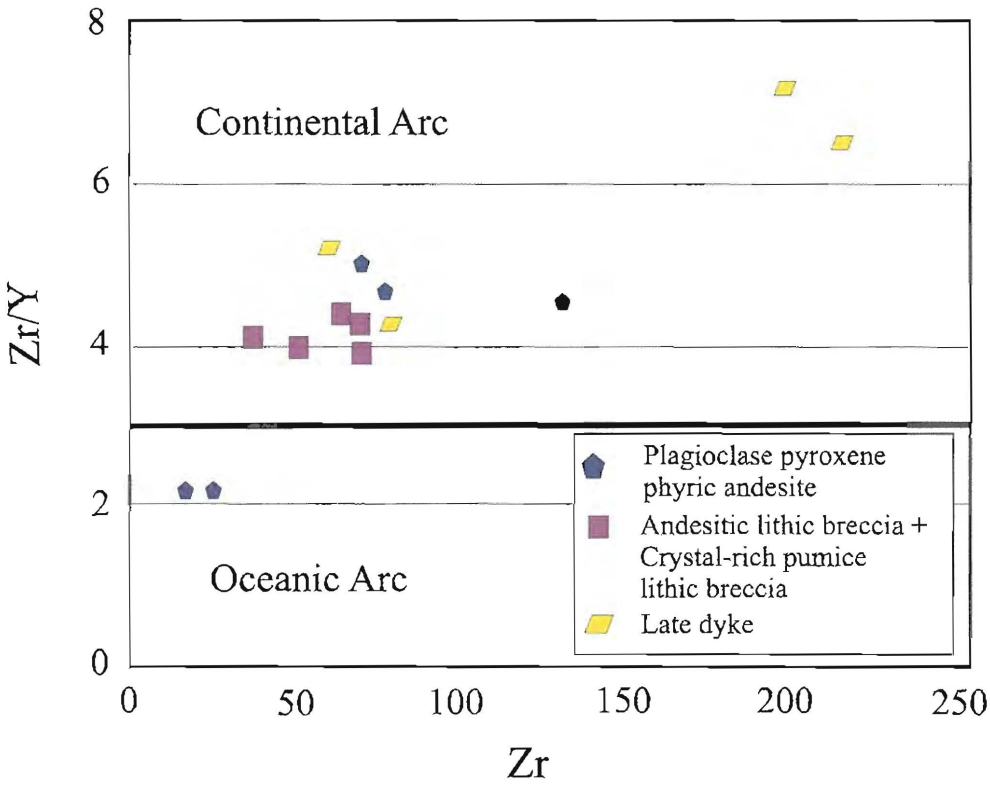

Figure 3.28. Plot of Zr and Zr/Y from host rock at the H zone shows continental and oceanic arc setting (After Pearce, 1983).

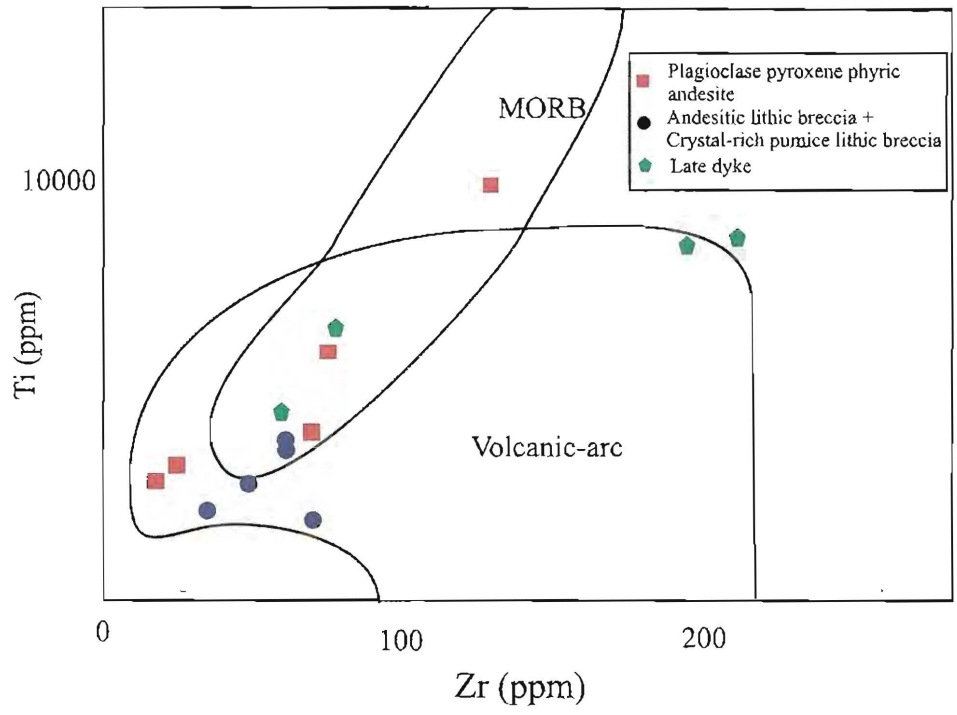

Figure 3.29. The Zr vs. Ti plot for tectonic setting (Pearce, 1982).

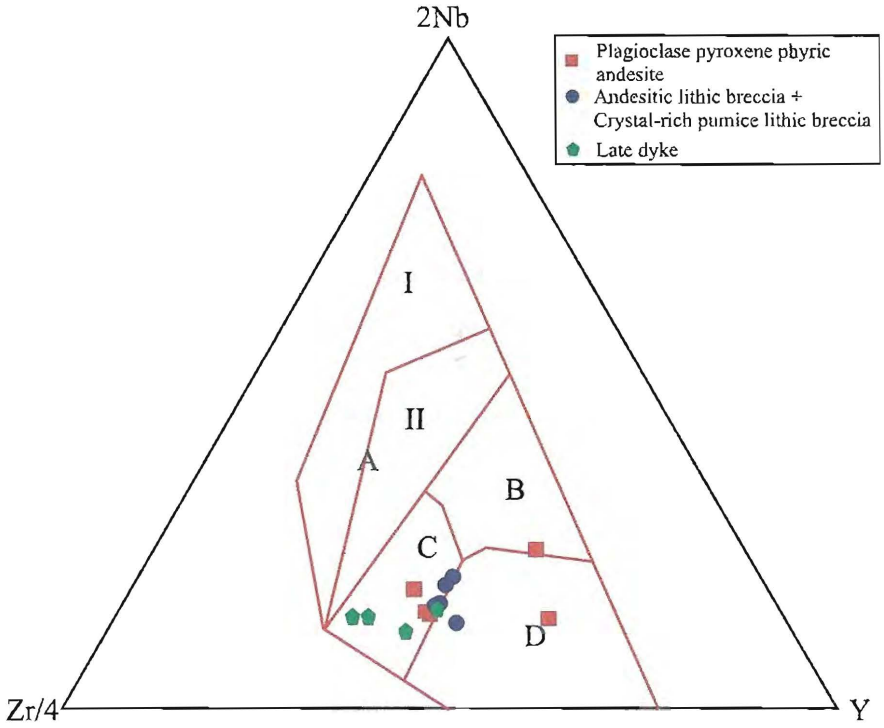

Figure 3.30. Plot of 2Nb - Zr/4 – Y. AI = within-plate alkali basalts; AII = within-plate alkali basalts and within-plate tholeiite; B = E-type MORB; C = within-plate tholeiite and volcanic-arc basalts; D = N-type MORB and volcanic-arc basalts (Meschede, 1986).

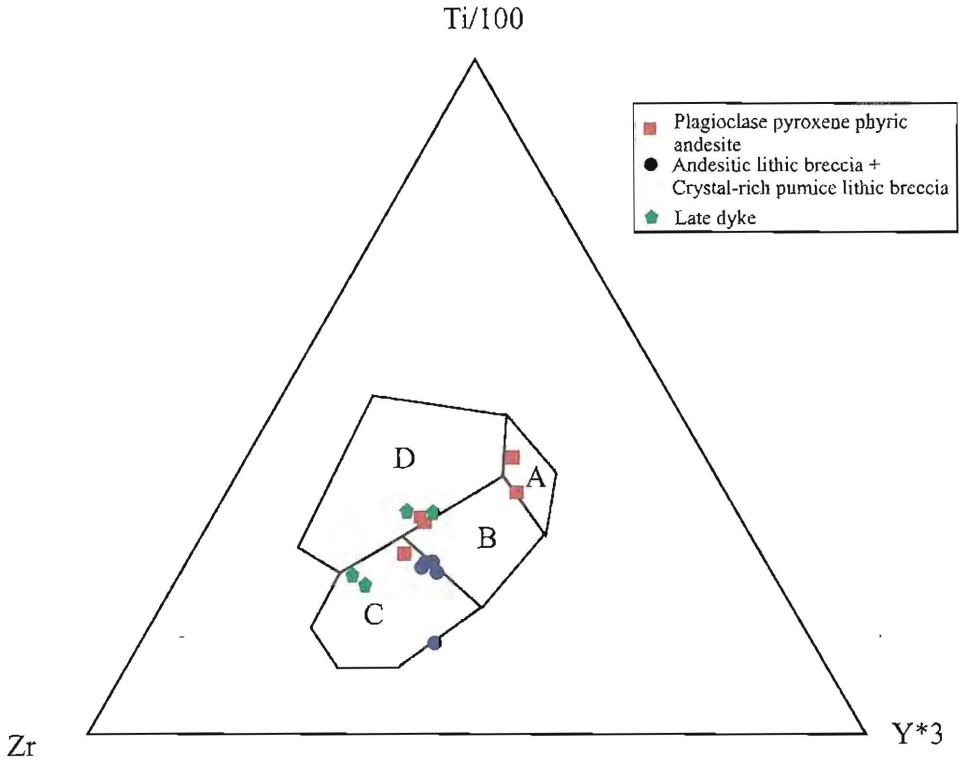

Figure 3.31. Ti - Zr-Y discrimination diagram for basalt from the H zone (after Pearce and Cann 1973); A = island-arc tholeiites, B = MORB, island-arc tholeiites and calc-alkali basalts, C = calc-alkali basalts, and D = within-plate basalts.

3.6. Depositional setting and environment

Observations at the H zone and previous descriptions by Dedenczuk (1998), Greener (1999), Barron (1998), Diemar (1999) and Cumming (2004) have been combined to present a geological model of the depositional environment of volcanic and volcaniclastic rocks preserved at the Chatree deposit.

Volcaniclastic units comprising crystal-rich quartz-feldspar lithic breccia, quartz-rich volcanic sandstone/mudstone and crystal-rich andesitic pumice breccia are present in both the open pits and drill cores as basal and upper sequences. The volcaniclastic units in the H zone can be correlated with the units in the A and D zones (Dedenczuk, 1998); quartz-andesite lithic muddy sandstone, quartz-rich sandstone and volcanic siltstone in the C zone (Greener, 1999), tuff or lapilli (Diemar, 1999) and pumice breccia facies (Cumming, 2004). The basal volcaniclastic rocks represent a minor sequence, intercalated with limestone (drill cores in the H and A zones) and andesitic lithic breccia/andesite. The upper sequences are dominantly massive crystal-rich andesitic pumice breccia, inter-layered with volcanic sandstone.

Andesitic breccias to coherent andesite form the majority of the volcanic pile in the H zone at Chatree. Andesitic sequences including andesitic lithic breccias and plagioclase-pyroxene-phyric andesite in the H zone can be correlated with autoandesitic breccias (Dedenczuk, 1998), porphyritic latitic and trachytic flows in the A and D zones (Barron, 1998) and polymictic andesitic lithic breccia and plagioclase phyric andesite (Cumming, 2004). Plagioclase-pyroxene-phyric andesite occurs as sills and dykes. Numerous dykes intrude and crosscut the early units. These have variable compositions including andesite, dacite, basalt and rhyolite. They generally crosscut the host rocks following main fractures. Coherent andesite with andesitic autobreccia and pyroclastic rocks are present at the Chatree deposit. Their low vesicularity suggested that they were rising slowly and possibly erupted by effusive processes.

The major environment of the volcanological succession is interpreted to be subaerial; however, some rock units were deposited in a shallow submarine environment. The Chatree deposit could have been deposited in subaqueous setting from volcanic eruptions under subaerial environment.

The evidence that indicates a shallow submarine deposition includes;

- Limestone containing fragments of bryozoa, crinoid stem and molluscs.

- Lithic fragments within limestone are recognised as clasts of hyaloclastite, suggesting the clasts were formed before limestone formation.
- Volcanic sandstone and siltstone contain fragments of radiolaria and plant remains suggesting a depositional environment not far from shore.
- The limestone is inferred to mark preserved shallow-marine carbonate horizons formed during times of reduced volcanism.

The evidence that indicates a subaerial deposition includes;

- There are basal beds of pyroclastic flows that are subaerial in origin. These overlie the coherent andesite and breccia.
- The pyroclastic flows show characteristics of block and ash flow deposits such as angular glass shards, crystal fragments, lithic fragment and no welded clasts.
- The basal pyroclastic beds that occur as crystal rich pumice lithic breccias are massive and poorly sorted and have angular clasts. They are overlain by thin parallel-bedded volcanic sandstone/mudstone layers.
- Some clasts of andesitic lithic breccia are red as a result of thermal oxidation.

Andesitic lithic breccias have been classified as autobreccias. Clasts typically show jigsaw-fit texture with matrix support, with a few examples of re-sedimented hyaloclastite with clast rotation. This suggests that the majority of the breccias may have formed by in situ collapse of existing andesitic rocks.

Plagioclase-pyroxene-phyric andesite intrudes and forms sills in the andesitic breccia. Pillow lavas and re-sedimented hyaloclastite are not found in the area, suggesting a subaerial depositional environment.

Clasts of pyroclastic units and andesitic breccia are angular and poorly sorted indicating textural and mineralogical immaturity with little reworking. From this evidence, the volcanic rocks were likely deposited proximal to the source vent. Greener (1999) suggested that materials were sourced from the north by size distribution of pyroclastic clasts.

Cumming (2004) proposed an eruptive-mineralisation sequence of events that comprises four stages:

1) The brecciation and rapid deposition of andesite lavas by a large scale collapse event, followed by the incorporation of the fragments into slurry flows and deposition in a subaqueous environment;

2) The intrusion of andesitic sills;
3) Hydrothermal alteration and mineralisation; and
4) Intrusion of dykes, cross cutting mineralisation.

3.7. Summary

The H zone occupies the western side of the Chatree deposit and consists of andesitic lithic breccia, plagioclase-pyroxene-phyric andesite, crystal-rich andesitic pumice breccias, crystal-rich quartz feldspar lithic breccia, quartz-rich volcanic sandstone and limestone. All units have been hydrothermally altered and cut by mineralised veins. Late andesitic-dacitic and basaltic dykes crosscut all units and most veins.

The dominant structural grain in the H zone is NE, with an inferred central fault striking 040° and dipping north-west at between 20° and 45°. The inferred fault has a normal movement suggesting an extensional setting. The H zone mineralisation occurs predominantly within the hanging wall shear zone and to a lesser degree, within the footwall shear zone. Shearing along the fault has occurred pre, syn and post mineralisation.

The geochemical data of samples from within the H zone suggests that the host rocks have an andesitic to basaltic composition and the late intrusive dykes have andesitic-dacitic and basaltic compositions. The geochemical data also suggests that the basaltic wallrocks have sub-alkali and calc-alkali characteristics. The volcanic host rocks may have formed in a volcanic arc, with most rocks of continental volcanic arc affinity.

The host rocks were deposited mainly in a subaerial to shallow submarine environment, proximal to the source vent and have then been transported from the north.

Chapter 4

Vein Mineralogy and Paragenesis

4.1. Introduction

This chapter documents the nature of mineralisation, and include descriptions of vein morphology, texture, mineralogy and paragenesis. Five vein stages have been identified in the H zone. The earliest vein stages are mainly quartz, whereas later stages are carbonate-rich. This also chapter documents the occurrence of electrum and other ore minerals (e.g., pyrite, chalcopyrite, sphalerite and galena) throughout all paragenetic stages.

4.2. Methodology

All data for the mineralogical study were collected from drill cores along 3 selected sections (including, Section 6100N, 6200N and 6350N) in the H zone and outcrop of the H pit (see Chapter 3; Figures 3.3 to 3.6). Observations of vein characteristics were made during detailed logging of diamond drill cores and petrographic examination using thin sections and polished thin sections. Polished thin sections were also used for electron microprobe analysis (EMP) to identify unknown minerals and determine compositional variation of minerals including electrum, pyrite, sphalerite and chlorite.

4.3. Vein morphology, texture, mineralogy and paragenesis

Quartz-carbonate veins with minor breccia characterise at the Chatree deposit. At the H zone, these veins exhibit a range of textures and a diverse mineralogy. There are five vein stages that have been classified by vein morphology, texture, mineralogy and paragenesis studies.

4.3.1. Stage 1

Stage 1 consists of hydrothermal breccia (early Stage 1) and grey quartz veins (late Stage 1). Stage 1 veins commonly occur along a main NE trending fault, and involve recrystallisation of quartz and fine-grained pyrite. Hydrothermal breccias or autobreccias of the H zone, shown in Sections 6100N and 6200N and the H pit, are 2 m thick and 20 m wide and they are located above and below the ore zone. The

hydrothermal breccia comprises quartz and fine-grained pyrite as matrix and angular andesite clasts that range from 1 cm to 30 cm in size showing jigsaw-fit texture (Figure 4.1). The late Stage 1 assemblage is grey quartz stockwork veins of 1-2 cm width. Stage 1 veins are crosscut by later stage veins (Stages 2-5) and often overprinted by white quartz.

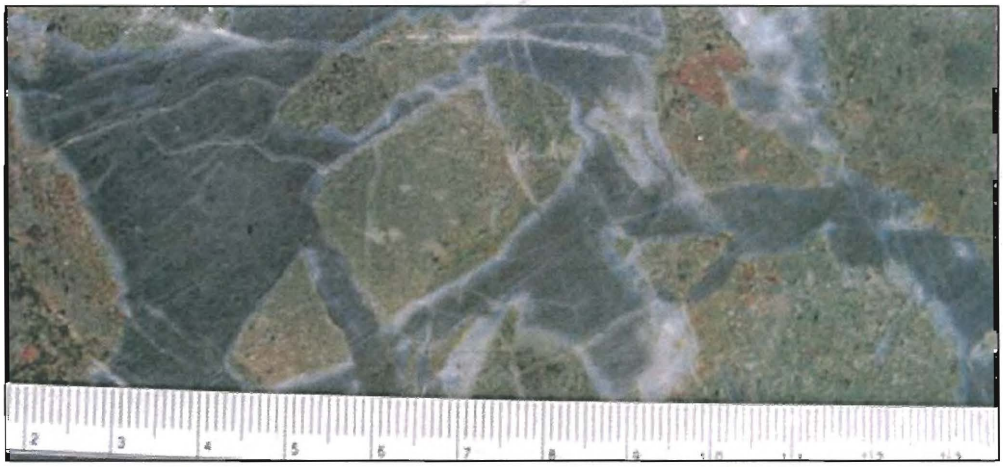

Figure 4.1. Photograph showing characteristics of vein Stage 1; hydrothermal breccia showing jigsaw-fit textures, sample from RCD 453 at depth 115m.

4.3.2. Stage 2

Vein Stage 2 is associated with gold mineralisation in the H zone of the Chatree deposit. Stage 2 veins are typically linear and show a strong sub-parallel alignment. They occur at shallow levels at which they were emplaced during brittle fracturing of the host rocks. They typically range up to 20 m wide. The veins generally dip 45° northwest in the southern part of the H zone and show a slightly flatter dip (20° northwest) at the northern end of the H zone. At the top and bottom of the zone containing Stage 2 veins, vein orientations change from parallel to form a stockwork through the host rock.

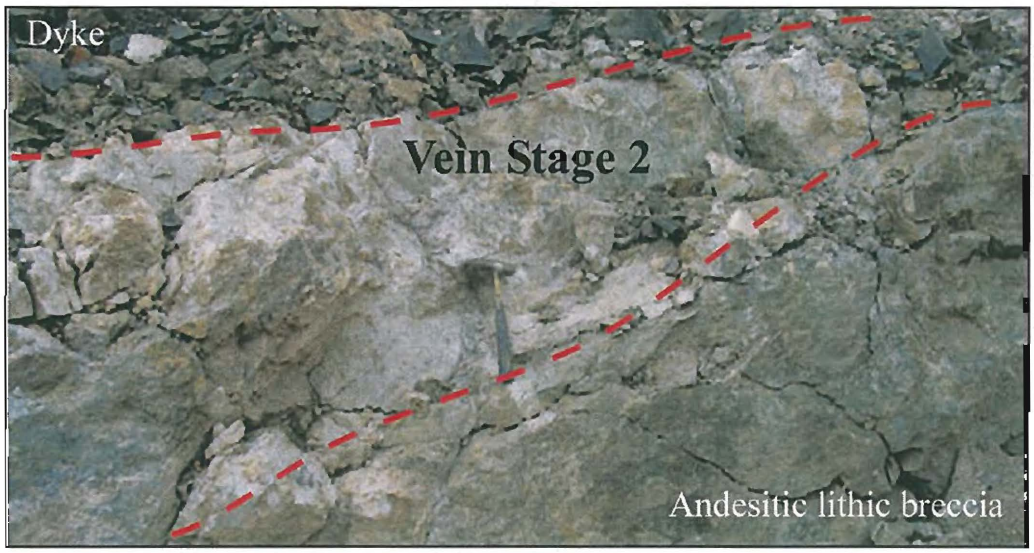

Figure 4.2. Photograph showing characteristic of Stage 2 veins crosscut in the host rocks (andesitic lithic breccia) at the H pit.

4.3.2.1. Stage 2 vein textures

The following vein textures are recorded in vein Stage 2,

a) Crustiform-colloform banding. Mineralised veins typically show crustiform and colloform banded textures (Figures 4.3 and 4.4) and are normally associated with ore grade Au-Ag mineralisation. Generally, crustiform-colloform banded veins contain 1-3 g/t Au on average, although some can be high-grade (such as sample No. RCD 357.89; 15.1 g/t Au and sample No. RCD 504.124; 35 g/t Au).

Figure 4.3. Photograph showing crustiform-colloform bands in vein Stage 2, Sample No. RCD 357.93.

Figure 4.4. Photograph showing crustiform-colloform texture of Stage 2 vein consisting of quartz-calcite-chlorite-pyrite. Sample contains a high gold grade (15.1 g/t), Sample No. RCD 357.89.

b) Comb textures. The comb-textured veins show bands of prismatic crystals of quartz with elongated euhedral shapes (Figure 4.5) and are characterised by low-grade gold. The bands of prismatic crystals may show alternating colour and composition.

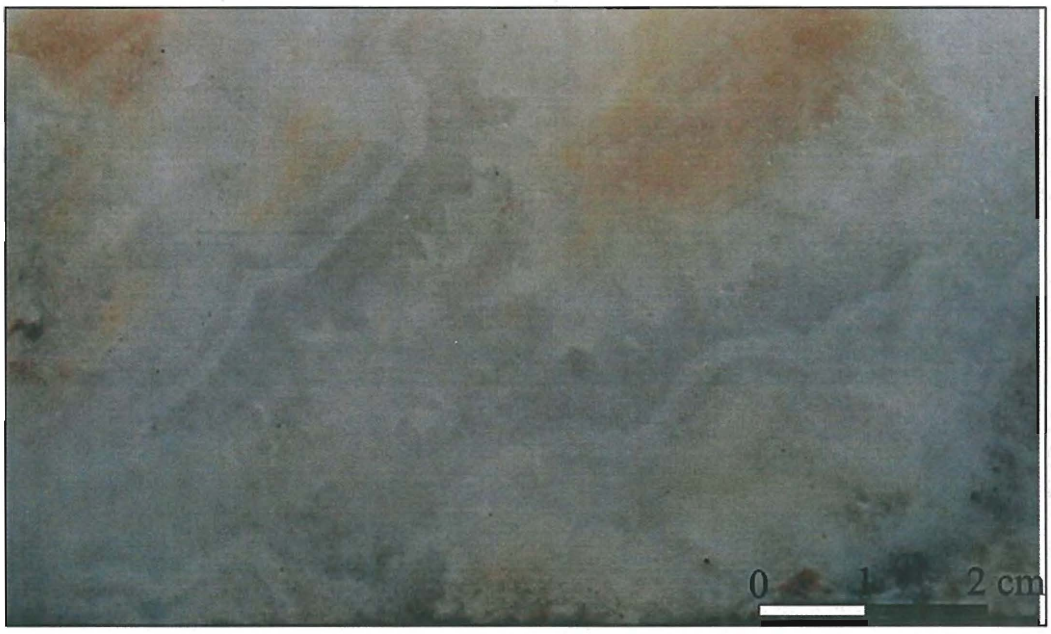

Figure 4.5. Photograph showing comb texture in vein Stage 2 with prismatic quartz, late quartz and calcite infill, Sample from RCD 357.

c) Breccia texture: Breccia texture is common in vein Stage 2. Generally, the texture is polymictic breccia that consists of fragments of host rock and early veins including andesite, calcite, quartz and grey quartz clasts (Figure 4.6). The clasts are usually angular to subangular, poorly sorted and matrix-supported. The vein breccias show alignment of similar clasts, including vein fragments and are crosscut by other stage 2 vein textures.

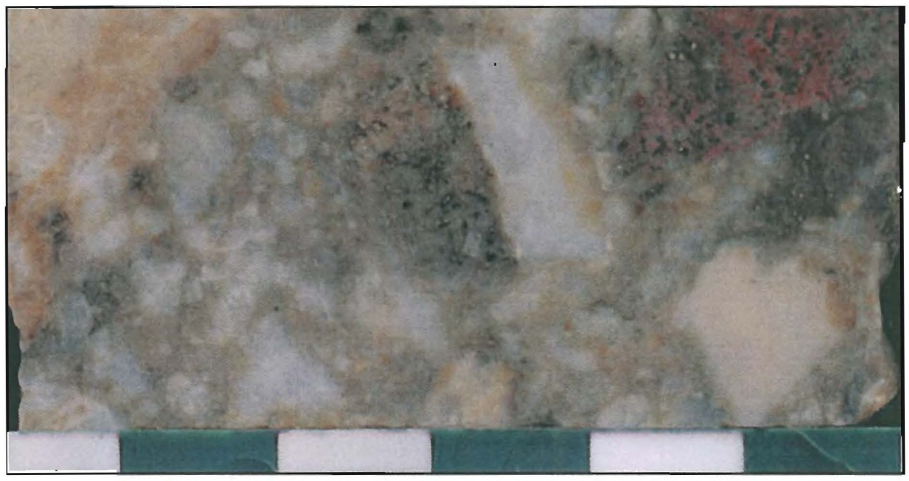

Figure 4.6. Photograph showing breccia texture in vein Stage 2, Sample No. RCD 357.90.

d) Vuggy quartz texture: Vuggy quartz has been recognised in drill cores RCD 356 at depth of ~15 to 20 m (Figure 4.7). This texture is associated with high Au grades (>100 g/t) and suggests supergene enrichment.

Figure 4.7. Photograph showing carbonate-leached vuggy quartz vein of Stage 2 associated with supergene enrichment, Sample No. RCD 312.105.

4.3.2.2 Vein mineralogy

The Stage 2 vein minerals (Figures 4.8 and 4.9) in the H zone are quartz, calcite, chlorite, illite, illite-smectite, sericite, ankerite, dolomite, epidote, adularia, pyrite, hematite, rhodochrosite, chalcedony, sphalerite, galena, chalcopyrite and electrum in decreasing order of abundance.

a) Quartz: Quartz is the most common mineral in this vein stage, and shows a range in colour including colourless, white, grey, and green and a range in size from <1 mm to 1 cm. It occurs as euhedral (such as prismatic crystals) to anhedral grains. Void spaces in Stage 2 veins typically have carbonate or quartz infill.

b) Carbonate: Carbonate minerals are common in Stage 2 veins and include calcite, dolomite, rhodochrosite and ankerite in order of abundance. Calcite formed as bands with quartz (Figure 4.9), infill in voids, and as replacement, and commonly shows euhedral to anhedral texture, and rhombohedral cleavage. Other carbonate minerals such as dolomite, rhodochrosite and ankerite occur as a replacement phase.

c) Chalcedony: Chalcedony in Stage 2 veins is pale grey and associated with quartz. It has a waxy lustre.

d) Adularia: Adularia is uncommon in Stage 2 veins and can be recognised only under the microscope, as colourless and rhomb-shaped crystals.

e) Sericite: Sericite occurs in Stage 2 veins as replacement of calcite and adularia during an alteration event.

f) Clay minerals: Clay minerals in Stage 2 veins have been identified by Portable Infrared Mineral Analyser (PIMA), and include illite and smectite, both of which occur replacing host rock.

g) Chlorite: Chlorite is present in Stage 2 veins and occurs as irregular patches, interlayered with quartz (Figure 4.9) and calcite and sometimes infilling vugs. Most chlorite is light green or colorless, but brown varieties are locally present. Compositions of chlorite are used in Chapter 5 to help determine the temperature of gold mineralisation.

h) Hematite: Hematite in the Stage 2 veins is red-brown in hand specimens (Figure 4.8).

i) Epidote: Epidote typically replaces the carbonate minerals, but in a few cases it is present as discrete clusters of grains within the vein matrix. It is usually yellowish-green in hand specimen.

j) Sulphide minerals: Sulphide minerals in Stage 2 veins include pyrite, chalcopyrite, sphalerite, and galena. Pyrite is the most abundant sulphide mineral, occurring as clustered, large, or intergrown euhedral crystals. Pyrite crystals formed after quartz and calcite but before other sulphide minerals and electrum. Sphalerite, chalcopyrite and galena occur as blebs and inclusions in pyrite.

k) Electrum: Electrum occurs as free blebs and inclusion in pyrite grains (see more details in 4.4 Ore mineralogy).

Figure 4.8. Photograph showing Stage 2 veins of quartz-carbonate-chlorite-hematite-pyrite-sericite, Sample No. RCD 1116.149.

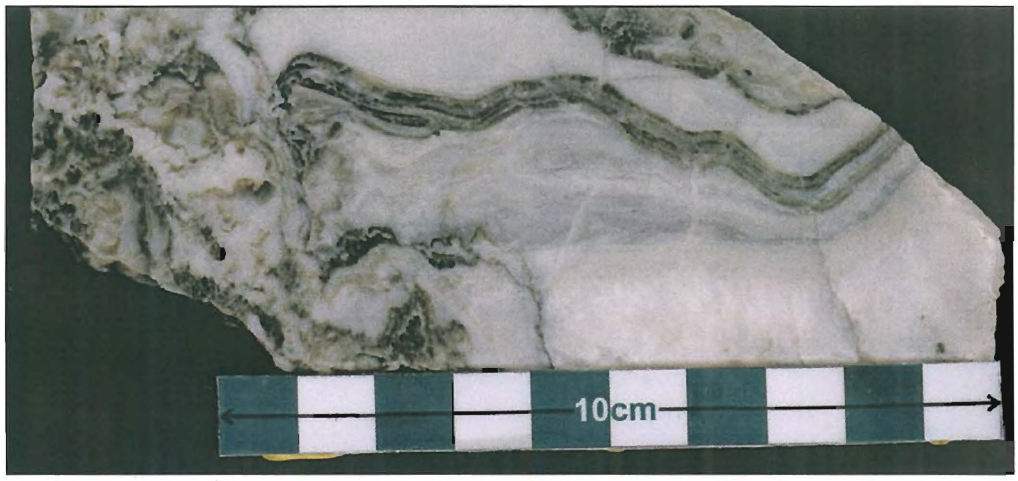

Figure 4.9. Photograph showing Stage 2 veins with quartz-calcite-chlorite bands, Sample No. RCD 505.110.

4.3.3. Stage 3

These veins crosscut vein Stages 1 and 2, and typically occur as 1-2 cm wide and rarely extend for more than 10-15 cm. Stage 3 veins are linear and clearly crosscut Stage 2 veins (Figure 4.10). Stage 3 veins are composed of recrystallised quartz; however, clusters of pyrite, K-feldspar, calcite and altered epidote are also present in minor amounts (Figure 4.11).

Figure 4.10. Photograph showing vein Stage 3 quartz crosscutting breccia textured vein Stage 2, Sample No. RCD 353.42.

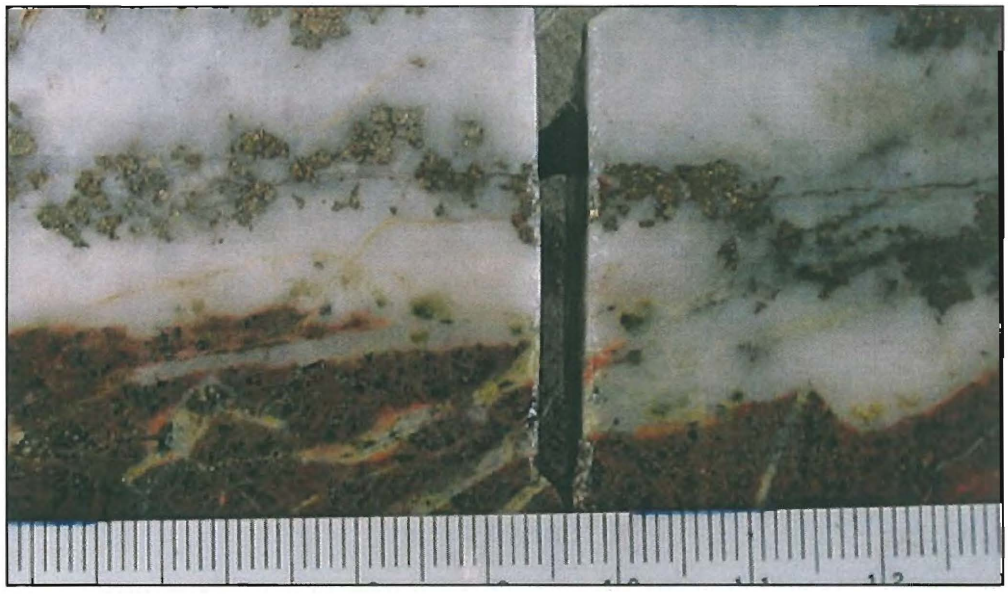

Figure 4.11. Photograph showing quartz-pyrite in Stage 3 veins, Sample from RCD 1122.

4.3.4. Stage 4

Calcite veinlets form the latest vein stage and crosscut all other vein stages and all rock units. Calcite veins are usually <1 mm wide. Calcite also exists as small patches, discontinuous trails and stockworks in the wall rock (Figure 4.12).

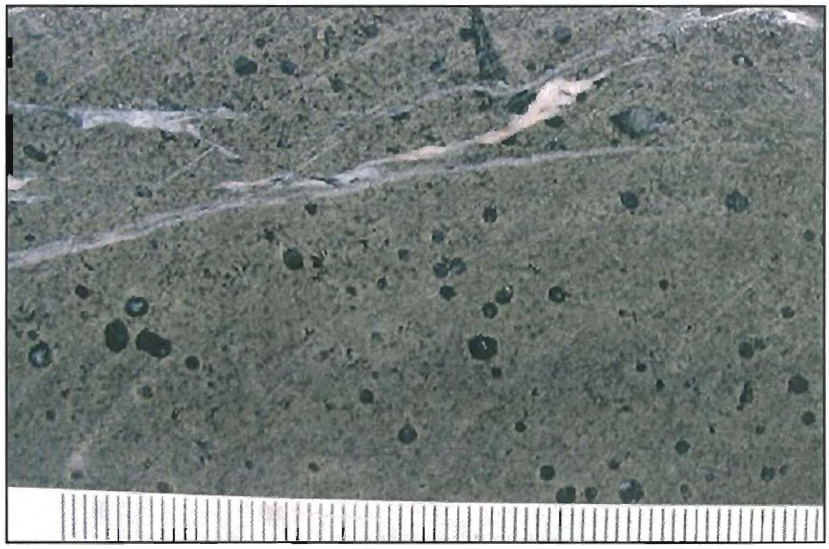

Figure 4.12. Photograph showing Stage 4 calcite veinlet crosscutting andesitic dyke, Sample No. RCD 312.105.

4.3.5. Stage 5

This stage consists of pink fibrous laumontite ($Ca_4(Al_8Si_{16}O_{48}).16H_2O$), that occurs as ~2 mm thick coating on fractures (Figure 4.13), and filling small cavities and some veins.

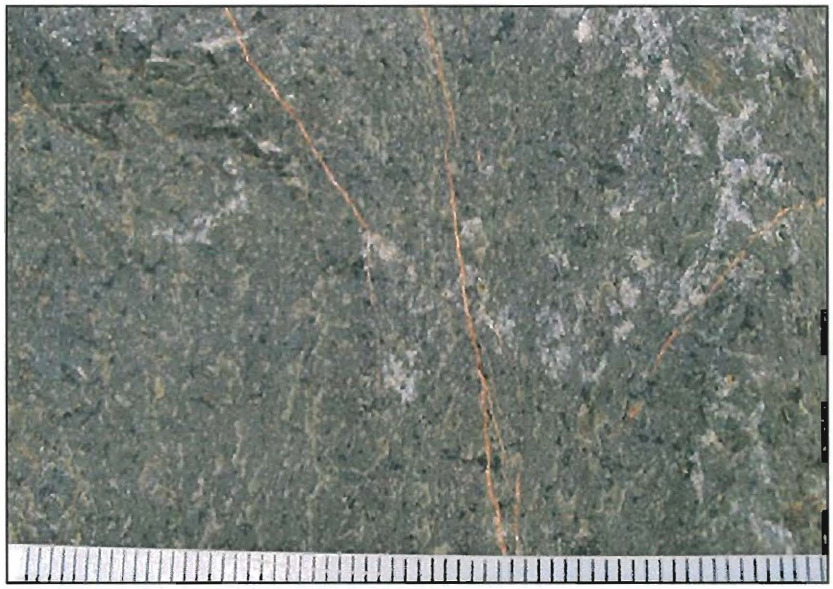

Figure 4.13. Photograph showing pink laumontite (Stage 5) coating calcite veinlet in plagioclase-pyroxene-phylic andesite, Sample No. RCD 1116.149.

Through the vein mineralogical study, paragenetic relationships of vein mineralisation have been represented in Figure 4.1.

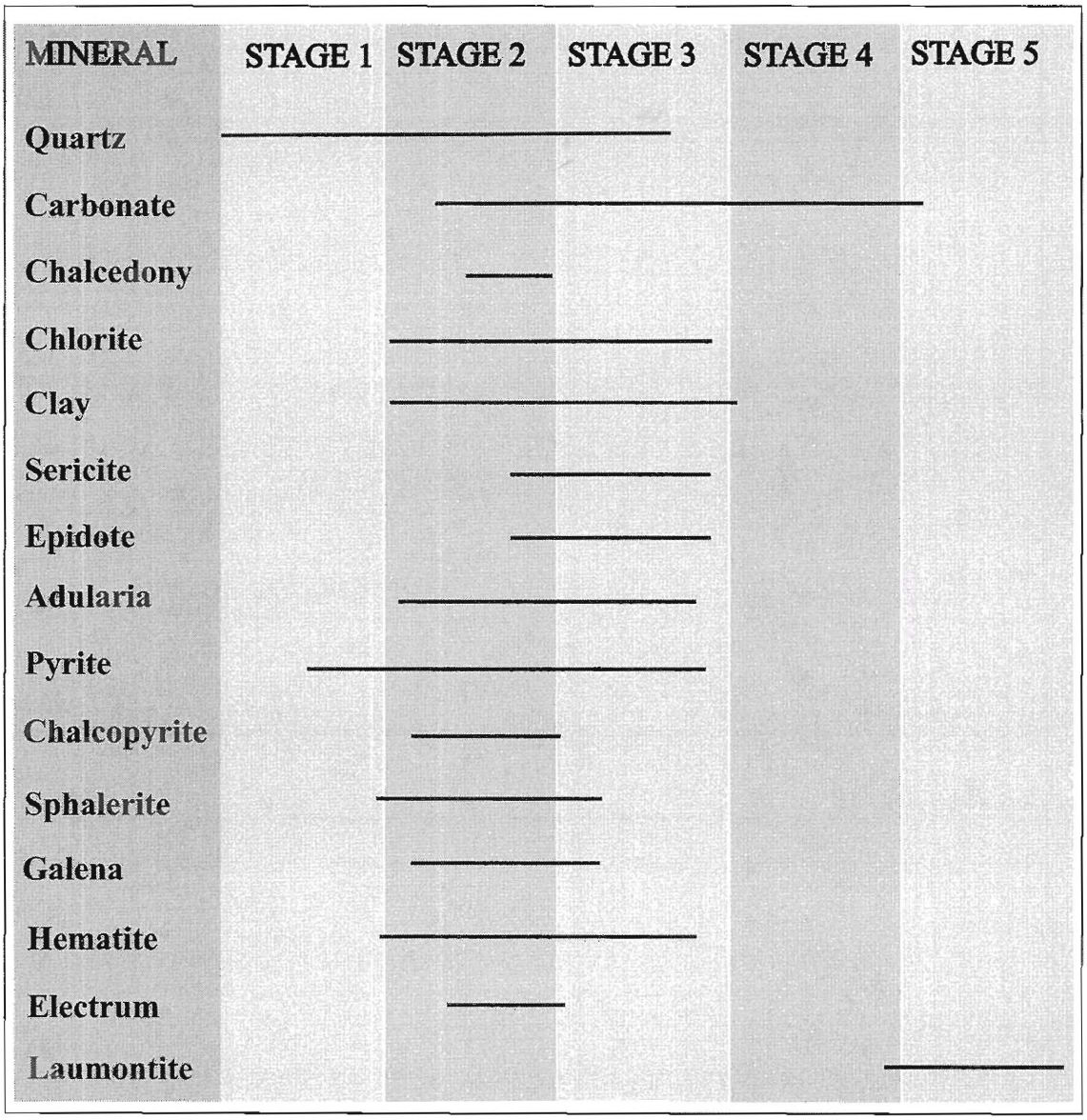

Figure 4.14. Paragenesis of different vein stages at the H zone, Chatree deposit, central Thailand.

4.4. Ore mineralogy

Gold is the most important ore mineral at the Chatree deposit and is normally associated with a significant quantity of alloy silver, which is described as electrum. Electrum is defined as gold with more than 20 wt% of silver (Boyle, 1979). The electrum in the H zone occurs as free grains, small inclusions in pyrite and in contact with other sulphide minerals including, pyrite, chalcopyrite, galena and sphalerite associated with fine-grained quartz and calcite gangue (Figures 4.15 to 4.21). Generally, the grade of Au in the deposit is fairly low (average 2-3 g/t Au). Gold as electrum is typically intergrown with sulphide minerals as fine grains and is difficult to locate and identify under the microscope. However, there are a few high-gold grade samples including Samples No. RCD 357.89 (15.1 g/t Au), RCD 357.92 (4.88 g/t Au) and RCD 504.124 (36.8 g/t Au). The gold in these samples were analysed by electron microprobe.

The following mineral abbreviations are used in Figures 4.15 to 4.21.
Pyrite = Py; Electrum = El; Sphalerite = Sph; Galena = Gal; Chalcopyrite = Chc.

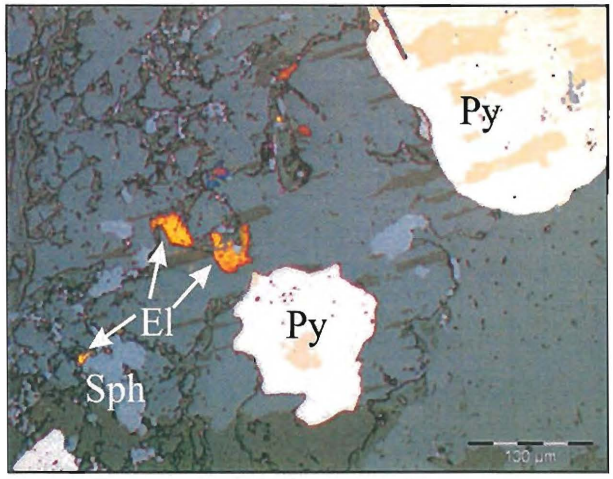

Figure 4.15. Photomicrograph showing electrum disseminated and in contact with sphalerite in reflected light, Sample No. 357.89.

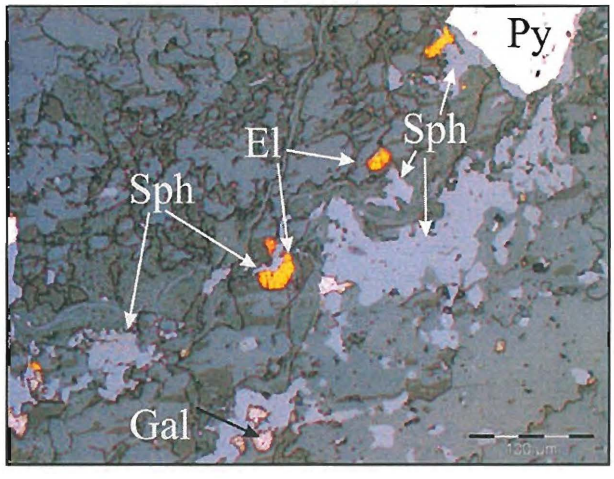

Figure 4.16 Photomicrograph showing electrum disseminated and in contact with sphalerite, galena on sphalerite in reflected light, Sample No. 357.89.

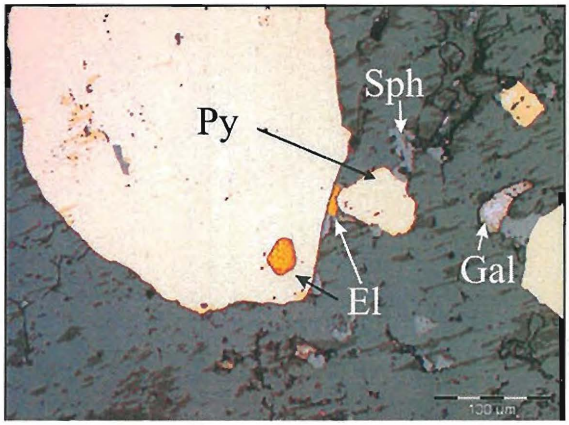

Figure 4.17. Photomicrograph showing an electrum inclusion in pyrite and in contact with pyrite and sphalerite in reflected light, Sample No. 357.89.

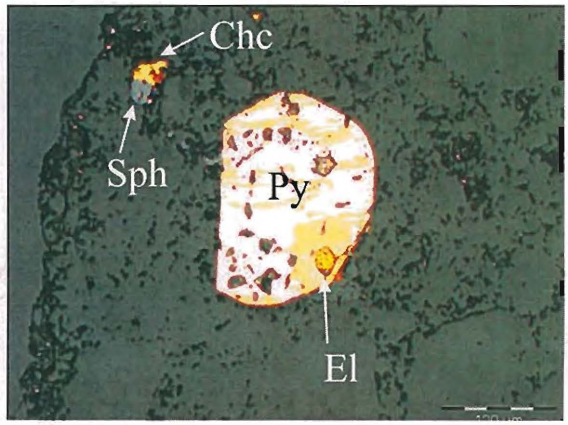

Figure 4.18. Photomicrograph showing electrum inclusions in pyrite and sphalerite in contact with chalcopyrite in reflected light, Sample No. 357.92.

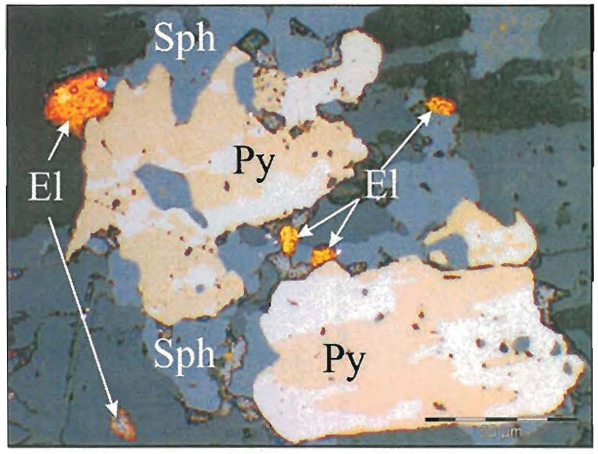

Figure 4.19. Photomicrograph showing electrum disseminated and in contact with pyrite and sphalerite in reflected light, Sample No. 357.89.

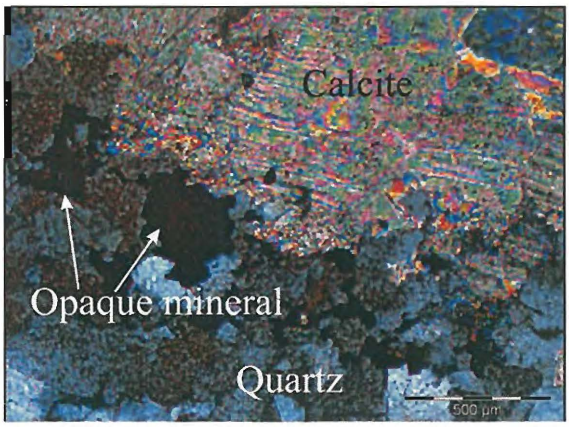

Figure 4.20. Photomicrograph showing opaque minerals (sulphide minerals and electrum) within calcite and quartz gangue in transmitted light, Sample No. 357.89.

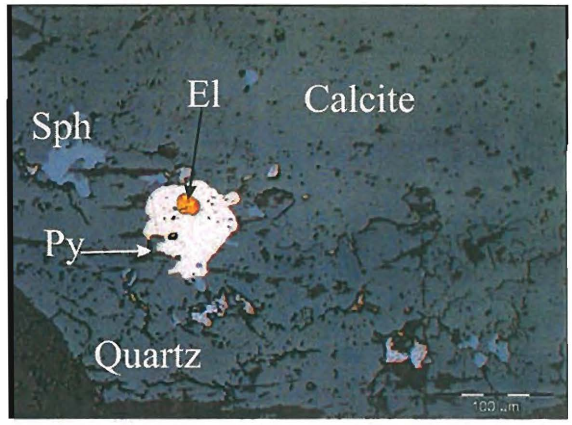

Figure 4.21. Photomicrograph showing electrum inclusion in pyrite within calcite and quartz gangue in reflected light, Sample No. 357.89.

4.4.1. Electrum and sulphide mineral paragenesis

Electrum is associated with sulphide minerals including pyrite, sphalerite, chalcopyrite, and galena. Electrum is anhedral with an average grain size of 30 microns. It normally occurs as irregular blebs within pyrite, and as inclusions, free blebs together with galena and sphalerite.

Euhedral to subhedral pyrite (average grain size = 100μm) is the most abundant sulphide mineral and has formed paragenetically earlier than other sulphide minerals. Pyrite is occasionally intergrown with sphalerite, chalcopyrite, galena and electrum. Fractured coarse-grained pyrite is rarely infilled by sphalerite and electrum.

Sphalerite forms anhedral crystals and blebs (average grain size = 50μm) intergrown with electrum and other sulphide minerals (e.g. pyrite, chalcopyrite, and galena). Sphalerite clearly overprinted pyrite. Sphalerite typically contains abundant fine-grained chalcopyrite as "chalcopyrite disease" (Figure 4.22). The sphalerite composition of grains from Stage 2 veins were analysed by electron microprobe and have low FeS contents (Table 4.1), ranging from 0.13 to 1.91 FeS mole%. The low iron content is consistent with other epithermal system and may suggest a high sulphur activity of the fluids responsible for mineralisation (Hedenquist et al., 2000).

Chalcopyrite forms anhedral grains (average grain size = 30μm) and inclusions in pyrite and sphalerite. Chalcopyrite occurs in contact with sphalerite and as free grains.

Galena forms anhedral grains (average grain size = 30μm) and occurs as inclusions within pyrite and in contact with pyrite and sphalerite. Galena grains show characteristic triangular cleavage pits. Recrystallised galena encloses pyrite and sphalerite.

Electrum and sulphide mineral paragenesis is shown in Figure 4.23.

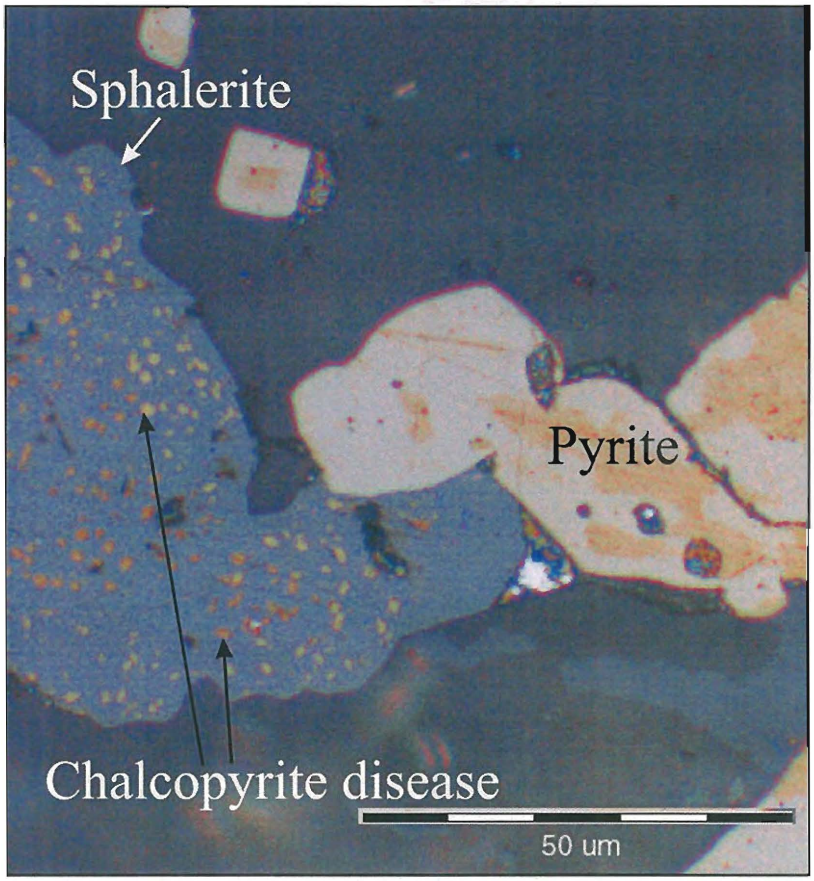

Figure 4.22. Photomicrograph showing chalcopyrite disease in sphalerite grain in reflected light, Sample No. 504.124.

Table 4.1. Sphalerite composition by electron microprobe analysis and FeS content.

Sample No.	S wt %	Mn wt %	Fe wt %	Zn wt %	Cd wt %	Se wt %	Cu wt %	Total wt %	FeS mole %
374.26_1_sph1	33.56	0.04	0.3	64.05	0.51	0.03	0.4	98.88	0.45
374.26_1_sph2	33.84	0.02	0.54	63.3	0.13	0.02	0.63	98.48	0.83
374.26_2_sph3	33.72	0.05	1.27	63.89	0.14	0.03	1.21	100.32	1.91
357.89_1_sph1	33.66	0.04	1.1	63.49	0.35	0.01	0	98.65	1.67
357.89_1_sph2	33.9	0.06	0.2	64.53	0.34	0.01	0.17	99.22	0.3
357.89_2_sph3	34.08	0.02	0.89	64.29	0.28	0.01	0.22	99.8	1.34
357.89_2_sph4	33.37	0.03	0.16	65.18	0.28	0.02	0.03	99.06	0.24
357.89_3_sph5	33.69	0.03	0.38	62.61	0.3	0.02	0.44	97.46	0.58
357.89_4_sph6	33.88	0.04	0.97	64.57	0.33	0.03	0.04	99.85	1.45
357.89_4_sph7	33.57	0.04	0.51	65.09	0.32	0.02	0.05	99.59	0.77
357.89_6_sph8	33.83	0.07	0.23	64.29	0.29	0.02	0.1	98.84	0.35

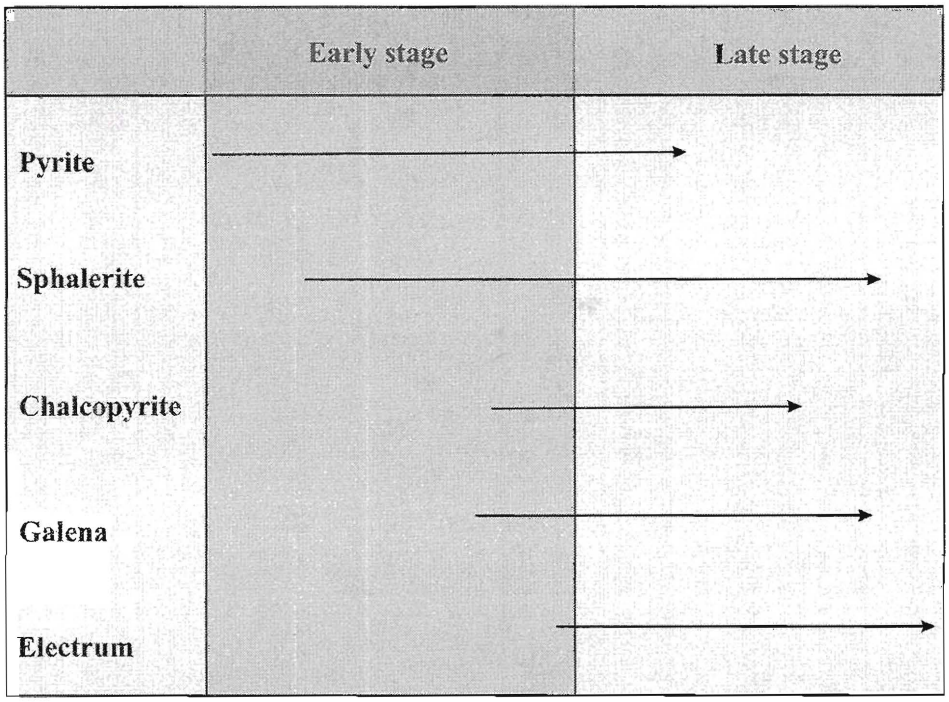

Figure 4.23. Paragenetic relationship between sulphide minerals and electrum, the H zone, Chatree deposit.

4.4.2. Ag:Au ratios

The silver:gold ratio in the H zone has been studied by using exploration assay data (whole rock analysis undertaken by Akara Mining) and electron microprobe (EMP) analysis of electrum grains at the Central Science Laboratory (CSL), University of Tasmania.

Silver and gold ratio from assay data: the Ag:Au ratio from whole rock assay data averages 4:1 (in samples where both Au and Ag are > 1 ppm: Appendix G). Contour maps of Au assay and Ag:Au ratio are shown in Figures 4.24 and 4.25.

Silver with gold from electron microprobe analysis: twenty electrum grains from three Stage 2 ore vein samples were analysed (Table 4.2) including Samples No. RCD 357.89 (15.1 g/t Au and 26.2 g/t Ag), RCD 357.92 (4.88 g/t Au and 7.1 g/t Ag) and RCD 504.124 (36.8 g/t Au and 33.3 g/t Ag). These grains were analysed for the chemical composition of gold and silver alloy. Element that were used for analysis including Au, Ag, Cu, As, and Hg (Appendix C).

Electrum in the H zone has Ag content ranging from 31.5 to 45.7 w% and Au content ranging from 53.1 to 68.2 wt% (Ag:Au ratio ~0.6:1). The Cu and As contents are less than 1 wt%. The Hg content of the samples could not be detected by an electron microprobe analyzer.

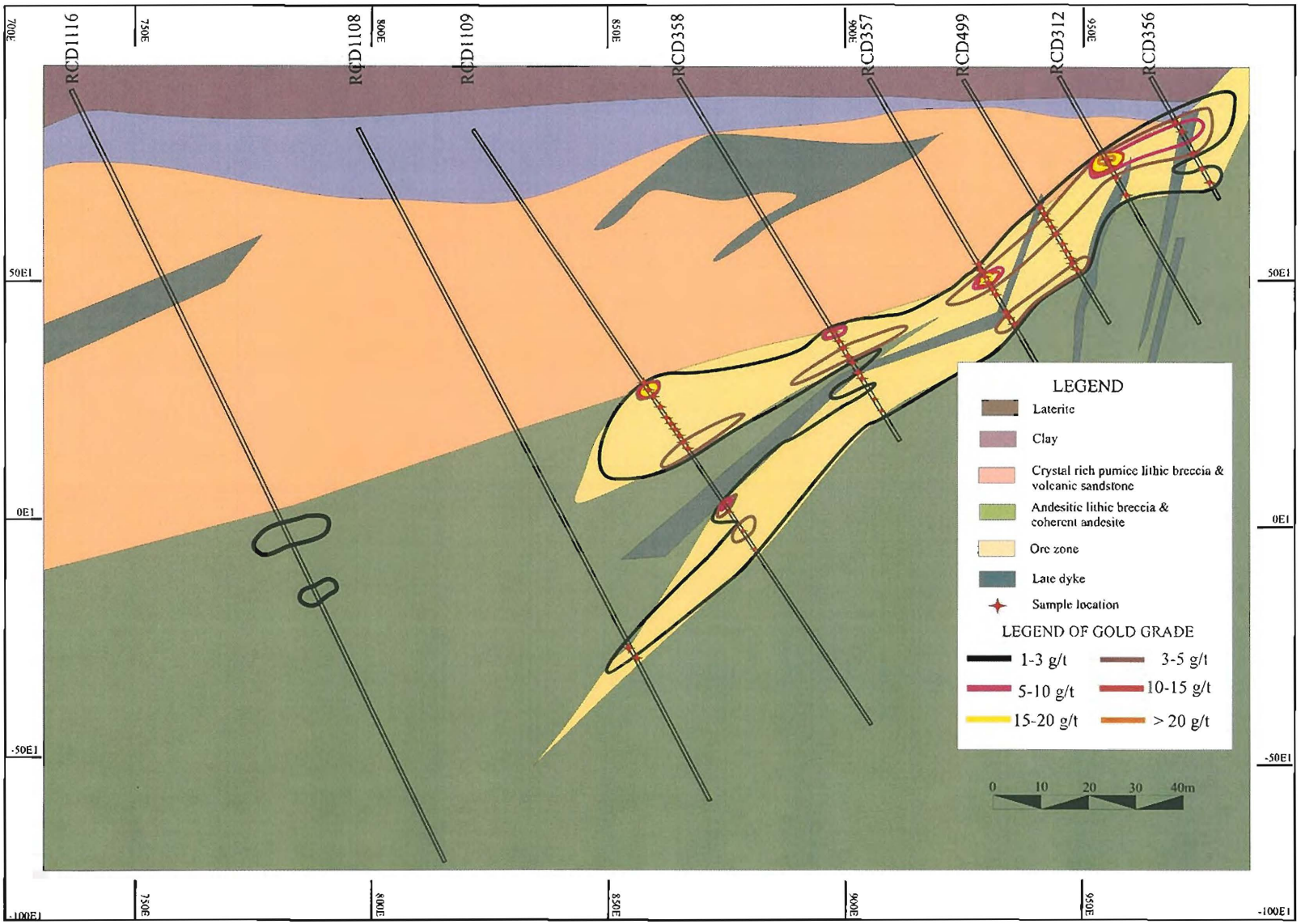

Figure 4.24. Cross section of gold grade contours for Section 6200N, the H zone, Chatree deposit, central Thailand.

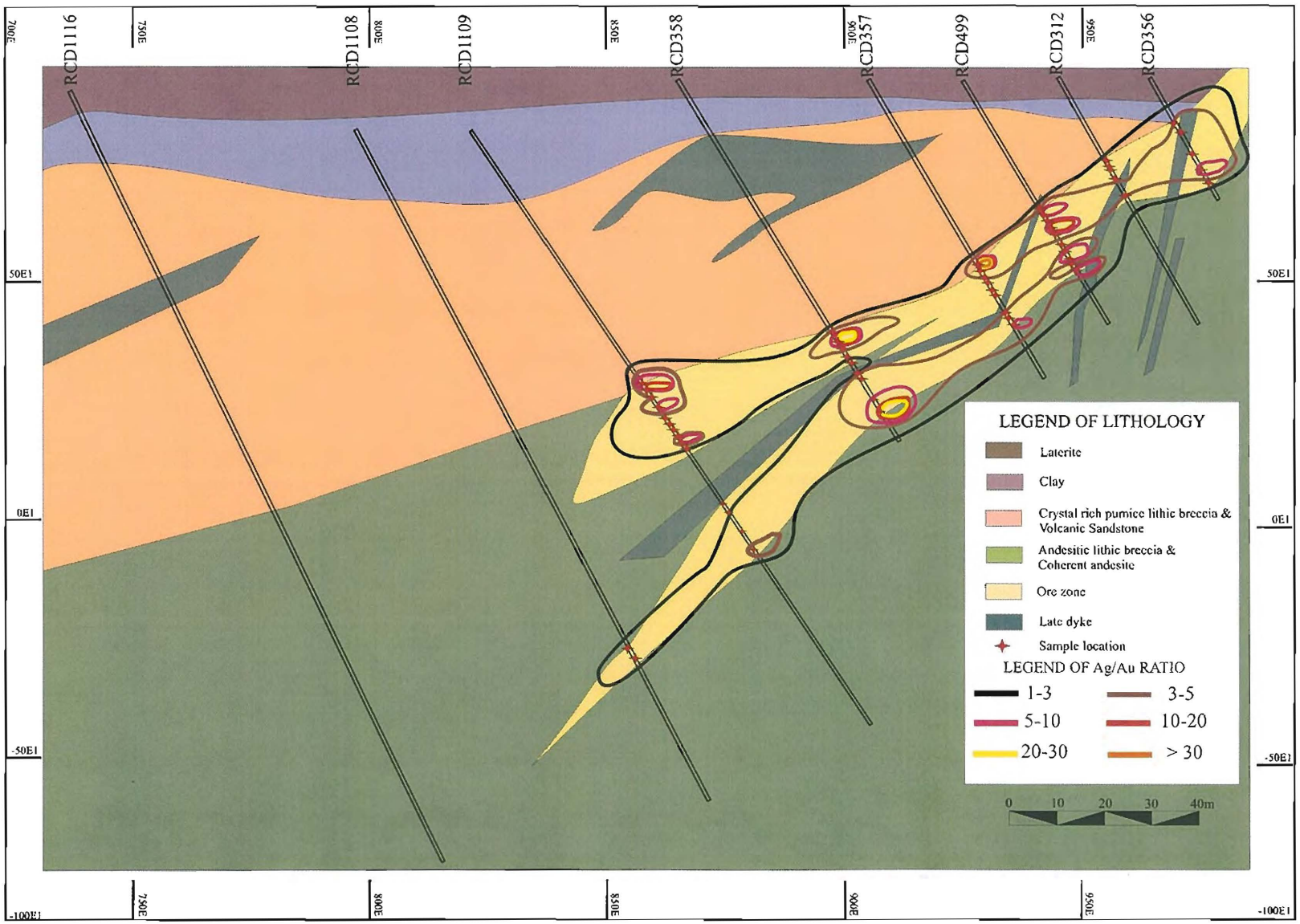

Figure 4.25. Cross section of silver to gold ratio contours for Section 6200N, the H zone, Chatree deposit, central Thailand.

Table 4.2. Compositional variation and associated mineral assemblage of electrum in the H zone, Chatree deposit, central Thailand.

Sample No.	Deportment	Associated Gangue	Size (μm)	Au wt %	Ag wt %	Gold fineness
357.89.01	Inclusion within pyrite	Fine quartz and calcite	20	61.9	41.3	600
357.89.02	In contact with pyrite and sphalerite	Fine quartz and adularia	25	64.1	39.9	616
357.89.03	In contact with galena and sphalerite	Fine quartz and adularia	10	43.2	32.3	572
357.89.04(core)	In contact with pyrite and sphalerite	Fine quartz and calcite	45	57.1	45.4	557
357.89.05(rim)	In contact with pyrite and sphalerite	Fine quartz and calcite	45	63.5	39.2	619
357.89.06	In contact with sphalerite	Fine quartz	25	59.4	42.3	584
357.89.07	In contact with pyrite	Fine quartz	30	55.9	43.6	562
357.89.08	In contact with sphalerite	Fine quartz	25	53.9	45.1	544
357.89.09 (core)	In contact with pyrite and sphalerite	Fine quartz	50	63.4	39.5	616
357.89.10 (rim)	In contact with pyrite and sphalerite	Fine quartz	50	62.6	40.8	605
357.89.11	In contact with sphalerite	Fine quartz	30	64.6	39.5	620
357.89.12	Disseminated	Fine quartz	15	53.1	37.2	588
357.89.13	In contact with galena and sphalerite	Fine quartz	40	62.8	40.3	609
357.89.14(core)	Disseminated	Fine quartz	30	64.7	39.3	622
357.89.15 (rim)	Disseminate in fracture	Fine quartz	30	65.2	39.1	625
357.89.16	Disseminate in fracture	Fine quartz	20	62.1	31.9	661
357.92.17(core)	Inclusion within pyrite and In contact with galena	Fine quartz	20	67.3	33.1	670
357.92.18 (rim)	Inclusion within pyrite and In contact with galena	Fine quartz	20	70.4	31.5	691
357.92.19	Inclusion within pyrite and In contact with galena	Fine quartz and sericite	10	68.2	33.2	672
504.124.20	In contact with pyrite	Fine quartz	15	55.6	45.7	549

Gold fineness, determined by the equation [Au/(Au+Ag)]*1000 in weight % (Fisher, 1945) for individual gold grains, provides an opportunity to determine Au/Ag variations. Gold fineness from the H zone ranges from 544 to 690 (Table 4.2), with an average of 609 (Figure 4.26).

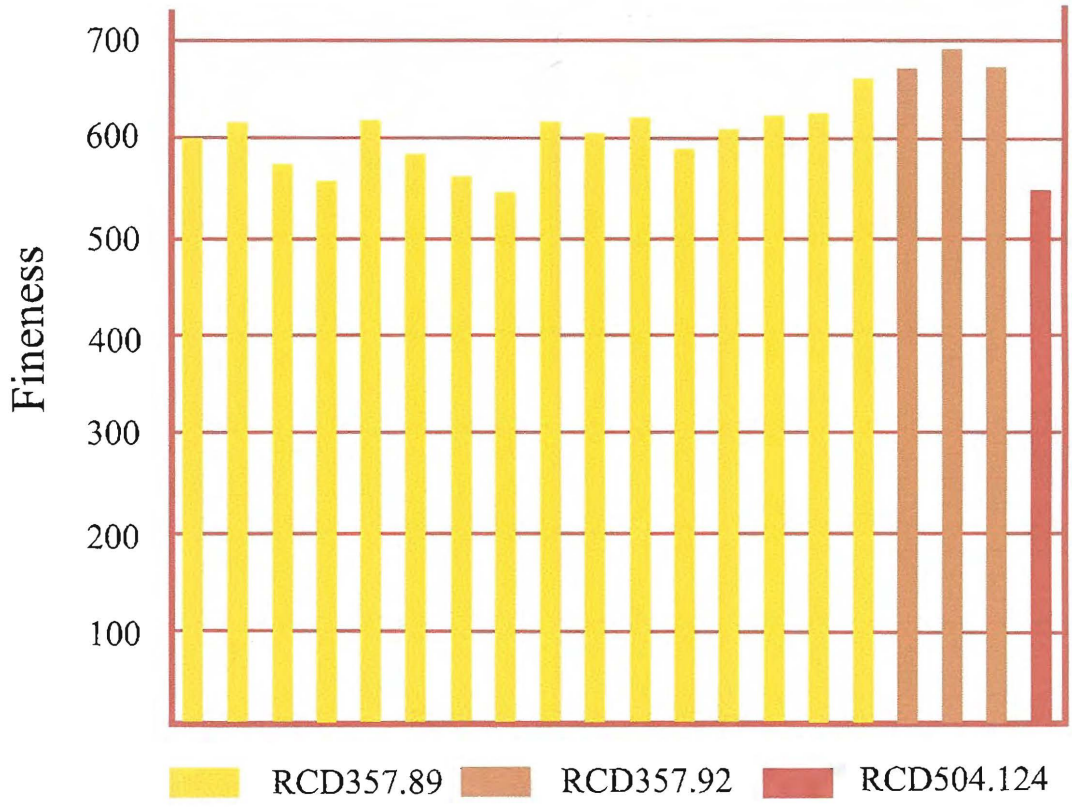

Figure 4.26. Distribution of gold fineness of individual grains from three different samples from the H zone, Chatree deposit, Thailand.

4.5. Discussion

4.5.1. Vein mineralogy

Veins and their characteristics can be interpreted in term of fluid conditions and physico-chemical processes of hydrothermal system.

The Stage 1 hydrothermal breccia and grey quartz that forms autobreccias may be classified as magmatic hydrothermal breccia due to its jigsaw breccia texture and the quartz-rich matrix. They are surrounded by andesitic rocks that hydrofractured due to sudden failure of the rock with the rapid influx of ore-forming fluids evolved from crystallising water-saturated magma.

Crustiform and colloform textures in vein Stage 2 may have formed by boiling during fluid flow, resulting in rapid semi-rhythmic deposition to produce finely layered banding (Lawless et al., 1999). Other minerals such as calcite replaced or infilled open spaces when conditions changed. Crustiform and colloform veins are fragmented by fault or hydraulic injection. Colloform band are mainly formed at shallow depth and caused by colloidal silica accumulation (Lingdgren, 1933).

Comb textures that present in Stage 2 veins are formed by hydrothermal solutions in open fissures. Bands of comb textures are deposited by variation in the impurities in crystals (Lawless et al., 1999).

The vuggy quartz similar to that in Stage 2 veins is generally found in overprinted, steam-heated, advanced argillic alteration zones, usually presents in high-sulphidation epithermal systems (Hedenquist et al., 2000). However, the vuggy vein texture at the H zone is more likely associated with supergene enrichment.

Adularia in Stage 2 ore veins suggests that a boiling zone similar to other low-sulphidation epithermal deposits is present (Cooke and Simmons, 2000).

Chalcedony, which typically forms in the upper levels of epithermal deposits(~15m from surface; Hedenquist et al., 2000), is not extensive in the H zone, suggesting that the upper parts of the H zone may have been eroded away.

4.5.2. Ore mineralogy

4.5.2.1. Ag:Au ratio

The Ag:Au ratio from individual electrum grains (electron microprobe; 0.6:1) and whole rock (assays; 4:1) are different. The assays show lower gold content but the individual grains show higher gold content. This probably reflects either inhomogeneity of the electrum grains, or that additional Ag is present as solid solution within other mineral phases (e.g. galena, argentite, copper sulphides, and sulphosalts).

The Ag:Au ratio depends on speciation of gold and silver in fluid and mechanisms of precipitation. The speciation of Au and Ag depends upon temperature, pressure, redox state, pH, salinity and activities of H_2S, S_2, and O_2 (Lawless et al., 1999). Generally, the Ag:Au ratio increases along a hydrological flow path. Gold compounds are less soluble and tend to be deposited first during cooling; while silver is transported further (Lawless et al., 1999). The Ag:Au ratio of the H zone increases with increasing grade that may suggest the direction of fluid flow to the top level. The high silver contents may also suggest that the H zone occurred distal from source of fluid.

The gold in epithermal environment is dominated by bisulphide complex [$Au(HS)_2^-$] and the silver is dominated by chloride complex [$AgCl_2^-$] under relatively reduced, neutral pH conditions and low temperature (<300°C; Seward and Barnes, 1997; Gammons and William-Jones, 1995) that characterised at the H zone (see Chapter 5).

Low Hg, Sb, and Cu contents of electrum indicate relatively hight activities of fS_2 conditions (Shikazono and Shimizu, 1987).

Gold fineness values for the H zone range between 549 to 691 with an average 609. The range is consistent with gold fineness values reported for other epithermal deposits i.e. 450 to 900 (Morrison et al., 1991). Morrison et al. (1991) suggested that the wide range of values could be explained by the variable ore-deposition mechanisms in epithermal systems including, cooling, boiling and mixing of ore fluids with meteoric fluids.

Epithermal deposits that formed in andesitic host rocks are generally characterised by high fineness values e.g. 720 – 980 based on observation data from Morrison et al. (1991). The H zone mineralisation at Chatree is hosted by andesitic rocks, and hence high gold fineness values could be expected. However, the H zone mineralisation is associated with a K-feldspar-sericite assemblage. This is consistent with the possible explanation for lower values suggested by Morrison et al. (1991).

The thermodynamic modelling of Huston et al. (1992) suggested that high gold fineness (>700) is due to hight temperature (>400°C). The mineralisation of the H zone formed at low temperature (100 to 300°C; based on alteration mineral assemblages), therefore, low gold fineness can be accounted for the H zone.

4.5.2.2. Chalcopyrite disease

Chalcopyrite disease is moderately common at Chatree (Figure 4.22). Traditional interpretations of this texture have suggested that it results from exsolution on cooling of the ore fluids after emplacement (e.g., Craig and Vaughan 1981; Kojima, 1990). However, chalcopyrite will not dissolve in sphalerite unless temperatures exceed 500°C (Craig and Vaughan, 1981). This is well in excess of the estimated temperatures for the H zone at Chatree (~100 to 300°C, see Chapter 5). In lower temperature environments, the texture is more likely to represent chalcopyrite intergrowths or replacement of sphalerite (e.g. Barton and Bethke, 1987; Parr et al., 1995).

4.5.2.3. Sphalerite content

The sphalerite of the H zone has a low Fe content (FeS = 0.13 to 1.91 mole%), consistent with the other epithermal Au-Ag vein-type deposits (Shikazono, 1977). In addition, Hedenquist et al. (2000) suggests that low Fe sphalerite may occur in an intermediate sulphidation-state deposit (Ag and base metal-rich), considered a subset of the low sulphidation style. Whole rock data from the H zone indicates a high silver – gold ratio. When considered with the Fe content of sphalerite, the observation is consistent with those of Vikre (1981), who recognised that the Fe content of sphalerite correlates inversely with the silver content. The low Fe content of sphalerite may also indicate a high sulphur activity of the hydrothermal fluids responsible for mineralisation (Petersen et al., 2004).

4.5.3. Comparative vein study of the H zone with A, D and C zones

Vein morphology, texture, mineralogy and paragenesis of the H zone can be compared with other zones (Table 4.3), including the A and D zones described by Dedenczuk (1998) and the C zone by Greener (1999).

The stages of vein at the Chatree deposit of the H zone with A, C, and D zones are differently interpreted numbers of stages (Table 4.3). However, vein texture and mineralogy are similar, including; crustiform-colloform band, comb, and breccia textures in the ore veins; electrum is the most important ore mineral occuring as disseminate, inclusion within pyrite and in contact with sulphide minerals (e.g. pyrite, sphalerite, chalcopyrite and galena) within quartz and calcite gangue.

The ore vein orientation in the H zone is distinct from the other zones. The A, D and C zones strike about 350° with dipping near vertical but the H zone strikes 250° and dips at 45° with which the other vein stages are associated. The major fault that delivered ore fluids up to H zone may have developed after the main structure (N-S trend), at the northern of the H zone, the major ore vein merges with the ore trend at C zone. The ore veins at H zone may have occurred later than other zones.

The gold fineness of H zone is in a range of the other zones but generally higher than the C zone (~400; Greener, 1999) and less than the A zone (~700; Dedenczuk, 1998).

Table 4.3. Comparison of vein mineralogy and characteristics of the H zone and A, D and C zones, the Chatree Deposit.

Character	A zone (Dedenczuk, 1998)	D zone (Dedenczuk, 1998)	C zone (Greener, 1999)	H zone (This study)
Number of Vein stages	4	6	3	4
Ore vein	Stage 2	Stage 3	Stage 2b	Stage 2
Ore vein orientation	350^0/ near vertical	350^0/ near vertical	350^0/ 50-60^0	250^0/ 45^0
Ore vein texture	Crustiform-colloform band, cockade	Crustiform-colloform band	Crustiform band, comb	Crustiform-colloform band, comb, breccia, vuggy
Ore vein mineralogy	Quartz, calcite, dolomite, jasper, illite/smectite, pyrite, electrum, chalcopyrite, adularia, epidote	Quartz, calcite, dolomite, jasper, illite/smectite, pyrite, electrum, chalcopyrite, adularia, epidote	Quartz, calcite, chalcedony, sphalerite, galena, chalcopyrite, tetrahedrite, electrum, prehnite, adularia, native silver	Quartz, calcite, chlorite, illite, illite-smectite, sericite, ankerite, dolomite, epidote, adularia, pyrite, hematite, rhodochrosite, chalcedony, sphalerite, galena, chalcopyrite, electrum
Ore mineralogy	Electrum with pyrite, chalcopyrite, sphalerite, galena and silver minerals	Electrum with pyrite, chalcopyrite, sphalerite, galena and silver minerals	Electrum with pyrite, chalcopyrite, sphalerite, galena and silver sulphide selenide	Electrum with pyrite, chalcopyrite, sphalerite, and galena
Gold/Silver assay*	1.8 g/t Au, 19 g/t Ag	2 g/t Au, 12 g/t Ag	2.1 g/t Au, 9 g/t Ag	2.1 g/t Au, 9 g/t Ag
Electrum occurrence	Disseminate and inclusion in sulphide minerals	Disseminate and inclusion in pyrite	Bleb with sulphide minerals	Disseminate, inclusion and adjacent with sulphide minerals
Gangue	Quartz and carbonate	Quartz	Quartz	Fine-grained quartz and calcite
Gold fineness	569 – 872	537 – 570	219 – 430	544 – 690

* Data from http://www.kingsgate.com.au, 2004.

4.6. Summary

Table 4.4 summarises the characteristics of vein morphology, vein textures, mineralogy, and paragenesis.

Table 4.4. Summary vein studies of the H zone, Chatree deposit, Thailand.

Stage	Morphology	Texture	Mineralogy	Comment
Stage 1: Hydrothermal Breccia	Irregular veins with 2 m thick and 20 m wide	Breccia - jigsaw-fit	Quartz and pyrite	Formed by failure of the rock with ore-forming fluids influx
Stage 2: Mineralised Vein	Linear and sub-parallel veins, Up to 20 m wide	Crustifrom-colloform banding, comb, breccia and vuggy	Quartz, calcite, chlorite, illite, illite-smectite, sericite, ankerite, dolomite, epidote, adularia, pyrite, hematite, rhodochrosite, chalcedony, sphalerite, galena, chalcopyrite and electrum	Crustiform-colloform banding formed by boiling; Vuggy quartz associated with supergene enrichment; Adularia indicating boiling
Stage 3: Quartz Vein	Linear veins, 2-3cm wide	-	Quartz, calcite pyrite, K-feldspar, and epidote	-
Stage 4: Calcite Veinlet	Linear veins, <1 mm wide	-	Calcite	-
Stage 5: Laumontite Coating	Coating in fractures, cavity fills	-	Laumontite	-

Electrum occurs as free grains, small inclusions and in contact with pyrite, chalcopyrite, galena and sphalerite in quartz and calcite gangue (Figures 4.15 to 4.21). The average gold grade in the H zone is 2-3 g/t. The Ag:Au ratios are 4:1 for the whole rocks and 0.6:1 for the individual grains. Gold fineness for the electrum ranges from 544 to 690 (average 609).

Chapter 5
Hydrothermal Alteration

5.1. Introduction

This chapter documents the mineralogy, distribution and timing of hydrothermal alteration assemblages that occur in the H zone at the Chatree deposit. The hydrothermal alteration study of the H zone was undertaken to better constrain the nature of fluid composition and ore formation.

Hydrothermal fluid has many effects on the wall rock that it flows through for example the removal or leaching of existing minerals in the wall rock, the replacement of the wall rock by secondary hydrothermal phases, and/or secondary minerals deposited via precipitation from the hydrothermal fluid. Hydrothermal mineral assemblages that are controlled by temperature, fluid composition, host rock composition and rock permeability (Thompson and Thompson, 1996) can be used as indicators of temperature range and fluid conditions (Christie and Brathwaite, 2004).

5.2. Methodology

Information regarding the alteration mineralogy in this study has been collected from drill core logging in three selected sections (i.e., 6100N, 6200N, and 6350N) and surface mapping in the H pit. Detailed observations were made on rocks from section 6200N. Alteration minerals were studied by standard optical microscopy. Select samples retrieved from drill cores were analysed by a Portable Infrared Mineral Analyser (PIMA). Mineral identification from individual-spectra was made using the Spectral Geologist v3.0 (Ausspec International) software. The PIMA measures reflectance in the SWIR range of 1,300 to 2,500 nanometers. This range absorbs compounds including H_2O, CO_3, NH_4, AlOH, MgOH and FeOH molecular bonds. Therefore, PIMA is useful to determine phyllosilicates, carbonates, hydroxylates silicates and sulphates. Estimation of relative abundances of the dominant minerals and mineral compositions were identified by using specialised software (TSG) to compare the relative magnitudes of absorption features at various wavelengths in SWIR reflectance spectra. The TSG software automates the interpretation process by matching the measured signal with reference mineral signatures present in its exclusive database. K-feldspar staining was used for identifying K-feldspar in host rocks and veins.

Electron microprobe analysis was used for studying mineral compositions for important phases such as chlorite. Chlorite occurs throughout the H zone and its Fe:Mg ratios were investigated to estimate the temperature of formation and test for any significant relationships to gold grade.

5.3. Alteration and mineralogy

This section describes alteration minerals, their textures, distribution of the minerals, and relationship with the central vein system.

5.3.1. Silica alteration assemblages

Silica alteration involves the infilling by quartz and chalcedony in void spaces (such as vesicles and open fracture), as partial to total replacement of both phenocrysts and groundmass in the host rocks (Figure 5.1) and quartz-carbonate veins. Silica alteration is extensive and recognised by multiple generations of quartz and chalcedony and best developed in the ore zone and ~15m below ore veins.

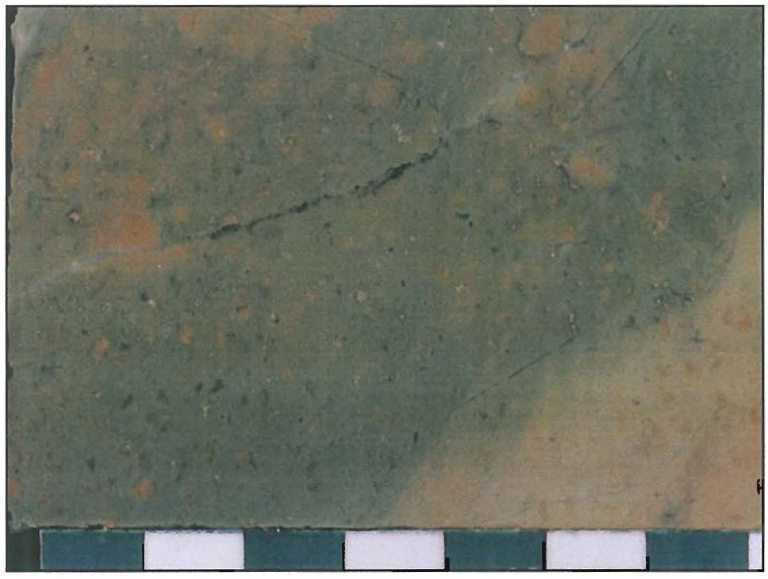

Figure 5.1. Photograph showing silica alteration in andesitic lithic breccia, Sample No. RCD 1112.48.

Quartz occurring in void space and replacing original minerals is typically characterised by microgranular/crystalline quartz with an average grain size of 10 μm (e.g. in Sample No. RCD 357.89; Figure 5.2). Quartz alteration occurs in quartz-carbonate veins with about 40 vol% quartz replacement of pre-existing quartz and calcite crystals. Quartz replacement of the host rocks is both selective and pervasive

within groundmass (less than 5 vol%) and within phenocrysts (less than 10 vol%), mostly occuring as fine, anhedral interlocking grains intergrown with chlorite, illite-smectite and adularia. Quartz infilling open space is coarser-grained (up to 5mm) and is associated with base metal minerals and other alteration minerals such as adularia, calcite, pyrite, chlorite and illite. Quartz also occurs as irregular veinlets that increase in abundance toward major veins (~5m from ore veins).

Chalcedony is cryptocrystalline silica that occurs in colloform-crustiform banded veins with quartz. It has formed after the first quartz alteration, with about 5 vol% replacement within quartz veins.

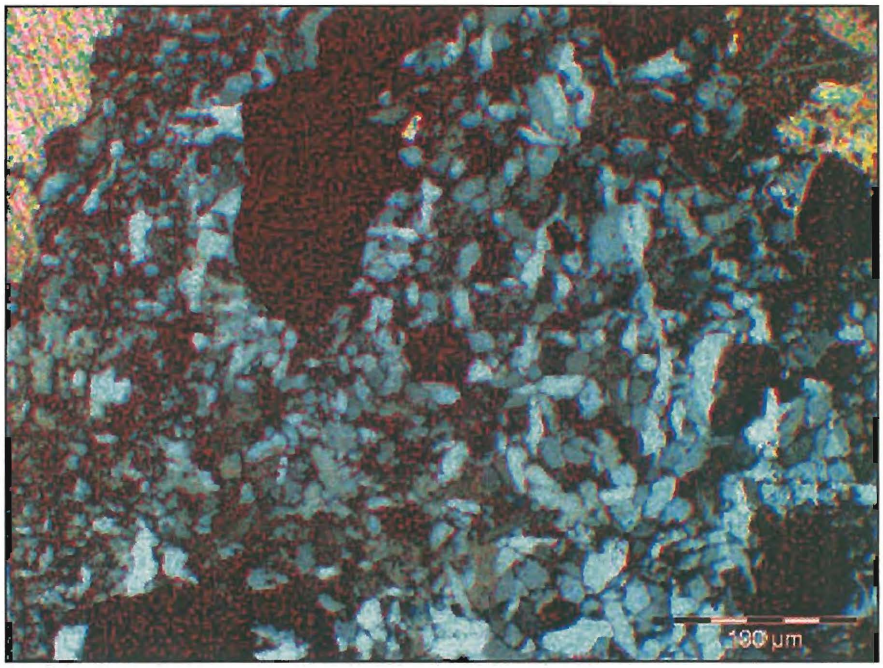

Figure 5.2. Photomicrograph showing fine-grained quartz alteration in quartz-carbonate mineralised vein (cross-polarised light), Sample No. RCD 357.89.

5.3.2. Albitic alteration assemblages

Albitic alteration assemblage may be as much as 10 vol% selective replacement by albite overgrowths on plagioclase phenocrysts and groundmass of the andesitic host rocks. Albite alteration is typically associated with sericite, chlorite, quartz and calcite in a distal zone from the mineralised veins (~20m from ore veins) and is replaced by chlorite, sericite and calcite. Albite alteration occurred earlier than other alteration assemblages.

5.3.3. Argillic alteration assemblages

Argillic alteration assemblages include kaolinite, montmorillonite, and interlayered illite-smectite (Figure 5.3). Argillic alteration assemblages occur widely in both veins and host rocks, and overprint other mineral alteration assemblages, both proximal and distal from the mineralised veins. Argillic alteration assemblages occur above the central veins in the H zone and are most common in crystal-rich andesitic pumice breccias.

Kaolinite occurs in sheared near surface hanging wall rocks and has been detected by PIMA. It occurs as a pervasive replacement (about 40-60 vol%) of the host rocks (e.g., Sample No. HP 01), as infill in veins and open-space or as a selective replacement of feldspars and quartz. Outcrops containing kaolinite are typically soft and white to tan colour.

Montmorillonite has been detected by PIMA in samples from the sheared hanging wall, associated with kaolinite in outcrop. Montmorillonite occurs as pervasive alteration of quartz and feldspar (30 vol% replacement).

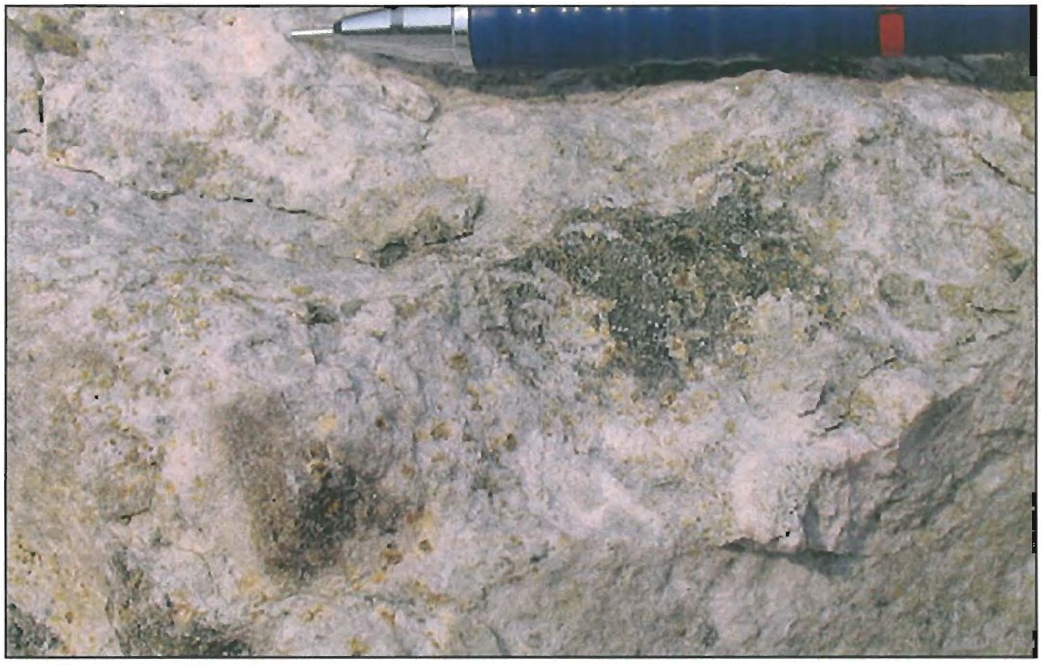

Figure 5.3. Photograph showing argillic alteration (characterised by kaolinite and montmorillonite) in the sheared hanging wall of the H pit.

5.3.4. Carbonate mineral alteration assemblages

Carbonate mineral alteration assemblage includes calcite, dolomite, ankerite, and rhodochrosite.

Calcite is the major carbonate minerals found in the H zone and is typically found in Stage 2 to 4 veins (see Chapter 4) but also replacing minerals in the wall rocks. Calcite is typically crystalline with distinct rhombohedral cleavage and varies in size up to 5 cm. Calcite alteration represents about 10 vol% when occurring as a selective replacement of the host rock, and 40 to 60 vol% when occurring in quartz veins (observed in all vein samples). Abundant calcite alteration occurs proximal to the mineralised veins. Calcite partly replaces phenocrysts of plagioclase and pyroxene and locally floods the groundmass. Late-stage calcite forms numerous massive and barren veins, veinlet (Stage 4 veins; see Chapter 4) and open-space fill within quartz-carbonate veins (Figure 5.4).

Other carbonate minerals including ankerite, rhodochrosite and dolomite have been confirmed by PIMA. Dolomite replaces ~5 to 10 vol% of calcite crystals. Ankerite and dolomite occur proximal to the mineralised veins. Rhodochrosite replaces calcite (Figure 5.5), and quartz, and has formed after the other carbonate minerals.

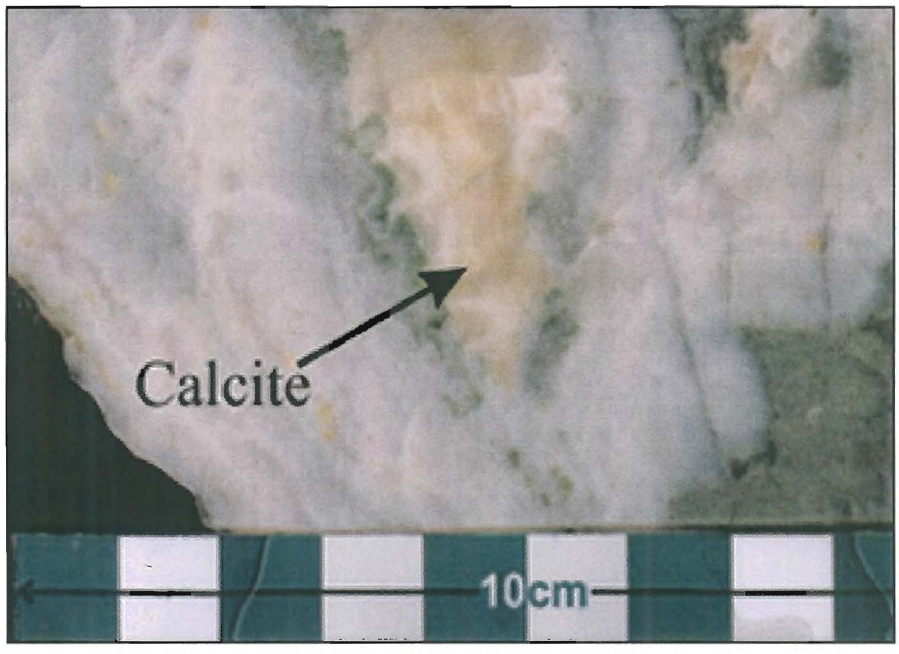

Figure 5.4. Photograph showing calcite infilling open-spaces in quartz within a quartz-carbonate mineralised vein, Sample No. RCD 499.97.

Figure 5.5. Photograph showing rhodochrosite in quartz-carbonate vein, Sample No. RCD 394.36.

5.3.5. Chloritic alteration assemblage

Chlorite is found in almost every sample and typically occurs in both host rocks and within veins and in the footwall of the H zone. It forms a pervasive alteration (~5 to 20 vol%) of the groundmass in the host rocks, and as a selective alteration of pyroxene and amphibole phenocrysts (up to 90 vol% replacement), lithic and pumice clast (~60 vol%), patches and bands in quartz-carbonate veins (~20 vol%; Figure 5.6). Chlorite and K-feldspar alterations often occur replacing lithic clasts of the andesitic lithic breccia (Figure 5.7). Chlorite is locally replaced by sericite, epidote and illite.

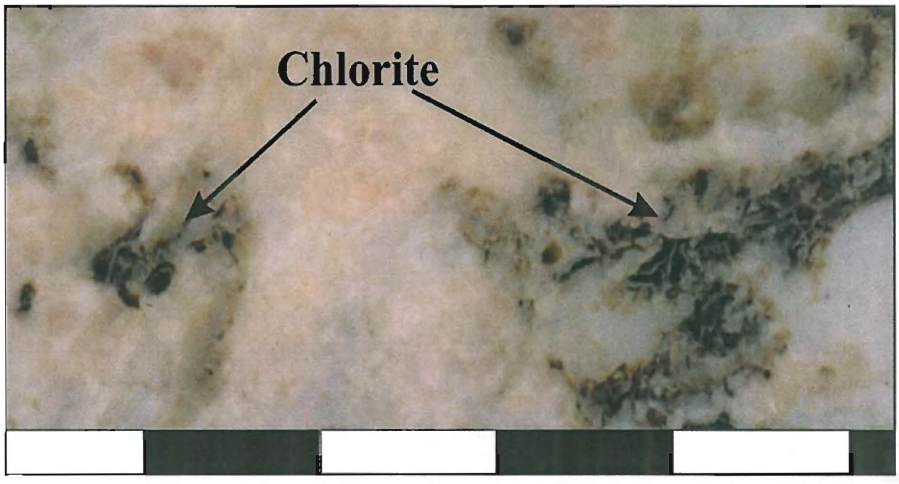

Figure 5.6. Photograph showing chlorite replacement in quartz-carbonate vein, Sample No. RCD 374.26.

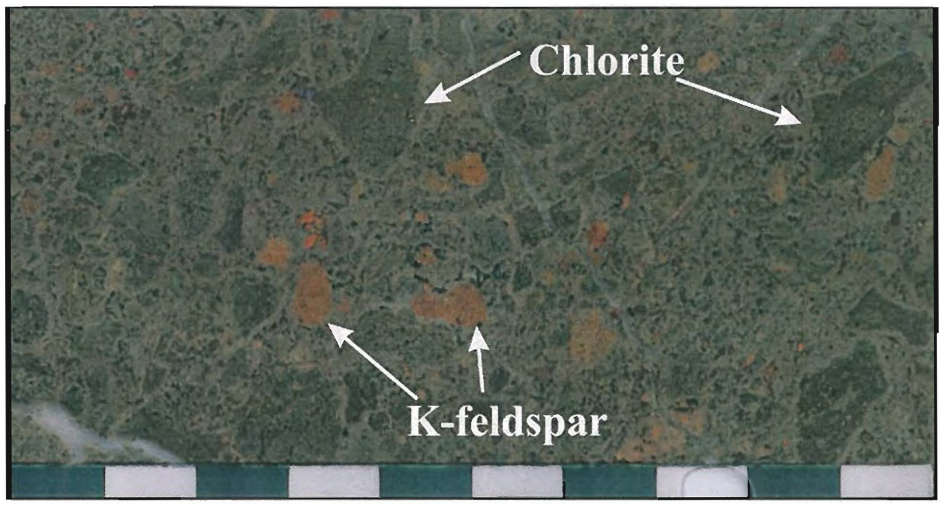

Figure 5.7. Photograph showing K-feldspar and chlorite alteration replacing lithic clasts of andesitic lithic breccia, Sample No. RCD 1113.121.

5.3.6. Potassic alteration assemblages

Adularia characterises the potassic alteration assemblages and occurs as pink vein selvages (<1cm; Figure 5.8), and euhedral rhombic crystals, typically less than 0.05mm across. Adularia is generally intergrown with quartz and calcite in the mineralised veins (~5 vol%) and as replacement of plagioclase phenocrysts and groundmass of the andesitic host rocks, and clasts of the breccia host rocks (~15 vol%). Adularia alteration is typically found in the central veins and ~10m from the central veins. Adularia is difficult to identify in hand specimens, however, chemical staining clearly distinguishes its occurrence (Figure 5.9). Secondary adularia maybe altered to illite (e.g. Sample No. RCD 357.89 and RCD 344.15; Figures 5.10 and 5.11).

Figure 5.8. Photograph showing K-feldspar halo around quartz veins that have undergone epidote replacement. Footwall at the H pit.

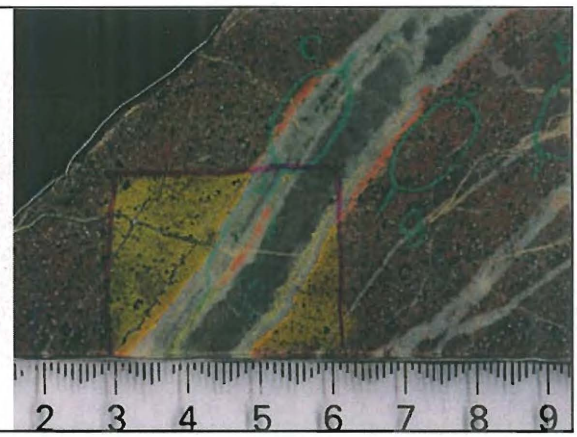

Figure 5.9. Photograph showing K-feldspar alteration highlighted by yellow staining of plagioclase-pyroxene-phyric andesite, Sample No. RCD 1122.24.

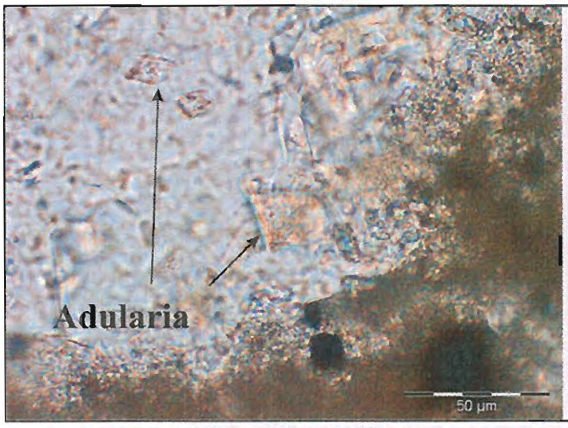

Figure 5.10. Photomicrograph showing adularia alteration of crystal-rich quartz-feldspar breccia, note rhomb-shaped adularia crystals (cross polarised light), Sample No. RCD 344.15.

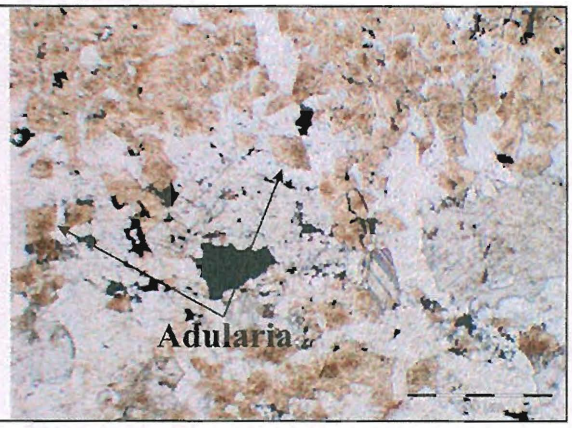

Figure 5.11. Photomicrograph showing adularia in a quartz-carbonate mineralised vein, note rhomb-shaped adularia crystals. Adularia is in turn being replaced by illite (cross polarised light), Sample No. RCD 357.89.

5.3.7. Phyllic alteration assemblages

Phyllic alteration assemblages are characterised by illite and sericite in association with quartz. They are responsible for a pervasive bleached appearance to the host rocks (Figure 5.12).

Illite and illite-smectite (as detected by PIMA) typically occur as a replacement of plagioclase and pyroxene phenocrysts and groundmass of andesite and form a significant constituent in the matrix and clasts of the host rocks (~20 vol% of original rocks), sometimes destroying the original texture. Illite and illite-smectite also replace adularia and calcite in quartz-carbonate veins. The amounts of illite and illite-smectite generally increase away from the central veins (Stage 2 veins see Chapter 4).

Sericite is a fine-grained white mica and typically white to pale yellow and is seen as vein selvage. Sericite occurs as both pervasive and selective alteration within most samples that proximal to central veins. It occurs selectively replacing pyroxene and feldspar phenocrysts, quartz and totally replacing calcite, adularia and epidote. Sericite replaces ~20 vol% of the original minerals (e.g. feldspar, pyroxene, quartz and adularia) in the host rock with up to 60 vol% replacement in veins (Figure 5.13).

Figure 5.12. Photograph showing sericite alteration halo around quartz-carbonate-chlorite vein, Sample No. RCD 1109.72.

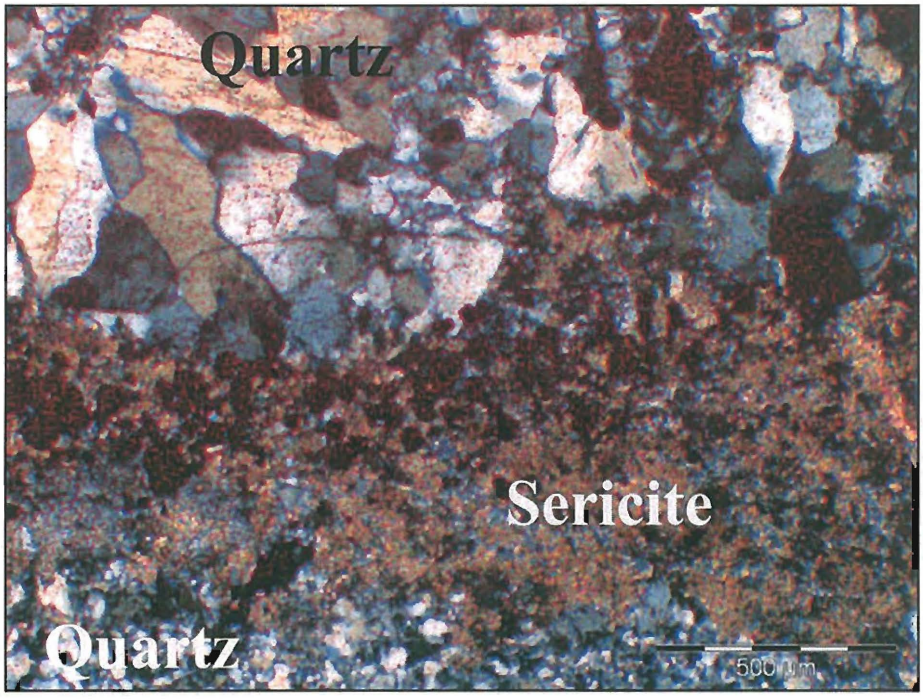

Figure 5.13. Photomicrograph showing sericite alteration in a quartz vein with pyrite alteration (cross-polarised light), Sample No. RCD 1109.75.

5.3.8. Propylitic alteration assemblages

Propylitic alteration assemblages comprise chlorite, epidote, prehnite, sericite, quartz, albite, carbonates, pyrite, and hematite.

Epidote selectively replaces plagioclase phenocryst, the groundmass of the andesitic host rocks (~5 vol%) and forms an open space infill and within veins (~10 vol%; Figure 5.14). Epidote forms clusters of euhedral columnar crystals intergrown with calcite, K-feldspar and quartz. Epidote generally occurs outside the ore zone (~20m from the central veins) and is associated with prehnite (Figure 5.15).

Hematite is fine-grained, giving a red stain to the host rocks, and occurs intergrown with other minerals in veins (Figures 5.14 and 5.15). Hematite is generally less than 5 vol% around grain boundaries and fractures. Hematite is found within the central veins and ~15m from the central ore veins.

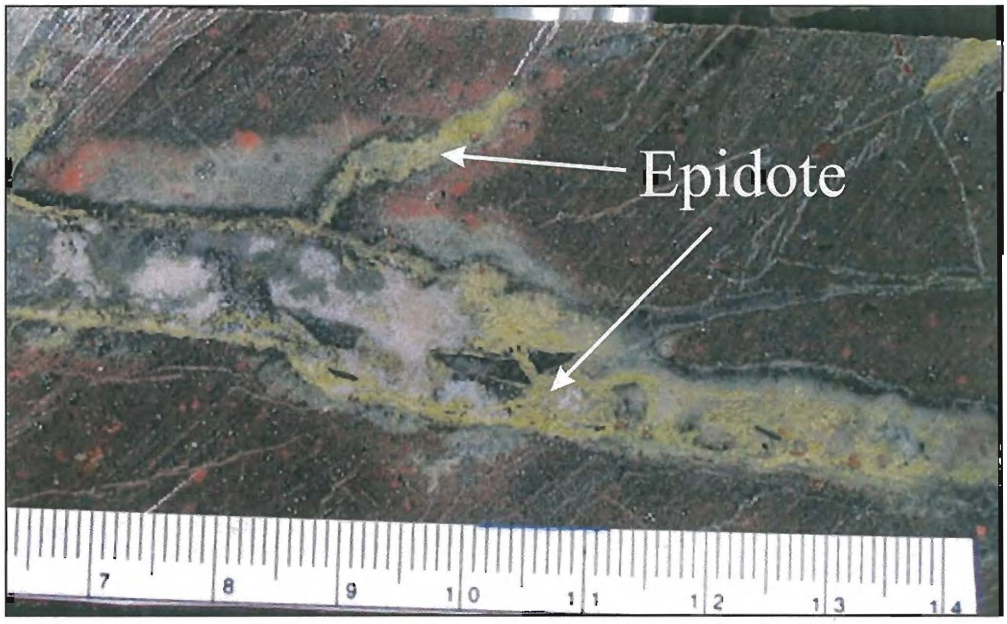

Figure 5.14. Photograph showing epidote alteration within carbonate-quartz vein, Sample from RCD 1122.

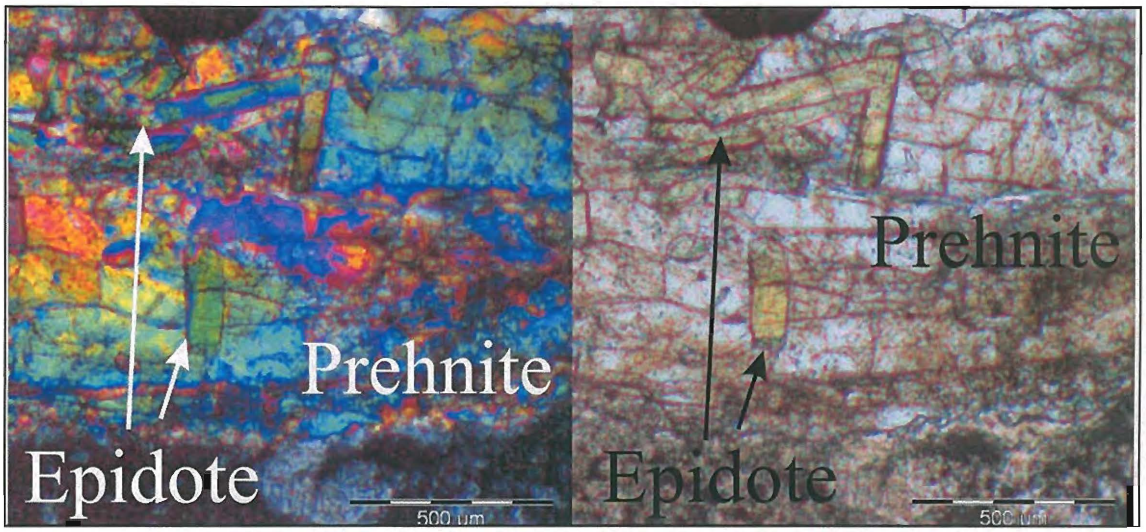

Figure 5.15. Photomicrograph showing epidote and prehnite alteration within carbonate-quartz vein (cross polarised light), Sample No. RCD 450.29.

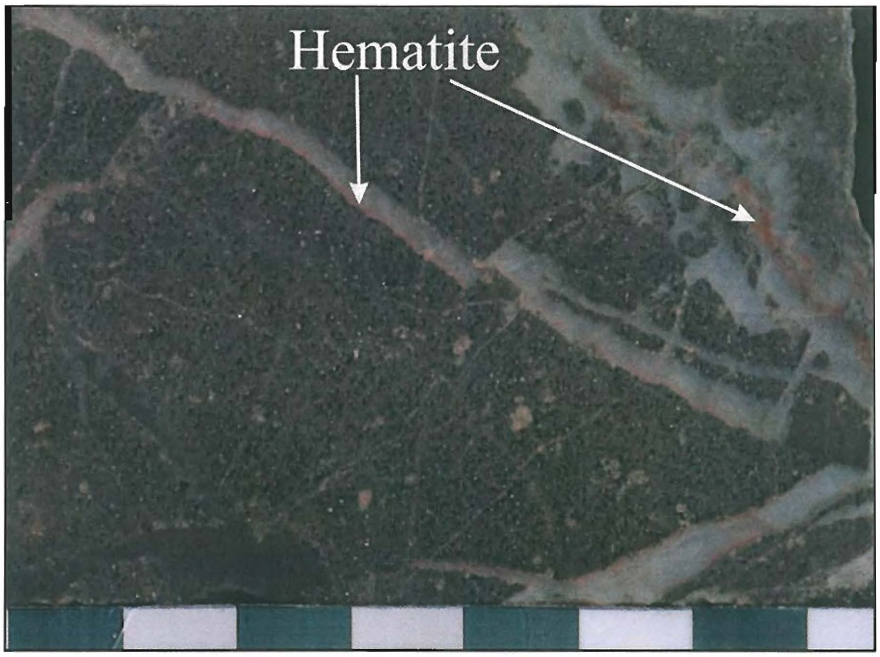

Figure 5.16. Photograph showing hematite alteration within quartz vein, Sample No. RCD 344.15.

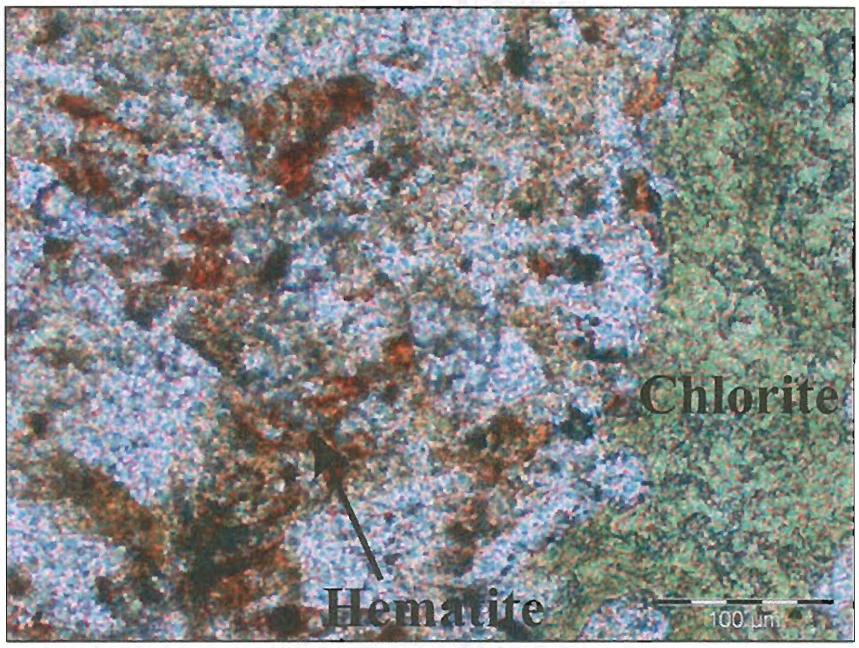

Figure 5.17. Photomicrograph showing hematite and chlorite alteration within quartz-carbonate mineralised vein (cross polarised light), Sample No. RCD 453.44.

5.3.9. Sulphide minerals

Sulphide minerals occurring in the H zone include pyrite, sphalerite, chalcopyrite and galena. Pyrite is the most abundant sulphide mineral and replaces phenocrysts and groundmass of the andesitic host rocks, clasts and matrix of breccia host rocks and quartz, calcite, chlorite and sericite within veins. Pyrite occurs as cubic crystals and generally found in the hanging wall host rocks where it represents ~10 vol% of the rocks (Figure 5.18). The other sulphide minerals (e.g., sphalerite, galena, and chalcopyrite) generally replace pre-existing minerals and represent ~5 vol% within quartz and calcite grains (Figure 5.19). Sphalerite, chalcopyrite and galena, rarely found in the host rocks, are more common within veins.

Figure 5.18. Photograph showing cubic pyrite in hanging wall rocks of the H pit.

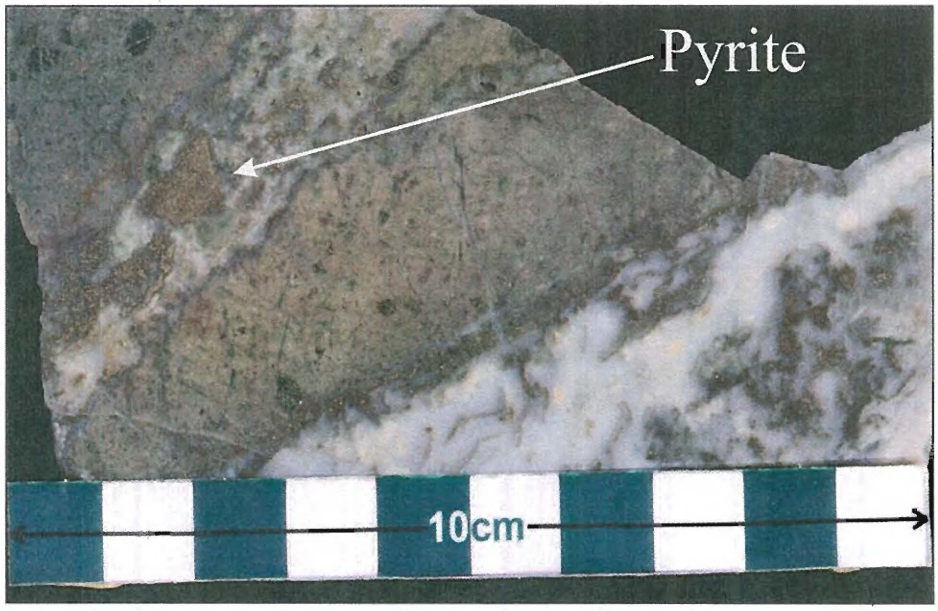

Figure 5.19. Photograph showing pyrite alteration within quartz-chlorite vein, Sample No. RCD 1109.75.

5.3.10. Zeolitic alteration assemblages

In the H zone, the most abundant zeolite mineral is laumontite. Pink laumontite occurs as a coating on fractures, cavity fills and within some veins. Laumontite represents <3 vol% and post-dates all other alteration assemblages.

Figure 5.20. Photograph showing pink laumontite occurs as a coating in fractures, Sample from RCD 1109.

5.4. Discussion

5.4.1. Alteration zones and equilibrium alteration assemblage

By studying alteration zones and the minerals assemblages, inferences can be made about the fluid conditions responsible for the alteration. There are many types of alteration minerals occurring in diverse assemblages in the H zone. Five broad alteration zones (Figure 5.21) have been identified in this study including;

- Zone I (Kaolinite - montmorillonite - illite - pyrite);
- Zone II (Quartz - carbonate - illite - chlorite - pyrite - sericite - adularia);
- Zone III (Illite - chlorite - adularia - quartz - carbonate - epidote – sericite – albite - prehnite);
- Zone IV (Epidote - chlorite - illite);
- Supergene enrichment alteration.

5.4.1.1. Zone I

Zone I is characterised by kaolinite and montmorillonite, with lesser amounts of pyrite and illite and has been classified as argillic alteration. Zone I occurs in the hanging wall at the shallow depth (~50m from the surface) above the gold-rich vein system and has a sheet-like geometry. The zone of alteration is intense, suggesting that the host rock had high permeability, however, many original textures are still preserved. Alteration affected crystal-rich andesitic pumice breccias with high permeability.

Kaolinite usually forms in the-near surface, steam-heated environment above the groudwater level, from low temperature acidic waters, at temperatures around 100°C (White et al., 1999) and with a pH of 2 - 3 (Lawless et al., 1999).

Montmorillonite occurs as a replacement of ferro-magnesian minerals from near-neutral pH, chloride hydrothermal waters, deuteric processes, or as a product of weathering. In the hydrothermal environment, montmorillonite forms from fluids less than 150°C (Lawless et al., 1999).

Kaolinite and montmorillonite occurring together at Zone I assume as coexist in equilibrium, Zone I is interpreted to have formed by low temperature (100°C to 150°C), acid to neutral hydrothermal fluids with low salinity. Simmons and Browne (2000) suggested that an argillic alteration (illite-smectite-calcite±kaolinite assemblage) at the shallow depths and on the margin of geothermal systems occurred by steam-heated waters. Zone I of the H zone that includes an argillic alteration may be also produced by steam-heated waters.

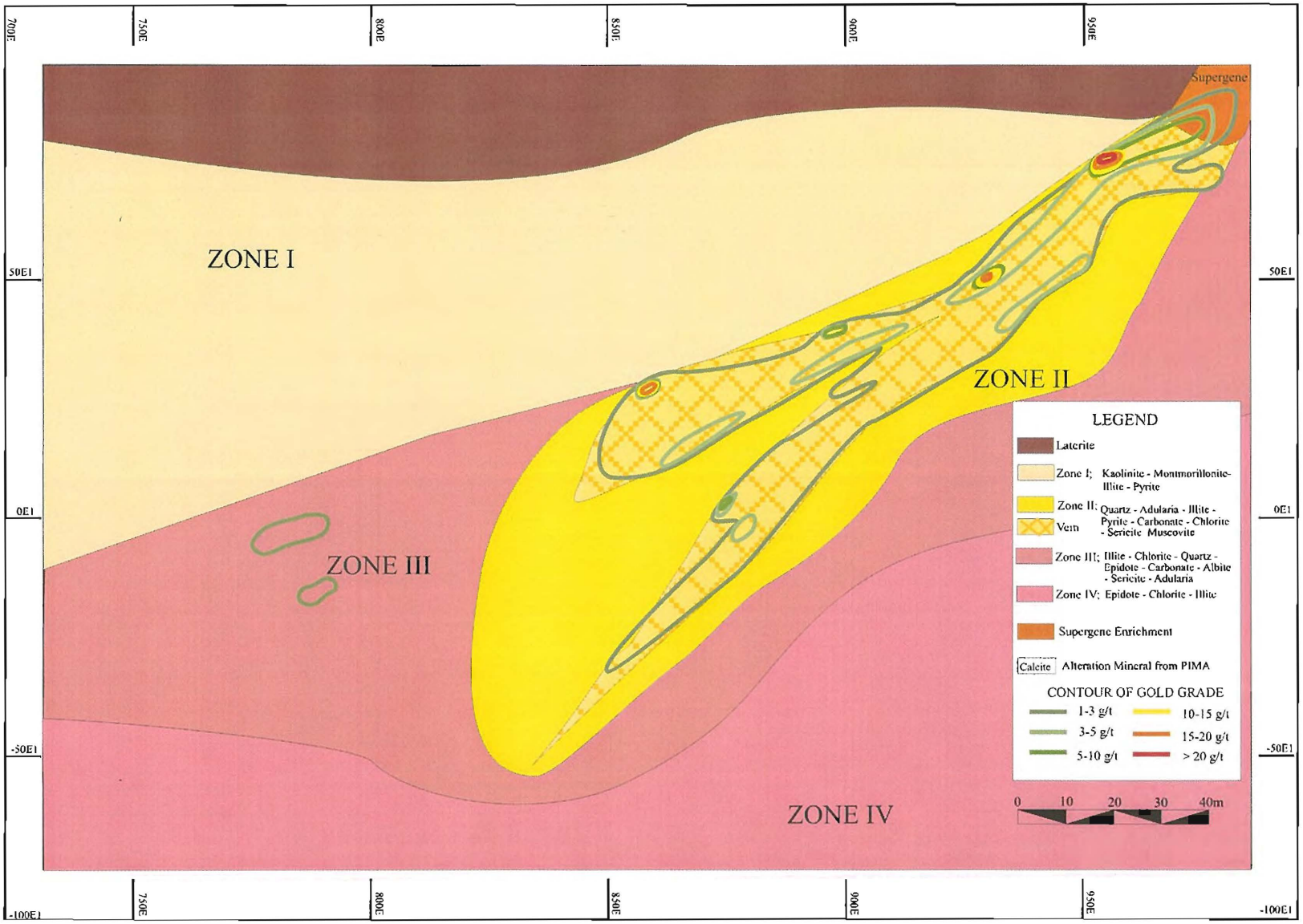

Figure 5.21. Cross-section for Section 6200N of the H zone showing alteration zones that have been identified by PIMA

5.4.1.2. Zone II

Zone II includes several alteration minerals assemblages, including silica, potassic and phyllic alteration assenblages and is proximal to the mineralised veins. The alteration minerals selectively replace the host rock within the altered vein envelope. Alteration halos are commonly characterised by white to pale yellow sericite and pink K-feldspar alteration.

Quartz is a common alteration mineral in this zone found in stockwork veins and silica flooding of the host rocks. Quartz precipitates in a wide temperature range and generally forms as a result of decreasing fluid temperature (Thompson and Thompson, 1996). Abundant fine-grained quartz suggests temperature were over 180 - 190°C (Simmons and Christenson, 1994).

Adularia is found in both the gold rich veins and as an alteration product of the host rock. Adularia formation may occur due to gas loss, pH increases and cooling and good permeability in reservoir production zones (Simmons et al., 2000). Studies of active geothermal sytems (Simmons and Christenson, 1994) and thermodynamic studies (Reed and Spycher, 1985) suggest that adularia in veins is a good indicator for boiling. Adularia precipitates from near neutral to alkaline fluid with pH > 5.2 (Lawless et al., 1999).

Illite dominates at temperature >220°C (Christie and Brathwaite, 2004), and forms from near-neutral pH to slightly acid fluids (Thompson and Thompson, 1996). Illite interlayered with illite-smectite suggests that temperatures were less than 200°C.

Sericite is fine-grained white mica that forms under slightly acid conditions with pH 4 - 6 and temperatures ~200 - 250°C (Thompson and Thompson, 1996). Sericite replaces other alteration types and is associated with fractures.

Carbonate minerals are mainly found in veins and have variable compositions, suggesting a range of fluid temperature, pressure and chemical conditions during their formation. Calcite is the major carbonate mineral in the H zone and forms over a wide temperature range. Calcite occurring in open-spaces may form from boiling and exsolution of CO_2. Dolomite overprints calcite, and is deposited from near-neutral fluids. It commonly precipitates from fluid with temperatures < 200°C and rarely > 250°C (Lawless et al., 1999). Ankerite is a late replacement phase in veins. Ankerite and dolomite may form by fluid mixing in cooler zones (Lawless et al., 1999).

Chlorite replaces both host rocks and alteration minerals. The presence of chlorite can indicate near neutral fluids of pH of 6 - 7 (Lawless et al, 1999), and

suggests the lack of intense ion exchange. Chlorite is commonly found in distal and impermeable zones (Lawless et al, 1999). Chlorite of the H zone is dominantly Mg-rich chlorite (Fe/Fe+Mg<0.5; Appendix C), which is considered to form during the interaction of cold meteoric water with hot hydrothermal fluid (Thompson and Thompson, 1996).

5.4.1.3. Zone III

Zone III occurs stratigraphically below Zone II. This zone is found about 20m from central veins (Stage 2 veins in Chapter 4). Major alteration minerals in Zone III include illite, chlorite, albite, adularia and sericite with minor quartz, calcite, rhodochrosite, epidote and prehnite.

Epidote typically forms at temperatures in excess of 230°C, from near-neutral pH fluid, with moderate to high Cl, low to moderate CO_2 and high Si (Thompson and Thompson, 1996). Epidote indicates the bottom of the epithermal zone (upper temperature limit).

Propylitic alteration occurs at low temperature (200 - 300°C) in a distal setting (Lawless et al., 1999) and forms from near-neutral pH fluids.

5.4.1.4. Zone IV

Zone IV is located in the deepest part of the deposit, and is typically not associated with ore-grade mineralisation. Zone IV consists of the propylitic alteration zone which is characterised by dark green epidote replacement of minerals within veins and selective replacement by chlorite and illite. Propylitic alteration forms at moderate temperatures (mostly 200 - 250°C), in the presence of near-neutral pH fluids with a range of salinities, usually in low permeability areas (Lawless et al., 1999). Zone IV can be associated with the assemblage of chlorite-calcite-illite-quartz where host rock is more permeable.

5.4.1.5. Supergene enrichment alteration

The data from Akara Mining shows unusual high gold assays in vuggy quartz breccia near the surface e.g. sample from drill core no. RCD356 that has gold grade >100 g/t is characterised by carbonate-leached quartz breccia. The vuggy quartz breccia has been resulted from supergene enrichment and occurs in an area where the water table lies close to the surface.

5.4.2. The Fe/(Fe+Mg) of chlorite and Au grade

Chlorite compositions were determined by using the PIMA and electron microprobe analyses. The PIMA generally detected more Mg-rich than Fe-rich chlorites. This abundance was confirmed by the electron microprobe, which indicated a Fe/(Fe+Mg) ratio from 0.09 to 0.45 (Table 5.1). Figure 5.22 shows a broad positive relationship between the Fe/(Fe+Mg) of chlorite and Au grade in the H zone. One of the determining factors causing Fe/Mg substitutions in chlorite is fO_2 (de Caritat et al. 1993). With increasing Fe contents relative to Mg are associated with low fO_2, suggesting that gold precipitation in the H zone may be related to redox condition of ore fluids.

5.4.3. Chlorite geothermometry

Chlorite alteration is abundant in both andesitic host rocks and Stage 2 veins. Electron microprobe analysis was conducted on 37 chlorites from the H zone to determine their average composition (Appendix C). Tetrahedral (Al^{IV}) was used to calculate temperature of formation for the respective chlorites by an equation (1) from Cathelineau and Nieva (1985).

$$T°C = -61.9229 + 321.9972\ (Al^{IV}) \qquad (1)$$

The calculated temperatures range from 132.6°C to 514.4°C (Table 5.1). There are no obvious distinctions in the composition or temperatures between chlorites from the host rocks and ore veins.

An interpretation of the complete alteration assemblage in the H zone at Chatree suggests that all minerals have been deposited at temperatures between 100°C to 300°C. This range is consistent with the temperature range found in other low sulphidation epithermal deposits (Hedenquist et al., 2000).

Most of the temperatures derived from chlorite geothermometry are not in agreement with the range interpreted for the entire alteration assemblage. It is generally accepted that chlorite geothermometry should be used with caution and/or in conjunction with other temperature determining methods (Walshe, 1986; Cathelineau, 1988; de Caritat et al. 1993). This is due to range of parameters that can influence the chlorite composition including fluid pH, bulk rock composition and fO_2 (de Caritat et al. 1993). The Fe:Mg ratio of chlorite coexisting with other silicates (e.g. K-feldspar + smectite, smectite + illite) at a fixed temperature and pressure is directly related to fO_2 (de Caritat et al. 1993). Chlorite from the H zone at Chatree is Mg-rich (Fe/(Fe+Mg)

ratio <0.5) suggesting that fO_2 has played a dominant role in determining the composition of the chlorite and not temperature.

Table 5.1. Table of geothermometry and composition of chlorite from the H zone, Chatree deposit, Thailand

Sample	Description	Si	Al	Mg	Fe	AlIV	Fe/(Fe+Mg)	Temperature
RCD499-95_chl1	from andesitic rocks	6.18	4.64	6.57	1.48	2.81	0.18	391
RCD499-95_chl2	from andesitic rocks	6.09	4.55	6.64	1.55	2.73	0.19	378
RCD499-95_chl3	from andesitic rocks	6.11	4.77	6.13	1.71	2.95	0.22	413
RCD499-95_chl4	from andesitic rocks	6.22	5.00	5.98	1.52	3.18	0.20	450
RCD499-95_chl5	from andesitic rocks	6.13	4.67	6.37	1.65	2.85	0.21	397
RCD499-95_chl6	from andesitic rocks	6.13	4.96	6.10	1.58	3.14	0.21	444
RCD394-35_chl7	from quartz-calcite vein	7.17	3.17	5.23	2.84	1.35	0.35	155
RCD394-35_chl8	from quartz-calcite vein	6.29	3.91	4.31	4.83	2.09	0.53	274
RCD394-35_chl9	from quartz-calcite vein	6.71	3.66	5.52	3.10	1.84	0.36	234
RCD394-35_chl10	from quartz-calcite vein	7.24	3.03	5.48	2.79	1.21	0.34	133
RCD1109.76_chl11	from quartz-calcite vein	5.97	4.54	5.43	3.40	2.72	0.39	376
RCD1109.76_chl12	from quartz-calcite vein	5.98	4.46	5.64	3.32	2.64	0.37	363
RCD1109.76_chl13	from quartz-calcite vein	5.95	4.47	5.59	3.41	2.65	0.38	365
RCD1109.76_chl14	from quartz-calcite vein	6.05	4.46	5.41	3.40	2.64	0.39	363
RCD499.94_chl15	from quartz-calcite vein	6.13	4.68	6.39	1.46	2.86	0.19	398
RCD499.94_chl16	from quartz-calcite vein	5.95	4.81	6.42	1.53	2.99	0.19	419
RCD499.94_chl17	from quartz-calcite vein	6.02	4.88	6.38	1.37	3.06	0.18	431
RCD504.124_chl18	from quartz-calcite vein	6.18	4.38	7.58	1.15	2.56	0.13	350
RCD504.124_chl19	from quartz-calcite vein	6.91	4.86	4.73	1.84	3.04	0.28	427
RCD504.124_chl20	from quartz-calcite vein	7.19	4.22	5.45	1.55	2.40	0.22	324
RCD505.110_chl21	from quartz-calcite vein	6.90	3.32	7.95	0.88	1.49	0.10	179
RCD505.110_chl22	from quartz-calcite vein	6.94	3.31	7.92	0.82	1.48	0.09	177
RCD505.110_chl23	from quartz-calcite vein	6.93	3.32	7.91	0.86	1.50	0.10	179
RCD358.80_chl24	from quartz-calcite vein	6.21	4.74	6.54	1.33	2.92	0.17	408
RCD358.80_chl25	from quartz-calcite vein	6.17	4.82	6.52	1.34	2.99	0.17	420
RCD358.80_chl26	from quartz-calcite vein	5.94	4.56	7.02	1.69	2.74	0.19	379
RCD358.80_chl27	from quartz-calcite vein	5.98	4.63	6.91	1.58	2.80	0.19	389
RCD358.80_chl28	from quartz-calcite vein	6.11	4.36	7.07	1.53	2.53	0.18	346
RCD505.111_chl29	from quartz-calcite vein	6.18	4.50	5.82	2.58	2.68	0.31	369
RCD505.111_chl30	from quartz-calcite vein	6.10	4.45	6.09	2.56	2.63	0.30	361
RCD505.111_chl31	from quartz-calcite vein	6.05	4.68	5.40	2.93	2.86	0.35	399
RCD505.111_chl32	from quartz-calcite vein	6.22	4.67	5.07	2.77	2.85	0.35	397
RCD505.111_chl33	from quartz-calcite vein	6.65	5.14	3.99	2.26	3.32	0.36	472
RCD1109.75_chl34	from andesitic rocks	5.76	5.40	4.45	3.82	3.58	0.46	514
RCD1109.75_chl35	from andesitic rocks	5.72	5.14	4.76	3.93	3.32	0.45	472
RCD1109.75_chl36	from andesitic rocks	5.64	5.12	4.99	3.98	3.30	0.44	469
RCD1109.75_chl37	from andesitic rocks	5.65	5.13	4.85	4.04	3.31	0.45	471

* Temperatures were calculated using equation from Cathelineau & Nieva (1985) ------ T°C = -61.9229 + 321.9972 (Al^{IV})

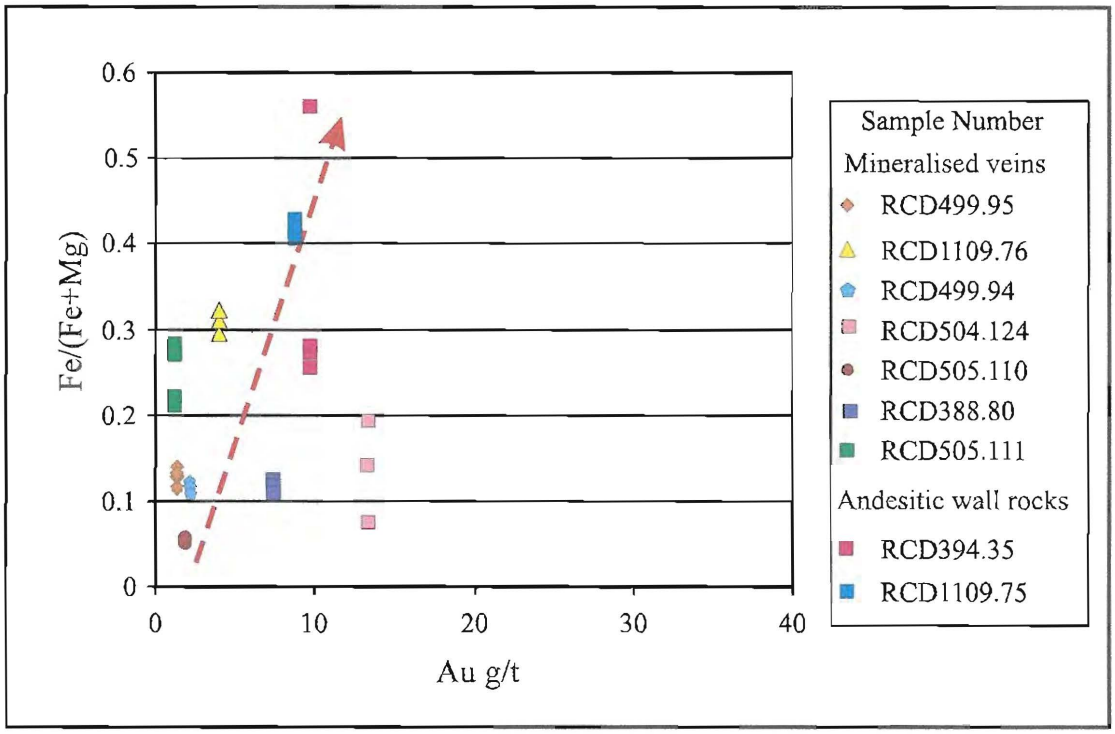

Figure 5.22. Relationship between Au grade and Fe/(Fe+Mg) of chlorite from samples of the H zone, Chatree deposit, Thailand.

5.4.4. Comparison between the H zone and low-sulphidation epithermal deposits

The nature of alteration zones and their distribution patterns at the H zone are similar to those encountered in other low-sulphidation epithermal deposits described by Hedenquist et al. (2000). Figure 5.23 shows the relationship between the alteration zone at the Chatree deposit and an idealised low-sulphidation system. Similarities between the H zone and other epithermal systems include;

- The upper sections of low-sulphidation deposits as capped with a blanket of kaolinite, cristobalite, smectite, locally alunite and native sulphur (advance argrillic alteration), which usually overlies the ore system in the hanging wall. This alteration assemblage is comparable with the Zone I of the H zone, although mineralogy in the H zone consists of kaolinite, montmorillonite, illite and pyrite, suggesting an argillic or intermediate argillic assemblage rather than advance argrillic alteration.
- Hedenquist et al. (2000) indicates that a chalcedony blanket underneath the water table and silica sinter may also be present. These are not observed in the H zone.
- The model of Hedenquist et al. (2000) indicates that ore veins occur within a zone of quartz, chalcedony, carbonates, adularia and barite ± fluorite. Zone II in the H zone, which hosts the ore zone and comprises similar minerals (e.g. quartz, chalcedony,

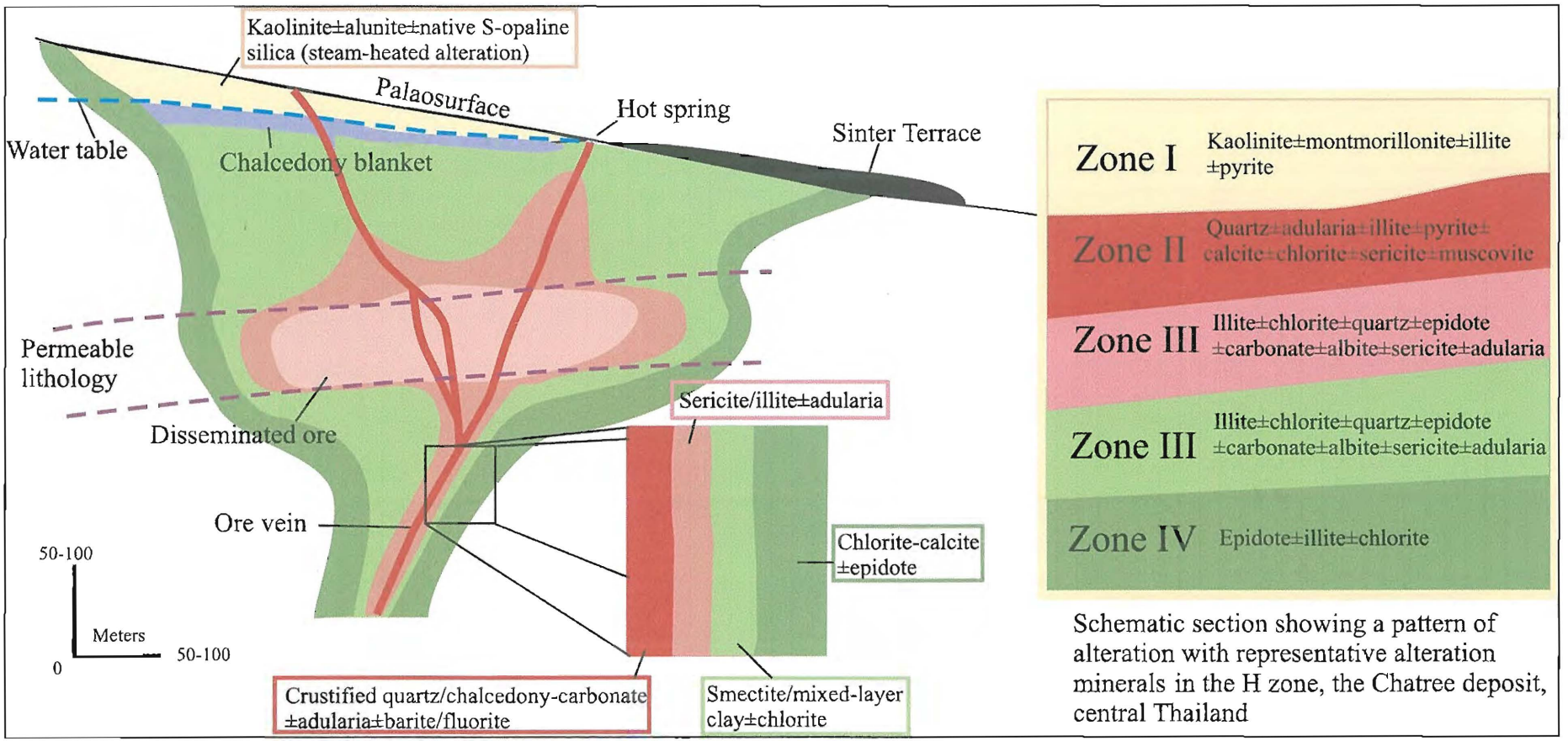

Schematic section showing a pattern of alteration with representative alteration minerals in the H zone, the Chatree deposit, central Thailand

Figure 5.23. Schematic diagram showing comparison of general low-sulfidation alteration pattern (after Hedenquist et al., 2000) and alteration zones in the H zone, the Chatree deposit, Thailand.

- Adularia, calcite, dolomite and rhodochrosite) although barite or fluorite is not observed in the H zone. However, barite is found in the Erawan epithermal deposit (see Chapter 1) which is located in the northeast of the Chatree deposit.
- The alteration zones of sercite/illite±adularia and smectite/mixed-layer clay±chlorite zones in Figure 5.23 are not clearly recognisable in the H zone at the Chatree deposit. However, Zone III contains illite, chlorite, adularia, quartz, carbonate, epidote, sericite and albite maybe comparable with those in the model.
- The chlorite, calcite and epidote zone in Figure 5.23 are comparable with Zone IV of the H zone. Zone IV does not contain some key minerals from the sercite/illite±adularia and smectite/mixed-layer clay±chlorite zones. This suggests there may be some overlap in the zones recognised in this study and those of the idealistic model.

5.5. Summary

Alteration assemblages formed by hydrothermal fluid-wall rock interactions at the H zone is shown in Table 5.2. The alteration mineral assemblages can be classified into five zones shown in Table 5.3.

Table 5.2. Mineral alteration assemblage of the H zone, the Chatree deposit, Thailand

Alteration Assemblage	Mineral
Silicic	Quartz and chalcedony
Albitic	Albite
Algillic	Kaolinite, montmorillonite and illite-smectite
Carbonate	Calcite, rhodochrosite, ankerite and dolomite
Chloritic	Chlorite
Potassic	Adularia
Phyllic	Illite, illite-smectite and sericite
Propylitic	Epidote, hematite
Sulphide Minerals	Pyrite, sphalerite, chalcopyrite and galena
Zeolitic	Laumontite

Table 5.3. Characteristics of the alteration zones at the H zone, the Chatree deposit, Thailand

Zone	Minerals	Temperature	pH	Standard Terminology	Environment of Formation	Interpreted Fluid Composition
I	Kaolinite-Montmorillonite-Illite-Pyrite	100 - 150^{0}C	Acid to neutral 2 - 6	Argillic	Occurs in hanging wall, shallow depth, replacement in permeable zone, blanket-like, maybe product of weathering	Chloride fluid
II	Quartz–Adularia-Illite–Pyrite-Carbonate–Chlorite–Sericite–Muscovite	180 - 300^{0}C	Near neutral 4 - 7	Potassic, silicic and phyllic	Occurs in wall rock around vein, in permeable zone, associated with fracture, maybe associated with boiling	Weakly chloride alkaline water
III	Illite–Chlorite–Quartz–Epidote–Carbonate–Albite–Sericite-Adularia	200 - 300^{0}C	Near neutral	Propylitic	Occurs in foot wall at low permeable zone	Moderate to high Cl, low to moderate CO_2 and high Si fluids
IV	Epidote–Chlorite-Illite	200 - 250^{0}C	Near neutral	Propylitic	Occurs in wall rock at distal setting, low permeable	Moderate to high Cl, low to moderate CO_2 and high Si fluids
Supergene enrichment zone	occurs near surface, unusually high gold grades occurring in carbonate-leached quartz breccias					

Chapter 6
Sulphur, Carbon and Oxygen Isotopes

6.1 Introduction

Stable isotope studies provide valuable information for the ore deposit study and have contributed significantly to our understanding of ore genesis. Stable isotopes have been utilised to constrain the source of ore solutions and metals, provide information on the chemical environment of mineral deposition, mechanism of transport, and composition of fluid (Ohmoto, 1972). Sulphur, carbon and oxygen isotopes have been studied in this chapter.

6.2. Sulphur Isotopes

Sulphur is a widely distributed constituent in the lithosphere where sulphur is present as sulphide minerals in a reducing environment and sulphate minerals in an oxidising environment. Sulphur isotope analysis can be used to investigate the origin of the sulphur in the fluid and processes of ore formation (Ohmoto, 1986). Field observation and mineralogical study (Chapter 4) at the H zone indicate that electrum is associated with the sulphide mineralisation. Therefore, determining the sources of sulphur can assist in understanding of genesis of the H zone.

6.2.1. Methodology

Eleven ore vein samples containing twenty-three pyrite grains from Section 6200N were analysed. The pyrite grains analysed are subhedral to euhedral, and considered to be of the same paragenetic stage as gold mineralisation (from Stage 2 quartz-carbonate veins). The sulphur isotope compositions of pyrite grains were analysed using the laser ablation method at the Central Science Laboratory (CSL), University of Tasmania. The samples were prepared as polished thin sections with 150 μm thickness. They were ablated in an oxygenated environment. The resultant SO_2 gas was separated from any CO_2 using several freezing and heating taps, prior to analysis in a VG Micromass SIRA Series II mass spectrometer. The gas was analysed and compared with the known standards, including galena from Broken Hill ($\delta^{34}S$ = 3.4‰) and Rosebery ($\delta^{34}S$ = 12.4‰). Repeat standard analysis gives an analytical uncertainty

of ~0.2‰ $\delta^{34}S$. As this study has used the laser ablation technique, a known correction factor of 5.8‰ $\delta^{34}S$ has been applied to all pyrite analyses.

6.2.2. Results

6.2.2.1. $\delta^{34}S$ values of the H zone

The sulphur isotopic results of pyrite from the ore veins of the H zone show $\delta^{34}S$ values between –1.7 to +5.3‰ (n=23; Table 6.1), with a mean of +2.1‰ and standard deviation of +3.7‰. Figures 6.1 and 6.2 show the spatial distribution of the data on Section 6200N and a frequency distribution histogram of the data respectively.

Table 6.1. The sulphur isotope values of the H zone from pyrite grains that associated with mineralisation (vein Stage 2) and gold grades.

Sample No.	δ34S Value	Gold assay (g/t)
RCD 1109.76.01	+5.0	3.86
RCD 1109.76.02	+4.3	3.86
RCD 357.89.01	+2.5	15.1
RCD 357.89.02	+5.3	15.1
RCD 1109.75.01	+2.0	8.73
RCD 1109.75.02	+1.6	8.73
RCD 358.82.01	+3.9	3.42
RCD 358.82.02	+4.8	3.42
RCD 358.87.01	0.2	1.16
RCD 358.87.02	+2.4	1.16
RCD 499.96.01	+3.3	4.38
RCD 499.96.02	+0.1	4.38
RCD 358.80.01	+3.2	7.35
RCD 358.80.03	+3.8	7.35
RCD 357.92.01	-1.7	4.88
RCD 357.92.02	+4.2	4.88
RCD 1108.69.01	-0.6	1.69
RCD 1108.69.02	+0.7	1.69
RCD 499.94.01	+3.2	2.2
RCD 499.94.02	+4.6	2.2
RCD 499.95.01	+5.0	1.39
RCD 499.95.02	+2.6	1.39
RCD 1108.68.02	+3.4	1.99

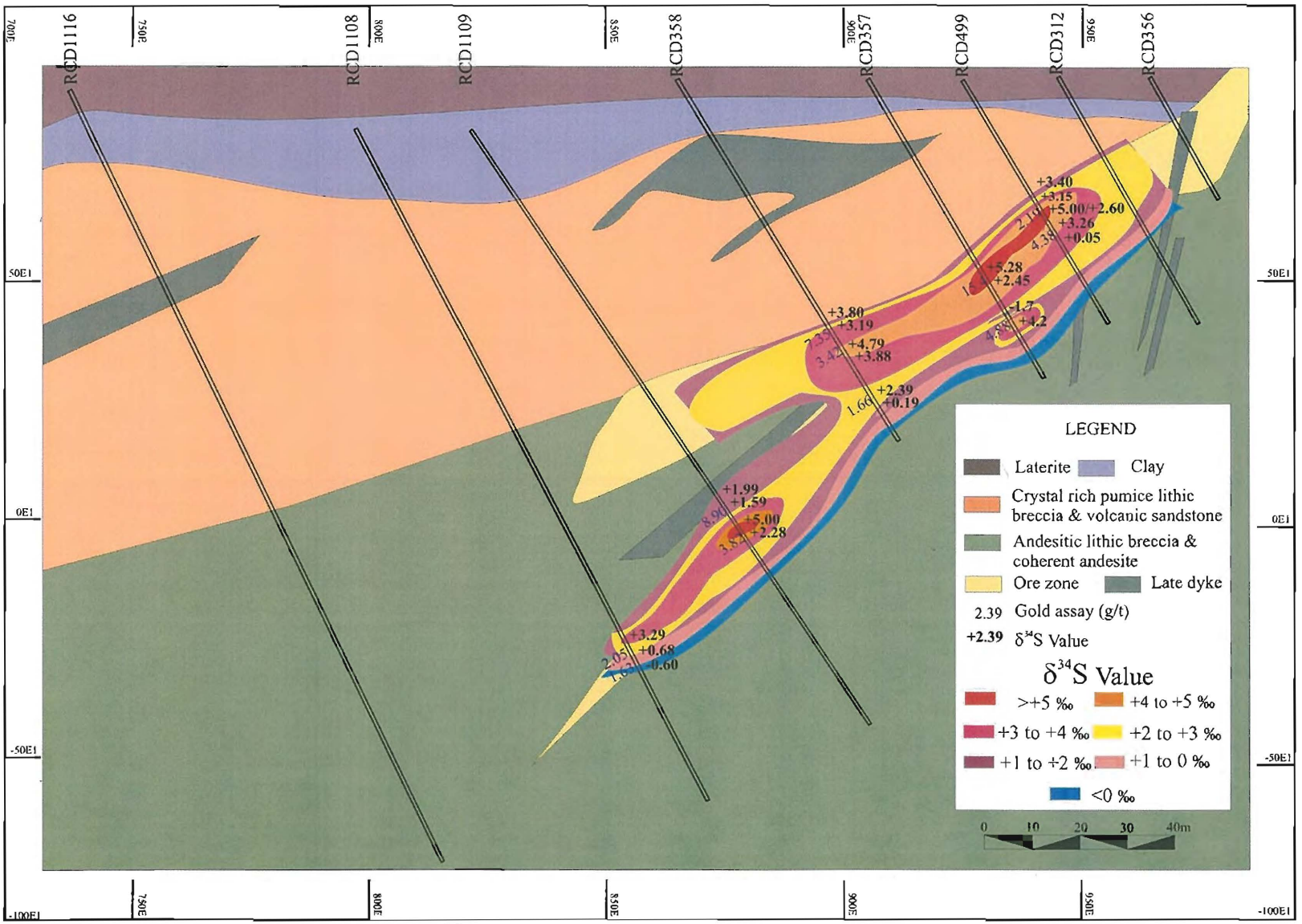

Figure 6.1. Distribution of $\delta^{34}S$ at Section 6200N, the H zone, Chatree deposit, Thailand.

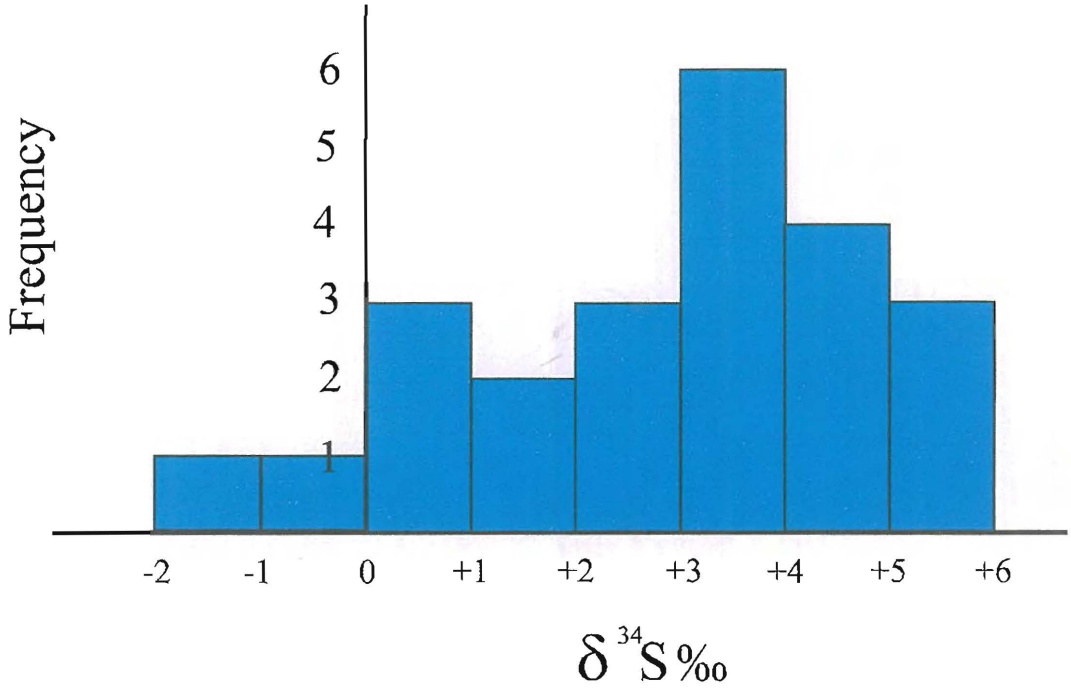

Figure 6.2. Frequency distribution histogram of $\delta^{34}S$ values (‰) of pyrites in ore veins of the H zone, Chatree, Thailand.

6.2.2.2. Comparison of $\delta^{34}S$ values of the H zone with the A, C and D zones of the Chatree deposit

Dedenczuk (1998) and Greener (1999) studied the sulphur isotopes from the wall rock and vein material from the A, C and D zones of Chatree deposit, respectively. Figure 6.3 shows a comparison of the $\delta^{34}S$ values from their earlier research with data from this study of the H zone with dividing into wall rock and ore vein groups.

The $\delta^{34}S$ values from all zones range between –9.4 to +9.6‰ with a mean of +3‰. Wall rock at the Chatree deposit comprises mainly volcanic and volcaniclastic rocks (see Chapter 3). $\delta^{34}S$ values of pyrite in the wall rock range between –6.6 to +9.6‰ with a mean of +3‰.

The $\delta^{34}S$ values from veins of the A, C, D and H zones range between –9.4 to +7.1‰ with a mean of +3‰ (Figure 6.3).

The $\delta^{34}S$ values from both the wallrock and veins at Zone A, C, D and H show a mean of +3‰ suggesting sulphide minerals have formed from the same fluids.

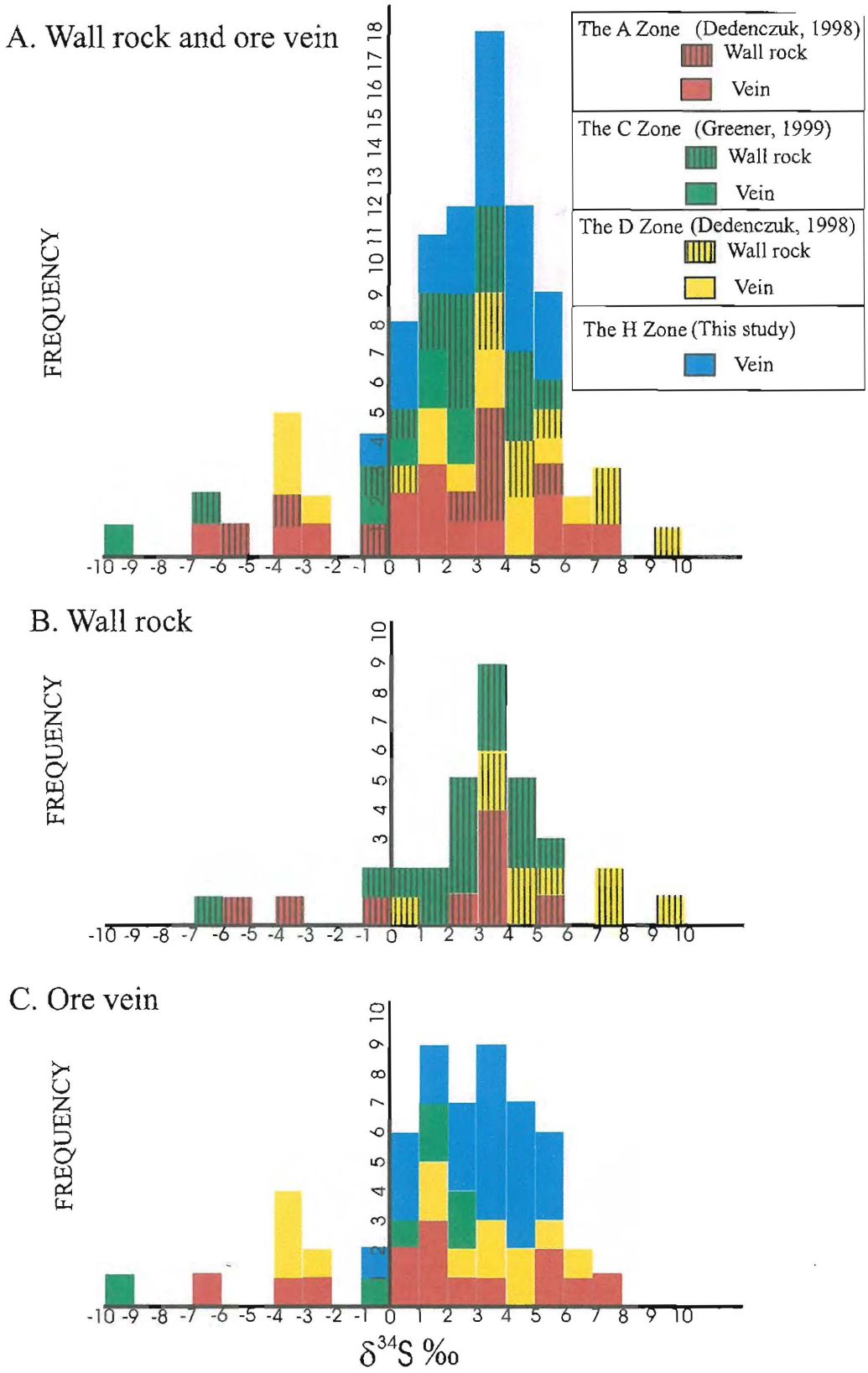

Figure 6.3. Comparison of the $\delta^{34}S$ values between the H zone and the A, C and D zones, the Chatree deposit from sulphide grains from wall rocks and veins. Note A: sulphide minerals from both wall rock and ore vein, B: sulphide minerals from wall rock and C: sulphide minerals from ore vein

6.2.3. Discussion

6.2.3.1. Source of sulphur

Typical $\delta^{34}S$ value of magmatic rocks is near zero per mil (Rollinsons, 1993). On this basis, the narrow range of $\delta^{34}S$ values for the H zone pyrite (–2 to +6‰) may imply that the source of sulphur was a magmatic body underneath the Chatree deposit. Alternatively, sulphur came directly from the volcanic rocks through which the ore fluid passed. Supporting a magmatic origin, sulphide minerals associated with electrum could be derived from leaching igneous-host rock sulphides rather than from direct magmatic fluids. The mean sulphur isotope value from the A, C, D and H zone is +3‰ in both host rock and mineralised veins (Figure 6.4). This suggests that a homogeneous sulphur source may be present for all zones. The low $\delta^{34}S$ values in some samples (e.g. –1.70‰) from the Chatree (Figure 6.3) may be a consequence of (1) high oxidation state of the fluid or mixing with two fluids (2) boiling which effectively remove the heavy isotope and (3) incorporation of wall rock sulphur from biogenetic source (Ohmoto and Rye, 1979).

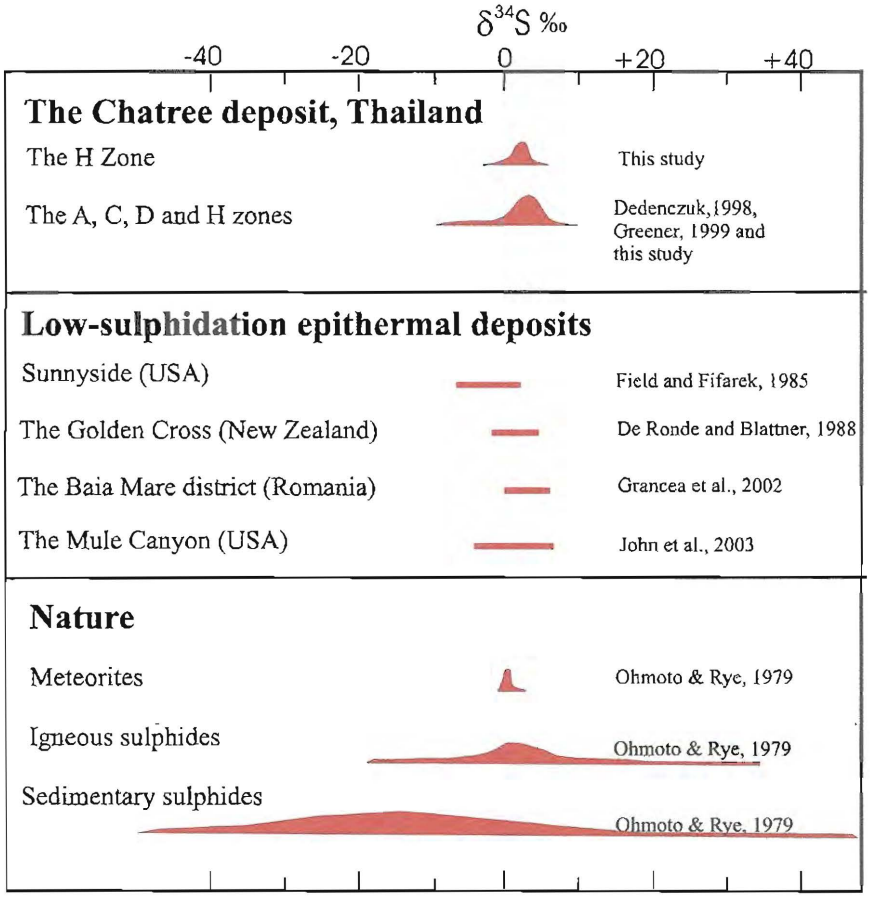

Figure 6.4. Comparison of $\delta^{34}S$ values in the H zone with different sulphur isotope data.

6.2.3.2. Sulphur isotope and pH/fO_2 controls

Most pyrite of the Chatree has been thought to have formed from reduced (H_2S^- predominant) fluids (Greener, 1999). The H_2S concentrates $\delta^{34}S$ relative to dissolved sulphide ions and increasing the pH that results directly in increasing the $\delta^{34}S$ of precipitated sulphides (Hoefs, 1996). From alteration assemblages established in Chapter 5, variations in the pH (from pH 4 to pH 6) probably occurred during the Stage 2 veins (central veins). This change in pH may have caused pyrite precipitation. Moreover, an increase of fO_2 has a strong effect on the $\delta^{34}S$ values (Ohmoto, 1972). When sulphide precipitation occurs, sulphur isotope fractionation can take place between dissolved sulphur species and sulphide minerals. The removal of sulphide from the fluids can cause a measurable fractionation on H_2S remaining in the fluids (Hoefs, 1996).

6.2.3.3. Sulphur isotope and boiling

Boiling of H_2S-rich fluid effectively removes the heavy isotope leading to partition into the SO_2 vapour phase. A consequence more depleted $\delta^{34}S$ values in pyrite could be consistent with boiling. Figure 6.1 shows $\delta^{34}S$ values of the H zone appear to become generally more depleted down hole and higher gold grade zones coincide with lighter isotope zones. The enrichment of $\delta^{34}S$ values at the higher level and the presence of adularia (see Chapter 4) at the top of mineralised vein suggest that boiling in the ore veins may have occurred. The high gold grades at the H zone are also broadly associated with $\delta^{34}S$ depletion (Figure 6.5) although there is a spread of data from some samples. The samples that are not consistent with the depleted trend may be resulted from more oxidise. This data may suggest the sulphur isotope may assist in delineating boiling zone (Buchanan, 1981). Dedenczuk (1998) also suggested that the $\delta^{34}S$ values of coarse grain pyrite in the D zone show depleted cores and enriched rims. This is interpreted as pyrite nucleating during a period of boiling with continuing growth occurring after boiling has ceased (Buchanan, 1981).

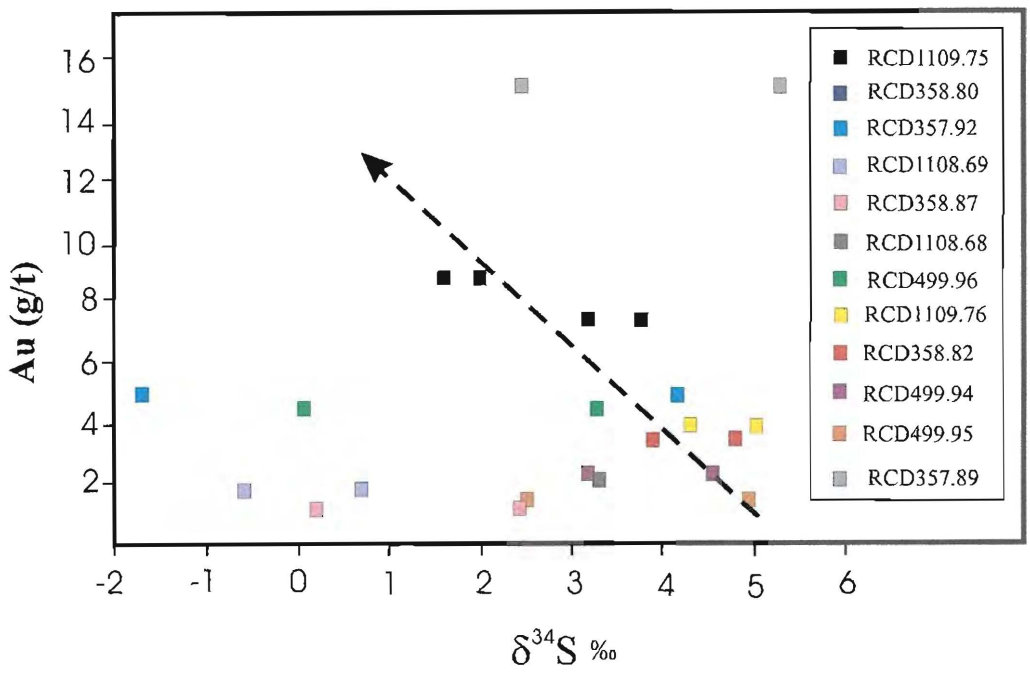

Figure 6.5. Relationship between $\delta^{34}S$ values (‰) with Au grades for pyrite grains of the H zone, Chatree deposit, Thailand.

6.3. Carbon and Oxygen Isotopes

Carbon and oxygen isotopes measured on the carbonates are useful for understanding of ore genesis. In this study, carbon and oxygen isotope data are used to constrain the source of carbon and oxygen in hydrothermal fluids (Davison, 2003). The carbon and oxygen isotopic covariations in carbonates associated with hydrothermal mineralisation have been used for obtaining information about the isotopic composition of hydrothermal fluid involved as an indicator of their origin, the nature of dissolved carbonate species and the nature of hydrothermal processes (eg. cooling, fluid mixing, fluid/rock interaction and secondary alteration).

6.3.1. Methodology

Seventeen samples containing different carbonate minerals were analysed. These samples were constrained paragenetically and included calcite and rhodochrosite in veins, amygdales and breccia matrix. Only one altered-limestone wall rock sample was analysed. The analysed carbonate minerals have been divided into three groups including;

- Ore stage carbonate (n = 8); calcite from breccia ore stage and from ore vein (Stage 2: Chapter 4);
- Late stage carbonate (n = 8); calcite from breccia wall rock, amygdale in andesite, calcite veinlet and rhodochrosite;
- Altered limestone (n = 1).

The samples were analysed at the University of Tasmania. Carbonate crystals were micro-drilled into powder and reacted with H_3PO_4 at 25°C for approximately 12 hours. The liberated CO_2 gas was analysed using VG Micromass SIRA Series II mass spectrometer. Results are relative to Vienna Standard Mean Ocean Water V-SMOW (oxygen) and the Pee Dee Belemnite PDB (carbon) standards. Repeat standard analysis reveals an analytical uncertainty of 0.05‰.

6.3.2. Results

6.3.2.1. $\delta^{13}C$ and $\delta^{18}O$ values of the H zone

The range of measured values varies from –0.8 to –7.3‰ for $\delta^{13}C$ and +7.5 to +14.9‰ for $\delta^{18}O$. The results from each paragenetic stage or grouping (see above) are presented in Table 6.2.

Calcite from the quartz-carbonate veins has $\delta^{13}C$ values of –1.7 to –2.4‰ (average –2.0‰) and $\delta^{18}O$ values of +7.5 to +11.6‰ (average 8.5‰). Calcite (inferred to formed after ore precipitation) as amygdales in andesite volcanic rocks, as a replacement mineral of the groundmass of andesitic breccia, calcite infill and calcite veins range in $\delta^{13}C$ and $\delta^{18}O$ values from –1.7 to –7.3‰ (average –4.9‰) and +8.6 to +14.9‰ (average +11.4‰), respectively. Hydrothermal rhodochrosite has $\delta^{13}C$ values of –0.8‰ and $\delta^{18}O$ values of +9.9‰ (Table 6.2).

Based on petrographic observations, the limestone analysed here is altered and returned anomalous values of –2.1‰ for $\delta^{13}C$ and +9.9‰ for $\delta^{18}O$. Figures 6.6 and 6.7 summarise this data for the H zone.

Table 6.2. $\delta^{13}C$ and $\delta^{18}O$ analysis from carbonate minerals of the H zone, Chatree deposit, Thailand.

Group	Sample Name	Description	$\delta^{13}C_{PDB}$	$\delta^{18}O_{PDB}$	$\delta^{18}O_{SMOW}$
Ore stage carbonate	RCD312.106 *	breccia (ore)	-2.3	-18.7	+11.6
	RCD357.92	breccia (ore)	-2.1	-21.6	+8.6
	RCD499.94	calcite in ore vein	-2.1	-21.3	+8.9
	RCD499.96	calcite in ore vein	-2.2	-21.3	+8.9
	RCD357.89	calcite in ore vein	-2.4	-22.1	+8.1
	RCD358.80	calcite in ore vein	-2.1	-22.7	+7.5
	RCD358.82	calcite in ore vein	-1.8	-21.4	+8.8
	RCD358.85	calcite in ore vein	-1.7	-21.2	+9.0
Late stage carbonate	RCD312.103 *	amygdale in andesite with chlorite	-4.3	-19.9	+10.3
	RCD1109.73 *	amygdale in andesite with chlorite	-3.6	-20.9	+9.4
	RCD1108.68	breccia (host rock)	-1.7	-21.6	+8.6
	RCD499.98	calcite infill	-7.3	-15.5	+14.9
	RCD357.93	calcite vein	-5.6	-17.7	+12.6
	RCD1109.77 *	calcite vein	-4.7	-19.7	+10.6
	RCD1116.67	calcite vein	-6.5	-15.5	+14.9
Rhodochrosite	RCD1109.72	rhodochrosite	-0.8	-20.4	+9.9
Altered limestone	RCD1116.64	limestone	-2.1	-20.4	9+.9

* cold finger used

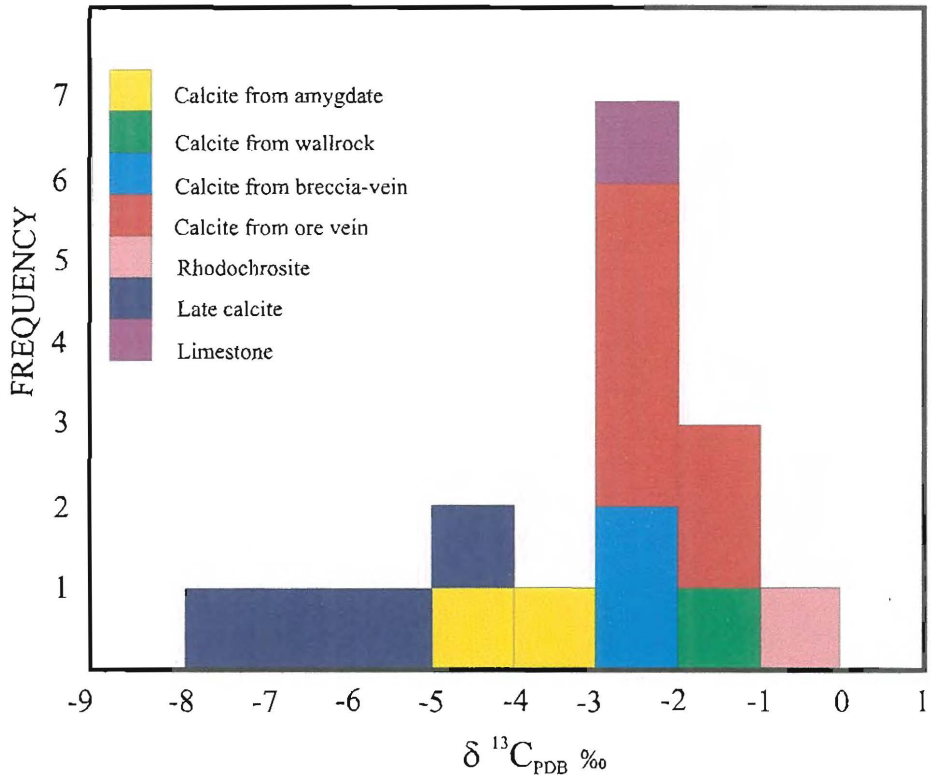

Figure 6.6. Histogram showing the $\delta^{13}C$ values of samples from the H zone, Chatree deposit, Thailand.

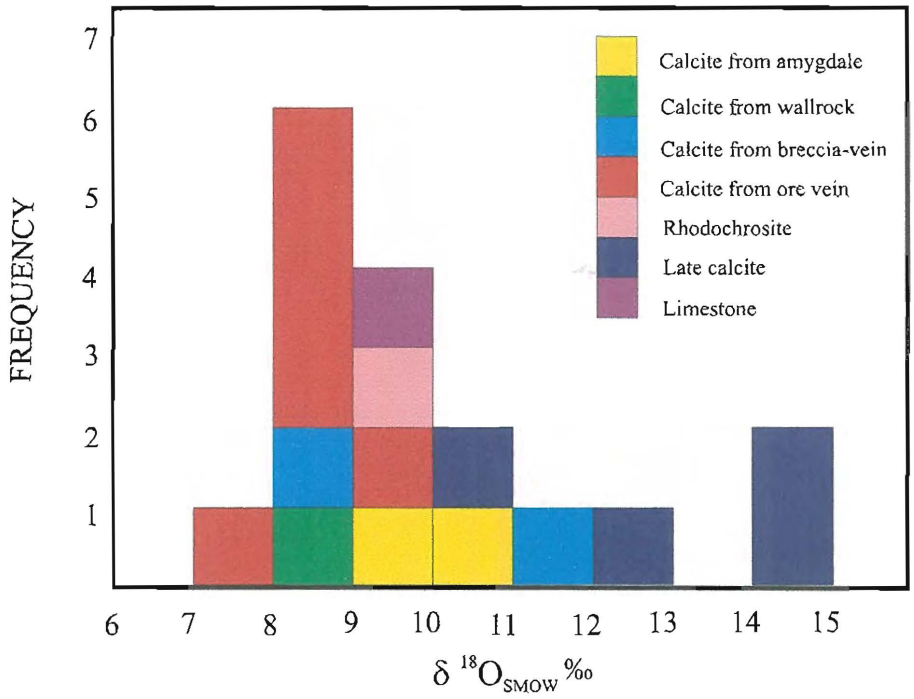

Figure 6.7. Histogram showing the $\delta^{18}O$ values of samples from the H zone, Chatree deposit, Thailand.

6.3.2.2. The $\delta^{13}C$ and $\delta^{18}O$ values of the A, C, D and H zones of the Chatree deposit

Carbon and oxygen isotope data of carbonates from the previous studies at the Chatree (Dedenczuk, 1998 and Greener, 1999) have been divided into two groups including ore carbonate stage and late stage calcite same as the H zone study. Figures 6.8 and 6.9 compare the $\delta^{13}C$ and $\delta^{18}O$ values from the A, C and D with data from this study of the H zone.

The $\delta^{13}C$ values of the ore stage carbonates from all zones have a narrow range between +0.2‰ to –6.6‰ with a mean of -3‰. The $\delta^{13}C$ values of the late stage carbonates from all zones range between +12.4‰ to –1.1‰ with a mean of -3‰. The $\delta^{18}O$ values of the ore stage carbonates from all zone range between +7.5‰ to 17.2‰ with a mean of +11‰. The $\delta^{18}O$ values of the late stage carbonates from all zones mostly range between +7.3‰ to 16.3‰ with two out range data of +4.2‰ and +20.2‰.

The carbon and oxygen isotopes of all zones are consistent but some samples from the C zone show more depleted $\delta^{13}C$ values and more enrichment in $\delta^{18}O$ values.

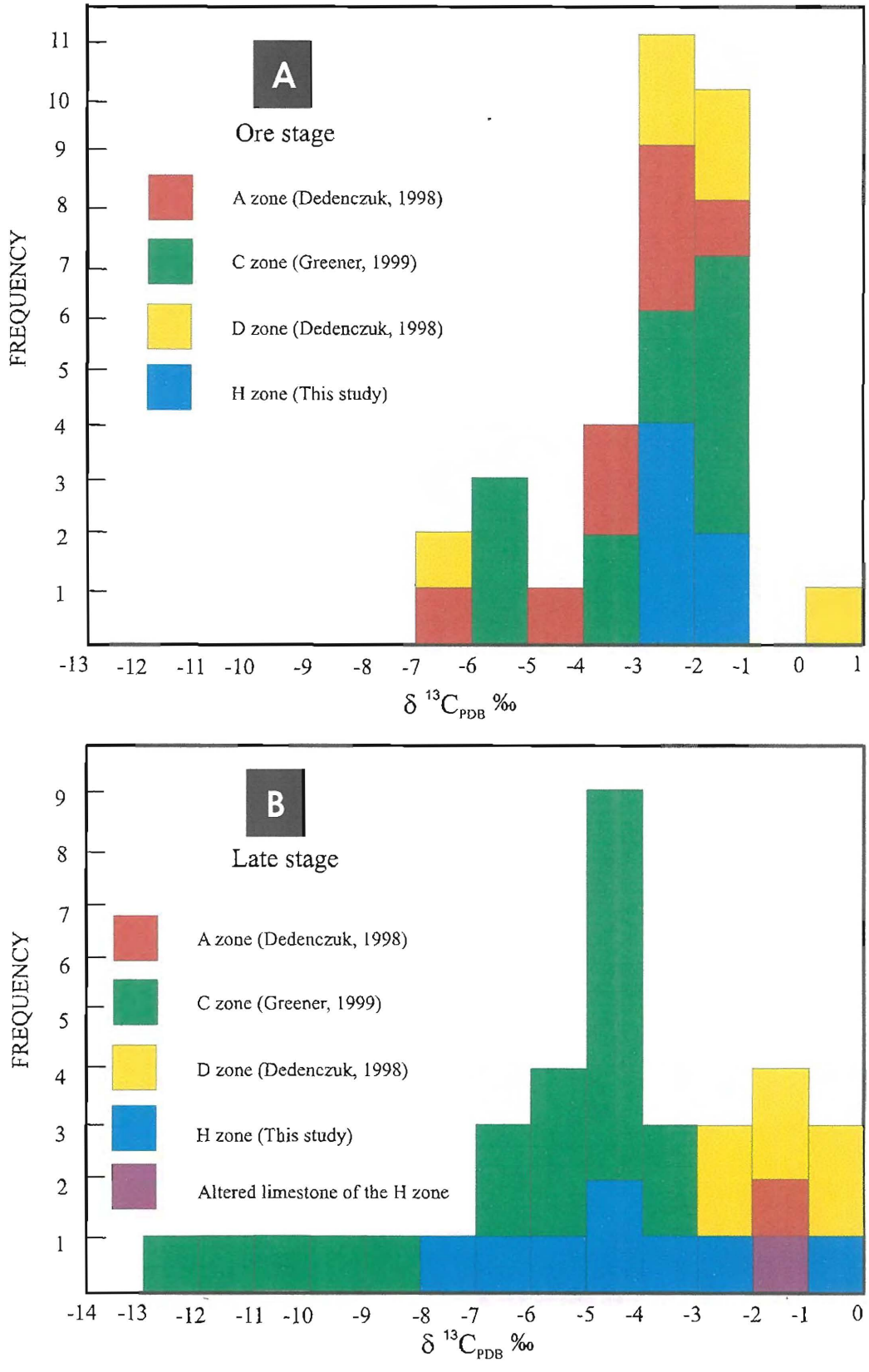

Figure 6.8. Comparison of the $\delta^{13}C$ values between the A, C, D and H zones of the Chatree deposit, Thailand.

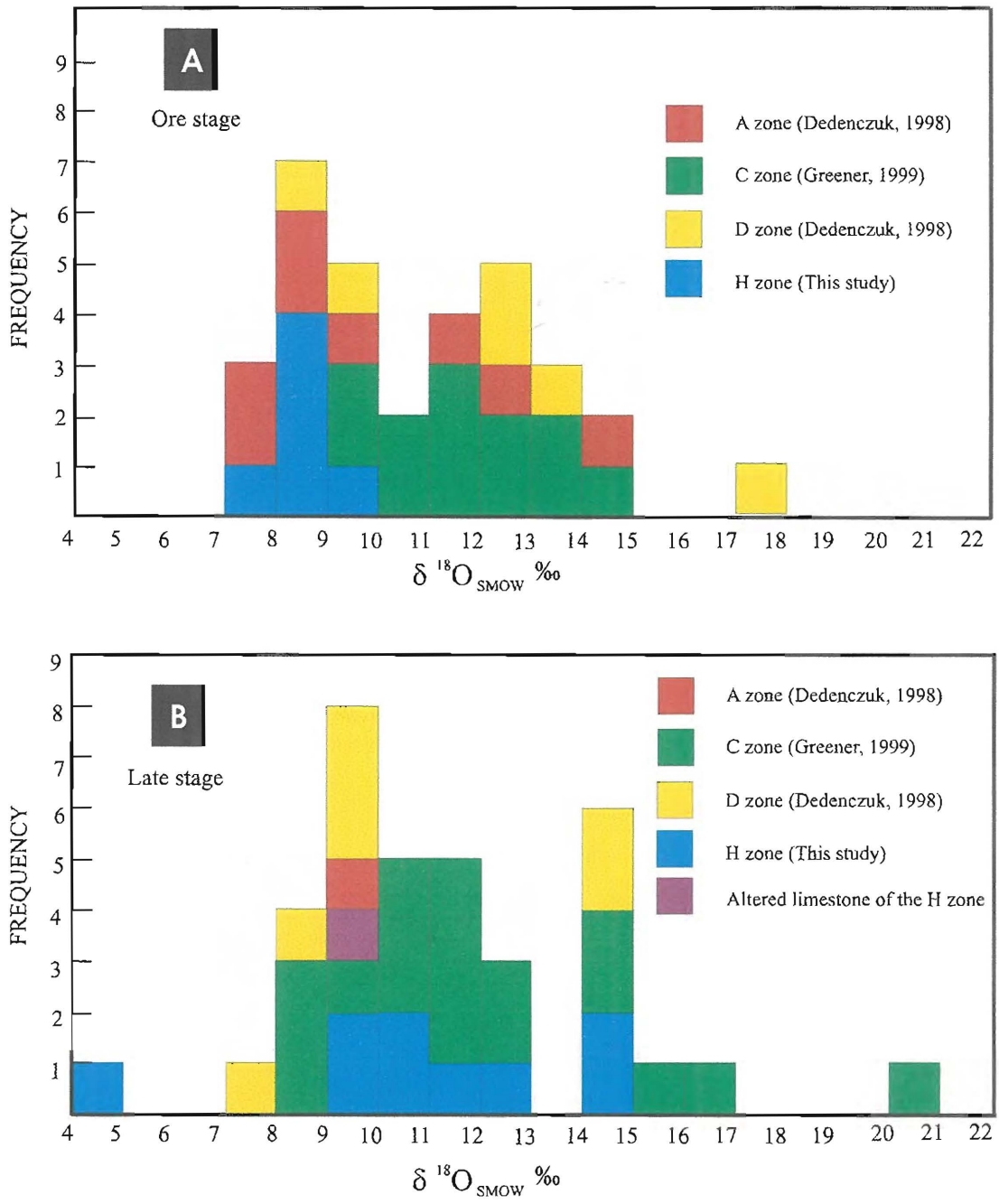

Figure 6.9. Comparison of the $\delta^{18}O$ values between the A, C, D and H zones of the Chatree deposit, Thailand.

6.3.3. Discussion

6.3.3.1. Data interpretation and source of fluid

1. Carbon Isotope

The $\delta^{13}C$ values of the H zone range between –0.8‰ to –7.3‰ (n = 17) suggesting the isotopic values are comparable to the compositions of the major global carbon reservoirs (Figure 6.10). Generally, values of $\delta^{13}C$ less than -5‰ can be considered to have derived from mixed compounds of light carbon reservoirs, such as igneous CO_2, sedimentary carbon, or carbon in meteoric water (Figure 6.10).

a) Calcite in quartz-carbonate veins (ore stage). The measured $\delta^{13}C$ compositions for ore stage of the H zone have a range of –1.7 to –2.4‰. This suggests that carbon may have been derived from magmatic, meteoric or marine limestone sources.

b) Calcite late stage. The $\delta^{13}C$ values for late stage calcite of the H zone have a wider range of –1.7 to –7.3‰ and are lighter than the ore stage group. However, the $\delta^{13}C$ values of late stage carbon are still in the range of magmatic, meteoric or marine limestone sources. More depleted $\delta^{13}C$ values may indicate a greater magmatic component when the fluids have been mixed. The magmatic composition may be inherited from the volcanic wall rock via fluid-rock interaction.

c) Limestone. The limestone analysed from the H zone (-2‰) is consistent with marine limestone (0±3‰; Rollinson, 1993). However, the $\delta^{13}C$ values of limestone is significantly shifted from $\delta^{13}C$ values expected for unaltered Permian limestone of +6‰ (Bottrell et al., 2001) to the more depleted value of –2‰ This shift suggests that fluid-rock interactions have modified the typical isotope composition of the limestone.

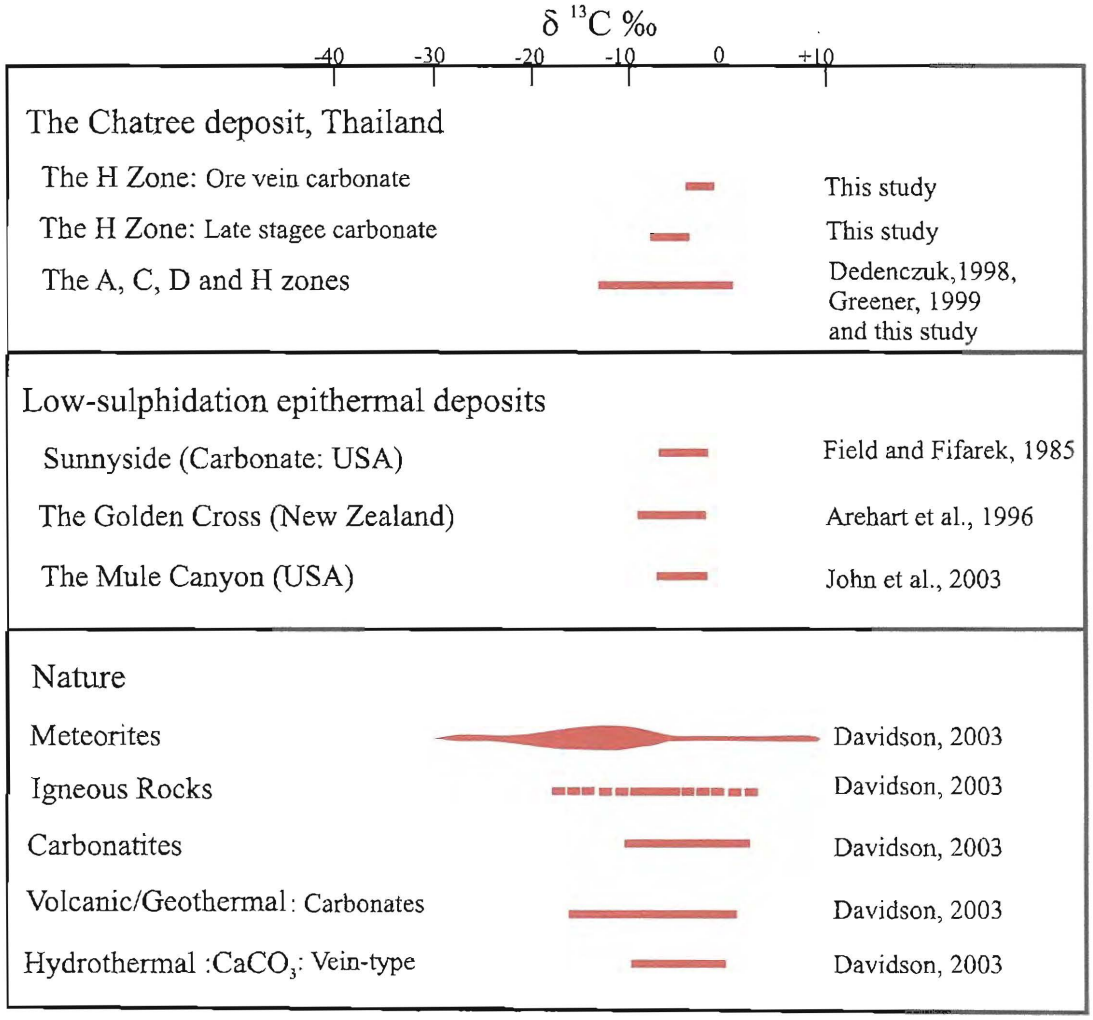

Figure 6.10. The $\delta^{13}C$ values of the H zone and the A, C and D zones of the Chatree deposit compare with source of Carbon and the other low-sulphidation epithermal deposits.

2. Oxygen isotope

The measured $\delta^{18}O$ compositions of the H zone range from +7.5 to +14.9‰ (n = 17; Figure 6.11), a range that overlaps with both pristine volcanic and metasedimentary rock values (Rollinson, 1993).

a) Calcite in quartz-carbonate veins (ore stage). The measured $\delta^{18}O$ compositions of calcite from the ore stage range between +7.5 to +11.6‰ (average +8.5‰). This suggests the source of oxygen has been derived mainly from a magmatic-water source (+7±2‰, Ohmoto, 1986) mixed with metasediments compositions (Rollinson, 1993).

b) Calcite late stage. The measured $\delta^{18}O$ compositions for late stage calcite range between +8.5 to +14.9‰ (average +12.0‰). The heavier than ore stage values can be interpreted to suggest the source of oxygen may have been derived from the same ore stage fluids, however with a greater influence from the metasediments or host volcanic pile.

c) Limestone. The measured $\delta^{18}O$ composition of limestone is +9.0‰, which is more depleted than accepted $\delta^{18}O$ values of Permian limestone (~18 to 33‰; Rollinson, 1993). The $\delta^{18}O$ values for the limestone can readily be explained by isotope resetting of the limestone during interaction with hydrothermal fluids.

The sulphur and carbon isotope data suggest that the dominant sources of fluids are likely a mixture of magmatic and meteoric waters. However, the oxygen isotope data does not show a significant meteoric component. Generally, meteoric waters have $\delta^{18}O$ values less than 0‰ (Campbell and Larson, 1998), however, the $\delta^{18}O$ values from the H zone are greater than 0‰. The absence of a distinct meteoric signature may result if the meteoric water have undergone a significant isotopic exchange, or have mixed with other fluids (e.g. magmatic fluids) and the composition is no longer that of the original precipitation (Campbell and Larson, 1998).

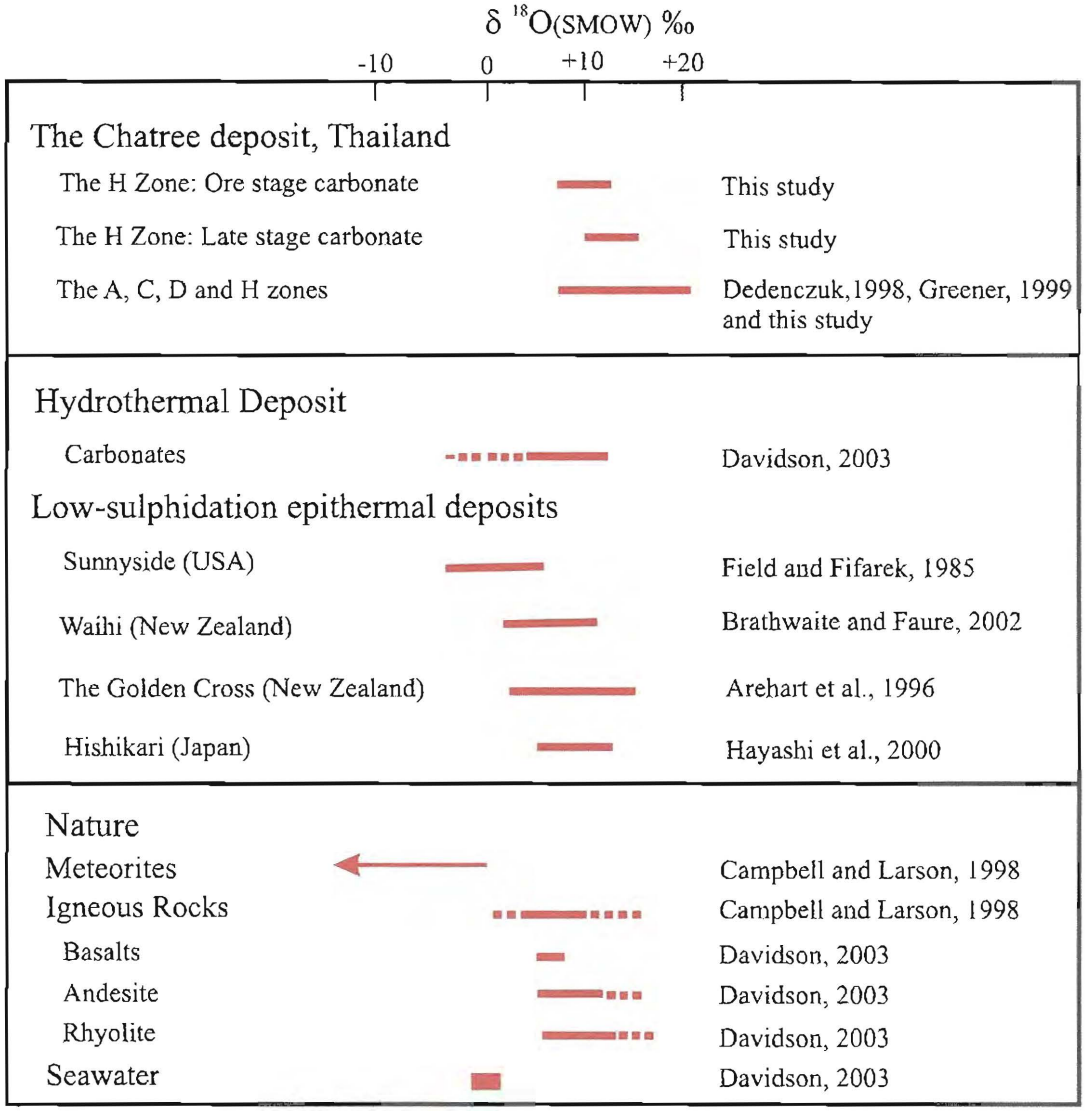

Figure 6.11. The $\delta^{18}O$ values of the H zone and the A, C and D zones of the Chatree deposit compare with source of Oxygen and the other low-sulphidation epithermal deposits.

6.3.3.2. Carbon and oxygen plot

Data from previous carbon-oxygen isotope studies in the A, C and D zones (Dedenczuk, 1999; Greener, 1999) have been used to supplement data from this study. The data have been classified by their paragenetic stages into 3 groups including ore stage carbonate, late stage carbonate and altered limestone.

Plotting the measured $\delta^{13}C$ versus $\delta^{18}O$ compositions of carbonate minerals from the H zone and the A, C and D zones shows that the $\delta^{13}C$ values decrease while $\delta^{18}O$ values increase; i.e., a strong negative correlation (trend 2) in ore stage carbonate minerals, while the late stage carbonate minerals shows a positive trend (trend 1).

6.3.3.3. Initial composition of fluid

Carbon and oxygen isotopic compositions of fluid responsible for the carbonates from the Chatree deposit were determined in order to interpret the deposition of fluid history. Determination of initial fluid composition during the carbonate formation has been documented by calculating the calcite fractionation curve at temperature from 300°C to 50°C using equation (1) of Ohmoto and Rye (1979) and equation (2) of Friedman and O'Neil (1977). The initial $\delta^{13}C$ and $\delta^{18}O$ values that have been used for calculation are 0‰ in both. The assumed constant composition of fluid (0‰) is summarised to constrain that the fluid could be formed from magmatic and meteoric waters (Figure 6.12).

$1000\ln (Calcite\text{-}CO_2) = 8.27\text{-}18.11*10^3/T+8.557*10^6/T^2\text{-}8.914*10^8/T^3$ ----------(1)

$1000\ln (Calcite\text{-}H_2O) = 2.78*10^6/T^2 - 2.89$ ----------(2)

Figure 6.12 shows the curves fit of the calculated $\delta^{13}C$ and $\delta^{18}O$ values from the H zone (this study) and the A, C, and D zones (Dedenczuk, 1998; Greener, 1999) with the ore stage carbonate trend (trend 1). Trend (1) that shows a positive correlation of $\delta^{13}C$ and $\delta^{18}O$ values broadly matches with the calculated cooling curve with an initial composition (-3‰ $\delta^{13}C$ and +2‰ $\delta^{18}O$ values). This initial composition can be interpreted to be modified meteoric water. The negative trend (trend 2) may suggest mixing of ore fluids (see below).

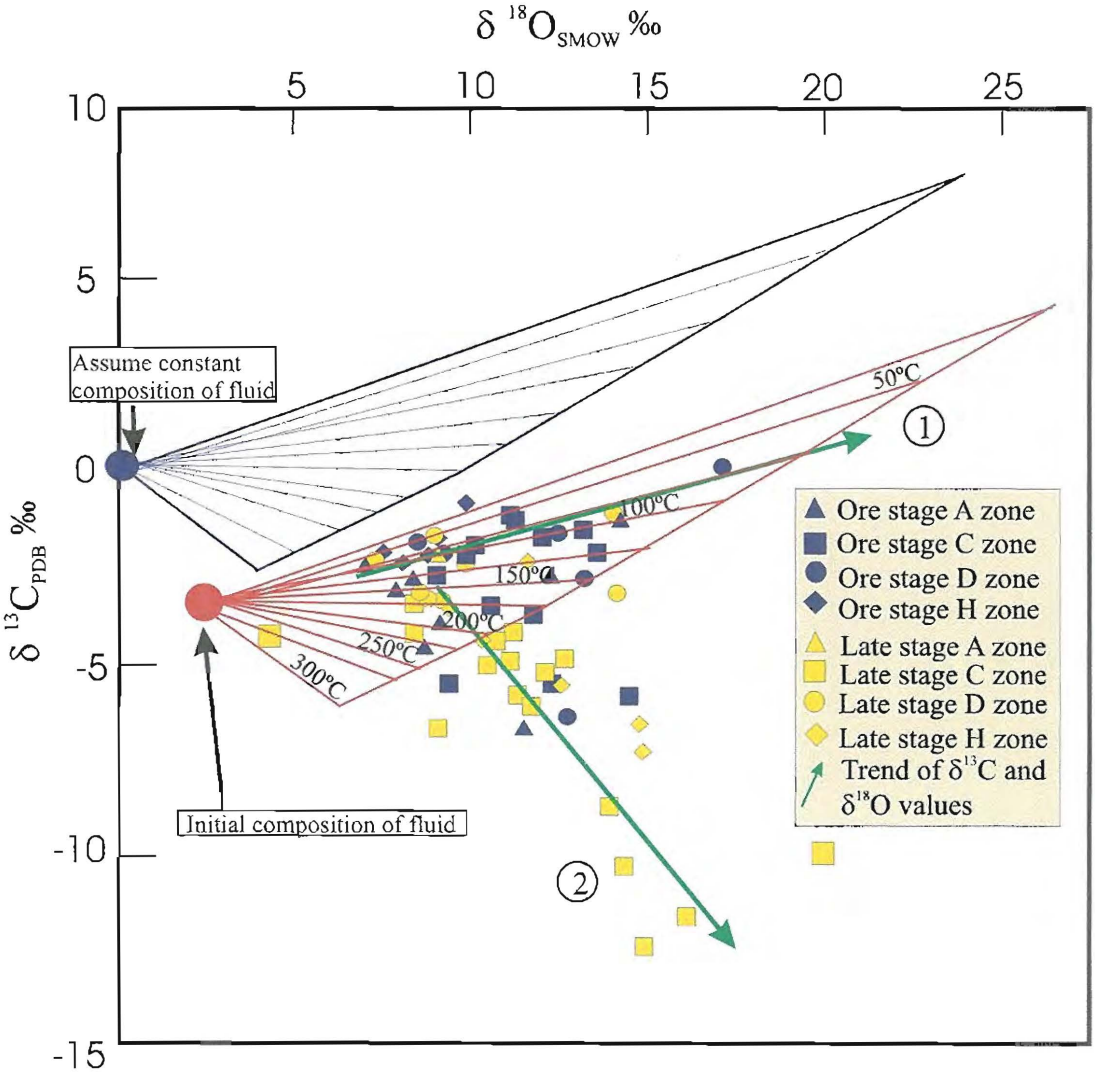

Figure 6.12. The carbon and oxygen isotope plot shows the positive (trend 1) in ore stage carbonates and negative trends (trend 2) in late stage carbonates; data of the A and D zones from Dedenczuk (1998), the C zone from Greener (1999) and the H zone from this study. The assuming composition of fluid has been used for calculating at 0‰ for both carbon and oxygen isotopic composition.

6.3.3.4. Carbon species

The carbon in carbonate minerals is typically contained within oxidised carbon species including CO_2, H_2CO_3, HCO_3^- and CO_3^{2-}. The H_2CO_3 and HCO_3^- species are considered to be the important sources of carbon in hydrothermal fluids (Davidson and Devis, 2001).

The plot of $\delta^{13}C$ and $\delta^{18}O$ values of carbonates of the H zone for determining species of the fluid that is presented in Figure 6.13. The curves in Figure 6.13 are equilibrium fractionation trends as function of temperature for calcite, assuming H_2CO_3 and HCO_3^- are dominant carbon species. Curves of H_2CO_3 and HCO_3^- that are calculated for $\delta^{13}C$ values of the fluid are taken as –2‰ and $\delta^{18}O$ as +3‰, respectively. The carbon-oxygen trends of the ore stage carbonate at the H zone suggests that both H_2CO_3 and HCO_3^- may be introduced as the dominant carbon species of the hydrothermal fluid at the H zone. The late stage carbonate of the H zone shows the trend that is different from H_2CO_3 and HCO_3^- curve. This may be interpreted as mixing or overprinting during the late stage carbonate precipitation from a different source.

The alteration assemblages of the H zone (Chapter 5) suggest that alkaline fluids at low temperature have precipitated these minerals. This supports the interpretation that HCO_3^- is the dominant carbon species in the H zone alteration minerals (Ohmoto, 1972). The change in carbon species is highly significant and may be caused by changes in pH and temperature during mineral precipitation.

Temperatures from a fluid inclusion study at the C zone (Greener, 1999) of late stage calcite (146°C and 285°C) have been used to estimate the $\delta^{13}C$ and $\delta^{18}O$ composition by using the fractionation equations of Friedman and O'Neil (1977). Greener (1999) suggested that calcite precipitating with H_2CO_3 as the dominant carbon species.

The carbon species of the Chatree deposit including the H zone may consist of H_2CO_3 and HCO_3^- species. The mixing between two species is more likely resulted in forming the carbonates in the H zone and the Chatree deposit.

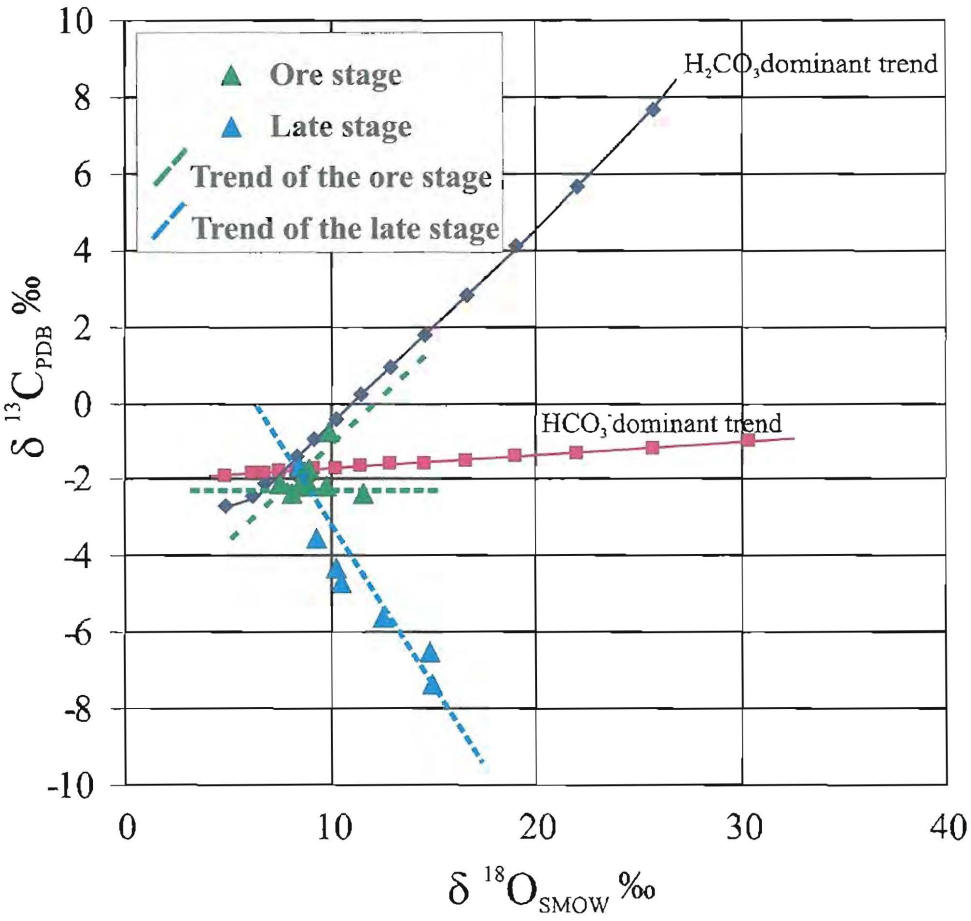

Figure 6.13. Plot of $\delta^{13}C$ and $\delta^{18}O$ values of carbonates from the H zone with the H_2CO_3 and HCO_3^- curves that are the dominant carbon species. The H_2CO_3 and HCO_3^- curves are calculated from $\delta^{13}C$ and $\delta^{18}O$ values of –2‰ and +3‰. Fractionation factors for carbon and oxygen isotopes between appropriate species were taken from Ohmoto and Rye (1979) and Deines et al. (1974).

6.3.3.5. Fluid-rock interaction

The altered limestone has the $\delta^{13}C$ and $\delta^{18}O$ values of -2.14 and 9.85‰. The $\delta^{13}C$ values of the limestone is consistent with marine limestone (0±3‰) but more depleted when compared with Permian limestone (~6‰; Bottrell et al., 2001). The $\delta^{18}O$ values are shifted and more depleted values than marine limestone (+18 to +33‰; Rollinson, 1993; Figure 6.14). The depletion in the $\delta^{18}O$ values is typically resulted from a strong alteration by a large water flux (Hoefs, 1996) through the wall rock exchanging heavy $\delta^{18}O$ isotopes with light isotopes in the hydrothermal fluids. During hydrothermal alteration, H_2CO_3, HCO_3^- and CO_2 maybe removed by dissolution or thermal decarbonation (Ohmoto, 1986) resulting in lighter $\delta^{13}C$ values and heavier $\delta^{18}O$ values. This essentially produces a second fluid end member.

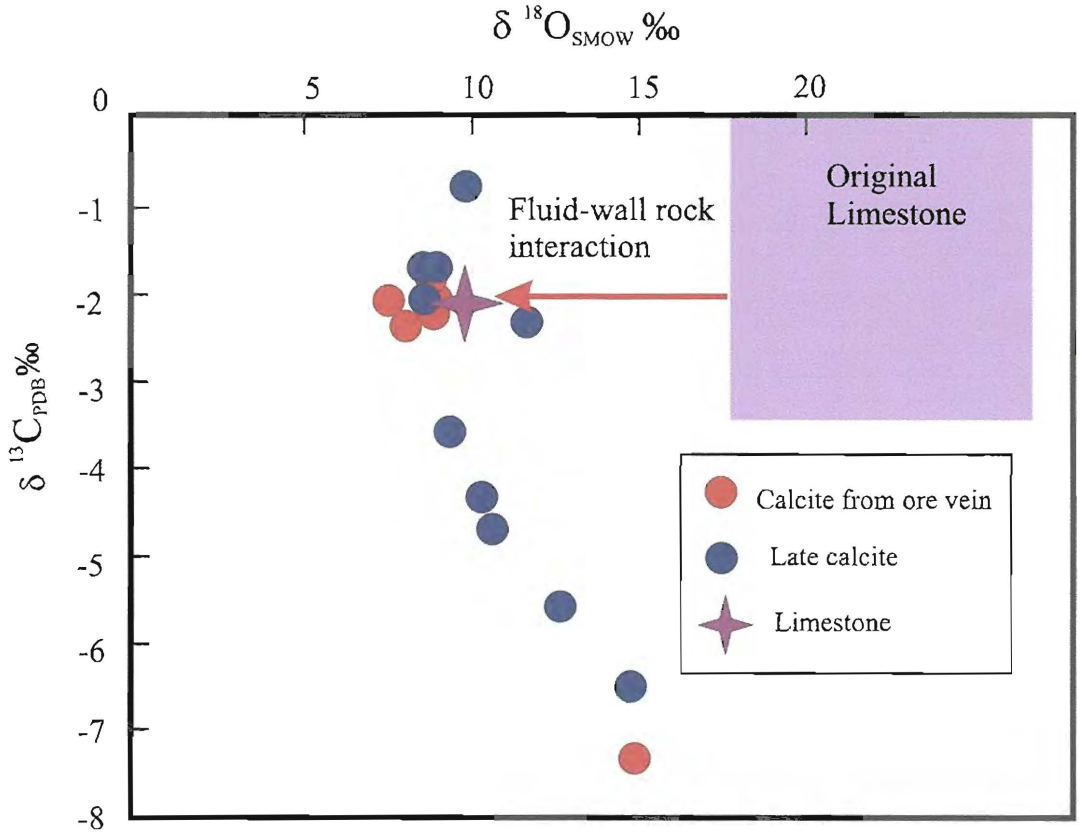

Figure 6.14. Plot of carbon and oxygen isotopes of the H zone showing the altered limestone having the $\delta^{18}O$ values (+9.85‰) shifted from the $\delta^{18}O$ values (+18 to +33‰; Rollinson, 1993) of marine limestone resulting from fluid-wall rock interaction.

6.3.3.6. The carbon-oxygen isotope - temperature relationships

To determine carbonate precipitation and temperature relationships from carbon-oxygen isotope data, the $\delta^{13}C$ and $\delta^{18}O$ values have been recalculated according to the fractionation equation for calcite-H_2O of Friedman and O'Neill (1977; equation 2), and the fractionation equation for calcite-CO_2 of Ohmoto and Rye (1979; equation 1). Initial temperatures of 150°C to 300°C derived from fluid inclusions (Greener, 1999) have been used. These temperatures are consistent with the mineral assemblages of the H zone (described in Chapter 5). The recalculated data has been plotted in Figure 6.15 and indicates a positive trend. A possible explanation for the positive correlation between the $\delta^{13}C$ and $\delta^{18}O$ values is the precipitation of ore stage carbonates due to a temperature decrease from 300 to 150°C from a large and homogeneous fluid reservoir with $\delta^{13}C \sim -2‰$ and $\delta^{18}O \sim +6‰$. The positive trend may suggest that calcite precipitation occurred in equilibrium with H_2CO_3 (dissolved CO_2; Zheng, 1990; Brathwaite and Faure, 2002). Typically, the solubility of calcite in fluids increases as temperature decreases, therefore the calcite deposition should be achieved when cooling is combined with continuous CO_2 degassing or continuous reaction with the wall rock (Zheng and Hoefts, 1993).

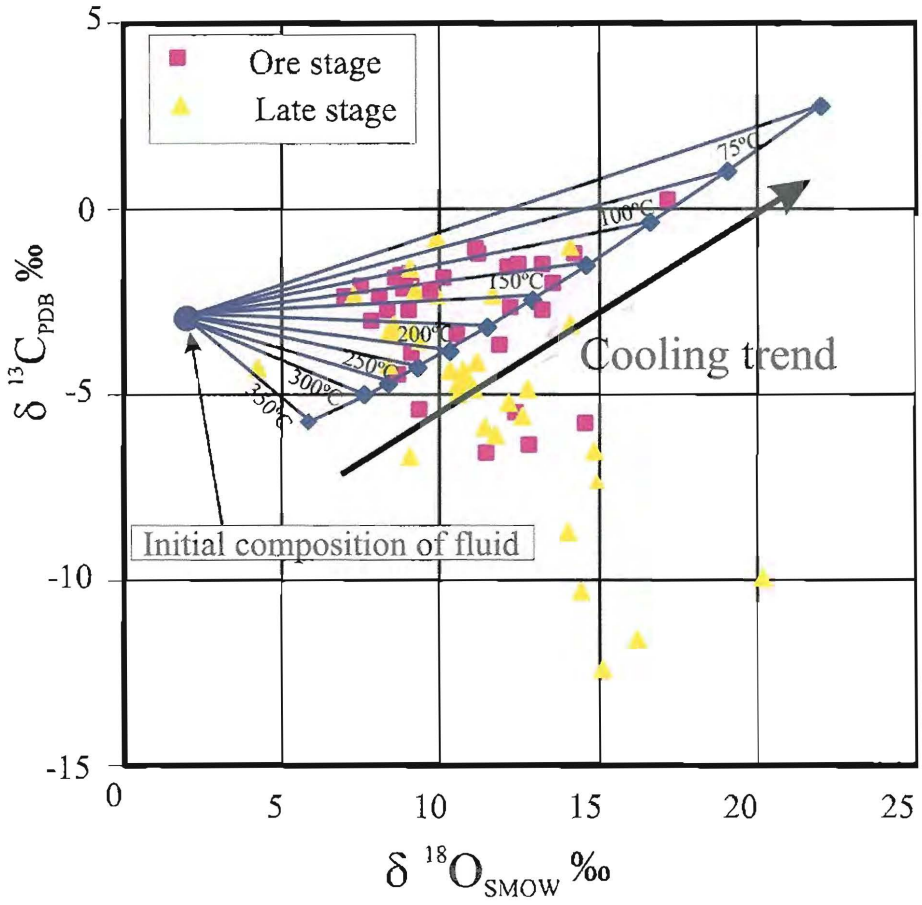

Figure 6.15. Plot of the $\delta^{13}C$ and $\delta^{18}O$ values from all zones with the decreasing temperature when the carbonate precipitating (cooling trend). The curve of cooling trend has been calculated by fractionation equations of Friedman and O'Neill (1977) and Ohmoto and Rye (1979) using $\delta^{13}C$ and $\delta^{18}O$ values of –2‰ and +3‰.

6.3.3.7. Fluid mixing

The negative slope of coupled carbon-oxygen trends may suggest carbonate precipitation due to mixing with two fluids with different alkali-chloride concentrations (Zheng and Hoeffs, 1993). The mixing fluid should be dominated by the carbon species (from H_2CO_3 to HCO_3^-) because the carbon species equilibrate very rapidly. The fluid mixing model (Figure 6.16) that has been suggested by Savard and Kontak (1998) is calculated using the equations of Deines et al. (1974; equations 3 and 4) and Friedman and O'Neil (1977; equation 2).

$1000\ln a(\text{Calcite-}CO_2) = 1.192*10^6/T^2 - 3.61$ ----------(3)

$1000\ln a(\text{Calcite-}HCO3^-) = 0.095*10^6/T^2 + 0.91$ ----------(4)

The fluid mixing model of the Chatree has been calculated from the assumed end member composition:

- Fluid I - $\delta^{13}C$~ 0‰ and $\delta^{18}O$~ +5‰ (magmatic water); and
- Fluid II - $\delta^{13}C$~ -10‰ and $\delta^{18}O$~ +22‰ (modified meteoric water).

The modified meteoric water may be occurred by mixture of cold meteoric water and magmatic water or cold meteoric water reaction with the igneous host rocks or sedimentary rocks near the Chatree deposit.

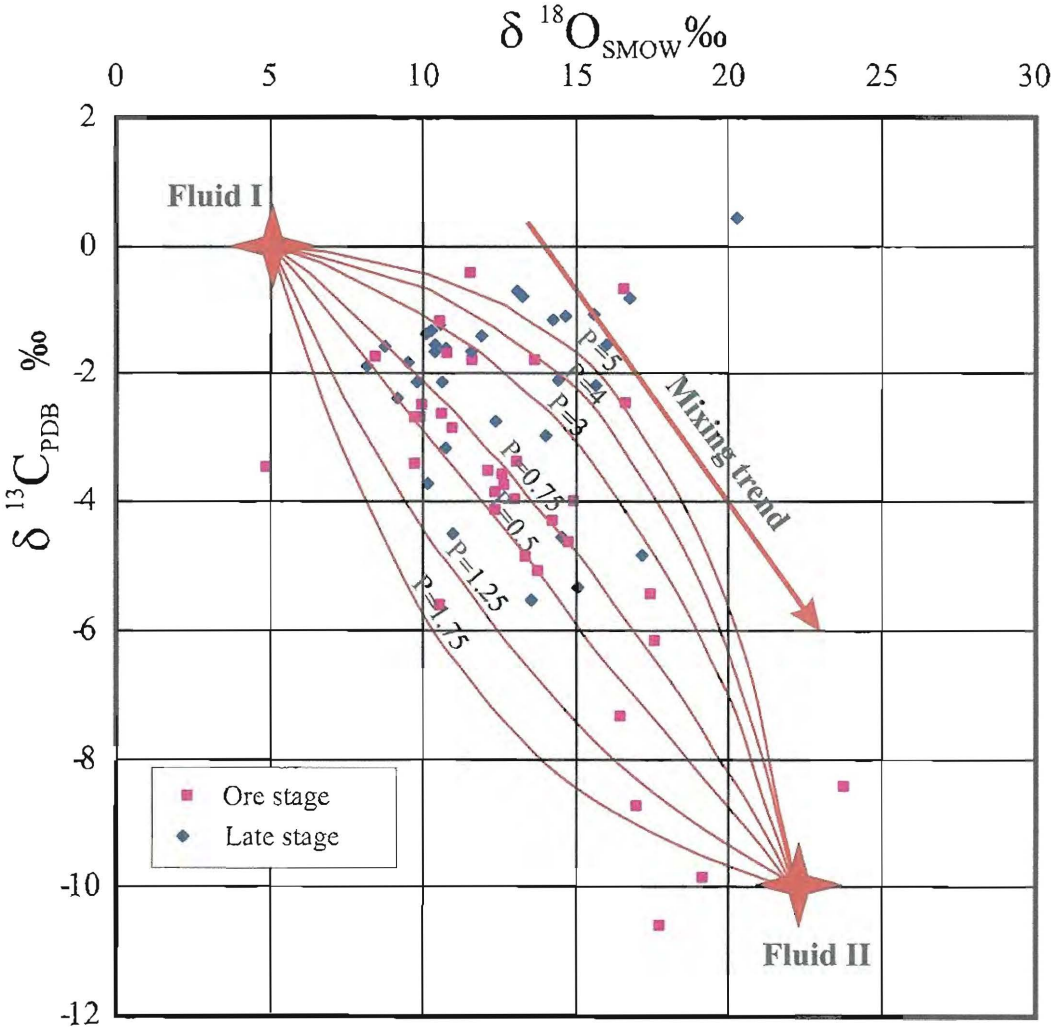

Figure 6.16. Plot of the $\delta^{13}C$ and $\delta^{18}O$ values from all zones with the mixing curves of fluid compositions by mixing of two fluids. Fluid I has $\delta^{13}C$ = 0‰ and $\delta^{18}O$ = +5‰; Fluid II has $\delta^{13}C$ = -10‰ and $\delta^{18}O$ = +22‰. P is the concentration ratio of total dissolved carbon in Fluid II to in Fluid I. The fluid mixing model of Savard and Kontak (1998) is calculated using the fractionation equations of Deines et al. (1974) and Friedman and O'Neill (1977).

6.4. Summary

The stable isotope study of the H zone has included sulphur, carbon and oxygen isotopes. Table 6.3 summarises the analytical data and interpretation.

Table 6.3. Summary of sulphur, carbon and oxygen isotopes data, source of fluids, species and related process for the H zone, Chatree deposit, Thailand.

Stable isotope	**Description**	**Result**	**Source of fluids**	**Species**	**Related processes**
Sulphur isotope	Pyrite from Stage 2 veins	$\delta^{34}S$ values = −1.7 to +5.3‰	Derived from magmatic waters (from magma or igneous host rocks)	H_2S predominant	Fluid mixing (magmatic and meteoric waters); Boiling
Carbon isotope	Ore stage carbonates	$\delta^{13}C$ values = −1.7 to −2.4‰	Derived from magmatic and meteoric waters	H_2CO_3 and HCO_3^-	Cooling and fluid mixing
Carbon isotope	Late stage carbonate	$\delta^{13}C$ values = −1.7 to −7.3‰	Derived from magmatic and meteoric waters	H_2CO_3 and HCO_3^-	Cooling and fluid mixing
Carbon isotope	Altered limestone	$\delta^{13}C$ values = -3‰	Derived from magmatic and meteoric waters	H_2CO_3 and HCO_3^-	Fluid-wall rock interaction
Carbon isotope	Initial fluid	$\delta^{13}C$ values = −2.1‰	Derived from magmatic and meteoric waters	H_2CO_3 and HCO_3^-	Cooling and fluid mixing
Oxygen isotope	Ore stage carbonates	$\delta^{18}O$ values = +7.5 to +11.6‰	Derived from magmatic and meteoric waters	H_2CO_3 and HCO_3^-	Cooling and fluid mixing
Oxygen isotope	Late stage carbonate	$\delta^{18}O$ values = +8.6 to +14.9‰	Derived from magmatic and meteoric waters	H_2CO_3 and HCO_3^-	Cooling and fluid mixing
Oxygen isotope	Altered limestone	$\delta^{18}O$ values = +9.9‰	Derived from magmatic and meteoric waters	H_2CO_3 and HCO_3^-	Fluid-wall rock interaction
Oxygen isotope	Initial fluid	$\delta^{18}O$ values = +2‰	Derived from magmatic and meteoric waters	H_2CO_3 and HCO_3^-	Cooling and fluid mixing

CHAPTER 7

Conclusions, Discussion and Genetic Model

7.1. Introduction

Previous chapters in this thesis document and discuss the geologic setting, vein paragenesis, ore mineralogy, hydrothermal alteration and stable isotopes of the H zone, Chatree deposit. This chapter combines and discusses the results of the previous chapters, compares the Chatree H Zone with other low-sulphidation epithermal deposits and proposes the genetic model.

7.2. Geological Setting

The H zone of the Chatree deposit is located in the Permo-Triassic Loei – Phetchabun Volcanic Belt and formed during subduction-arc magmatism (Bunopas and and Vella, 1983). The H zone is hosted by andesitic volcaniclastic succession and late dykes. The host rock consists of:

- Coherent plagioclase-pyroxene-phyric andesite;
- Andesitic lithic breccias;
- Crystal-rich andesitic pumice breccias;
- Crystal-rich quartz-feldspar lithic breccia;
- Quartz-rich volcanic sandstone and mudstone;
- Limestone; and
- Andesitic-dacitic and basaltic dykes.

Andesitic lithic breccia was formed by the in-situ collapse of existing andesitic rocks. Plagioclase-pyroxene phyric andesite intrudes and forms as sills into the andesitic lithic breccia. Crystal-rich quartz-feldspar lithic breccia and rare limestone occur as thin layers within the andesitic lithic breccia. Pyroclastic massive crystal-rich andesitic pumice breccia is inter-layered with volcanic sandstone/mudstone that overlies the andesitic lithic breccia. Late andesitic, andesitic-dacitic and basaltic dykes crosscut the volcanic and pyroclastic units. The late dykes have similar orientations to the major faults.

The Chatree deposit area has major faults trending NNW, NW and NE. Major structures of mineralised zones (the A, C and D zones) are NNW and NW directions but a major structure of the H zone is NE with a fault striking 040° and dipping north-west at between 20° and 45°. The fault has been inferred to normal movements syn- and post-mineralisation fault. The post mineralisation fault movement has been resulted in a major hanging wall shear in the crystal-rich andesitic pumice breccias and quartz-rich volcanic sandstone/mudstone units and subordinate footwall shear in the plagioclase-pyroxene-phyric andesite and andesitic lithic breccias units.

Whole rock geochemical data suggest that the host rock compositions are andesite, andesite-basalt to calc-alkaline basalt. The volcanic host rocks were erupted in both oceanic and continental arc setting with most rocks forming in continental arc setting.

The depositional environment of the host rock deposition is mainly in subaerial environment with minor shallow submarine environment. The host rocks have been deposited proximal to the volcanic source vent and have then been transported from the north (Greener, 1999; Cumming, 2004).

7.3. Vein mineralogy and paragenesis

Five vein stages have been identified within the H-zone by including:

- Stage 1 hydrothermal breccia and grey quartz formed along a main NE trending fault by ore-forming fluids evolved from crystallising water-saturated magma.
- Stage 2 mineralised veins consisting of quartz, calcite, chlorite, illite, illite-smectite, sericite, ankerite, dolomite, epidote, adularia, pyrite, hematite, rhodochrosite, chalcedony, sphalerite, galena, chalcopyrite and electrum with crustiform-colloform, comb, breccia and vuggy textures. Stage 2 veins are typically linear, showing strong sub-parallel alignment and grade through stockworks to the host rocks. The veins generally dip 45° to the NW with slightly flatter dips to the north of the H zone.
- Stage 3 veins are typically 1-2 cm wide linear veins, consisting of quartz, k-feldspar, carbonate, epidote, and pyrite.
- Stage 4 veinlets contain calcite. They are the latest vein generation and crosscut all previous vein stages and all rock units.
- Stage 5 is a joint surface coating consisting of laumontite in fractures, cavities and some veins.

Gold occurs as electrum in the Stage 2 veins of the H zone. Electrum occurs as: disseminations, inclusions within pyrite and in contact with pyrite, sphalerite, chalcopyrite and galena associated with fine-grained quartz and calcite gangue. The gold grade of the H zone is average 2-3 g/t. Whole rock gold and silver assays indicate a silver-gold ratio averaging 4:1. Average gold fineness for the electrum ranges from 544 to 690 (average 609) with Ag content ranging from 31.5 to 45.7 w% and Au content ranging from 53.1 to 68.2 w% (Ag:Au ratio ~0.6:1). The gold at the H zone is inferred to have been transported as bisulphide complex ($Au(HS)_2^-$) and the silver is transported dominantly by chloride complex ($AgCl_2^-$, Dedenczuk, 1998; Greener, 1999) similar to other epithermal deposits (Hedenquist et al., 2000). The sphalerite of the H zone has low FeS contents (<2 mole%) that may indicate a high sulphur activity in the hydrothermal fluids responsible for mineralisation in the H zone.

7.4. Hydrothermal alteration

Mineral alteration assemblages of the H zone are classified into 4 alteration zones defined by overprinting relationships and detailed textural studies using petrographic and PIMA study. These include:

- Zone I (Kaolinite - illite - montmorillonite - pyrite) occurs in the hanging wall with a sheet-like geometry. It can be classified as argillic alteration and is characterised by strong alteration intensity suggesting the host rock had high permeability. Zone I alteration is interpreted to have formed by low temperature (100°C to 150°C), acid to neutral and low salinity hydrothermal fluids.
- Zone II (Quartz - carbonate - illite - chlorite - pyrite - sericite - adularia) forms proximal to the mineralised veins. It is classified as potassic, silicic and phyllic alterations and is interpreted to have formed at temperatures ranging between 100°C to 300°C, from neutral to slightly alkaline hydrothermal fluids in impermeable zone.
- Zone III (Illite - chlorite - adularia - quartz - calcite - dolomite - ankerite - epidote - sericite - albite) occurs within 10 m of the ore zone. It is classified as propylitic alteration and is interpreted to have formed at temperatures ranging between 200°C to 300°C, from near-neutral pH fluids with range of salinities in areas of low permeability.
- Zone IV (Epidote - chlorite - illite) forms 30m from the ore zone. The zone is classified as propylitic alteration, and the alteration is interpreted to have formed at

temperatures ranging between 200°C to 250°C from near-neutral pH fluids with a range of salinities.

- Supergene enrichment alteration is present near the surface and is indicated by unusually high gold assays (>100 g/t). It is interpreted to result from the water table being close to the surface.

Chlorite of the H zone is Mg-rich chlorite with a Fe/(Fe+Mg) ratio from 0.09 to 0.45. The gold grades and the Fe/(Fe+Mg) of chlorite at the H zone have a positive relationship that may suggest gold precipitation in the H zone related to the redox condition of the ore fluids.

7.5. Sulphur, carbon and oxygen isotopes

Sulphur, carbon and oxygen isotopes have been analysed to assist with an understanding of ore fluid chemistry and sources of the ore fluids.

Pyrite of vein Stage 2 has $\delta^{34}S$ values ranging between –1.7 to +5.3‰, with a mean of 2.1‰ and a standard deviation of 3.7‰, consistent with $\delta^{34}S$ values for magmatic sulphur either as magmatic fluids or by dissolution of igneous sulphides. The relation of the $\delta^{34}S$ values and gold grades of the H zone suggests that sulphur isotope variation may be related to boiling and the data can be used to assist in delineating boiling zone.

Carbon and oxygen isotope data were obtained from various stages of limestone, ore-stage and post ore stage carbonates. The values of $\delta^{13}C$ of the carbonates range between –0.8‰ to –7.3‰ and the data suggest that carbon was derived from mixed compounds of igneous CO_2 and carbon in meteoric water. The $\delta^{18}O$ values range between +7.5‰ to +14.9‰. These values partly overlap with those from pristine volcanic rocks and are similar to values from metasediments (Rollinson, 1993). A dominant fluid with initial composition of $\delta^{13}C$ and $\delta^{18}O$ values of -3‰ and +2‰ was assumed to involve in the H zone and the fluid is interpreted to be modified meteoric water.

Sulphur, carbon, oxygen isotopes from the H zone suggest that there has been a significant amount of meteoric waters mixing with magmatic fluids. The meteoric water circulation was probably due to a convective hydrothermal system induced by heat derived from an underlying igneous rock source.

The carbon species of the Chatree deposit including the H zone consists of both H_2CO_3 and HCO_3^- species that are associated with the mixing process. The carbon and oxygen isotopes of limestone suggest that fluid-wall rock interaction occurred in the deposit resulting in metasomatic alteration of the limestone. A Plot of $\delta^{13}C$ versus $\delta^{18}O$ values of the Chatree deposit indicates that the ore stage carbonates have a positive trend and the late stage carbonates have shows a negative trend. The positive trend suggests that the carbonate precipitation was related to decrease in temperature of the ore fluid. The negative trend suggests that mixing of two carbonate sources has occurred during the late stage carbonate deposition.

7.6. Geochemistry of the ore fluid

The geochemistry of the H zone ore fluid is estimated from mineralogical studies. Features of the fluid including temperature, pressure, oxygen-carbon dioxide fugacity, pH and sulphur fugacity are interpreted from equilibrium mineral assemblages.

7.6.1. Temperature

The mineral assemblages presented in Table 5.1 (see Chapter 5) suggest temperatures in the H zone ranging between 100 to 300°C, consistent with Dedenczuk (1998) and Greener (1999) who suggested that the fluid temperature ranged between 100°C to 300°C from the fluid inclusion studies in the A, C and D zones. Temperature of the H zone from fluid inclusion is not studied in this work because there is no suitable fluid inclusion for analysis.

The wide temperature range explains the range of different minerals found in the H zone. Table 5.3 in Chapter 5 shows temporal variations in temperature of hydrothermal systems by using the relationship of alteration minerals and their respective vein stages. The highest temperature range is found from vein Stage 2 with muscovite at 300°C.

7.6.2. pH and salinity

In Chapter 5, alteration assemblages of the H zone indicate that the pH of the fluid is near neutral as evident by the presence of quartz, pyrite, illite, chlorite, adularia and epidote (Hedenquist et al., 2000). Moreover, adularia is precipitated in the mineralised veins and the wall rocks of the H zone according to the reaction;

$$K^+ + Al(OH)_3 + 3H_4SiO_4 = KAlSi_3O_8 + H^+ + 7H_2O \quad (1)$$

$Al(OH)_3$ is the predominant aluminium species in near-neutral-pH low-salinity waters (Lawless et al., 1999).

The mineral assemblages of quartz, adularia, chlorite, illite, calcite, and pyrite suggest formation from alkaline chloride water (Simpson et al., 1995). The abundance of carbonate minerals suggests that fluid have relatively high concentrations of dissolved CO_2. Studies of the alteration zones of the H zone in Chapter 5 show a near neutral to slightly acid pH fluid that is mainly meteoric origin with a small magmatic volatile input. Salinity of fluids at the H zone has not been determined due to the lack of suitable fluid inclusions for analysis. However, Greener (1999) and Dedenczuk (1998) suggested that the Chatree ore fluids have low salinity (< 3 wt% NaCl equiv.) based on fluid inclusion studies of the A, C and D zones.

7.7. Depositional process

Gold and silver being the most important ore elements in the Chatree deposit was probably transported as a bisulphide complex, whereas silver travels as both bisulphide and chloride complex. The interpretation of gold and silver speciation is based on experimental studies (e.g., Gammons and William-Jones, 1995, 1997; Benning and Seward, 1996). Gold of the H zone is transported as $Au(HS)_2^-$ in dilute, reduced, near neutral pH waters (Cooke and Simmons, 2000) and precipitated from the solution with an equation:

$$2Au(HS)_2^- + H_2 + 2H^+ = 2Au + 4H_2S \quad (2)$$

By the equation, gold deposition of the H zone is dependent on temperature, pH, salinity, fS_2 and fO_2 condition. Depositional mechanisms that caused gold precipitation include conductive cooling, boiling, fluid mixing and water-rock interaction.

7.7.1. Conductive cooling

Cooling is a process that is related to the loss of heat by conduction to the country rocks. It may occur when fluids rise in a conduit (Cooke and Gemmell, 1996). At the H zone, the effects of cooling from 300 to 100°C are seen based on the carbon and oxygen isotope study. The pH of a cooling fluid seems to decrease because acids dissociate with decreasing temperature or because of precipitation of minerals such as muscovite and pyrite (Cooke and McPhail, 2001). Quartz + muscovite + pyrite +

sphalerite at the deeper level were precipitated between 300 and 190°C and quartz + pyrite + kaolinite near surface were formed between 185 and 100°C (Cooke and McPhail, 2001). The conductive cooling may be a significant depositional process in the upper level of the H zone based on comparing mineral assemblages of the lower level (quartz + muscovite + pyrite + sphalerite assemblages) and the upper level (quartz + pyrite + kaolinite). The dominant fluid of the H zone is interpreted as an alkaline-reduced fluid by alteration minerals assemblages. Precipitation of quartz vein (97% quartz) with traces of pyrite, K-feldspar, calcite, sphalerite, galena, chalcopyrite, dolomite and muscovite that is predicted to occur at about 200°C (Cooke and Gemmell, 1996) also occurs in the H zone. This process is interpreted to remove all lead, zinc and silver from the solution but the low initial metal concentrations in the fluid allowed only traces of base metal sulphide to be deposit in the H zone. Although acnthite is not found in the H zone, silver of the H zone may occur as extraction of acanthite over a small temperature interval, equivalent to a restricted vertical interval of mineralisation in a fault based on observation of Cooke (1992) at the Acupan vein system, Philippines. The conductive cooling process is unlikely to be the predominant process to precipitate Gold at the H zone because it is very difficult to cool 300°C water without boiling or mixing in the upper few kilometre from the surface (Cooke and McPhail, 2001).

7.7.2. Boiling

Boiling occurs when hydrothermal fluids ascend through a near neutral environment with a decrease in pressure. Boiling of the H zone is suggested by adularia precipitate in the mineralised veins (see Chapter 4; Reed and Spycher, 1985). Boiling results in the reduction and loss of temperature, CO_2 and H_2S. By the equation(2), loss of H_2S due to boiling drives the equation to the right, increasing the pH and depositing gold. The pH increase was caused by gas loss to vapour state (Reed and Spycher, 1985). The loss of CO_2 and H_2S lead to the association of bicarbonate and bisulphide species. The pH increase is partly offset by precipitation of sulphide (e.g., pyrite) and carbonate minerals (e.g., calcite and rhodochrosite). Loss of CO_2 also causes the fluid to become more alkaline and result in gold precipitation. Gold precipitation begins during the first increment of boiling. Boiling is complicated by associated pH changes that may prevent higher grades of gold from being deposited (Lawless et al., 1999). High gold grades of the H zone that form in smaller localised zones may be caused by an abrupt pressure release process such as dilation due to tectonic movement that can result in

hydrothermal fracturing and brecciation. Repeated dilatational processes such as fault movement, hydrothermal fracturing and brecciation may form economic gold veins of the H zone. These processes occur because the dilatational zones are often self-sealing with quartz and carbonate minerals. The self-sealing process results in the depth interval of boiling zone changing and giving rise to spatial overlapping of different chemical regimes (Reed and Spycher, 1985). Boiling of an alkaline reduced brine results in the precipitation of quartz (59 vol%), calcite (31 vol%), rhodochrosite (9 vol%) and traces of other minerals such as pyrite, K-feldspar, sphalerite, galena, chalcopyrite and dolomite (Cooke and Gemmell, 1996). The quartz-carbonate vein assemblage of the H zone is consistent with these observations, suggesting that they may be products of boiling hydrothermal fluids.

7.7.3. Fluid mixing

Mixing of fluids is related to changes in temperature and ligand concentrations, which may result in precious and base metal deposition (Henley, 1990). Fluid mixing typically occurs in the near surface environment (Cooke, 1992). Sulphur, carbon and oxygen isotope data of the A, C, D and H zones (see Chapter 6) from sulphide minerals co-existing with gold and carbonate minerals of ore stage, late stage and limestone suggest that fluid mixing occurred at Chatree. The sulphur, carbon and oxygen isotope studies at the Chatree also suggest that fluid mixing is an important mechanism controlling the deposition of ore and other minerals. The mixing process occurred due to mixing of cold meteoric water with a hot metal bearing hydrothermal fluid. This process may also dilute the gold concentration and cool the fluids. The deep ore veins were formed by hotter condition that typically forms veins rich in sulphides with chlorite and pyrite gangue. Progressive mixing as deep fluid migrated to the upper part of the system resulted in increasing silver-rich ores (Gemmell and Cooke, 1996). Sphalerite and galena may be precipitated during the initial stage of mixing.

7.7.4. Water-rock interaction

The zonation of wall rock alteration assemblages of the H zone resulted from the interaction of hydrothermal fluid with the andesitic host rock and limestone. Interaction of fluid with the host rock can be a potential site for the deposition of gold. However, ore-grade gold mineralisation of the H zone is only occurred associated with veins, suggesting that water-wallrock interactions were not an important process for deposition

of the precious metals. The alteration generally forms halos around the veins and represents the dominant process at the H zone.

7.8. H zone compared to other low-sulphidation epithermal deposits

The Chatree deposit has many features that are consistent with a low-sulphidation epithermal deposit (Dedenczuk, 1998; Deimar, 1999, Greener, 1999 and this study). These features include the age, tectonic setting, and host rocks. Most low sulphidation epithermal gold deposits are found in Cretaceous or younger rocks (Sillitoe, 1993), and are usually associated subaerial with volcanism and calc-alkali magmas (Cooke, 2000). The mineralised veins of the Chatree deposit, including the H zone, are hosted by Permo-Triassic age, sub-alkali and calc-alkali basalt and andesite associated with a volcanic arc affinity (see Chapter 3). Epithermal deposits are often related to areas of well-developed tensional fracture systems and normal faults, indicating extensional tectonic settings (Gemmell, 2004). This study suggests the structural setting of the H zone as a dilational jog formed by extension along a NE trending normal fault (see Figure 3.2 in Chapter 3).

Cooke (2000) indicates that a low sulphidation epithermal gold deposit generally forms at shallow depths (within 1 km of the surface), moderate pressures and temperatures of less than 300°C. Gold mineralisation in the H zone occurs in veins <200m from the current surface. Most ores in low-sulphidation epithermal systems are found in quartz veins, stockworks, and breccias carrying gold, silver, electrum, argentite and pyrite with variable amounts of sphalerite, chalcopyrite, galena, rare tetrahedrite and sulphosalt minerals (Panteleyev, 1996). The most common emplacement form is open space fillings, including cockscomb textures, crustifications, drusy cavities and symmetrical banding (Gemmell 2004). Common gangue minerals include quartz, calcite, fluorite, barite, and pyrite. In the H zone, electrum (gold + silver) with associated pyrite, sphalerite, chalcopyrite and galena occur in crustiform-colloform bands, comb textures, and breccia veins. The ore and sulphide minerals are associated with a quartz and calcite gangue (see Chapter 4).

The mineral alteration assemblages (e.g., quartz, calcite, illite, chlorite, pyrite, and adularia) in this study suggest that hydrothermal fluids of the H zone have near neutral pH and low salinity characteristics (see Chapter 5). Cooke (2000) indicates that similar assemblages and hydrothermal fluid characteristics are typical for low sulphidation epithermal systems. This study interprets the alteration assemblages

present in the H zone to have formed by hydrothermal fluids of temperatures between 100°C to 300°C (see Chapter 5). The major mechanisms for gold deposition in epithermal environments such as boiling and fluid mixing suggested by Cooke (1996), are also interpreted to have been vital mechanisms in the deposition of gold in the H zone, based on mineralogy, sulphur, carbon and oxygen isotope studies.

Table 7.1 summarises some characteristics of the H zone at the Chatree deposit with similar features for "typical" low-sulphidation epithermal deposits and two major low-sulphidation epithermal deposits (the Golden Cross, New Zealand and Hishikari, Japan). Table 7.1 indicates that the majority of features found in the H zone at Chatree are comparable to these examples.

Table 7.1. Comparison of the characteristics of the H zone, the Chatree deposit, Thailand and other low-sulphidation epithermal deposits.

	Typical low-sulphidation epithermal	**The H zone, Chatree deposit, Thailand**	**The Golden Cross, NZ**	**Hishikari, Japan**
Tectonic setting	Extensional continental and island arc	Continental and oceanic arc	Continental arc	Oceanic arc
Igneous suite	Calc-alkaline	Calc-alkaline	Calc-alkaline	Calc-alkaline
Igneous rock	Rhyolite-basalt	Andesite	Andesite and dacite	Andesite
Metal signature	Au-Ag	Au-Ag	Au-Ag	Au-Ag
Au/Ag assay (g/t)	Low Au grade	2.1 / 14	2.4 / 9.64	130 / 64
Ag/Au ratio	0.5-20	8	4	0.47
Deposit form	Vein, stockwork, vein breccia, breccia infill, dissemination	Vein, stockwork and breccia	Quartz-Adularia Vein	Quartz-Adularia Vein
Ore texture	Open-space, colloform-crustiform band, comb structure, and multiple brecciation	Open-space, colloform-crustiform band, zone crystal and breccia	Vein , breccia and stockwork	Bladed quartz, Lattice and Open space
Gangue mineral	Quartz, calcite, adularia, chalcedony, illite, chlorite, fluorite	Fine grained quartz, calcite, chlorite and adularia	Quartz, adularia and calcite	Quartz and Adularia
Proximal alteration	Quartz, illite, smectite and adularia	Quartz, calcite, illite, chlorite, pyrite, sericite and adularia	Chlorite, illite, smectite, and pyrite	Chlorite and sericite
Fluids	150°-300°C, <2 wt%NaCl equiv.	100°-300°C, <3 wt%NaCl equiv.	190°-295°C, <2 wt%NaCl equiv.	210°C<2 wt%NaCl equiv.
Fluid charateristic	Meteoric± magmatic near neutral, reduced	Meteoric± magmatic near neutral, reduced	Meteoric± magmatic near neutral, reduced	Meteoric±magmatic near neutral, reduced
Reference	Gemmell, 2004; Panteleyev, 1996; Hedenquist et al., 2000; Brathwaite and Christie, 2000.	This study; Greener, 1999 (fluids data)	Ronde and Blattner, 1988; Brathwaite and Blattner, 1995; Brathwaite and Faure, 2002; Simpson et al., 1995	Nakayama, 1995; Etoh et al., 2002; Izawa et al., 1990

7.9. Genetic model

In the previous sections, it is documented that the H zone of the Chatree deposit is a low-sulphidation epithermal gold deposit. It formed in a tectonically active setting (subduction zone) along the Loei – Phetchabun volcanic belt. An intrusive rock is inferred to be present at depth, and this is the source of heat and metals of the hydrothermal system, which led to the deposition of gold and silver at shallow level (< 1 km depth), forming the Chatree deposit. The formation of Chatree low-sulphidation epithermal gold deposit is a combination of processes that involved linking magmatism, structural, deformation, geochemical evolution and hydrothermal of ore fluids.

- **Phase 1 - Pre-magmatism ground preparation.** The volcanic and pyroclastic host rocks at the Chatree deposit were deposited predominantly in a subaerial environment with minor shallow submarine transgressions. Major NW trending strike-slip faults resulted in dilation jogs forming NE/40° veins of the H zone (Figure 7.1).

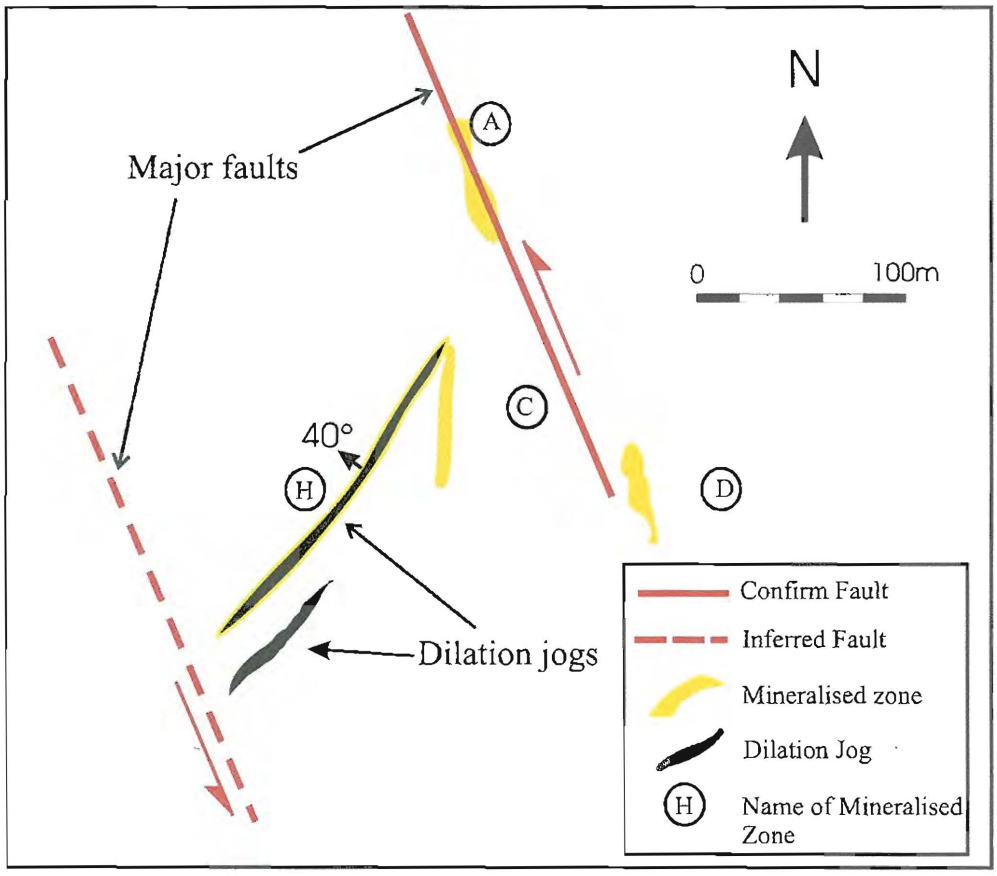

Figure 7.1. Major NW fault movement at the Chatree resulting in dilation jog of the H zone.

- **Phase 2 – Intrusion-related heated source.** Hydrothermal activity in a low-sulphidation deposit typically began with a high temperature (600°C; Hedenquist et al., 2000) intrusion at depth that may also be suggested in the H zone. The heat source generates a convection cell that circulates predominantly meteoric water into deeper levels. Continually recharging meteoric water mixes with magmatic volatiles (from sulphur, carbon and oxygen isotope interpretation) and fluids derived from the intrusion produced a dilute brine of near-neutral pH fluid (Figure 7.2).

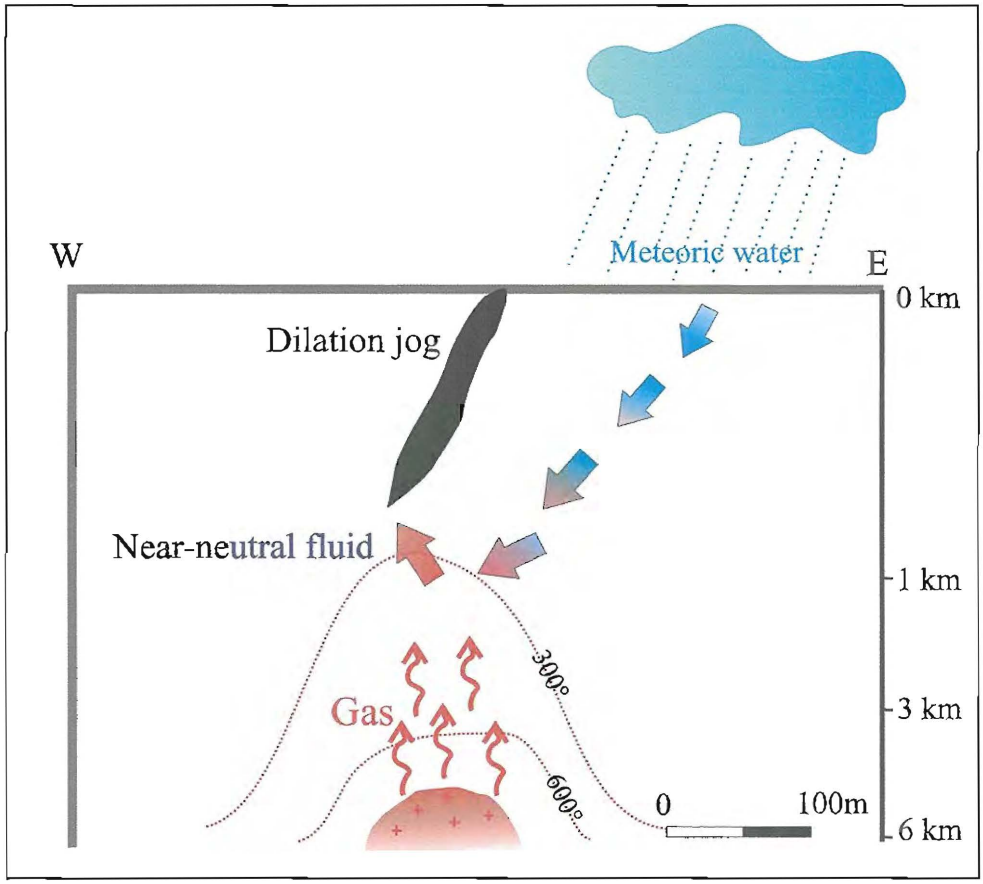

Figure 7.2. Cartoon cross-section illustrating the meteoric water mixes with magmatic volatile and fluids in the H zone (modified after Hedenquist et al., 2000; Cooke and Simmons, 2000)

- **Phase 3 - Hydrothermal breccia and boiling.** The near-neutral to slightly alkali fluids rise along the fractures that formed by dilational jogs of the major faults (Figure 7.3A). The fluids have sufficient energy to transports clasts of andesitic host rocks along fracture (Figure 7.3B), forming hydrothermal breccia with grey quartz matrix. Fluid flow continued until the fractures become blocked or until fluids were exhausted. Hydrothermal fluids ascending through the fracture underwent the rapid pressure reduction, resulting in boiling.

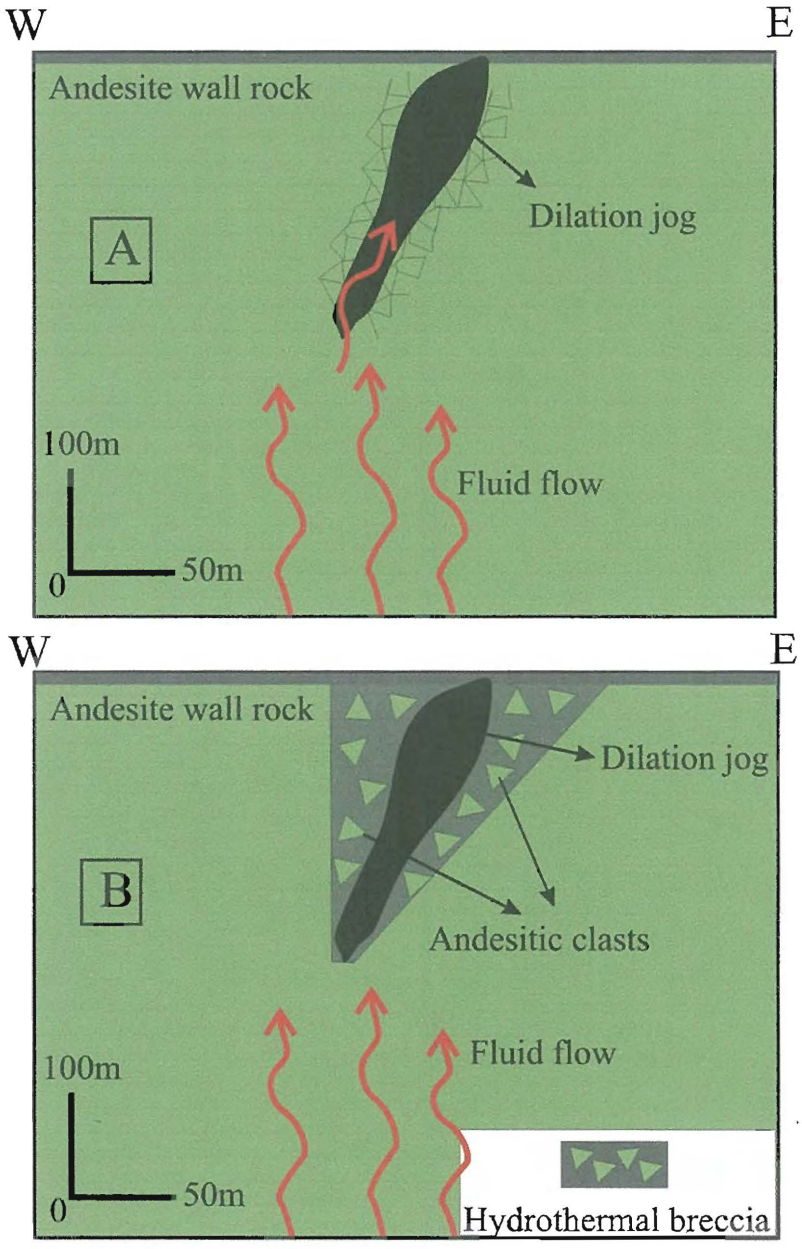

Figure 7.3. Cartoon illustrating formation of the hydrothermal breccia of the H zone, Chatree deposit, Thailand.

- **Phase 4 Gangue precipitation.** The temperature of fluids during boiling is varying when fluids circulate. From Phase 3, boiling is resulted from pressure drop then the fluid temperature was suddenly dropped and steam fraction was increased to maintain water-steam saturation conditions. The fluid temperature is increased due to a combination of heat transferred to the host rock. The increasing of fluid flow leads to amorphous silica deposition between the hotter host rock and cooler fluid (Figure 7.4). The amorphous silica deposition will be alternating periods from different flow regimes and temperature, producing a dilatant depositional cycles and producing the fine rhythmically band (colloform-crustiform quartz band). Sometimes silica precipitate sealed themselves that can cause breccia texture. These processes occurred repeatedly. Boiling resulted in adularia precipitation with quartz in veins (Lawless et al., 1999). Quartz and adularia deposition reduced primary permeability in the host rocks (Lawless et al., 1999). Carbonate deposition occurred by a CO_2-rich water increasing temperature, leading to release of CO_2 that promotes carbonate depositing (Hedenquist et al., 2000). The ascending of near neutral fluid of the H zone also resulted in illite-smectite and silicic alteration of the wall rock.

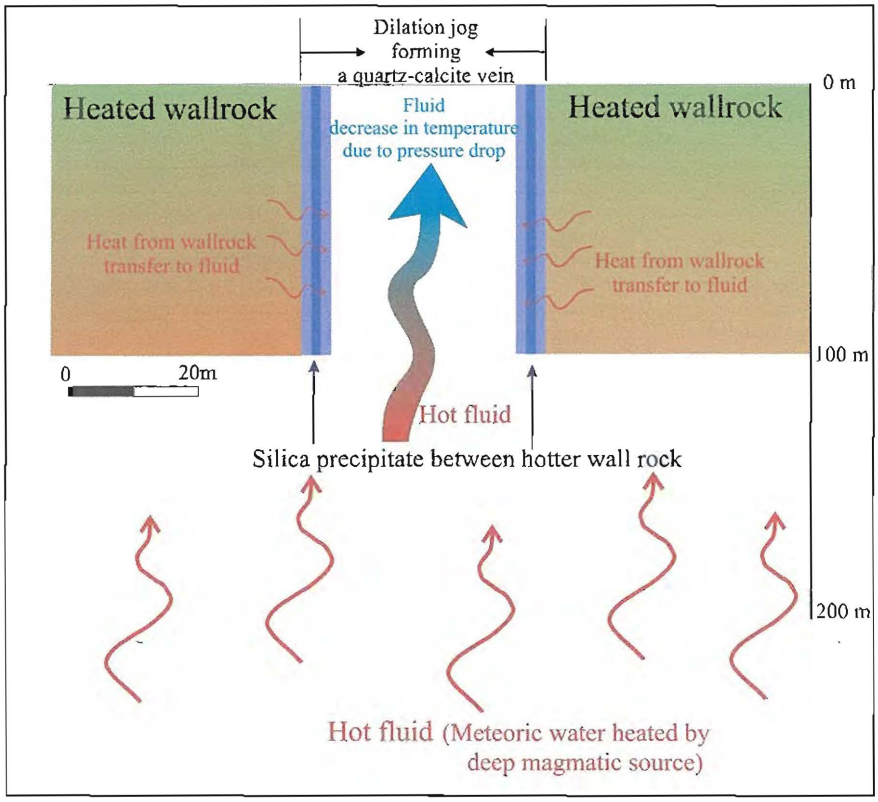

Figure 7.4. Cartoon cross-section illustrating the deposition of silica gangue minerals at the H zone, the Chatree deposit, Thailand.

- **Phase 5 - Electrum precipitation.** Electrum in the H zone is commonly co-depositional with galena, pyrite, chalcopyrite and sphalerite in fine grained quartz, calcite, pyrite with minor adularia. Electrum that generally deposited at a temperature range of 260° to 190°C from a fluid range of 1.0 to 0.2 wt% NaCl equiv. of salinity (Lawless et al., 1999) maybe assumed in the H zone. Hot hydrothermal fluid mixing with cold groundwater will dilute the gold concentration and resulted in fluid cooling. Fluid mixing at depth typically forms veins rich in sulphides with hematite, chlorite and pyrite gangue.

- **Phase 6 - Late mineral precipitation and steam-heated zone.** At shallow level of hydrothermal systems, acid sulphate water is typically occurred from gas condensation (White, 2004). Acid sulphate waters may be formed at near surface of the H zone. Calcium-bearing acid-sulphate waters that formed above boiling zone ascended to near surface and mixed with the hydrothermal fluid producing the carbonate-bearing vein and alteration assemblage. The acid sulphate waters near the surface are heated and become CO_2-rich steam heated water on the margin of the system. Steam-heated water forms a blanket of kaolinite, montmorillonite, illite-smectite and pyrite (Figure 7.5). It is not directly associated with ore but overlies the ore zone in the hanging wall of the H zone.

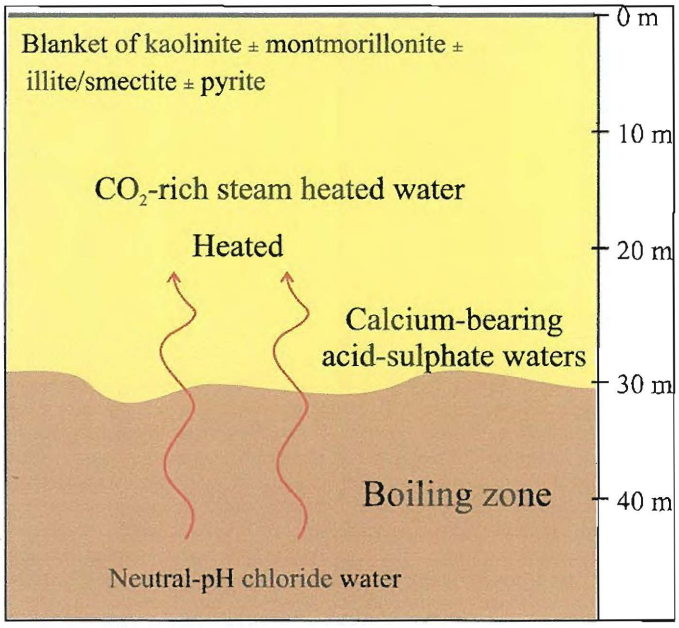

Figure 7.5. Cartoon illustrating the blanket of kaolinite, montmorillonite, illite-smectite and pyrite by steam heated water (modified after White, 2004).

- **Phase 7 - Post mineralisation.** Shearing in the hanging wall occurred after mineralisation by late fault movement although shearing may have initially begun during mineralisation. The late dyke that crosscuts the earlier host rocks and veins occurred after shearing (Figure 7.6). The late stage calcite veinlet that crosscut all units may have formed by effect of late dyke providing heating and cooling of the host rock.

- **Phase 8 - Supergene enrichment.** Supergene oxidation occurred where water table lies close to the surface (Hedenquist et al., 2000). The oxide-sulphide interface is generally subhorizontal because it is controlled by paleowater table (Chávez, 2000).

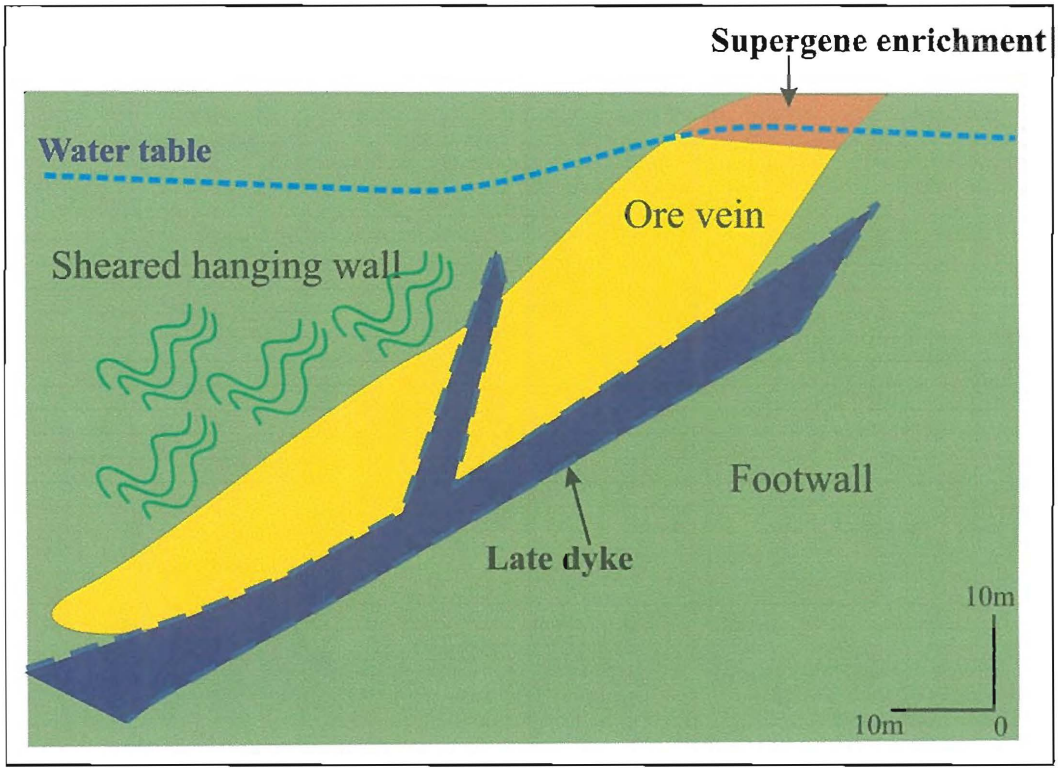

Figure 7.6. Cartoon illustrating the late dyke crosscuts ore vein of the H zone and also results in sheared hanging wall.

References

Achache, J., Courtillot, V., and Besse, J., 1983, Palaeomagnetic constraints on the Late Cretaceous and Cenozoic tectonics of southeastern Asia: Earth and Planetary Science Letters, v. 63, p. 123-136.

Arehart, G. B., Christenson, B. W., Lindsay, J. M., Sano, Y., and Anonymous, 1996, Palaeofluids at the Golden Cross epithermal mine, New Zealand: Abstracts with Programs - Geological Society of America, v. 28, p. 93.

Barr, S. M., and James, D. E., 1990, Trace element characteristics of upper Cenozoic basaltic rocks of Thailand, Kampuchea and Vietnam: Journal of Southeast Asian Earth Sciences, v. 4, p. 233-242.

Barr, S. M., and Macdonald, A. S., 1987, Nan River suture zone, northern Thailand; with Suppl. Data 87-32: Geology, v. 15, p. 907-910.

—, 1991, Toward a late Palaeozoic-early Mesozoic tectonic model for Thailand: Journal Thai Geoscience, v. 1, p. 11-12.

Barron, B. J., 1998, Petrological examination of twenty rock samples from the Chatree gold project, Thailand: Akara Mining Limited, unpublished report, 20 p.

Barton, P. B. Jr., and Bethke, P. M., 1987, Chalcopyrite disease in sphalerite: pathology and epidemiology, Am Mineral, v. 72, p. 451-67.

Benning, L. G., and Seward, T. M., 1996, Hydrosulphide complexing of Au(I) in hydrothermal solutions from 150-400 degrees C and 500-1500 bar: Geochimica et Cosmochimica Acta, v. 60, p. 1849-1871.

Bottrell, S. H., Crowley, S., and Self, C., 2001, Invasion of a karst aquifer by hydrothermal fluids: Evidence from stable isotopic compositions of cave mineralization: Geofluids, v. 1, p. 103-121.

Boyle, R. W., 1979, The geochemistry of gold and its deposits: Geological Survey of Canada, Bulletin 280, 583 p.

Brathwaite, R. L., and Blattner, P., 1995, The Waihi epithermal gold-silver-quartz vein system, New Zealand: A high-throughput geothermal system of late Miocene age: Publication Series - Australasian Institute of Mining and Metallurgy, v. 9/95, p. 75-80.

Brathwaite, R. L., Christie, A. B., and Anonymous, 2000, Deposit types and paleo-depth extents of Coromandel epithermal Au-Ag deposits: Crown Minerals Publicity Unit, New Zealand Ministry of Economic Development.

Brathwaite, R. L., and Faure, K., 2002, The Waihi epithermal gold-silver-base metal sulfide-quartz vein system, New Zealand: Temperature and salinity controls on electrum and sulfide deposition: Economic Geology, v. 97, p. 269-290.

Buchanan, L. J., 1981, Precious metal deposits associated with volcanic environments in the Southwest: Arizona Geological Society Digest, v. 14, p. 237-262.

Bunopas, S., 1981, Paleogeographic history of Western Thailand and adjacent parts of Southeast Asia-A plate tectonics interpretation: Unpublished Ph.D. thesis, Wellington, New Zealand, Victoria University of Wellington, 810 p.

Bunopas, S., 1992, Regional stratigraphic correlation in Thailand: Potential for Future Developt.Piancharoen, C., editor-in-chief, Department of Mineral Resources, Bangkok, Thailand, 17-24 November, 1992, 2, p. 2-24.

Bunopas, S., 2002, Growing of Asia in the Late Triassic Continental-continental Collision of Shan-Thai and Indochaina against South China, In: The Symposium on Geology of Thailand, Bangkok, Thailand, 26-31 Ausgust, 2002, p. 129-135.

Bunopas, S., and Vella, P., 1983, Tectonic and geologic evolution of Thailand: Stratigraphic Correlation of Thailand and Malaysia, Haad Yai, Thailand, 1983, Proceedings, p. 307-322.

Burrett, C., and Stait, B., 1987, China and Southeast Asia as part of the Tethyan margin of Cambro-Ordovician Gondwanaland: In: shallow Tethys 2. Proceedings of the International Symposium on Shallow Thethys 2 McKenzie, K. G., Ed, Balkema, Rotterdam, p. 65-77.

Burrett, C., Long, J., and Stait, B., 1990, Early-middle Palaeozoic biogeography of Asian terranes derived from Gondwana: Memoir - Geological Society of London, v. 12, p. 163-174.

Campbell, A. R., and Larson, P. B., 1998, Introduction to stable isotope applications in hydrothermal systems: Reviews in Economic Geology, v. 10, p. 173-193.

Cathelineau, M., 1988, Cation site occupancy in chlorites and illites as a function of temperature, in Bain, D. C., Ed., Clay Minerals, 23: London, Mineralogical Society, p. 471-485.

Cathelineau, M., and Nieva, D., 1985, A chlorite solid solution geothermometer; the Los Azufres (Mexico) geothermal system: Contributions to Mineralogy and Petrology, v. 91, p. 235-244.

Chaodumrong, P., 1992, Stratigraphy, sedimentology and tectonic setting of the Lampang Group, Central North Thailand: Unpublished Ph.D. thesis, University of Tasmania, Hobart, Australia, 230 p.

Charoenpravat, A., Sripongpan, P., Thammadusadee, V., and Wolfrat, R., 1987, Geology of Amphoe Sop Prap and Amphoe Wang Chin, Thailand. Geology Ib. B65. Hanover, 52p.

Charusiri, P., 1989, Lithophile metallogenic epochs of Thailand: A geological and geochronological investidation: Unpub. PhD thesis, Queen University, Kingston, Ontario, Canada, 891p.

Charusiri, P., Daorerk V., Archibald, D., Hisada, K. and Ampaiwan, T., 2002. Geotectonic Evolution of Thailand: A New Synthesis: Journal of the Geological Society of Thailand, No.1, p. 1-20.

Chavez, W. X., Jr., 2000, Supergene oxidation of copper deposits: Zoning and distribution of copper oxide minerals: SEG Newsletter, v. 41, p. 10-21.

Cooke, D. R., 1992, Numerical models of mineral deposition for the Acupan vein system, Philippines, in Kharaka, Y. K., and Maest, A. S., eds., Proceedings - International Symposium on Water-Rock Interaction, v.7: Sub-Group on Water-Rock Interaction, International Association of Geochemistry and Cosmochemistry and Alberta Research Council, p. 1579-1582.

Cooke, D. R., and Gemmell, J. B., 1996, Low Sulfidation Epithermal Gold Deposit, in Master of Economic Geology Course Work Manual 5, p. 3.133-3.137, Centre of Ore Deposit Research (CODES).

Cooke, D. R., and McPhail, D. C., 2001, Epithermal Au-Ag-Te mineralization, Acupan, Baguio District, Philippines: Numerical simulations of mineral deposition: Economic Geology, v. 96, p. 109-131.

Cooke, D. R., and Simmons, S. F., 2000, Characteristics and genesis of epithermal gold deposits: Reviews in Economic Geology, v. 13, p. 221-244.

Craig, J. R. and Vaughan, D. J., 1981, Ore microscopy and ore petrography, John Wiley & Sons, New York, 406 p.

Christie, A. B. and Brathwaite, R. L., 2004, Palaeodepth assessment of epithermal golds-silver deposits in New Zealand: SEG 2004 Predictive Mineral Discovery Under Cover, Centre for Global Metallogeny, The University of Western Australia, Publication No.33, p. 208-211.

Cumming, G. V., 2004, An assessment of the volcanic facies at the Chatree mine and other selected volcanics in the Loei-Petchabun Volcanic belt, B.Sc (Hons) thesis (unpublished), Centre of Ore Deposit Research, School of Earth Sciences, University of Tasmania, Hobart, Australia, p 101.

Davison, G. J., 2003, Carbon/Oxygen Isotopes-their principles and uses in the exploration and understanding of fossil hydrothermal systems, in Master of Economic Geology Course Work on Ore deposit geochemistry, hydrology and geochronology, v. 1, Centre of Ore Deposit Research (CODES), University of Tasmania, Hobart, Australia.

Davidson, G. J. and Davis, B., 2001, Some controls on oxidation state variation of oxide Cu-Au systems [abs.]: Geological Society of America, Abstracts with Programs, v. 33, p. 2.

Dedenczuk, D., 1998, Epithermal gold mineralisation at Khao Sai, B.Sc (Hons) thesis (unpublished), Centre of Ore Deposit Research, School of Earth Sciences, University of Tasmania, Hobart, Australia.

Deer, W. A., Howie, R. A., and Zussman, J., 1992, An introduction to the rock-forming minerals: Hong Kong, Longman Group, 696p.

de Caritat, P., Hutcheon, I., and Walshe, J. L., 1993, Chlorite geothermometry; a review: Clays and Clay Minerals, v. 41, p. 219-239.

de Ronde, C. E. J., and Blattner, P., 1988, Hydrothermal alteration, stable isotopes, and fluid inclusions of the Golden Cross epithermal gold-silver deposit, Waihi, New Zealand: Economic Geology, v. 83, p. 895-917.

Diemar, M. G., 1990, TGF 1508 summary, report to Thai Gold Fields Limited (unpublished).

Diemar, M. G., 1999, The Chatree epithermal gold-silver deposit, Phichit-Phetchabun Provinces, Thailand, In: Symposium on Mineral, Energy, and Water Resource of Thailand: Toward the year 2000 October 28-29, Bangkok, Thailand.

Diemar, M. G., http://www.smedg.org.au/chatree2.html

Diemar, M. G., and Diemar, V. A., 1999, Geology of the Chatree epithermal gold deposit, Thailand: Publication Series - Australasian Institute of Mining and Metallurgy, v. 4-99, p. 227-231.

Deines, P., Langmuir, D., and Harmon, R. S., 1974, Stable carbon isotope ratios and the existence of a gas phase in the evolution of carbonate ground waters: Geochimica et Cosmochimica Acta, v. 38, p. 1147-1164.

Department of Mineral Resources, 1994, Report on semi-detailed Mineral Exploration at Chon Dean - Thap Klo selected area No. 16-1994, (unpublished) report to Department of Mineral Resources, Thailand (in Thai).

Department of Mineral Resources, 1999, Geology of Thailand, Department of Mineral Resources, Bangkok, Thailand (in Thai).

Department of Mineral Resources, 2002, Geology and Mineral Resources of Thailand Conference, Department of Mineral Resources, Bangkok, Thailand (in Thai).

Dewey, J. F., Cande, S. C., and Pitman, W. C., III, 1989, Tectonic evolution of the India/Eurasia collision zone: Eclogae Geologicae Helvetiae, v. 82, p. 717-734.

Dewey, J. F., Shackleton, R. M., Chang, C., Sun, Y., and Yin, J., 1988, The tectonic evolution of the Tibetan Plateau: Philosophical Transactions of the Royal Society of London, Series A: Mathematical and Physical Sciences, v. 327, p. 379-413.

Etoh, J., Taguchi, S., and Sekine, R., 2002, Bladed quartz and its relationship to gold mineralization in the Hishikari low-sulfidation epithermal gold deposit, Japan: Economic Geology, v. 97, p. 1841-1851.

Ewart, A., 1982, The mineralogy and petrology of Tertiary-Recent orogenic volcanic rocks: with special reference to the andesitic-basaltic compositional range: in Thorpe, R. S., ed.: Chichester, John Wiley & Sons.

Field, C. W., and Fifarek, R. H., 1985, Light stable-isotopes systematics in the epithermal environment: Reviews in Economic Geology, v. 2, p. 99-128.

Fisher, N. H., 1945, The fineness of gold, with special reference to the Morobe gold field, New Guinea: Economic Geology, v. 40, p. 449-495.

Friedman, I., O'Neil, J. R., and Fleischer, M., 1977, Compilation of stable isotope fractionation factors of geochemical interest, U.S. Geological Survey Professional Paper, no. 440-KK.

Gammons, C. H., and Williams-Jones, A. E., 1995, The solubility of Au-Ag alloy+AgCl in HCl/NaCl solutions at 300 degrees C; new data on the stability of Au(I) chloride complexes in hydrothermal fluids: Geochimica et Cosmochimica Acta, v. 59, p. 3453-3468.

Gammons, C. H., and Williams-Jones, A. E., 1997, Chemical mobility of gold in the porphyry-epithermal environment: Economic Geology, v. 92, p. 45-59.

Gatinsky, Y. G., Hutchinson, C. S., Minh, N. N., and Tri, T. V., 1984, Tectonic evolution of Southeast Asia, *in* Yanshin, A. L., Gatinsky, Y. G., Kropotkin, P. N., Perfiliev, Y. S., Shvolman, V. A., and Shlezinger, A. E., eds., Report of the Session - International Geological Congress, v. 27: location varies, International Geological Congress, p. 225-240.

Gemmell, J. B., and, Cooke, D. R., 1996, Low Sulphidation Epithermal Deposit, in Master of Economic Geology Course Work Manual 5, p. 3.1-3.121, Centre of Ore Deposit Research (CODES).

Gemmell, J. B., 2004, Low- and intermediate-sulphidation epithermal deposit, in 24 carat Au Workshop, CODES Special Publication 5, Centre for Ore Deposit Research (CODES), University of Tasmania, Hobart, Australia.

Greener, S., 1999, Wall rock alteration and vein mineralogy of low sulphidation epithermal deposit, Thailand, B.Sc (Hons) thesis (unpublished), Centre for Ore Deposit Research, School of Earth Sciences, University of Tasmania, Hobart, Australia.

Grancea, L., Bailly, L., Leroy, J., Banks, D., Marcoux, E., Milesi, J. P., Cuney, M., Andre, A. S., Istvan, D., and Fabre, C., 2002, Fluid evolution in the Baia Mare epithermal gold/polymetallic district, Inner Carpathians, Romania: Mineralium Deposita, v. 37, p. 630-647.

Harder, S. H., 1991, Extensional tectonics in the Gulf of Thailand and South China Sea: Proceedings of the Seventh Regional Conference on Geology, Mineral and Energy Resources of Southeast Asia (GEOSEA VII), Bangkok, Abstract volume, p. 47.

Harker, A., 1909, The natural history of igneous rock, Macmillan, New York, 384 pp.

Hayashi, K. I., Maruyama, T., and Satoh, H., 2000, Submillimeter scale variation of oxygen isotope of vein quartz at the Hishikari Deposit, Japan: Resource Geology, v. 50, p. 141-150.

Hedenquist, J. W., Arribas R, A., and Gonzalez-Urien, E., 2000, Exploration for epithermal gold deposits: Reviews in Economic Geology, v. 13, p. 245-277.

Henley, R. W., 1990, Ore transport and deposition in epithermal environments, in Herbert, H. K., and Ho, S. E., (Eds.), Publication - Geology Department and Extension Service, University of Western Australia, v. 23: Geology Department and Extension Service, University of Western Australia, p. 51-69.

Hoefs, J., 1996, Stable Isotope Geochemistry, Springer, Heidelberg, 201p.

Huston, D. L., Bottrill, R. S., Creelman, R. A., Zaw, K., Ramsden, T. R., Rand, S. W., Gemmell, J. B., Jablonski, W., Sie, S. H., and Large, R. R., 1992, Geologic and geochemical controls on the mineralogy and grain size of gold-bearing phases, eastern Australian volcanic-hosted massive sulfide deposits: Economic Geology, v. 87, p. 542-563.

Huston, D. L., Power, M., Gemmell, J. B., Large, R. R., 1995, Design, calibration and geological application of the first operational Australian laser ablation sulphur isotope microprobe: Australian Journal of Earth Sciences, v. 42, no. 6, pp. 549-555.

Hutchinson, C. S., 1989, Geologic evolution of Southeast Asia. Oxford Monographs on Geology and Geophysics. No.13, Oxford University Press, 368p.

http://www.kingsgate.com.au

Intasopa, S., 1993, Petrology and Geochronology of the volcanic rocks of central Thailand volcanic belt, Ph.D. thesis, University of New Brunswick, p. 242.

Izawa, E., Urashima, Y., Ibaraki, K., Suzuki, R., Yokoyama, T., Kawasaki, K., Koga, A., and Taguchi, S., 1990, The Hishikari gold deposit; high-grade epithermal veins in Quaternary volcanoes of southern Kyushu, Japan: Journal of Geochemical Exploration, v. 36, p. 1-56.

John, D. A., Hofstra, A. H., Fleck, R. J., Brummer, J. E., and Saderholm, E. C., 2003, Geologic setting and genesis of the Mule Canyon low-sulfidation epithermal gold-silver deposit, north-central Nevada: Economic Geology, v. 98, p. 425-463.

Jungyasuk, N. and Khosithanont, S., 1992, Volcanic rock and associated mineralisation in Thailand, in: Piancharoen, C. (Ed), Potential for future development, Bangkok, p. 522-537.

Kamvong, T., 2004, Geochemistry and genesis of Phu Lon copper-gold skarn deposit northeast Thailand, B.Sc (Hons) thesis (unpublished), Centre for Ore Deposit

Research, School of Earth Sciences, University of Tasmania, Hobart, Australia, p. 96.

Khin Zaw, Burrett, C. F., Berry, R. F., Bruce, E. and Pasqua, D. F., 1999, Geological, tectonic and metallogenic relations of mineral deposits in mainland SE Asia, Geochronological studies, AMIRA project P390A: Final Report: December 1999(unpublished), Centre of Ore Deposit Research (CODES), University of Tasmania, Hobart, Australia.

Kojima, S, 1990, A coprecipitation experiment on intimate association of sphalerite and chalcopyrite and its bearings on the genesis of Kuroko ores, Mining Geol., v. 40 (3), p. 147-158.

Large, R. R, 2003, The use of stable isotopes in ore deposit research and exploration, in Masters of Economic Geology Course Work Manual; Ore deposit geochemistry, hydrology and geochronology; May 2003, Centre for Ore Deposit Research (CODES), University of Tasmania, Hobart, Australia.

Lawless, J. V., White, P. J., Bogie, I., Cartwright, A. J., 1999, Finding Mineralisation is Easy; Why is it so Hard to Find A Mine?, Kingstone Morisson, Short Course PacRim 99 Congress, Bali, 9-10 October 1999, Indonesia.

Le Maitre, R. W., Bateman, P., Dudek, A., Keller, J., Lameyre Le Bas, M. J., Sabine, P. A., Schmid, R., Sorensen, H., Streckeisen, A., Wolley, A. R., and Zanettin, B., 1989, A classification of igneous rocks and glossary of terms, Blackwell, Oxford.

Lin, J., and Watts, D. R., 1988, Palaeomagnetic constraints on Himalayan-Tibetan tectonic evolution: Philosophical Transactions of the Royal Society of London, Series A: Mathematical and Physical Sciences, v. 326, p. 177-188.

Lindgren, W., 1933, Mineral Deposits (4^{th} ed.), McGraw-Hill, New York.

Mantajit, N., 1997, Stratigraphy and tectonic evolution of Thailand, GEOTHAI'97: The International Conference on Stratigraphy and Tectonic Evolution of Southeast Aia and the South Pacific, v.1, p. 1-6.

Meesook, A., Suteethon, V. and Wongprayoon, T., 1994, a preliminary report on Jarssic Cretaceous non-marine bivalves of northeast Thailand, Geological Survey Division, Department of Mineral Resources, Bangkok, Thailand, 11p (in Thai).

Meschede, M., 1986, A method of discriminating between different types of mid-ocean ridge basalts and continental tholeiites with the Nb-Zr-Y diagram: Chemical Geology, v. 56, p. 207-218.

Metcalfe, I., 1986, Late Palaeozoic palaeogeography of Southeast Asia: Some stratigraphical, palaeontological and palaeomagnetic constraints: Bulletin Geological Society of Malaysia, v. 19, p. 153-164.

—, 1988, Origin and assembly of Southeast Asian continental terranes: Geological Society Special Publications, v. 37, p. 101-118.

—, 1990, Allochthonous terrane processes in Southeast Asia: Philosophical Transactions of the Royal Society of London, Series A: Mathematical and Physical Sciences, v. 331, p. 625-640.

Metcalfe, I., and Anonymous, 1984, Stratigraphy, palaeontology and paleogeography of the Carboniferous of Southeast Asia: Memoires de la Societe Geologique de France, Nouvelle Serie, v. 147, p. 107-118.

Molnar, P., and Tapponnier, P., 1975, Cenozoic tectonics of Asia: Effects of a continental collision: Science, v. 189, p. 419-426.

Morrison, G. W., Rose, W. J., and Jaireth, S., 1991, Geological and geochemical controls on the silver content (fineness) of gold in gold-silver deposits: Ore Geology Reviews, v. 6, p. 333-364.

Nakayama, K., 1995, Case history of the discovery of the Hishikari gold deposit, Japan, *in* Mauk, J. L., and St George, J. D., eds., Publication Series - Australasian Institute of Mining and Metallurgy, vol.9/95: Parkville, Australasian Institute of Mining and Metallurgy, p. 429-434.

Ohmoto, H., 1972, Systematics of Sulfur and Carbon Isotopes in Hydrothermal Ore Deposits: Economic Geology, v. 67, p. 551-578.

—, 1986, Stable isotope geochemistry of ore deposits: Reviews in Mineralogy, v. 16, p. 491-559.

Ohmoto, H., and Rye, R. O., 1979, Isotopes of sulfur and carbon, in Barnes, H.L., (Ed.), Geochemistry of hydrothermal ore deposits (2d. ed.): Wiley, p. 509-567.

Panteleyev, A., 1996, Epithermal Au-Ag-Cu; high sulphidation: Mines and Petroleum Resources, British Columbia Ministry of Energy.

Parr, J. M., Murao, S. and Binns, R. A., 1995, A comparison of massive sulfide deposits forming at the PACMANUS (Manus Basin, PNG) and Jade (Okinawa Trough, South China Sea) seafloor hydrothermal fields, Publication Series - Australasian Institute of Mining and Metallurgy, v.9, p. 453-458.

Pearce, J. A., 1982, Trace element characteristics of lavas from destructive plate boundaries, in: Thorpe R.S. (Ed.), Andesites, Wiley, Chichester, p. 525-548.

Pearce, J. A., 1996, A user's guide to basalt discrimination diagrams, in D. A., Wyman (Ed.), Trace element geochemistry of volcanic rocks: Applications for massive sulphide exploration, Geological Association of Canada Short Course Notes, v.12, p. 79-113.

Pearce, J. A., and Cann, J. R., 1973, Tectonic setting of basic volcanic rocks determined using trace element analyses: Earth and Planetary Science Letters, v. 19, p. 290-300.

Pearce, J. A., Hawkesworth, C. J., and Norry, M. J., 1983, Role of the sub-continental lithosphere in magma genesis at active continental margins, in: Hawkesworth C. J. and Norry M. J. (Eds.) Continental basalts and continental xenoliths, Shiva, Nantwich, p. 230-249.

Peccerillo, A., and Taylor, S. R., 1976, Geochemistry of Eocene calc-alkaline volcanic rocks from the Kastamonu area, northern Turkey: Contributions to Mineralogy and Petrology, v. 58, p. 63-81.

Petersen, S., Herzig, P. M., Schampera, U. S., Hannington, M. D. and Jonasson, I. R., 2004, Hydrothermal precipitates associated with bimodal volcanism in the Central Bransfield Strait, Antarctica: Mineralium Deposita, v. 39, No. 3, p. 358 - 379.

Pisutha-Arnond, V., Vedchakanchana, S., and Sangiemsak, S., 1984, Some features of the gold skarn prospect at Ban Na Lom, Changwat Prachinburi, in Thiramongkol, N., Nakapadungrat, S., and Pisutha-Arnond, V., (Eds.): Dep. Geol., Chulalongkorn Univ.

Reed, M. H., and Spycher, N. F., 1985, Boiling, cooling, and oxidation in epithermal systems: A numerical modelling approach: Reviews in Economic Geology, v. 2, p. 249-272.

Rodmanee, T., 2000, Genetic model of Phu Thap Fah gold deposit Ban Huai Phuk Amphoe Wang Saphung Changwat Loei, Ph.D. thesis, Chiang Mai University.

Rollinson, H. R., 1993, Using Geochemical Data: Evaluation, Presentation, Interpretation: New York, Longman Group, 352 p.

Savard, M. M., Kontak, D. J., and Sangster, D. F., 1998, $\delta^{13}C$-$\delta^{18}O$-$^{87}Sr/^{86}Sr$ covariations in ore-stage calcites at and around the Gays River Zn-Pb deposit (Nova Scotia, Canada); evidence for fluid mixing: Economic Geology, v. 93, p. 818-833.

Sengor, A. M. C., 1984, The Cimmeride orogenic system and the tectonics of Eurasia. Geol. Soc Am. Spec. , Paper 195, 88p.

Seward, T. M., and Barnes, H. L., 1997, Metal transport by hydrothermal ore fields, in Barnes, H. L., ed.: New York, John Wiley & Sons, p. 435-486.

Shikazono, N., 1977, Vein-type deposits, In Fundamental Aspects of the Study of Deposits, University of Tokyo Press, p. 188-202.

Shikazono, N., and Shimizu, M., 1987, The Ag/Au ratio of native gold and electrum and the geochemical environment of gold vein deposits in Japan: Mineralium Deposita, v. 22, p. 309-314.

Sillitoe, R. H., 1993, Giant and bonanza gold deposits in the epithermal environment; assessment of potential genetic factors: Special Publication - Society of Economic Geologists, v. 2, p. 125-156.

Simmons, S. F., and Browne, P. R. L., 2000, Hydrothermal minerals and precious metals in the Broadlands-Ohaaki geothermal system; implications for understanding low-sulfidation epithermal environments: Economic Geology, v. 95, p. 971-999.

Simmons, S. F., and Christenson, B. W., 1994, Origins of calcite in a boiling geothermal system: American Journal of Science, v. 294, p. 361-400.

Simmons, S. F., Mauk, J. L., Simpson, M. P., and Anonymous, 2000, The mineral products of boiling in the Golden Cross epithermal deposit: Crown Minerals Publicity Unit, New Zealand Ministry of Economic Development.

Simpson, M. P., Simmons, S. F., Mauk, J. L., and McOnie, A. W., 1995, The distribution of hydrothermal minerals at the Golden Cross epithermal Au-Ag deposit, Waihi, New Zealand: Publication Series - Australasian Institute of Mining and Metallurgy, v. 9/95, p. 551-556.

Songpope, P., Praditan, S., Tongtaow, C., Janmaha, S., Intrawijitr, K., and Sangsuwan, U., 1991, Development of Cenozoic basins in Thailand: Marine and Petroleum Geol. v8, p. 84-97.

Tapponnier, P., Peltzer, G., and Armijo, R., 1986, On the mechanics of the collision between India and Asia: Geological Society Special Publications, v. 19, p. 115-157.

Thompson, A. J. B., and Thompson, J. F. H., 1996, Atlas of alteration: A field guide and petrographic guide to hydrothermal alteration minerals: Newfoundland, Geological Association of Canada, 119p.

Vikre, P. G., 1981, Silver mineralization in the Rochester District, Pershing County, Nevada: Economic Geology, v. 76, p. 580-609.

Walshe, J. L., 1986, A six-component chlorite solid solution model and the conditions of chlorite formation in hydrothermal and geothermal systems: Economic Geology, v. 81, p. 681-703.

White, N. C, 2004, Epithermal Gold Deposit, in Master of Economic Geology Course Work Manual: Ore Deposit Model, Centre of Ore Deposit Research (CODES), University of Tasmania, Hobart, Australia.

White, N. C., Hedenquist, J. W., Wilson, B., Cox, J., Brummer, J., Saderholm, E., Carlson-Carnejo, C., Read, J., Casteel, M.V., Schmidt, K., Goldstrand, P., Bernard, J., and Sandberg, J., 1999, Epithermal gold deposits: Styles, characteristics and exploration: Special Publication - Geological Society of Nevada, v. 29, p. 159-171.

Wielchosky, C. C. and Young, J. D., 1985, Regional facies variations in Permian rocks of the Phetchabun fold and thrus belt, Thailand, in P. Thanvarachorn, S. Hokjaroen, and W. Youngme, eds., Proceedings of the Conference on Geology and Mineral Resources Development of the Northeast Thailand, Khon Kaen University, Khon Kaen, Thailand, November, p. 41-55.

Winchester, J. A., and Floyd, P. A., 1976, Geochemical magma type discrimination; application to altered and metamorphosed basic igneous rocks: Earth and Planetary Science Letters, v. 28, p. 459-469.

Winchester, J. A., and Floyd, P. A., 1977, Geochemical discrimination of different magma series and their differentiation products using immobile elements: Chemical Geology, v. 20, p. 325-343.

Wongsomsuk, S., 1989, Geological Mapping Report; scale 1 : 50,000 Sheet Ban Khao Sai and Sheet Ban Wong Sai Poon Nai, Geological Survey Section, Department of Mineral Resources, Bangkok, Thailand (in Thai).

Zheng, Y. F., 1990, Carbon-oxygen isotopic covariation in hydrothermal calcite during degassing of CO_2: A quantitative evaluation and application to the Kushikino gold mining area in Japan: Mineralium Deposita, v. 25, p. 246-250.

Zheng, Y. F., and Hoefs, J., 1993, Carbon and oxygen isotopic covariations in hydrothermal calcites: Theoretical modeling on mixing processes and application to Pb-Zn deposits in the Harz Mountains, Germany: Mineralium Deposita, v. 28, p. 79-89.

APPENDICES

APPENDIX A: XRF analysis

XRF ANALYSES, CODES-SES, University of Tasmania, Hobart, Tasmania

Analyst :Phil Robinson, XRF sample preparation: Katie McGoldrick
Sample Crushing (WC mill) by
Kamonporn Khromkhun

Sample	SiO2	TiO2	Al2O3	Fe2O3	MnO	MgO	CaO	Na2O	K2O	P2O5	BaO	Loss inc S-	Total
RCD 341.02	51.60	0.55	17.95	10.06	0.44	5.12	4.70	1.63	3.33	0.13	0.18	4.39	100.08
RCD 499.10	50.66	0.68	15.77	8.25	0.27	3.24	4.48	0.09	9.66	0.27	0.16	6.29	99.82
RCD 394.39	50.88	0.47	18.12	7.84	0.68	4.86	4.08	1.19	7.42	0.11	0.30	3.87	99.82
HP 07	37.99	1.67	15.76	10.09	0.25	4.76	11.77	0.23	2.74	0.23	0.01	13.94	99.45
HP 09	48.65	1.00	17.55	8.99	0.19	5.14	7.76	3.96	0.87	0.24	0.05	5.27	99.68
RCD1108.70	56.63	0.59	15.03	6.92	0.33	4.08	3.23	0.43	8.03	0.22	0.13	4.43	100.06
F 03	69.09	0.35	9.30	4.64	0.27	1.87	4.05	0.67	4.69	0.14	0.15	4.30	99.52
HP 02	64.45	0.32	13.99	3.78	0.11	1.26	4.77	2.89	1.27	0.08	0.04	6.64	99.59
HP 06	62.17	0.47	11.22	9.44	0.43	3.89	3.07	<0.03	2.57	0.16	0.05	6.65	100.12
HP 10	56.47	0.66	15.79	8.18	0.38	2.98	2.41	1.39	7.01	0.25	0.28	3.64	99.44
RCD 312.102	53.08	1.44	14.68	9.48	0.17	4.12	4.56	4.09	1.45	0.39	0.03	6.06	99.55
RCD 505.109	50.00	1.08	18.26	9.39	0.19	5.26	7.73	3.38	0.66	0.25	0.03	3.76	99.97
HP 05	52.36	0.77	18.01	7.23	0.18	4.47	7.15	4.11	0.84	0.16	0.02	4.66	99.96
HP 11	52.96	1.49	15.85	9.41	0.18	4.10	6.74	3.87	1.30	0.41	0.02	3.66	100.01

XRF ANALYSES (continued)

Sample	Y	U	Rb	Th	Pb	As	Bi	Zn	Cu	Ni
RCD 341.02	11	<1.5	68	<1.5	<1.5	<3	<2	85	216	14
RCD 499.10	14	<1.5	145	<1.5	3	17	<2	101	58	17
RCD 394.39	8	<1.5	92	<1.5	2	14	<2	74	124	9
HP 07	29	<1.5	56	<1.5	10	13	<2	101	62	80
HP 09	16	<1.5	12	<1.5	3	12	<2	78	34	25
RCD1108.70	14	<1.5	134	<1.5	2	12	<2	75	91	12
F 03	9	<1.5	66	<1.5	18	21	<2	86	154	8
HP 02	18	<1.5	14	<1.5	0	<3	<2	48	15	2
HP 06	13	<1.5	56	<1.5	373	102	<2	1056	69	11
HP 10	16	<1.5	112	<1.5	2	9	<2	90	118	14
RCD 312.102	27	<1.5	23	2	6	6	<2	99	122	22
RCD 505.109	18	<1.5	10	<1.5	4	4	<2	91	65	26
HP 05	11	<1.5	9	<1.5	2	5	<2	103	37	47
HP 11	33	<1.5	17	2	6	8	<2	116	126	29
detection limit (ppm)	1	1.5	1	1.5	1.5	3	2	1	1	1

XRF ANALYSES (continued)

Sample	Nb	Zr	Sr	Cr	Ba	Sc	V	La	Ce	Nd
RCD 341.02	1	25	247	19	1671	37	324	<2	6	3
RCD 499.10	3	70	127	7	1325	28	247	7	18	7
RCD 394.39	2	17	357	22	2574	30	270	<2	4	<2
HP 07	5	129	71	146	110	38	267	5	11	12
HP 09	3	76	535	52	482	23	233	5	17	12
RCD1108.70	3	63	103	10	1137	24	291	6	12	8
F 03	2	36	98	14	1282	14	128	3	7	3
HP 02	3	69	105	6	380	18	63	4	11	8
HP 06	3	50	41	9	448	20	202	4	16	6
HP 10	3	68	136	8	2274	24	233	7	14	4
RCD 312.102	6	196	121	34	275	28	292	13	32	21
RCD 505.109	3	78	631	54	246	26	247	6	18	12
HP 05	2	59	223	136	138	23	191	5	15	10
HP 11	7	213	403	40	199	25	290	19	40	25
detection limit (ppm)	1	1	1	1	4	2	1.5	2	4	2

XRF ANALYSES (continued)

Recalculate in major elements

Sample	SiO2	TiO2	Al2O3	Fe2O3	MnO	MgO	CaO	Na2O	K2O	P2O5	BaO	Total	Loss inc S-
RCD 341.02	53.93	0.58	18.76	10.51	0.46	5.35	4.91	1.71	3.48	0.13	0.19	100	4.39
RCD 499.10	54.17	0.73	16.86	8.82	0.29	3.46	4.79	0.10	10.33	0.29	0.17	100	6.29
RCD 394.39	53.03	0.49	18.88	8.17	0.71	5.07	4.25	1.24	7.73	0.11	0.31	100	3.87
HP 07	44.42	1.95	18.44	11.80	0.29	5.57	13.77	0.27	3.21	0.27	0.01	100	13.94
HP 09	51.54	1.06	18.59	9.52	0.21	5.44	8.22	4.19	0.92	0.25	0.06	100	5.27
RCD1108.70	59.22	0.61	15.72	7.24	0.35	4.27	3.38	0.45	8.39	0.23	0.14	100	4.43
F 03	72.56	0.37	9.77	4.87	0.29	1.96	4.26	0.71	4.93	0.14	0.15	100	4.3
HP 02	69.34	0.35	15.05	4.07	0.11	1.36	5.13	3.11	1.36	0.08	0.05	100	6.64
HP 06	66.51	0.50	12.00	10.10	0.46	4.16	3.28	0.03	2.75	0.17	0.05	100	6.65
HP 10	58.94	0.69	16.48	8.54	0.40	3.11	2.52	1.45	7.32	0.26	0.29	100	3.64
RCD 312.102	56.78	1.54	15.70	10.14	0.18	4.41	4.88	4.37	1.55	0.42	0.03	100	6.06
RCD 505.109	51.97	1.12	18.98	9.76	0.19	5.47	8.03	3.51	0.68	0.25	0.03	100	3.76
HP 05	54.95	0.81	18.90	7.58	0.19	4.69	7.50	4.31	0.88	0.17	0.02	100	4.66
HP 11	54.97	1.55	16.46	9.77	0.19	4.26	6.99	4.02	1.35	0.42	0.02	100	3.66

APPENDIX B: PIMA

PIMA RESULT

NO.HOLE	SAMPLE	DEPTH(m)	2004								2003							
			A		B		C		D		A		B		C		D	
RCD1116	1116.60	131.10-131.20	phengite	epidote	Int Chlorite	phengite	montmorillo	epidote	Int Chlorite		IntChlorite		Phengite	Epidote				
	1116.61	149.10-149.20	Int Chlorite		Int Chlorite						IntChlorite	Illite	Epidote		IntChlorite			
	1116.62	160.00-160.15	Int Chlorite								Epidote	Illite	Muscovite	Epidote	Illite	Montmorillonite		
	1116.63	172.70-172.60	Int Chlorite								IntChlorite	Epidote	IntChlorite					
	1116.64	178.40-178.50	Muscovite	epidote	?Fe chlorite	?ankerite												
RCD1108	1108.65	87.58-87.70	Int Chlorite	phengite	phengite	ankerite	Int Chlorite	phengite										
	1108.66	102.70-102.80																
	1108.67	100.65-100.75	Int Chlorite		Int Chlorite		phengite	opal			IntChlorite		Phengite	Epidote	FeChlorite	Ankerite		
	1108.68	123.70-123.81	calcite		?calcite	?illite	?calcite	muscovite			Brucite	Calcite	Calcite	Illite				
	1108.69	125.59-125.70	Ankerite	phengite	ankerite	muscovite	null				Muscovite	Ankerite	Illite			Epidote		
	1108.70	135.27-135.37									Illite	Epidote	IntChlorite		IntChlorite	Muscovite		
	1108.71	152.90-153.00	Muscovite	epidote	Fe Chlorite		Int Chlorite	Muscovite	Muscovite	Opal	Muscovite	Opal	Illite	Epidote	IntChlorite	Muscovite		
RCD1109	1109.72	90.10-90.24	Int Chlorite	Illite	Illite	Opal	Fe Chlorite	Illite			FeChlorite	Illite	Illite	Ankerite	Illite	Ankerite	Illite	IntChlorite
	1109.73	92.20-92.32	Mg Chlorite	Illite														
	1109.74	94.00-94.10	Int Chlorite	Illite														
	1109.75	95.90-96.00	Illite	Calcite	Illite	ankerite	Calcite	Illite	Illite	Ankerite	Illite	IntChlorite	Illite	Calcite	Illite	Ankerite		
	1109.76	103.10-103.20	?Ankerite	Muscovite			Int Chlorite				IntChlorite	Muscovite	Phengite	Ankerite				
	1109.77	112.90-112.99	Epidote		Int Chlorite													
	1109.78	121.80-121.90	Int Chlorite	epidote	Fe Chlorite	Mg Chlorite												
	1109.79	135.80-135.90																
RCD 358	358.80	63.30-63.45	Mg Chlorite	Calcite	Mg Chlorite	Calcite	?Ankerite	?Illite			MgChlorite	Ankerite	MgChlorite	Calcite	IntChlorite	Calcite		
	358.81	63.90-63.97	Int Chlorite	Muscovite	Int Chlorite	Muscovite												
	358.82	67.29-67.45	calcite	Mg Chlorite	Mg Chlorite	Calcite	Mg Chlorite	Calcite			MgChlorite	Calcite	Calcite	MgChlorite	MgChlorite	Calcite		
	358.83	70.72-70.86	Int Chlorite	Muscovite	Int Chlorite	Muscovite					Prengite	Brucite	IntChlorite	Muscovite	IntChlorite	Illite		
	358.84	72.26-72.36	Int Chlorite															
	358.85	75.08-75.20	phengite	epidote	Int Chlorite						Prengite	Ankerite	IntChlorite		Prengite	Ankerite		
	358.86	76.43-76.52	Int Chlorite		Int Chlorite		Int Chlorite				Prengite	Epidote						

PIMA RESULT (continued)

NO.HOLE	SAMPLE	DEPTH(m)	2004								2003							
			A		B		C		D		A		B		C		D	
RCD 358	358.87	79.70-79.83	?Ankerite	?Gypsum	Calcite						IntChlorite		MgChlorite	Epidote				
RCD 357	357.89	49.43-49.55	calcite		Calcite	?Phlogopite1	Mg Chlorite	Calcite			Prehnite	Calcite	IntChloite	Calcite	MgChloite	Calcite		
	357.90	52.00-52.15	calcite	?Phlogopite1	calcite	?Phlogopite1					MgChloite		MgChloite	Calcite	MgChloite	Calcite		
	357.91	55.30-55.40	null															
	357.92	59.22-59.32	Int Chlorite	Ankerite	Int Chlorite	?Brucite					MgChloite	Calcite	IntChlorite	Ankerite				
	357.93	65.60-65.72	Prehnite	?Phlogopite2	Int Chlorite		Int Chlorite				IntChlorite	FeChlorite	Prehnite	Phlogopite2				
RCD 499	499.94	32.75-32.85	calcite		ankerite	Halloysite	Calcite	Illite	Calcite	Dolomite	Ankerite	Holloysite	Ankerite	Holloysite				
	499.95	35.86-36.00	Mn Chlorite	Ankerite	Calcite	Illite	Mg Chlorite	Calcite										
	499.96	36.70-36.83	calcite	Phlogopite1	Calcite		calcite	Phlogopite1			Calcite	Phlogopite	Calcite		MgChlorite			
	499.97	45.60-45.71	Int Chlorite	Illite							IntChlorite	Ankerite	Muscovite	Ankerite	IntChlorite	Ankerite		
	499.98	47.00-47.12									Phengite	Ankerite	MgChlorite	Epidote	Illite	Prengite		
	499.99	50.10-50.20	Int Chlorite															
	499.100	59.05-59.25	Fe Chlorite	Mg Chlorite														
RCD 312	312.101	43.88-43.90	Epidote	Calcite														
	312.103	45.80-45.90	Int Chlorite	Illite	Int Chlorite	Illite	Int Chlorite	Illite										
	312.104	48.83-48.90	?Fe Chlorite	Illite														
	312.105	50.95-51.15	Illite		Illite		Illite											
	312.106	56.00-56.15	Illite	Int Chlorite	Illite	Fe Chlorite	Illite	Int Chlorite			Illite		Illite	Intchlorite	Illite	Fe Intchlorite		
RCD 356	356.107	11.30-11.40	Illite	?Na_Alunite														
	356.108	18.20-18.30																
RCD 341	341.01	55.46-55.56									Ankerite	Phengite	Ankerite	Phengite				
	341.05	130.40-130.97									Palygorskite	Illite	Phengite	Halloysite				
RCD 460	460.06	36.55-36.42									IntChlorite	Muscovite						
	460.07	45.50-45.60									Calcite		Calcite		Calcite			
	460.08	64.85-64.95									MgChlorite	Illite	Calcite					
	460.09	70.99-71.09									Illite	Ankerite	Illite		Illite	Montmorillonite		
	460.12	118.73-118.82									IntChlorite	Muscovite	Phengite	Ankerite				

PIMA RESULT (continued)

NO.HOLE	SAMPLE	DEPTH(m)	2004								2003							
			A		B		C		D		A		B		C		D	
RCD 459	459.20	93.10-93.15									Illite	IntChlorite						
	459.22	125.04-125.16									Illite		Illite					
RCD 374	374.24	48.64-48.70									Illite		Illite	Ankerite				
	374.26	67.21-67.30									Illite	Calcite	Calcite	Illite	MgChlorite	Calcite		
RCD 450	450.27	53.75-53.87									Ankerite	Montmorillo	Calcite		Calcite			
	450.28	84.45-84.55									Calcite	Dolomite	MgChlorite	Ankerite	Calcite			
	450.30	93.35-93.47									IntChlorite	Illite	Illite	Opal	IntChlorite			
	450.32	125.05-125.18									IntChlorite	Ankerite						
RCD 394	394.35	51.19-51.30									Prehnite	Phlogopite	Prehnite	Epidote	Prehnite	Ankerite		
	394.36	64.30-64.44									Calcite	K_Alunite						
	394.37	74.55-74.65									IntChlorite	Illite	Illite	Epidote				
	394.38	79.45-79.45?									Epidote	Brucite	Brucite	Epidote				
	394.39	84.60-83.94?									Muscovite	Brucite						
	453.40	70.30-70.41									FeChlorite							
RCD 453	453.41	82.10-82.20									Illite	IntChlorite	Illite	Ankerite	Illite	Calcite		
	453.42	88.50-88.62									Illite	Ankerite	Ankerite	Illite	Illite	Epidote		
	1120.45	118.20-118.32									Illite	MgChlorite	IntChlorite		Phengite	Illite	Illite	Phengite
RCD 1120	1120.47	145.90-146.00									Illite		Illite	FeChlorite	Illite	Ankerite		
	1120.49	193.50-169.60									Epidote	Illite	IntChlorite					
	1123.53	136.00-136.09									Illite	Phengite						
RCD1123	1123.54	141.40-141.51									Illite	MgChlorite	Illite	MgChlorite				
	1123.55	148.60-149.70									MgChlorite	Ankerite	IntChlorite		Illite	Calcite		
	1123.58	167.92-168.00									Muscovite	Epidote	Muscovite	Epidote				
RCD 505	505.110	50.86-51.00									MgChlorite	Magnesium_	Ankerite	Montmorillonite				
	505.111	55.60-55.80									IntChlorite		IntChlorite		Ankerite			
RCD1113	1113.117	119.50-119.66									Calcite		IntChlorite					
	1113.118	121.70-121.80									Illite		Illite	Ankerite				

PIMA RESULT (continued)

NO.HOLE	SAMPLE	DEPTH(m)	2004								2003							
			A		B		C		D		A		B		C		D	
RCD1113	1113.119	125.23-125.35									IntChlorite	Illite	IntChlorite	Illite				
	1113.120	129.25-129.90									Muscovite	Calcite	IntChlorite		IntChlorite			
	1113.121	131.88-132.00									Epidote	Illite	IntChlorite	Muscovite				
RCD 504	504.124	37.10-37.26									Montmorillo	Ankerite	Montmorillo	Ankerite	Holloysite	Montmorillonite		
	504.126	45.10-45.22									Calcite	Illite	Illite	Calcite				
	504.127	45.89-46.00									Illite		Illite					
Outcrop	H03	hangingwall									Palygorskite	Gypsum	IntChlorite					
Outcrop	H05	vein									IntChlorite	Paragonite	Paragonite					
Outcrop	H08	breccia									Epidote	Haloysite						
Outcrop	H09	breccia									Illite							
Outcrop	H10	hangingwall									Illite	Monmorillor	Illite	Magnesium_clay				
Outcrop	H11	breccia									Illite	Calcite						
Outcrop	H13	footwall									MgChlorite	Epidote						
Outcrop	H19	hangingwall									Illite							
Outcrop	H22	hangingwall									Palygorskite	Gypsum						
Outcrop	H25	vein									Ankerite	Illite	IntChlorite	Illite				

APPENDIX C: Electron Microprobe analysis

Electrum analysis:

Sample	Cu	As	Ag	Au	Hg	Total
357.89_1	0.005264	0.018417	41.32067	61.90026	-0.14061	103.2446
357.89_2	0.048515	0.031179	39.85449	64.05527	-0.16638	103.9894
357.89_3	0.050816	0.012472	32.26739	43.20861	-0.02443	75.53928
357.89_4	0.013811	0.024399	45.39027	57.06348	-0.09518	102.492
357.89_5	-0.00372	0.025002	39.16531	63.54863	-0.14117	102.7389
357.89_6	0.023754	0.010737	42.3406	59.43428	-0.01724	101.8094
357.89_7	0.054132	0.022513	43.58306	55.85585	-0.03456	99.51556
357.89_8	0.430018	0.097744	45.11728	53.93009	-0.03107	99.57513
357.89_9	-0.00706	0.024553	39.47079	63.39553	-0.09001	102.8909
357.89_10	0.003508	0.022494	40.84113	62.63582	-0.0965	103.503
357.89_11	0.023307	0.011529	39.52903	64.57333	-0.10329	104.1372
357.89_12	-0.03228	0.028678	37.20012	53.11686	-0.03133	90.34565
357.89_13	0.002767	0.004859	40.31892	62.79906	-0.14227	103.1256
357.89_14	-0.00496	0.033095	39.31219	64.74133	-0.12847	104.0866
357.89_15	0.021955	0.023213	39.13137	65.18924	-0.13163	104.3658
357.89_16	-0.17082	-0.07141	31.88189	62.07153	-1.0152	93.95341
357-92_17	0.0392	0.0094	33.098	67.2679	0.4323	100.8469
357-92_18	0.0041	0.0203	31.5098	70.3932	0.3185	102.2459
357-92_19	-0.0025	0.0254	33.2281	68.2046	0.2657	101.7239
504-124_20	0.0351	0.0044	45.6964	55.5767	0.3636	101.6762

Sphalerite analysis

Sample No.	S (wt %)	Mn (wt %)	Fe (wt %)	Zn (wt %)	Cd (wt %)	Se (wt %)	Cu (wt %)	Total (wt %)
374.26_1_sph1	33.5604	0.03856	0.29561	64.0496	0.50579	0.02784	0.40082	98.87861
374.26_1_sph2	33.8363	0.02494	0.54209	63.3031	0.12987	0.01938	0.62711	98.4827
374.26_2_sph3	33.7186	0.05322	1.26518	63.8901	0.1435	0.03419	1.21036	100.3151
357.89_1_sph1	33.6633	0.03751	1.09952	63.4925	0.34991	0.00762	0.00233	98.65272
357.89_1_sph2	33.9004	0.06226	0.19983	64.5302	0.34459	0.01434	0.16883	99.2205
357.89_2_sph3	34.0846	0.02083	0.89377	64.293	0.28292	0.00518	0.21673	99.79698
357.89_2_sph4	33.3703	0.02726	0.15716	65.1778	0.2775	0.02039	0.02648	99.05688
357.89_3_sph5	33.6877	0.03063	0.3758	62.6097	0.30287	0.01712	0.43631	97.46011
357.89_4_sph6	33.8776	0.03606	0.97091	64.5706	0.32889	0.02748	0.03607	99.84762
357.89_4_sph7	33.5655	0.03627	0.51373	65.0865	0.32238	0.02167	0.04673	99.5928
357.89_6_sph8	33.8338	0.06752	0.23394	64.293	0.28939	0.02295	0.09516	98.83572
357.89_7_sph9	33.6646	0.04687	0.18613	65.4839	0.29708	0.02633	0.06763	99.77259
357.89_7_sph10	29.2191	0.04274	0.12855	57.6919	0.24755	0.02196	0.07899	87.43083
357.89_8_sph11	33.6151	0.04904	0.09025	65.7914	0.3081	0.02319	0.02559	99.90263

Chlorite analysis

Sample	Si	Ti	Al	Cr	Mg	Ca	Mn	Fe	Ni	Zn	Ba	OH	Na	K	F	Total	AlIV	Fe/(Fe+Mg)	half tetra	Temperature
RCD499-95_chl1	6.18	0.00	4.64	0.00	6.57	0.06	0.57	1.48	0.00	0.02	0.00	15.96	0.02	0.01	0.04	35.54	2.81	0.18	1.41	391
RCD499-95_chl2	6.09	0.01	4.55	0.00	6.64	0.06	0.70	1.55	0.00	0.01	0.00	15.99	0.01	0.01	0.01	35.64	2.73	0.19	1.37	378
RCD499-95_chl3	6.11	0.00	4.77	0.00	6.13	0.05	0.70	1.71	0.00	0.02	0.00	15.97	0.01	0.02	0.03	35.53	2.95	0.22	1.47	413
RCD499-95_chl4	6.22	0.00	5.00	0.00	5.98	0.04	0.51	1.52	0.00	0.00	0.00	15.97	0.00	0.04	0.04	35.31	3.18	0.20	1.59	450
RCD499-95_chl5	6.13	0.00	4.67	0.00	6.37	0.03	0.66	1.65	0.00	0.01	0.01	15.98	0.01	0.01	0.02	35.55	2.85	0.21	1.43	397
RCD499-95_chl6	6.13	0.00	4.96	0.00	6.10	0.03	0.57	1.58	0.00	0.01	0.00	15.99	0.01	0.01	0.01	35.40	3.14	0.21	1.57	444
RCD394-35_chl7	7.17	0.00	3.17	0.00	5.23	0.42	0.37	2.84	0.00	0.01	0.01	15.97	0.04	0.03	0.03	35.29	1.35	0.35	0.67	155
RCD394-35_chl8	6.29	0.01	3.91	0.00	4.31	0.07	0.35	4.83	0.00	0.00	0.01	15.96	0.01	0.01	0.04	35.78	2.09	0.53	1.04	274
RCD394-35_chl9	6.71	0.00	3.66	0.01	5.52	0.15	0.31	3.10	0.00	0.00	0.01	15.97	0.03	0.01	0.03	35.49	1.84	0.36	0.92	234
RCD394-35_chl10	7.24	0.01	3.03	0.00	5.48	0.31	0.37	2.79	0.00	0.00	0.01	15.95	0.06	0.02	0.05	35.30	1.21	0.34	0.60	133
RCD1109.76_chl11	5.97	0.00	4.54	0.00	5.43	0.03	0.37	3.40	0.00	0.01	0.01	15.95	0.00	0.05	0.05	35.81	2.72	0.39	1.36	376
RCD1109.76_chl12	5.98	0.01	4.46	0.00	5.64	0.03	0.37	3.32	0.00	0.00	0.00	15.94	0.00	0.02	0.06	35.82	2.64	0.37	1.32	363
RCD1109.76_chl13	5.95	0.00	4.47	0.00	5.59	0.02	0.39	3.41	0.00	0.00	0.00	15.93	0.01	0.00	0.07	35.85	2.65	0.38	1.32	365
RCD1109.76_chl14	6.05	0.00	4.46	0.00	5.41	0.04	0.34	3.40	0.00	0.01	0.01	15.95	0.01	0.05	0.05	35.78	2.64	0.39	1.32	363
RCD499.94_chl15	6.13	0.01	4.68	0.00	6.39	0.08	0.77	1.46	0.00	0.00	0.01	16.00	0.00	0.01	0.00	35.53	2.86	0.19	1.43	398
RCD499.94_chl16	5.95	0.00	4.81	0.00	6.42	0.06	0.86	1.53	0.00	0.01	0.00	16.00	0.00	0.00	0.00	35.64	2.99	0.19	1.49	419
RCD499.94_chl17	6.02	0.00	4.88	0.00	6.38	0.05	0.83	1.37	0.00	0.01	0.01	16.00	0.00	0.00	0.00	35.54	3.06	0.18	1.53	431
RCD504.124_chl18	6.18	0.00	4.38	0.00	7.58	0.04	0.28	1.15	0.00	0.01	0.00	15.97	0.02	0.05	0.03	35.68	2.56	0.13	1.28	350
RCD504.124_chl19	6.91	0.00	4.86	0.00	4.73	0.11	0.14	1.84	0.00	0.02	0.01	16.00	0.02	0.04	0.00	34.69	3.04	0.28	1.52	427
RCD504.124_chl20	7.19	0.00	4.22	0.00	5.45	0.12	0.09	1.55	0.00	0.02	0.01	15.98	0.04	0.09	0.02	34.77	2.40	0.22	1.20	324
RCD505.110_chl21	6.90	0.01	3.32	0.00	7.95	0.13	0.30	0.88	0.00	0.01	0.00	15.90	0.00	0.00	0.10	35.49	1.49	0.10	0.75	179
RCD505.110_chl22	6.94	0.00	3.31	0.00	7.92	0.12	0.31	0.82	0.00	0.02	0.00	15.93	0.01	0.01	0.07	35.46	1.48	0.09	0.74	177
RCD505.110_chl23	6.93	0.00	3.32	0.00	7.91	0.07	0.33	0.86	0.00	0.01	0.00	15.94	0.01	0.00	0.06	35.44	1.50	0.10	0.75	179

Chlorite analysis (continued)

Sample	Si	Ti	Al	Cr	Mg	Ca	Mn	Fe	Ni	Zn	Ba	OH	Na	K	F	Total	AlIV	Fe/(Fe+Mg)	half tetra	Temperature
RCD358.80_chl24	6.21	0.00	4.74	0.00	6.54	0.04	0.51	1.33	0.00	0.02	0.01	15.95	0.00	0.05	0.05	35.47	2.92	0.17	1.46	408
RCD358.80_chl25	6.17	0.00	4.82	0.00	6.52	0.03	0.53	1.34	0.00	0.01	0.00	15.94	0.01	0.06	0.06	35.48	2.99	0.17	1.50	420
RCD358.80_chl26	5.94	0.00	4.56	0.00	7.02	0.04	0.51	1.69	0.00	0.02	0.00	15.99	0.01	0.01	0.01	35.79	2.74	0.19	1.37	379
RCD358.80_chl27	5.98	0.00	4.63	0.00	6.91	0.03	0.54	1.58	0.00	0.04	0.00	15.94	0.01	0.01	0.06	35.74	2.80	0.19	1.40	389
RCD358.80_chl28	6.11	0.00	4.36	0.00	7.07	0.04	0.57	1.53	0.01	0.04	0.01	15.96	0.02	0.01	0.04	35.75	2.53	0.18	1.27	346
RCD505.111_chl29	6.18	0.01	4.50	0.00	5.82	0.05	0.42	2.58	0.00	0.01	0.00	15.99	0.00	0.06	0.02	35.61	2.68	0.31	1.34	369
RCD505.111_chl30	6.10	0.00	4.45	0.00	6.09	0.05	0.44	2.56	0.00	0.02	0.01	15.94	0.00	0.02	0.07	35.72	2.63	0.30	1.31	361
RCD505.111_chl31	6.05	0.00	4.68	0.00	5.40	0.04	0.46	2.93	0.01	0.01	0.00	15.95	0.01	0.11	0.05	35.69	2.86	0.35	1.43	399
RCD505.111_chl32	6.22	0.00	4.67	0.00	5.07	0.04	0.51	2.77	0.00	0.04	0.00	16.00	0.00	0.24	0.00	35.57	2.85	0.35	1.43	397
RCD505.111_chl33	6.65	0.00	5.14	0.00	3.99	0.04	0.34	2.26	0.00	0.02	0.01	15.98	0.01	0.65	0.02	35.11	3.32	0.36	1.66	472
RCD1109.75_chl34	5.76	0.00	5.40	0.01	4.45	0.03	0.05	3.82	0.00	0.00	0.01	15.94	0.00	0.09	0.06	35.62	3.58	0.46	1.79	514
RCD1109.75_chl35	5.72	0.00	5.14	0.00	4.76	0.02	0.06	3.93	0.00	0.03	0.00	15.98	0.01	0.10	0.02	35.77	3.32	0.45	1.66	472
RCD1109.75_chl36	5.64	0.00	5.12	0.00	4.99	0.00	0.06	3.98	0.00	0.02	0.00	15.97	0.00	0.02	0.03	35.83	3.30	0.44	1.65	469
RCD1109.75_chl37	5.65	0.01	5.13	0.00	4.85	0.01	0.06	4.04	0.00	0.02	0.00	15.95	0.01	0.02	0.05	35.81	3.31	0.45	1.65	471

Note: Temperature data were calculated using the equation of Cathelineau & Nieva, (1985).

APPENDIX D: Carbon, oxygen and sulphur isotopes

Carbon and Oxygen Isotope

Sample No.	Description	$\delta\ ^{13}C_{PDB}$	$\delta\ ^{18}O_{PDB}$	$\delta\ ^{18}O_{SMOW}$	Depth
RCD312.103 *	Amygdale in andesite with chlorite	-4.321	-19.902	10.344	45.80
RCD1109.73 *	Amygdale in andesite with chlorite	-3.555	-20.870	9.346	92.20
RCD312.106 *	breccia	-2.332	-18.646	11.639	123.70
RCD357.92	breccia	-2.053	-21.605	8.588	59.22
RCD1108.68	breccia	-1.672	-21.639	8.553	123.70
RCD499.94	ore vein	-2.057	-21.317	8.885	32.75
RCD499.96	ore vein	-2.190	-21.334	8.868	36.70
RCD499.98	ore vein	-7.335	-15.465	14.918	47.00
RCD357.89	ore vein	-2.372	-22.061	8.118	49.43
RCD358.80	ore vein	-2.074	-22.666	7.495	63.30
RCD358.82	ore vein	-1.794	-21.422	8.777	67.29
RCD357.93	calcite vein	-5.588	-17.733	12.580	65.60
RCD358.85	calcite vein	-1.711	-21.203	9.003	75.08
RCD1109.77 *	calcite vein	-4.694	-19.687	10.565	112.90
RCD1116.67	calcite vein	-6.515	-15.537	14.844	100.65
RCD1109.72	rhodocosite	-0.766	-20.349	9.883	90.10
RCD1116.64	limestone	-2.139	-20.377	9.854	178.40

*Cold finger used

Carbon and oxygen Isotope data of carbonates for the A, C, D and H zones, the Chatree deposit, Thailand.

The A zone			The C zone			The D zone			The H zone		
Dedenczuk, 1998			Greener, 1999			Dedenczuk, 1998			This study		
Sample No.	$\delta^{13}C$	$\delta^{18}O$	Sample No.	$\delta^{13}C$	$\delta^{18}O$	Sample No.	$\delta^{13}C$	$\delta^{18}O$	Sample No.	$\delta^{13}C$	$\delta^{18}O$
Ore stage			Ore stage			Ore stage			Ore stage		
D32 35.60	-2.73	8.37	C171.36.1	-3.43	10.55	D195 28 33.25.	-1.53	12.47	RCD312.106	-2.33	11.64
D32 45.40	-3.02	7.86	C172.72.5	-5.44	9.37	D195 72.60	-6.40	12.82	RCD357.92	-2.05	8.59
D37 91.45	-6.62	11.52	C201.48.1	-2.72	9.05	D196 36.60	-2.79	13.31	RCD499.94	-2.06	8.89
D39 92.83	-2.43	7.01	C172.72.1	-5.50	12.40	D196 98.60	0.20	17.23	RCD499.96	-2.19	8.87
D41 72.10	-2.69	12.29	C277.45	-2.04	13.62	D224 40.40	-1.85	8.62	RCD357.89	-2.37	8.11
D41 81.25	-4.53	8.68	C200.13.8	-3.66	11.93	D224 60.45	-2.10	9.17	RCD358.80	-2.07	7.50
D62 71.10	-3.89	9.17	C439.57.1	-1.88	10.14				RCD358.82	-1.79	8.78
D62 22.33	-1.21	14.27	C200.62.9	-1.10	11.16				RCD358.85	-1.71	9.00
			C202.40.5	-1.20	11.27				RCD1109.72	-0.77	9.88
			C384.67.7	-1.50	13.24						
			C201.27	-1.60	12.14						
			C277	-5.80	14.58						
Late stage			Late stage			Late stage			Late stage		
D62 91.05	-2.19	9.20	C404.95.9	-10.27	14.43	D246 47.85	-3.08	14.15	RCD312.103	-4.32	10.34
			C404.79A	-5.02	10.53	D246 53.00	-2.33	9.92	RCD1109.73	-3.56	9.35
			C404.79B	-5.21	12.15	D195 28.05	-1.05	14.09	RCD1108.68	-1.67	8.55
			C404.106.6	-5.85	11.38	D195 72.60	-3.14	8.55	RCD499.98	-7.34	14.92
			C201.49.1	-4.26	4.23	D212 48.8	-1.63	9.04	RCD357.93	-5.59	12.58
			C404.82.7	-3.34	8.48	D214 43.95	-2.29	7.26	RCD1109.77	-4.69	10.57
			C202.19	-3.35	8.34	D214 53.20	-3.30	9.10	RCD1116.67	-6.52	14.85
			C404.82.7	-4.19	8.35				Limestone		
			C384.67.7	-4.37	10.74				RCD1116.64	-2.14	9.85
			C172.66.8	-4.85	12.73						
			C172.86.6	-4.57	10.81						
			C202.21.6	-8.67	14.00						
			C172.45.3	-6.70	9.00						
			C384.104.5	-9.91	20.16						
			C172.66.8	-4.16	11.14						
			C171.40.9	-6.09	11.74						
			C200.107.8	-4.83	11.08						
			C404.99.9	-11.56	16.25						
			C384.78.6	-12.42	15.10						

$\delta^{34}S$ value from wall rock and ore vein pyrite grains of the A, C, D and H zones, the Chatree deposit, Thailand.

The A zone			The C zone			The D zone			The H zone		
Dedenczuk, 1998			Greener, 1999			Dedenczuk, 1998			This study		
Sample No.	$\delta^{34}S$(‰)	Sample type	Sample No.	$\delta^{34}S$(‰)	Sample type	Sample No.	$\delta^{34}S$(‰)	Sample type	Sample No.	$\delta^{34}S$(‰)	Sample type
D32 35.60	-3.19	ore vein	200.41	3.1	ore vein	D195 66.70	4.75	wall rock	RCD 409.76.01	+5.00	ore vein
D32 35.60	0.87	ore vein	172.79	1.7	ore vein	D195 84.94	3.88	wall rock	RCD 409.76.02	4.28	ore vein
D32 35.60	1.05	ore vein	404.95	0.5	ore vein	D195 84.94	4.01	ore vein	RCD 357.89.01	+2.45	ore vein
D32 38.65	3	wall rock	169.20.5	-0.3	ore vein	D196 21.10	6.03	ore vein	RCD 357.89.02	+5.28	ore vein
D32 38.65	5.39	ore vein	277.46.4	2.4	ore vein	D196 24.55	1.17	ore vein	RCD 1109.75.01	+1.99	ore vein
D32 43.70	2.34	ore vein	489.28	2.6	ore vein	D196 36.60	5.59	wall rock	RCD 1109.75.02	+1.59	ore vein
D32 45.40	5.56	ore vein	169.43.9	-9.4	ore vein	D196 56.60	9.58	wall rock	RCD 358.82.01	+3.88	ore vein
D37 89.45	3	ore vein	202.20.5	4.2	wall rock	D212 27.90	5.86	ore vein	RCD 358.82.02	+4.79	ore vein
D39.69.45	-5.14	ore vein	340.54.5	2.8	wall rock	D212 69.60	4.2	wall rock	RCD 358.87.01	0.19	ore vein
D39 90.65	1.28	ore vein	171.22.8	1.6	wall rock	D214 43.95	3.79	ore vein	RCD 358.87.02	+2.39	ore vein
D39 92.83	-3.12	wall rock	171.66	2.3	wall rock	D224 22.80	-3.76	ore vein	RCD 499.96.01	+3.26	ore vein
D39 97.40	-0.74	wall rock	404.86.7	-6.6	wall rock	D224 44.35	2.17	ore vein	RCD 499.96.02	+0.05	ore vein
D41 39.80	3.69	wall rock	172.106.2	2.8	wall rock	D224 44.35	3.67	ore vein	RCD 358.80.01	+3.19	ore vein
D62 22.30	6.29	ore vein	171.90.7	4.3	wall rock	D224 59.85	7.09	wall rock	RCD 358.80.03	3.80	ore vein
D62 57.25	2.52	wall rock	201.41	3.4	wall rock	D224 67.30	4.28	ore vein	RCD 357.92.01	-1.70	ore vein
D62 71.10	5.42	wall rock	404.66	3.1	wall rock	D224 67.30	7.53	wall rock	RCD 357.92.02	4.20	ore vein
D62 96.55	7.8	wall rock	404.66	4.2	wall rock	D246 20.60	3.1	wall rock	RCD 1108.69.01	-0.60	ore vein
D62 100.70	3.07	dyke	384.119.2	5.1	wall rock	D246 34.14	0.39	wall rock	RCD 1108.69.02	0.68	ore vein
			200.107	1.9	wall rock	D246 43.00	1.99	wall rock	RCD 499.94.01	3.15	ore vein
			439.67.8	-0.4	wall rock	D247 41.85	-3.19	ore vein	RCD 499.94.02	4.60	ore vein
			172.66.6	2.2	wall rock	D247 41.85	-2.86	ore vein	RCD 499.95.01	5.00	ore vein
			202.42.5	0.2	wall rock	D247 41.85	-3.17	ore vein	RCD 499.95.02	2.60	ore vein
			202.29.6	1.8	ore vein				RCD 1108.68.02	3.40	ore vein
			439.57.4	-4.8	wall rock						

APPENDIX E: List of samples

List of samples

Sample No.	Tas No.	Depth(m)	Rock name	Thin-section	Polish-section	Stainning	XRF	PIMA	S_Isotope	C_isotope	Electron Microprobe		
											Electrum	Sphalerite	Chlorite
Drill Core													
RCD341.01	155623	55.46-55.56	Dyke	X				X					
RCD341.02	155624	84.25-84.40	Plagioclase-pyroxene-phyric andesite	X			X						
RCD341.05	155625	130.40-130.9	Plagioclase-pyroxene-phyric andesite					X					
RCD460.06	155626	36.55-36.42	Andesitic lithic breccias					X					
RCD460.07	155627	45.50-45.60	Quartz carbonate vein		X	X		X					
RCD460.08	155628	64.85-64.95	Andesitic lithic breccias					X					
RCD460.09	155629	70.99-71.09	Quartz carbonate vein		X	X		X					
RCD460.12	155630	118.73-118.8	Andesitic lithic breccias					X					
RCD460.12.	155631	47.22-47.32	Plagioclase-pyroxene-phyric andesite	X			X						
RCD344.15	155632	172.54-172.7	Crystal-rich lithic breccias	X			X						
RCD459.18	155633	41.71-41.80	Quartz carbonate vein		X			X					
RCD459.19	155634	61.40-61.59	Andesitic lithic breccias					X					
RCD459.20	155635	93.10-93.15	Andesitic lithic breccias					X					
RCD459.22	155636	125.04-125.1	Plagioclase-pyroxene-phyric andesite					X					
RCD374.24	155637	48.64-48.70	Quartz-breccia vein					X					
RCD374.26	155638	67.21-67.30	Quartz carbonate vein		X	X		X				X	
RCD450.27	155639	53.75-53.87	Quartz-carbonate breccia vein					X					
RCD450.28	155640	84.45-84.55	Quartz carbonate vein		X			X					
RCD450.29	155641	86.55-86.67	Andesitic lithic breccias	X									
RCD450.30	155642	93.35-93.47	Andesitic lithic breccias		X	X		X					

List of samples (continued)

Sample No.	Tas No.	Depth(m)	Rock name	Thin-section	Polish-section	Stainning	XRF	PIMA	S_Isotope	C_isotope	Electron Microprobe		
											Electrum	Sphalerite	Chlorite
RCD450.31	155643	99.16-99.28	Late dyke	X									
RCD450.32	155644	125.05-125.1	Plagioclase-pyroxene-phyric andesite					X					
RCD394.35	155645	59.19-59.30	Andesitic lithic breccias		X	X		X					X
RCD394.36	155646	64.30-64.44	Quartz carbonate vein					X					
RCD394.37	155647	74.55-74.65	Quartz carbonate vein		X	X		X					
RCD394.38	155648	79.45-79.45	Andesitic lithic breccias		X	X		X					
RCD394.39	155649	84.60-83.94	Plagioclase-pyroxene-phyric andesite	X			X	X					
RCD453.40	155650	70.30-70.41	Late dyke					X					
RCD453.41	155651	82.10-82.20	Quartz carbonate vein			X		X					
RCD453.42	155652	88.50-88.62	Quartz carbonate vein					X					
RCD453.43	155653	115.71-115.8	Plagioclase-pyroxene-phyric andesite			X		X					
RCD453.44	155654	114.00-114.1	Plagioclase-pyroxene-phyric andesite	X									
RCD1120.45	155655	118.20-118.3	Plagioclase-pyroxene-phyric andesite			X							
RCD1120.46	155656	132.25-132.4	Late dyke										
RCD1120.47	155657	145.90-146.0	Andesitic lithic breccias					X					
RCD1120.49	155658	193.50-169.6	Late Dyke					X					
RCD1123.53	155659	136.00-136.0	Quartz lithic breccia			X		X					
RCD1123.54	155660	141.40-141.5	Quartz lithic breccia					X					
RCD1123.55	155661	148.60-149.7	Quartz carbonate vein					X					
RCD1123.58	155662	167.92-168.0	Andesitic lithic breccias			X		X					
RCD1123.59	155663	181.01-181.1	Andesitic lithic breccias	X									

List of samples (continued)

Sample No.	Tas No.	Depth(m)	Rock name	Thin-section	Polish-section	Stainning	XRF	PIMA	S_Isotope	C_isotope	Electron Microprobe		
											Electrum	Sphalerite	Chlorite
RCD1116.60	155664	131.10-131.2	Plagioclase-pyroxene-phyric andesite	X				X					
RCD1116.61	155665	149.10-149.2	Andesitic lithic breccias					X					
RCD1116.62	155666	160.00-160.1	Andesitic lithic breccias					X					
RCD1116.63	155667	172.70-172.6	Crystal-rich lithic breccias	X			X	X					
RCD1116.64	155668	178.40-178.5	Limestone	X									
RCD1108.65	155669	87.58-87.70	Plagioclase-pyroxene-phyric andesite	X									
RCD1108.67	155670	100.65-100.7	Andesitic lithic breccias					X		X			
RCD1108.68	155671	123.70-123.8	Quartz carbonate vein			X		X	X	X			
RCD1108.69	155672	125.59-125.7	Quartz carbonate vein			X		X	X				
RCD1108.70	155673	135.27-135.3	Andesitic lithic breccias				X	X					
RCD1108.71	155674	152.90-153.0	Anesitic breccia and andesite					X					
RCD1109.72	155675	90.10-90.24	Plagioclase-pyroxene-phyric andesite					X		X			
RCD1109.73	155676	92.20-92.32	Plagioclase-pyroxene-phyric andesite							X			
RCD1109.75	155677	95.90-96.00	Andesitic lithic breccias		X	X		X	X				X
RCD1109.76	155678	103.10-103.2	Quartz carbonate vein		X	X		X	X				X
RCD1109.77	155679	112.90-112.9	Andesitic lithic breccias	X						X			
RCD358.80	155680	63.30-63.45	Quartz carbonate vein		X	X		X	X	X			X
RCD358.81	155681	63.90-63.97	Plagioclase-pyroxene-phyric andesite										
RCD358.82	155682	67.29-67.45	Quartz carbonate vein		X			X	X	X			
RCD358.83	155683	70.72-70.86	Andesitic lithic breccias					X					
RCD358.84	155684	72.26-72.36	Late dyke							X			

List of samples (continued)

Sample No.	Tas No.	Depth(m)	Rock name	Thin-section	Polish-section	Stainning	XRF	PIMA	S_Isotope	C_isotope	Electron Microprobe		
											Electrum	Sphalerite	Chlorite
RCD358.85	155685	75.08-75.20	Plagioclase-pyroxene-phyric andesite			X		X		X			
RCD358.86	155686	76.43-76.52	Plagioclase-pyroxene-phyric andesite	X				X					
RCD358.87	155687	79.70-79.83	Quartz carbonate vein		X	X		X	X				
RCD357.88	155688	46.30-46.30	Quartz carbonate vein			X		X					
RCD357.89	155689	49.43-49.55	Quartz carbonate vein		X			X	X	X	X	X	
RCD357.90	155690	52.00-52.15	Quartz-carbinate breccia vein			X		X					
RCD357.92	155691	59.22-59.32	Quartz-carbinate breccia vein		X			X	X	X	X		
RCD357.93	155692	65.60-65.72	Plagioclase-pyroxene-phyric andesite					X		X			
RCD499.94	155693	32.75-32.85	Quartz carbonate vein		X			X	X	X			X
RCD499.95	155694	35.86-36.00	Quartz carbonate vein		X				X				X
RCD499.96	155695	36.70-36.83	Quartz carbonate vein		X			X	X	X			
RCD499.97	155696	45.60-45.71	Quartz carbonate vein					X					
RCD499.98	155697	47.00-47.12	Quartz carbonate vein		X	X		X		X			
RCD499.100	155698	59.05-59.25	Late dyke	X			X						
RCD312.101	155699	43.88-43.90	Late dyke				X						
RCD312.102	155700	44.65-44.73	Late dyke	X									
RCD312.103	155701	45.80-45.90	Plagioclase-pyroxene-phyric andesite							X			
RCD312.105	155702	50.95-51.15	Andesitic lithic breccias										
RCD312.106	155703	56.00-56.15	Andesitic lithic breccias					X		X			
RCD505.109	155704	42.00-42.10	Late dake				X						
RCD505.110	155705	50.86-51.00	Quartz carbonate vein		X			X					X

List of samples (continued)

Sample No.	Tas No.	Depth(m)	Rock name	Thin-section	Polish-section	Stainning	XRF	PIMA	S_Isotope	C_isotope	Electron Microprobe		
											Electrum	Sphalerite	Chlorite
RCD505.111	155706	55.60-55.80	Quartz breccia		X			X					X
RCD505.114	155707	62.70-63.83	Late dyke	X									
RCD1113.11	155708	111.35-111.4	Late dyke with vein	X									
RCD1113.11	155709	115.45-115.6	Plagioclase-pyroxene-phyric andesite	X									
RCD1113.11	155710	119.50-119.6	Andesite with vein stock work					X					
RCD1113.11	155711	121.70-121.8	Andesite with vein stock work		X	X		X					
RCD1113.11	155712	125.23-125.3	Andesitic lithic breccias			X		X					
RCD1113.12	155713	129.25-129.9	Andesitic lithic breccias			X		X					
RCD1113.12	155714	131.88-132.0	Andesitic lithic breccias				X	X					
RCD504.124	155715	37.10-37.26	Quartz carbonate vein		X			X			X		X
RCD504.125	155716	40.47-40.60	Late dyke	X									
RCD504.126	155717	45.10-45.22	Quartz carbonate vein					X					
RCD504.127	155718	45.89-46.00	Andesitic lithic breccias					X					

List of samples (continued)

Sample No.	Tas No.	Depth(m)	Rock name	Thin-section	Polish-section	Stainning	XRF	PIMA	S_Isotope	C_isotope	Electron Microprobe		
											Electrum	Sphalerite	Chlorite
H pit													
H03	155719	hanging wall	Crystal-rich andesitic pumice breccias					X					
H05	155720	quartz vein	Quartz carbonate vein					X					
H08	155721	breccia zone	Quartz carbonate vein					X					
H09	155722	breccia zone	Quartz carbonate vein					X					
H10	155723	hanging wall	Crystal-rich andesitic pumice breccias					X					
H11	155724	breccia zone	Breccia mineralised vein		X			X					
H13	155725	footwall	Plagioclase-pyroxene-phyric andesite					X					
H19	155726	hanging wall	Crystal-rich andesitic pumice breccias					X					
H22	155727	hanging wall	Crystal-rich andesitic pumice breccias					X					
H25	155728	quartz vein	Quartz carbonate vein					X					
F04	155729	footwall	Plagioclase-pyroxene-phyric andesite				X						
HP01	155730	hanging wall	Crystal-rich andesitic pumice breccias	X			X						
HP02	155731	hanging wall	Crystal-rich andesitic pumice breccias	X			X						
HP03	155732	hanging wall	Volcanic beded sandstone	X			X						
HP04	155733	footwall	Plagioclase-pyroxene-phyric andesite	X									
HP05	155734	footwall	Late dyke	X			X						
HP06	155735	footwall	Andesitic lithic breccias	X			X						
HP07	155736	footwall	Plagioclase-pyroxene-phyric andesite	X									
HP08	155737	footwall	Late dyke	X									
HP09	155738	footwall	Plagioclase-pyroxene-phyric andesite	X			X						

List of samples (continued)

Sample No.	Tas No.	Depth(m)	Rock name	Thin-section	Polish-section	Stainning	XRF	PIMA	S_Isotope	C_isotope	Electron Microprobe		
											Electrum	Sphalerite	Chlorite
HP10	155739	footwall	Andesitic lithic breccias	X			X						
HP11	155740	footwall	Late dyke	X			X						
HP12	155741	footwall	Late dyke	X									
HP13	155742	hanging wall	Crystal-rich andesitic pumice breccias	X									
HP14	155743	ore zone	Quartz carbonate vein		X								
HP15	155744	ore zone	Quartz carbonate vein		X								
HP16	155745	ore zone	Quartz carbonate vein		X								
HP17	155746	ore zone	Quartz carbonate vein		X								

APPENDIX F: Gold and silver assay

provided by Akara Mining Company

Drill hole	**Sample No.**	**Depth(m)**	Au g/t	Ag g/t	Ag/Au	**Drill hole**	**Sample No.**	**Depth(m)**	Au g/t	Ag g/t	Ag/Au
RCD 341	341.01	55.46-55.56	no data	no data	no data	RCD1116	1116.60	31.10-131.2	0.52	3.00	5.77
	341.02	84.25-84.40	no data	no data	no data		1116.61	49.10-149.2	0.05	2.00	40.00
	341.03	98.25-99.00	no data	no data	no data		1116.62	60.00-160.1	0.15	2.00	13.33
	341.04	126.43-126.51	no data	no data	no data		1116.63	72.70-172.6	0.03	1.00	33.33
	341.05	130.40-130.97	no data	no data	no data		1116.64	78.40-178.5	0.01	3.00	300.00
RCD 460	460.06	36.55-36.42	0.05	no data	no data	RCD1108	1108.65	87.58-87.70	0.15	2.00	13.33
	460.07	45.50-45.60	1.20	7.10	5.92		1108.66	02.70-102.8	0.13	2.00	15.38
	460.08	64.85-64.95	0.26	2.50	9.62		1108.67	00.65-100.7	0.05	2.00	40.00
	460.09	70.99-71.09	11.20	20.60	1.84		1108.68	23.70-123.8	0.14	2.00	14.29
	460.10	101.50-101.65	0.05	2.00	40.00		1108.69	25.59-125.7	1.63	3.00	1.84
	460.11	113.16-113.24	0.30	4.90	16.33		1108.70	35.27-135.3	0.05	2.00	40.00
	460.12	118.73-118.82	0.28	1.00	3.57		1108.71	52.90-153.0	0.06	2.00	33.33
	460.12.1	47.22-47.32	0.47	4.60	9.79	RCD1109	1109.72	90.10-90.24	0.02	2.00	100.00
RCD 344	344.13	70.26-70.35	no data	no data	no data		1109.73	92.20-92.32	0.01	2.00	200.00
	344.14	93.25-93.37	no data	no data	no data		1109.74	94.00-94.10	8.90	7.00	0.79
	344.15	172.54-172.70	no data	no data	no data		1109.75	95.90-96.00	8.90	7.00	0.79
	344.16	180.26-180.38	no data	no data	no data		1109.76	03.10-103.2	0.20	3.00	15.00
RCD 459	459.17	32.43-32.53	0.03	no data	no data		1109.77	12.90-112.9	0.18	2.00	11.11
	459.18	41.71-41.80	2.25	13.60	6.04		1109.78	21.80-121.9	0.03	2.00	66.67

Drill hole	Sample No.	Depth(m)	Au g/t	Ag g/t	Ag/Au	Drill hole	Sample No.	Depth(m)	Au g/t	Ag g/t	Ag/Au
RCD 459	459.19	61.40-61.59	0.13	1.30	10.00	RCD1109	1109.79	35.80-135.9	0.06	2.00	33.33
	459.20	93.10-93.15	0.46	1.60	3.48	RCD 358	358.80	63.30-63.45	7.35	7.10	0.97
	459.21	104.80-104.88	0.47	1.30	2.77		358.81	63.90-63.97	0.37	1.40	3.78
	459.22	125.04-125.16	0.37	1.10	2.97		358.82	67.29-67.45	3.42	4.20	1.23
	459.23	137.30-137.43	0.01	no data	no data		358.83	70.72-70.86	0.38	9.30	24.47
RCD 374	374.24	48.64-48.70	13.30	117.00	8.80		358.84	72.26-72.36	0.01	no data	no data
	374.25	61.89-61.97	0.01	no data	no data		358.85	75.08-75.20	0.02	no data	no data
	374.26	67.21-67.30	3.25	5.30	1.63		358.86	76.43-76.52	0.87	1.70	1.95
RCD 450	450.27	53.75-53.87	22.20	265.00	11.94		358.87	79.70-79.83	1.66	10.80	6.51
	450.28	84.45-84.55	0.19	1.00	5.26	RCD357	357.88	46.30-46.30	1.41	44.40	31.49
	450.29	86.55-86.67	0.06	no data	no data		357.89	49.43-49.55	15.40	27.20	1.77
	450.30	93.35-93.47	0.49	no data	no data		357.90	52.00-52.15	2.28	6.40	2.81
	450.31	99.16-99.28	0.06	no data	no data		357.91	55.30-55.40	0.01	no data	no data
	450.32	125.05-125.18	0.74	2.00	2.70		357.92	59.22-59.32	4.88	7.10	1.45
RCD 394	394.33	51.70-51.82	0.01	no data	no data		357.93	65.60-65.72	0.72	1.80	2.50
	394.34	54.15-54.24	0.01	no data	no data	RCD 499	499.94	32.75-32.85	2.19	7.30	3.33
	394.35	59.19-59.30	9.72	6.40	0.66		499.95	35.86-36.00	1.39	11.50	8.27
	394.36	64.30-64.44	0.14	1.00	7.14		499.96	36.70-36.83	4.38	6.40	1.46
	394.37	74.55-74.65	0.10	1.90	19.00		499.97	45.60-45.71	2.70	4.30	1.59
	394.38	79.45-79.45?	4.90	4.40	0.90		499.98	47.00-47.12	1.00	4.10	4.10

Drill hole	Sample No.	Depth(m)	Au g/t	Ag g/t	Ag/Au	Drill hole	Sample No.	Depth(m)	Au g/t	Ag g/t	Ag/Au
RCD 394	394.39	84.60-83.94	2.34	2.70	1.15	RCD 499	499.99	50.10-50.20	0.01	no data	no data
RCD 453	453.40	70.30-70.41	no data	no data	no data		499.100	59.05-59.25	0.07	no data	no data
	453.41	82.10-82.20	6.67	6.10	0.91	RCD 312	312.101	43.88-43.90	no data	no data	no data
	453.42	88.50-88.62	2.63	36.70	13.95		312.102	44.65-44.73	no data	no data	no data
	453.43	115.71-115.85	1.89	3.80	2.01		312.103	45.80-45.90	no data	no data	no data
	453.44	114.00-114.10	1.89	3.80	2.01		312.104	48.83-48.90	no data	no data	no data
RCD 1120	1120.45	118.20-118.32	0.54	4.00	7.41		312.105	50.95-51.15	0.19	no data	no data
	1120.46	132.25-132.45	0.03	2.00	66.67		312.106	56.00-56.15	0.03	no data	no data
	1120.47	145.90-146.00	0.64	5.00	7.81	RCD 356	356.107	11.30-11.40	4.35	9.40	2.16
	1120.48	175.07-175.20	0.01	1.00	200.00		356.108	18.20-18.30	3.78	12.80	3.39
	1120.49	193.50-169.60	0.03	1.00	33.33	RCD 505	505.109	42.00-42.10	0.03	no data	no data
	1120.50	202.40-202.50	0.01	1.00	200.00		505.110	50.86-51.00	2.24	103.00	45.98
	1120.51	228.70-228.80	0.08	1.00	12.50		505.111	55.60-55.80	2.23	7.10	3.18
RCD1123	1123.52	134.70-134.78	0.01	2.00	200.00		505.112	59.10-59.18	0.89	6.60	7.42
	1123.53	136.00-136.09	0.02	1.00	50.00		505.113	61.75-61.89	0.32	1.50	4.69
	1123.54	141.40-141.51	0.01	2.00	200.00		505.114	62.70-63.83	0.10	no data	no data
	1123.55	148.60-149.70	0.03	4.00	133.33	RCD1113	1113.115	11.35-111.4	0.43	3.00	6.98
	1123.56	155.36-155.45	0.02	3.00	150.00		1113.116	15.45-115.6	0.07	3.00	42.86
	1123.57	165.35-165.45	0.50	3.00	6.00		1113.117	19.50-119.6	0.97	3.00	3.09
	1123.58	167.92-168.00	0.34	4.00	11.76		1113.118	21.70-121.8	0.33	3.00	9.09

Drill hole	**Sample No.**	**Depth(m)**	Au g/t	Ag g/t	Ag/Au	**Drill hole**	**Sample No.**	**Depth(m)**	Au g/t	Ag g/t	Ag/Au
RCD1123	1123.59	181.01-181.10	0.34	2.00	5.88	RCD1113	1113.119	25.23-125.3	0.51	4.00	7.84
RCD 504	504.124	37.10-37.26	14.30	13.10	0.92		1113.120	29.25-129.9	0.03	2.00	66.67
	504.125	40.47-40.60	0.01	no data	no data		1113.121	31.88-132.0	0.29	2.00	6.90
	504.126	45.10-45.22	1.83	83.50	45.63	RCD 504	504.122	26.32-26.40	0.01	no data	no data
	504.127	45.89-46.00	0.18	2.50	13.89		504.123	33.00-33.17	1.19	4.10	3.45

APPENDIX G: Sample and drill hole location

Sample locations and drill hole positions

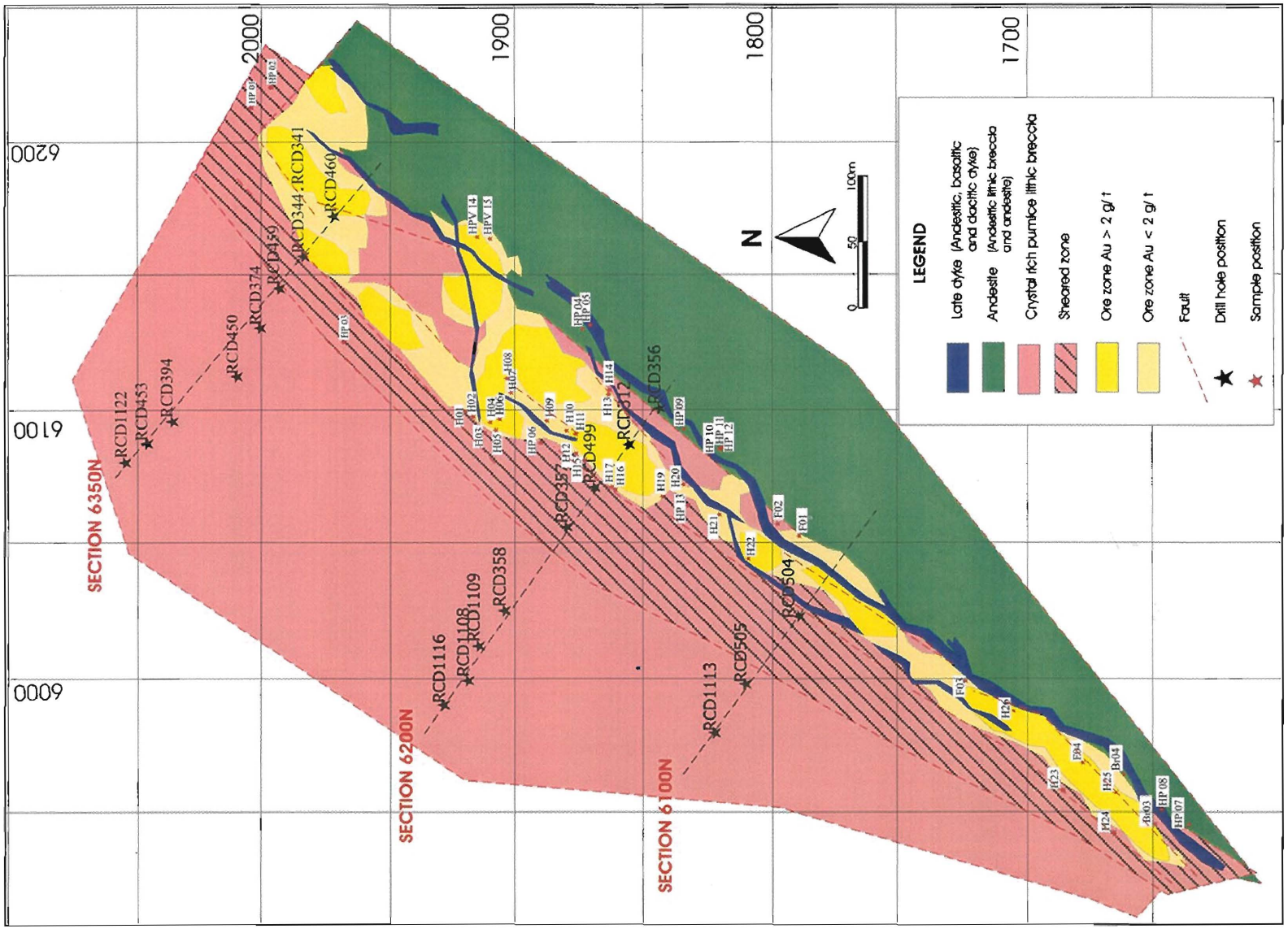

Sample locations of Section 6100N

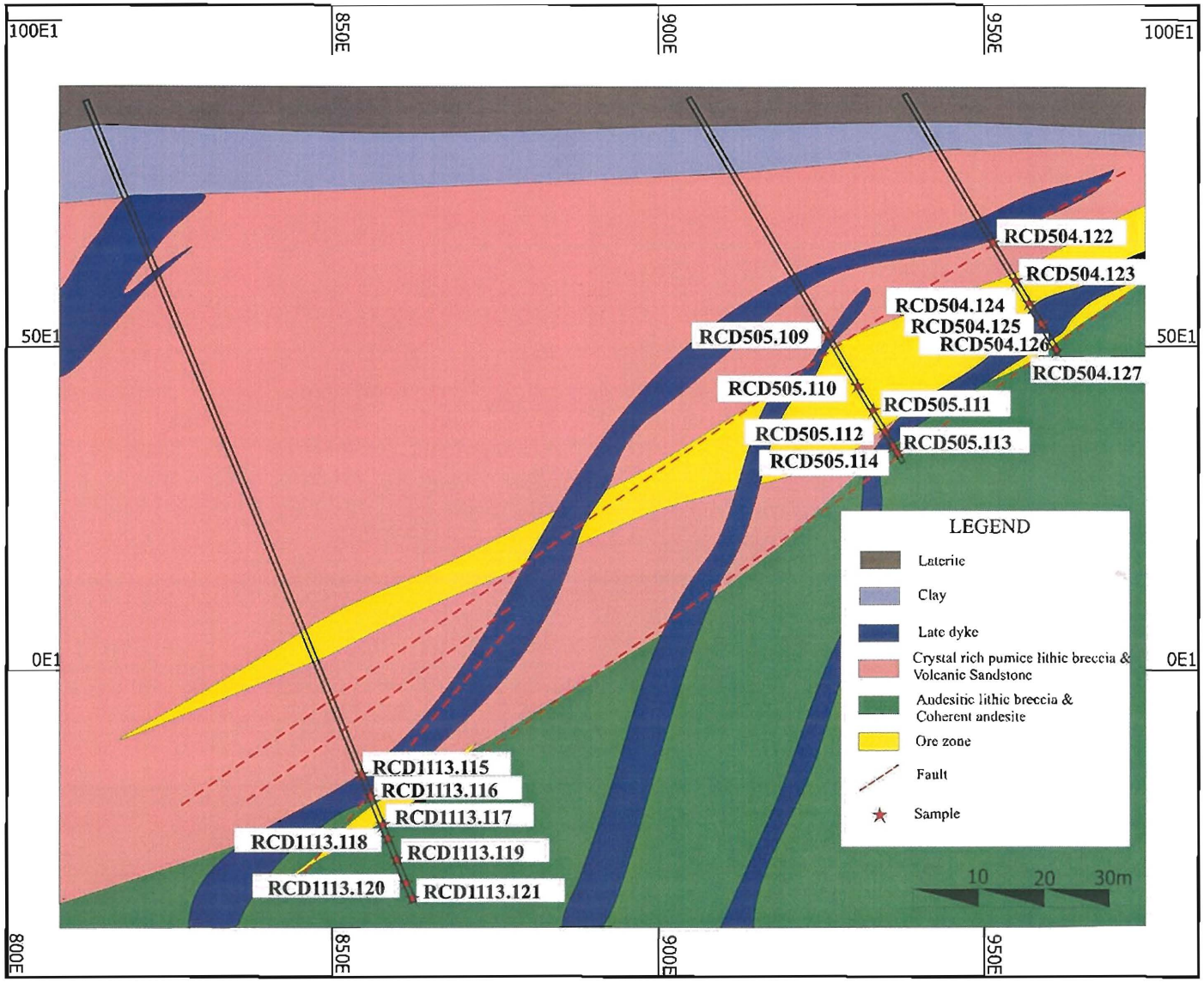

Sample locations of Section 6200N

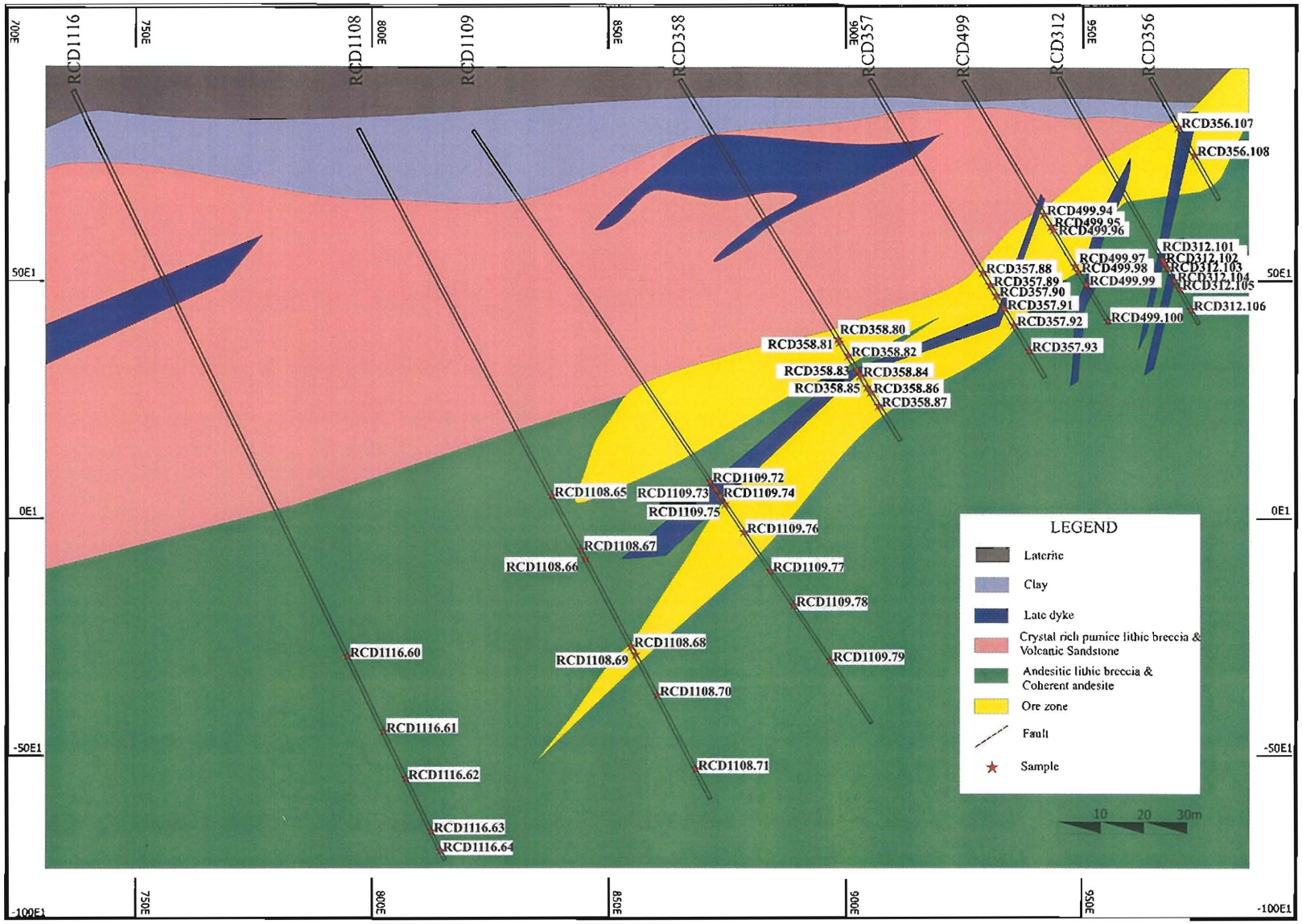

Sample locations of Section 6350N